IAEA-TECDOC-1065

Production technologies for molybdenum-99 and technetium-99m

INTERNATIONAL ATOMIC ENERGY AGENCY IAEA

The originating Section of this publication in the IAEA was:

Industrial Applications and Chemistry Section
International Atomic Energy Agency
Wagramer Strasse 5
P.O. Box 100
A-1400 Vienna, Austria

PRODUCTION TECHNOLOGIES FOR
MOLYBDENUM-99 AND TECHNETIUM-99m
IAEA, VIENNA, 1999
IAEA-TECDOC-1065
ISSN 1011–4289

Printed by the IAEA in Austria
February 1999

The IAEA does not normally maintain stocks of reports in this series.
However, copies of these reports on microfiche or in electronic form can be obtained from

INIS Clearinghouse
International Atomic Energy Agency
Wagramer Strasse 5
P.O. Box 100
A-1400 Vienna, Austria
E-mail: CHOUSE@IAEA.ORG
URL: http://www.iaea.org/programmes/inis/inis.htm

Orders should be accompanied by prepayment of Austrian Schillings 100,–
in the form of a cheque or in the form of IAEA microfiche service coupons
which may be ordered separately from the INIS Clearinghouse.

FOREWORD

Nuclear medicine as it has been practised for the last 30 years or so owns in part its tremendous impact in medical diagnostics procedures to the availability of ^{99m}Tc from compact, easy to use, relatively economical, transportable ^{99}Mo generators. Technetium-99m (6.02 h) is and promises to remain the most widely used radioisotope in nuclear medicine, accounting for more than 80% of all diagnostic nuclear medicine procedures. This amounts to 7 million per annum in Europe alone and to 8 million per annum in the United States of America. The world demand, currently estimated at approximately 6000 Ci (6 day pre-calibration), is expected to increase by about 5% per year.

Recently, a matter of concern has been the availability and supply of ^{99}Mo for the manufacturing of generators. These concerns arose from several factors including, amongst others, the shutdown of some nuclear reactors, uncertainty of reliable operating condition for radioisotope production and easy availability of enriched ^{235}U target material. On the research and development front, efforts are directed towards the development of low enriched uranium (LEU, <20% ^{235}U) target technology including the required modifications of the ^{99}Mo separation processes.

More recently, the utilization of charged particle accelerators, be they LINAC's or cyclotrons, has been discussed as a potential alternative technology to the fission route. These discussions have been prompted by basic research concerns as well as the need to explore new production routes to offset the perceived situation of future problems with the availability of ^{99}Mo if no new dedicated reactors are licensed.

To discuss these issues, the IAEA organized a consultants meeting. The meeting took place at the National Accelerator Centre at Faure, South Africa, from 10 to 12 April 1997.

This publication covers several aspects related to the production of ^{99}Mo and ^{99m}Tc. They range from nuclear reactor production of ^{99}Mo by (n,γ) and (n,fission reactions), including novel aspects of target technology particularly when utilizing LEU materials, to the feasibility of producing both of these radioisotopes by means of particle accelerators. The IAEA officer responsible for this publication is H. Vera Ruiz of the Division of Physical and Chemical Sciences.

EDITORIAL NOTE

In preparing this publication for press, staff of the IAEA have made up the pages from the original manuscripts as submitted by the authors. The views expressed do not necessarily reflect those of the IAEA, the governments of the nominating Member States or the nominating organizations.

Throughout the text names of Member States are retained as they were when the text was compiled.

The use of particular designations of countries or territories does not imply any judgement by the publisher, the IAEA, as to the legal status of such countries or territories, of their authorities and institutions or of the delimitation of their boundaries.

The mention of names of specific companies or products (whether or not indicated as registered) does not imply any intention to infringe proprietary rights, nor should it be construed as an endorsement or recommendation on the part of the IAEA.

The authors are responsible for having obtained the necessary permission for the IAEA to reproduce, translate or use material from sources already protected by copyrights.

CONTENTS

SUMMARY

Technetium-99m (6.02 h) is the most widely used radioisotope in nuclear medicine, accounting for more than 80% of all diagnostic nuclear medicine procedures. This amounts to 7 million per annum in Europe alone, and to 8 million per annum in the United States of America. Technetium-99m is almost exclusively produced from the decay of its 66-h parent ^{99}Mo. The present world demand for ^{99}Mo was estimated at approximately 6000 Ci per week (6 days pre-calibrated). Further growth in demand has been predicted. The present installed processing capacity is substantially larger than the above mentioned demand, and the capacity for irradiation of targets is even higher. The large demand for ^{99}Mo has given it an "industrial scale production" status.

The present sources of ^{99}Mo are research reactors by using the (n,γ) nuclear reaction with natural Mo (^{98}Mo, ~24%), resulting in inexpensive but low-specific activity ^{99}Mo, or by neutron-induced fission of ^{235}U, which results in expensive but high specific activity ^{99}Mo. The technology requirements for processing of ^{99}Mo from the (n,γ) "activation method" is rather simple, and is within the reach of most developing countries operating research reactors. In the "fission method", the technological and infrastructure requirements are more complex, and possibly can be sustained only by countries with advanced nuclear technology.

The potential use of accelerators for these purposes is another issue of current scientific and technological interest, particularly in view of recent advances being made in accelerator technology.

Against this background, it was considered worthwhile for the IAEA to review the recent developments in these areas, and to take a long term view regarding the availability of these two vitally important radioisotopes. To this effect, a Consultants meeting was organized to discuss the current status and future perspectives of the required technologies for the production of ^{99}Mo and ^{99m}Tc. The meeting took place at the premises of the National Accelerator Centre of South Africa, Faure, from 10 to 12 April 1997.

At the meeting the current available scientific literature for the production of these two radioisotopes via the use of nuclear research reactors and accelerators was reviewed and assessed. The main conclusions of the meeting can be summarised as follows:

Technetium-99m remains the most important radioisotope for nuclear medicine. Indications are that this should remain the case for the foreseeable future, due to a number of factors such as the inertia among users to stay with known modalities, the development of new labelling kits, and the emergence of new markets. Growth might be influenced by competition from non-nuclear diagnostic techniques, more effective use of generators, and fractionation of kits in order to achieve multiple patient studies with each vial of kit.

The present world demand for ^{99}Mo was estimated at approximately 6000 Ci per week (6 days pre-calibrated). Further growth in demand has been predicted in a US review.

At present nearly the entire demand for ^{99}Mo is supplied by a few large producers employing reactor-based production by means of thermal neutron induced fission of enriched uranium. The processing technology has been proven and licensed, and the ^{99}Mo as well as the down-stream products have been approved by pharmaceutical regulatory authorities. Sophisticated processing infrastructure exists and is being expanded by some producers.

The presently installed processing capacity is substantially larger than the above mentioned demand, and the capacity for irradiation of targets is even higher.

Due to the existing investment in production infrastructure and in the approval of ^{99}Mo and derived products, there will have to be a substantial economic incentive for a large producer of ^{99}Mo or ^{99m}Tc generators to change to a new process.

Any new process having a potential influence on the product quality, compared to existing processes, will have to be demonstrated and licensed fully. The product should be qualified by the various regulatory authorities, which is a long and expensive process adding to the market inertia referred to previously.

When modifications to existing processes or the possible implementation of new technologies are considered, the implications regarding waste treatment and disposal should receive high priority.

Fission ^{99}Mo production was regarded as outside the capabilities of most developing countries because of its complex nature. Where some level of self-sufficiency in ^{99m}Tc generator supply was sought by such countries, the meeting was of the opinion that one of the following avenues could be followed:

- the importation of finished generators for direct use, or
- the importation of fission ^{99}Mo from one of the producers in the world,
- followed by manufacture of chromatographic generators, or
- domestic production of $(n,\gamma)^{99}$Mo for use in alternative generator types.
- A prerequisite for this option is the availability of a reactor with a medium to high neutron flux being operated on a suitable schedule.

The production of ^{99}Mo via the ^{100}Mo(p,pn) reaction was evaluated. A good agreement was found among the different excitation functions available. However, because of the rather low cross-section values found in these measurements, the production of ^{99}Mo via this potential process was found to be largely impractical. A significant limiting factor of this approach appears to be the need for a large inventory (tens of kg quantities) of enriched ^{100}Mo, the logistical considerations of its distribution and recovery, and the cost (~US $2/mg). Furthermore, proton accelerators delivering mA beam on target would be required including the development of high power targets.

The production of ^{99m}Tc via the ^{100}Mo(p,2n) reaction was also evaluated, and the cross section data available were found to be consistent and in good agreement. Extrapolating ^{99m}Tc yields obtained from this data, using the operational conditions of existing 30 MeV accelerator technologies (i.e. ~200 μA, high power metallic targets currently used for the production of radionuclides, e.g. ^{201}Tl, ^{67}Ga, ^{111}In, ^{57}Co), suggest that large-scale (kCi) production of ^{99m}Tc is possible.

With this approach, with available accelerator and target technologies, logistical factors would prevail for local/regional production and distribution. However, the "instant ^{99m}Tc" approach is being utilized successfully, particularly in developing countries operating research reactors. A distinct advantage of this new approach is the possibility to produce and provide single-

photon radiopharmaceuticals (i.e. ^{201}Tl, ^{67}Ga, ^{123}I, and ^{111}In), therapy radionuclides (i.e. ^{103}Pd, ^{124}I, etc.) as well as positron emitting radionuclides such as ^{18}F, ^{11}C, ^{15}O, ^{13}N.

There is a requirement for experimental measurements of the thick target yield and the determination of the radionuclidic purity of the ^{100}Mo(p,2n)^{99m}Tc reaction under optimized conditions for the production of ^{99m}Tc using highly enriched isotopic targets. It was considered essential that the cross sections for co-production of long lived Tc radioisotopes be determined, since the isotopic composition of ^{98}Mo and other stable Mo isotopes is variable.

High energy proton-induced fission of ^{238}U, in combination with secondary prompt neutron induced fission within the target, was also evaluated. Tens of kCi/week production capabilities appear feasible, but require a large R&D effort to integrate the use of yet-to-be developed high-energy (120–150 MeV), high-intensity (1–2 mA) proton accelerators, and targets with which to maximize secondary neutron production, thermalization, and reflector techniques, in the same target. In view of the current effort to enhance the production capability of fission ^{99}Mo, by means of more conventional methods, this option appears to be of lower priority.

The status of nuclear data of deuteron induced reactions is not satisfactory. Low energy production routes such as ^{98}Mo(d,p)^{99}Mo and ^{98}Mo(d,n)^{99m}Tc are not competitive because of low yields. The production of ^{99}Mo at higher deuteron energies (E_d = 50 MeV) has a moderate yield (~13 mCi/μAh) but has serious problems of routine recovery of the enriched target material from the generators. Nuclear data are available only up to 21 MeV. The direct production of ^{99m}Tc using the ^{100}Mo(d,3n) nuclear reaction on enriched ^{100}Mo is more promising having high production yield (~55 mCi/μAh in an energy range up to 40 MeV). Additional measurements are required at higher energies (up to 50 MeV). The high energy deuteron induced reactions give high yields, but require a higher energy and high beam current accelerators than the proton induced reactions and are not likely to be utilized in the foreseeable future.

The contributed papers reflect the current status of the technology and discuss potential alternative methodologies for the production of ^{99}Mo and ^{99m}Tc for medical use. The first four papers address the technologies using nuclear reactors, including the description of a new method using an aqueous homogeneous reactor core for the production of fission ^{99}Mo and the latest development efforts to fabricate ^{235}U low enriched targets (LEU, <20% ^{235}U). The next five papers discuss the potential of utilizing particle accelerators and assess the current status of the available nuclear data for the production of both, ^{99}Mo and ^{99m}Tc with proton and deuteron beams. The last paper discusses a new technology based on gel systems for the preparation of ^{99}Mo/^{99m}Tc generators using low specific activity ^{99}Mo produced in research reactors by the neutron activation of natural and inexpensive molybdenum oxide targets.

CHARACTERISTICS OF NUCLEAR REACTORS USED FOR THE PRODUCTION OF MOLYBDENUM-99

R.M. BALL*
Ball Systems Company,
Lynchburg, Virginia,
United States of America

Abstract

The paper describes nuclear fission reactor characteristics as neutron producers and their use with targets of molybdenum-98 and uranium-235 to produce ^{99}Mo. Tabulations of reactors used and their characteristics are shown. A new method for ^{99}Mo production using an aqueous homogenous reactor is described showing the potential for 1/100th the waste, uranium consumption and power level for a given quantity of ^{99}Mo. A graph is shown of the expected growth in ^{99}Mo use and world-wide costs. The use of low-enriched (less than 20 % ^{235}U) in the homogenous reactor system is possible.

1. NUCLEAR REACTORS FOR THE PRODUCTION OF MOLYBDENUM-99

1.1. Why nuclear reactors?

The usual production of molybdenum-99 (^{99}Mo) for nuclear medicine depends either: 1) on the transmutation of an atom of ^{98}Mo to ^{99}Mo by the absorption of a neutron; or 2) on the fission of uranium-235 (^{235}U) which is also caused by the absorption of a neutron. Thus, for either method, at least one neutron is required for the reaction.

Neutrons can be produced from accelerator reactions where charged particles strike heavy atoms, and also from alpha or gamma reactions with light atoms, such as beryllium or lithium. However, to produce the large quantities of neutrons needed for production of useful quantities of ^{99}Mo, the most effective source is a critical nuclear reactor operating at powers in the range of megawatts. Each fission of an atom of ^{235}U produces an average of about 2.5 neutrons. In an operating reactor, these neutrons are either absorbed by materials in the reactor or escape from the boundaries of the reactor. One neutron must cause fission in another ^{235}U atom. Of the remaining 1.5 neutrons from each fission in a critical reactor, some small fraction are available for production.

Nuclear reactors are designed and built to trade non-productive absorption's or leakage for productive absorption's. The "trading" is usually between control rods and the "target" material. The amount available for trade is called "excess reactivity" and represents the fraction of tradable neutrons per fission. In a typical multipurpose reactor, this fraction is about 0.02. Thus, a reactor operating at one megawatt (3E16 fissions per second), the tradable neutrons amount to 6E14 neutrons per second. Theoretically, if all these neutrons could be captured by a target, the production rate could be up to 6E14 atoms per second or 1E-9 mol/sec. A theoretical possible equilibrium activity for ^{235}U would be 6E5 GBq (16,216 curies).

*Previously with Babcock & Wilcox - Nuclear Environmental Services, Inc.,

In practice, one cannot productively capture all the neutrons available and a comparison among reactor types, shown later, is based on the average flux in the volume where a target can be placed.

1.2. ^{99}Mo Production rate with targets in a nuclear reactor

1.2.1 Irradiation of ^{98}Mo

The basic equation for production of ^{99}Mo in a reactor by activation of ^{98}Mo is:

$$P = F \cdot S \qquad (1)$$

where:

P is the production rate of ^{99}Mo (atoms.s^{-1}.gm^{-1}(^{98}Mo))
F is the average neutron flux in the volume of the target, neutrons.cm^{-2}.s^{-1}, (nvth)
S is the average macroscopic cross section of ^{98}Mo cm^2.g^{-1}

at equilibrium, the production rate is equal to the decay rate, or the specific activity is:

$$A = P/1E9 \text{ GBq/gm}, \quad (1 \text{ GBq} = 1E9 \text{ disintegrations/second}) \qquad (2)$$

where

A is the specific activity, GBq g^{-1}.

This formulation is slightly different from convention and is used to simplify the determination of specific activity, GBq g^{-1} of molybdenum.

The cross section of ^{98}Mo for the (n,γ) reaction by thermal neutrons is 0.13 barns [1]. The resonance energy integral cross section is 7.2 barns and in reactors with large intermediate energy flux, can increase the reaction rate; however, the calculation is based on thermal flux.

More than 70% of the operational research reactors have their thermal neutron fluxes lower than 3.5E13 n.cm^{-1}.s^{-1} [2] Therefore, as illustration, a neutron flux of 1E13 n.cm^{-2}.s^{-1} is used. At this flux, the maximum specific activity achievable is 2.0 GBq g^{-1} (^{98}Mo). This assumes that the molybdenum in the target has been enriched to over 98% ^{98}Mo.

1.2.2. Irradiation of Uranium-235 Targets

Similarly, the equation for production of ^{99}Mo in a reactor by the fissioning of ^{235}U in the target is

$$P = F \cdot Sf \cdot Y$$

where

Sf is the fission macroscopic cross section for ^{235}U, 1.49 cm^2.g^{-1},
Y is the cumulative fission yield for ^{99}Mo from the fissioning of ^{235}U, 0.061 [1]

A determination of the specific activity of the ^{99}Mo at equilibrium must consider the formation of other isotopes of molybdenum as a result of fission (^{97}Mo, ^{98}Mo, ^{100}Mo) and thus,

with a thermal neutron flux of 1E13 nv, the specific activity is 4.4E6 GBq.g^{-1}(Mo), decreasing slowly with longer exposure in the reactor.

1.2.3. Variations with Reactor Flux

In the case of activation of ^{98}Mo, the specific activity is a direct function of the reactor flux. Thus, for a flux of 2E15 nvth (a flux achievable in the High Flux Isotope Reactor (HFIR) at Oak Ridge National Laboratory, USA), the specific activity would be 400 GBq.g^{-1}.

For fission targets, the production of molybdenum isotopes are a constant ratio with each other but the difference in half-life (many are stable isotopes) reduces the specific activity slowly over time.

Note that even with a high flux reactor used for activation of ^{98}Mo, the specific activity of fission ^{99}Mo is four orders of magnitude greater than irradiation ^{99}Mo.

1.2.4 Saturation Activity

Targets are not left in reactors indefinitely but are removed in 3 to 10 days after insertion. ^{99}Mo decays while in the reactor and a balance must be struck between processing costs, specific activity, and reactor operation costs. Fig. 1 shows the reduction in ^{99}Mo available per ^{99}Mo produced as a function of time in the reactor.

1.3. Reactors usable for ^{99}Mo production by target irradiation

All reactors are a source of neutrons but not all are suitable for ^{99}Mo production. The factors which determine suitability are power level, neutron flux available for target irradiation and the amount of volume into which targets can be placed. Where targets are fissionable isotopes, specifically ^{235}U, a further consideration is the removal of heat from the targets.

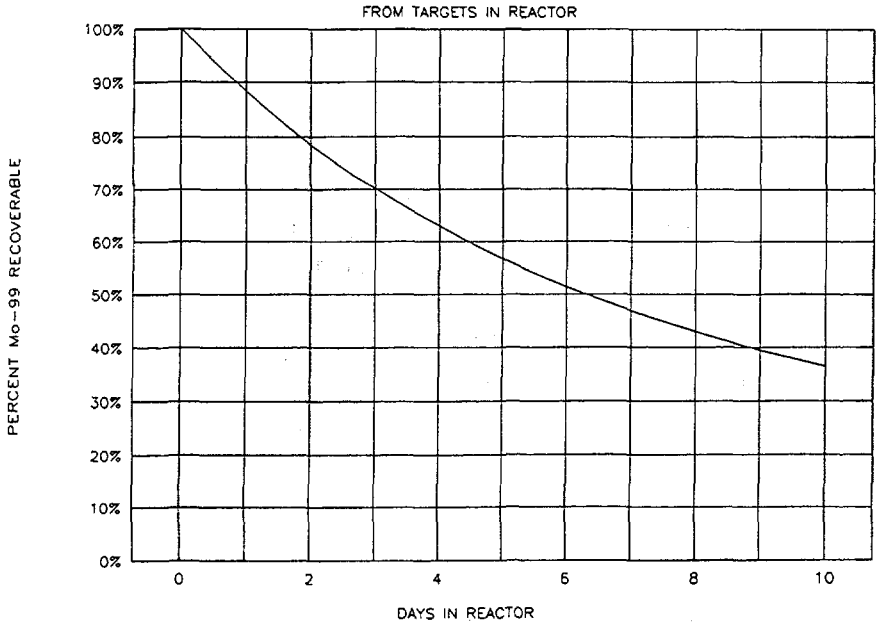

FIG. 1. Recoverable ^{99}Mo from targets in a reactor.

TABLE I. CHARACTERISTICS OF REACTORS USED TO IRRADIATE TARGETS FOR ^{99}MO PRODUCTION

Reactor Name	Location	Power kWth	Flux nvth	Target Vol. cm^3 (1 tar.)
NRU	Canada	135,000	1.5E14	90.5
HFR	Netherlands	45,000	0.6E14	182
ACRR	USA	2,000	3.7E12	363
HFIR	USA	85,000	2.1E15	--
TRIGA	USA	2,000	8.0E13	--
MURR	USA	10,000	4.5E14	--
SAFARI-1	South Africa	20,000	2.0E14	--
HIFAR	Australia	10,000	1.4E14	--

1.3.1. NRU Reactor

This reactor is located at the Chalk River Laboratory in Ontario, Canada. It is the workhorse (around 80% of the world's production) for the production of ^{99}Mo from the fission of ^{235}U. The reactor began operation in 1957. It is heavy water moderated and cooled. Presently, targets are made from alloys of aluminum and operate at about 60 kW each. Up to 20 targets are irradiated for from one to two weeks.

Replacement reactors, called "MAPLE-X's" are being planned for Chalk River to operate at 10 MWth and be dedicated to ^{99}Mo production.

1.3.2. HFR Reactor

This multipurpose reactor is located at the Petten site in The Netherlands. It began operation in 1962 and currently operates at 45 MWth. The reactor is light water moderated and cooled and has numerous locations which are used for the production of isotopes. The targets for the production of ^{99}Mo are aluminum clad and an aluminum-uranium alloy. The uranium is fully enriched. Irradiated targets are transported primarily to the Institute of RadioElements (IRE) in Fleurus, Belgium. IRE also uses the BR-2 in Mol, Belgium and SILOE in France.

1.3.3. ACRR Reactor

The ACRR is located at Sandia National Laboratory. It is being converted to irradiate targets (fully enriched uranium) made by electroplating the inside of a cylinder which is then sealed. The reactor originally was used for defense work in the USA and operated in a pulse mode. The present steady-state power is 2 MWth with plans to upgrade to 4 MWth. Test

quantities of ^{99}Mo have been made in 1997. The reactor is owned and operated under contract for the U.S. Department of Energy. It is stated to be a "backup" for other commercial sources of ^{99}Mo.

1.3.4. HFIR Reactor

The High Flux Isotope Reactor is located at Oak Ridge National Laboratory in Oak Ridge, Tennessee. It began operation in 1965. The mission of the reactor is the creation of high Z isotopes and, with the central flux trap, produces the highest thermal neutron flux in the world. Recently work has been done to irradiate ^{98}Mo for the production of ^{99}Mo. The high flux can create high specific activity ^{99}Mo (see 1.2.3).

1.3.5. TRIGA Reactor

TRIGA refers to a large number of reactors which have been designed and built by General Atomics in San Diego, California. They are deployed throughout the world and several models have been used to irradiate targets for isotope production. The TRIGA Mark II can operate at 2 MWth at 8E13 nvth. Upgradable TRIGAs, with forced cooling are capable of 25 MWth.

1.3.6. MURR Reactor

This reactor is at the University of Missouri, Columbia, in the USA. It operates at 10 MWth, has an annulus pressure vessel and operates 6.5 days per week. It has logged greater than 90% operation since 1977 and is capable of power upgrades to 25 MWth. It does not now routinely provide irradiation of targets to produce ^{99}Mo but is the primary non-DOE source of research radionuclides in the USA [3].

1.3.7. SAFARI-1

This reactor is a 20 MW Oak Ridge type Materials Testing Reactor at Pelindaba near Pretoria in South Africa. Targets are irradiated in core positions and target plates can be loaded and retrieved while the reactor is on power. ^{99}Mo is produced commercially for internal use and for export to India, and China. Most recently, during an interruption of production in Canada (a strike at the NRU in June 1997), ^{99}Mo was supplied to the Amersham company of the UK, and used also in the USA.

1.3.8. HIFAR

This is a heavy water research reactor operating at 10 MW in Australia. The reactor operates full time. As is characteristic of heavy water reactors, there are large volumes available for irradiation. Much of the ^{98}Mo target irradiation has been carried out in the HIFAR.

1.3.9. Other reactors

The reactors listed in Table I are far from a complete list. They merely represent reactors which are being used to produce ^{99}Mo or which could be used.

Other reactors, such as the ATR (USA), HFBR (USA) and SILOE (France) are all capable of producing research or commercial radionuclides. Some reactors are restricted to provide products for use by DOE facilities.

1.4. Heat removal requirements for targets used to make ^{99}Mo

1.4.1. Irradiation of ^{98}Mo Targets

The deposition of energy in ^{98}Mo targets is almost entirely from the reactor radiation absorbed by the mass of the target constituents. These are the container and the chemical material, such as TiMo, or ZrMo gels as described in Chapter 10. The energy deposition has been measured for a water cooled, swimming pool type reactor, the BSF at Oak Ridge National Laboratory [4]. At a power of one megawatt, at the center of the reactor, the heat deposition is 0.17 watts/gram of material. The chemical form of the material does not change the value substantially. Thus, a system of 500 grams would require 83 watts of heat removal, usually within the capability of the reactor coolant system.

1.4.2. Irradiation of Fission Targets

Heat production from fission is much larger than that from activation. A flux of 1E13 nvth on one gram of ^{235}U will produce about 1.5E13 fissions per second. The conversion to watts is 3E10 fissions/s per watt. Thus, a 20 gram ^{235}U target will generate 10kW of heat. With proper target design, this heat can also be transferred to the reactor coolant but may require forced cooling. A reactor with 20 targets must remove 200 kW of heat just from the targets.

1.5. Relationship of ^{99}Mo production to target fission power

The reactor fissions required to produce the neutrons which in turn cause fission in the targets also create ^{99}Mo as a fission product but unless the fuel elements are dismantled and the fission products extracted, this ^{99}Mo is lost or is unrecoverable. Since the ratio of reactor power to target power can be from 10 to 1 to 100 to 1, this represents a cost in uranium consumption and waste production which must be added to that of the targets.

Target power and ^{99}Mo production are directly linked. For a target power of 100 kW, ^{99}Mo is produced at the rate of 4.6E4 GBq d^{-1}. If targets are removed at the end of seven days, the percent recoverable is 47% or 2.16E4 GBq (see Fig. 1).

1.6. Relationship of ^{99}Mo production to target ^{235}U consumption

For a target power of 100 Kw, as in the above example, seven days of fissioning in the target would consume (at 1.2 gm ^{235}U per MW-day) 0.84 grams of ^{235}U. If the mass of ^{235}U in 10 targets (producing 100 kW) is 200 grams, the fractional burnup is 0.42%. Thus, over 99% of the uranium is not used and must be recycled or stored.

1.7. Production of ^{99}Mo using an aqueous homogeneous reactor

Although the experience with the fission target system of ^{99}Mo production has been proven successful, there are many possible improvements. Consider a reactor system which:

(1) Uses no targets, thus eliminating the production costs and transportation logistics.

(2) Is dedicated to the production of short lived fission isotopes and produces these isotopes on demand. Can operate at powers in t he kilowatt range; therefore, without forced cooling systems.

(3) By using daily extraction of ^{99}Mo, eliminates the unrecoverable losses from target decay within the reactor (see Figure 1).

(4) Reduces the amount of fission product waste produced by a factor of 100 and stores long lived wastes within the reactor solution.

(5) Requires only the ^{235}U replacement for material which has actually produced usable ^{99}Mo.

(6) Can operate with low enriched uranium (less than 20% ^{235}U) and does not require high enriched uranium for targets.

The "Medical Isotope Production Reactor" (MIPR) system has been designed to meet these goals.

1.7.1. *History of Solution Reactors*

In 1944, at Los Alamos, New Mexico, Richard Feynman suggested the design of an aqueous solution containing enriched uranium salts. The reactor was constructed as a 15 liter stainless sphere with 580 grams of ^{235}U (LOPO) [5]. The enrichment was 14.7% ^{235}U /total U. The LOPO reactor operated at a fraction of a watt but successor reactors (SUPO) went up to 45 kW.

The power coefficient of reactivity for this type reactor has a large negative value and thus is extremely safe and self-regulating. The first reactor built at a non-government site (North Carolina State at Raleigh, North Carolina USA) was selected to be an aqueous solution reactor because of the inherent safety. Later, other reactors were built in the midst of large population sites (for example: Washington, DC and Chicago, Illinois). World-wide, about 40 such reactors were constructed.

1.7.2. MIPR Characteristics

The design features of a solution reactor intended to produce ^{99}Mo have been developed by the USA companies of Babcock & Wilcox and Ball Systems. The relationship of reactor power to ^{99}Mo production have been previously discussed and the MIPR power can be up to 200 kWth. This power level should permit the system to be passively cooled by submerging the reactor container in a "swimming pool", similar to research reactors using plate type fuel elements.

A "Modular MIPR" design has been developed and is shown in Fig. 2. The reactor system is mounted within a structural frame. The main features are: 1) Dump tanks which hold the aqueous solution when the reactor is not operating; 2) Pumps and valves which permit the solution to be pumped up to the reactor tank; 3) Control and safety rods which are used to bring the reactor critical and maintain its power; 4) Catalytic converters to recombine the hydrogen and oxygen gas and other fission gas handling; 5) Extraction columns which strip the ^{99}Mo from the solution after the reactor is shutdown. The solution passes through the columns and is placed in the dump tank until the next operating cycle.

All of the equipment is assembled and tested with the instrumentation and control system in a fabrication shop prior to shipment to the site where the system is to be operated. Prior construction at the site would include a building housing a swimming pool with an area

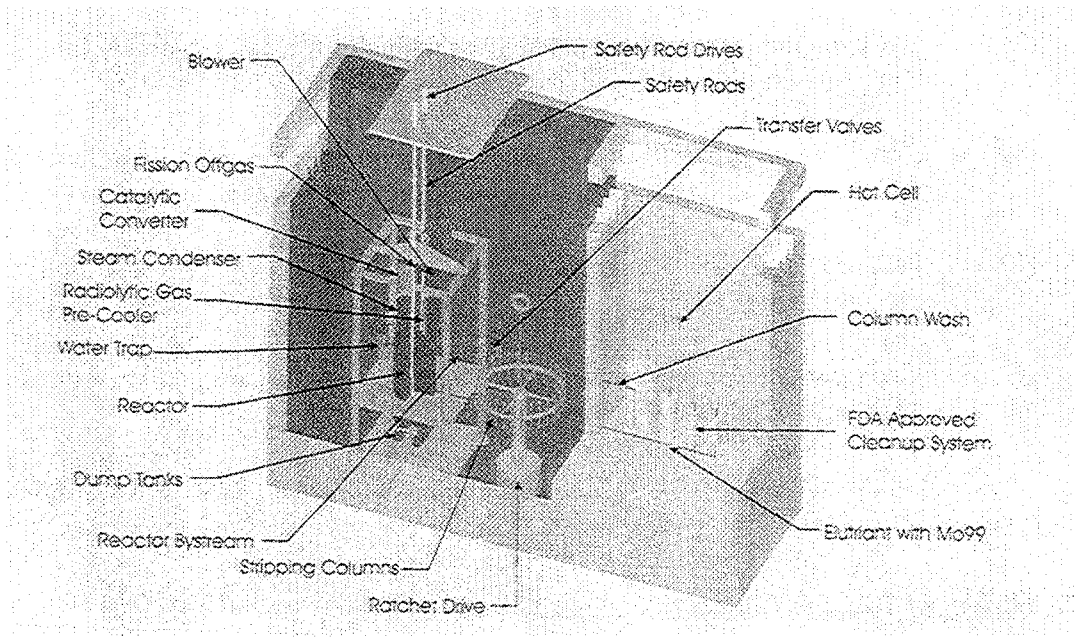

FIG. 2. Sketch of modular MIPR in swimming pool.

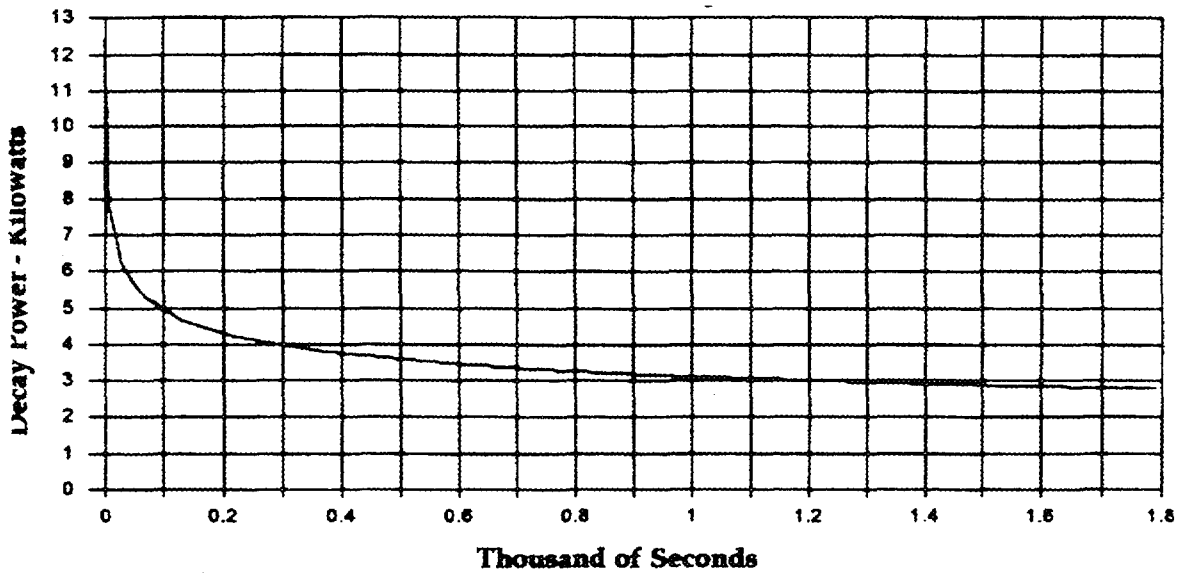

FIG. 3. Decay heat in solution immediately after shutdown-200 kW-1day.

of 3 meters by 3 meters and depth of at least 7 meters. Other utilities would also be installed at the site.

The final purifications, which require a hot cell facility sized to accommodate the activity of the ^{99}Mo (the major sources of radiation from fission products remain behind in the reactor solution) can be adapted from an existing hot cell or one constructed specifically for ^{99}Mo purification. The shipment of the Modular MIPR after testing can be handled by normal commercial means. The uranium solution is shipped and handled separately under licenses. The shielding and cooling system, which are the swimming pool water, are part of the prior site installation.

The recoverable production rate of ^{99}Mo at 200 kW at the end of one day is 81,600 GBq/day (2200 C · d^{-1}). After an operation for about one day, the reactor is shut down and allowed to decay for about 1000 s. Fig. 3 shows the decay of the reactor solution immediately after shutdown. This reduces the short lived fission product activity by a factor of 4. The solution is then run through an ion exchanger which permits the uranium and most fission products to pass through but holds up about 90% of the molybdenum [6]. The molybdenum is then eluted with a basic solution and the solution purified with further filtering and ion exchange.

Fig. 4 and Fig. 5 compare the process steps for Target Produced ^{99}Mo and MIPR Produced ^{99}Mo. A major difference is the elimination of targets and the retention of fission products, other than those to be sold commercially, within the reactor solution. This is similar to the fission products being retained in solid fuel as the reactor continues to operate.

Eventually, in the range of 10 years of operation, the reactor solution will require replacement and disposal of the long lived fission products remaining. Again, there is an advantage in not having a dissolution step required prior to treatment.

The gaseous fission products come out of solution with the radiolytic gasses and are trapped with filters and gas traps. Gases such as iodine are recovered for processing and commercial sale. The evolution of hydrogen and oxygen as radiolytic gas is extensive (about 1 $l.s^{-1}$ at 200 kW) and is recombined by a catalytic converter using platinized alumina. The resulting steam is condensed and the water returned to the reactor container.

1.7.3. Accumulation of Fission Products

As the MIPR operates at power, long lived fission products accumulate in the aqueous solution. Figure 6 shows the result of ORIGEN runs for a selected group of isotopes after the MIPR has operated at 200 kW for 1 y and 10 y. The concentrations are less than one gram per liter for even the largest contributor, zirconium.

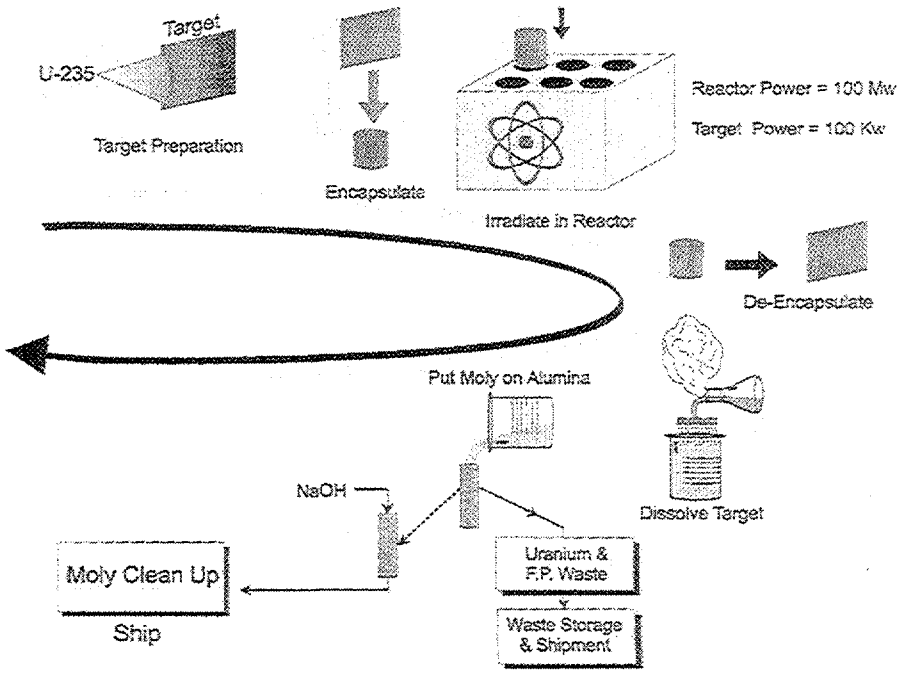

FIG. 4. Process cycle for reactor/target system.

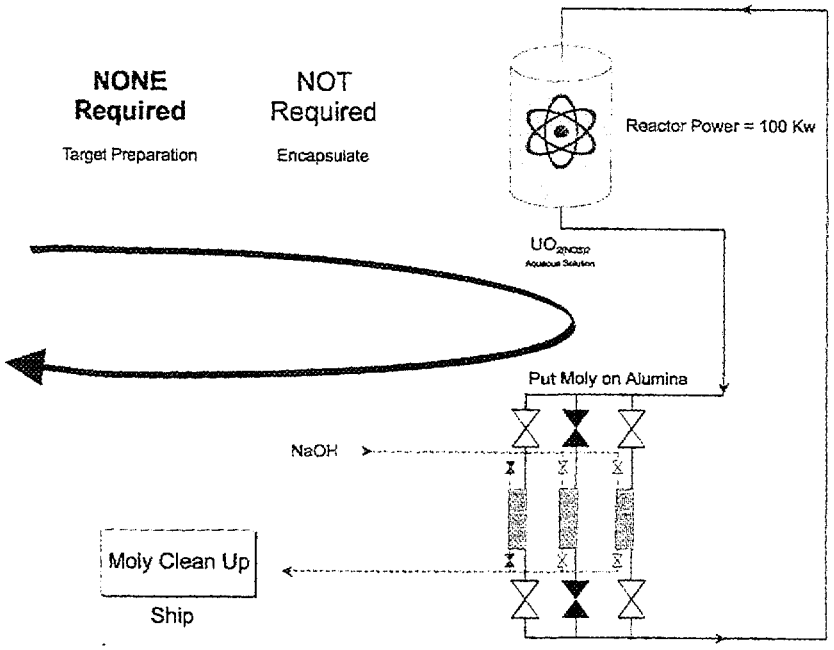

FIG. 5. Process cycle using solution (MIPR) system.

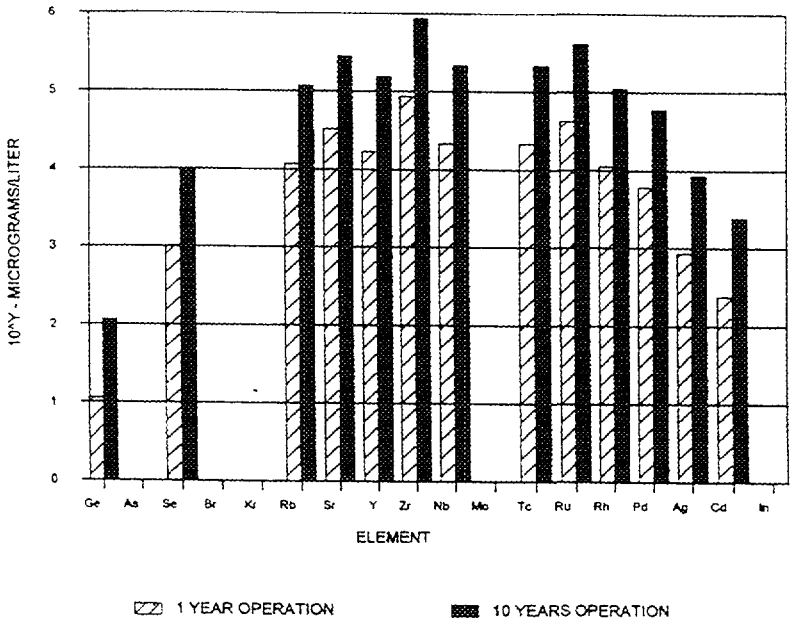

FIG. 6. Elements in solution after 1 and 10 years of MIPR operation.

1.7.4. Use of Low Enriched Uranium

As noted in the description of LOPO, the MIPR could operate with a uranium enrichment of 20%. The extraction of ^{99}Mo with a low enriched uranium solution has not been demonstrated but only a slight modification from high enriched extraction is expected. The benefit of a low enrichment solution would be the conformity with non-proliferation treaty requirements.

1.7.5. Downscaling the MIPR for Lower Production Requirements

Some developing countries may desire a lower production rate, perhaps 8000 GBq week^{-1}. With three days of production, the reactor could be operated at less than 10 kW. The amount of uranium and the hardware requirements for reactor operation are much the same but the consumption of consumables and the production of radioactive waste are greatly reduced.

1.7.6. Uranium Consumption in a MIPR

Since almost all of the uranium fissions are used to produce ^{99}Mo, the consumption of fissionable material is about 1/100th that of the target system where uranium must be supplied to the neutron producing "driver" reactor. At 200 kWth, the ^{235}U is burned at the rate of 0.12 grams per full power day. This burnup can be replaced by adding periodically a solution of concentrated uranium salt.

1.7.7. Economics of ^{99}Mo Production with a MIPR

The costs of operation depend on: 1) consumables, 2) payback of capital investment, 3) cost of waste handling and disposal. The advantages, compared with the target irradiation method are largely in the elimination of the targets with the production and shipping costs and the great reduction of waste. These are detailed in the article by Glenn [5]. Recent cost estimates for the construction of a new reactor which can be used to irradiate ^{235}U targets are about US $100 million. MIPR estimates for the reactor and its housing and operating systems (but not the hot cell facility for purification) are about 1/3rd of that [7].

The costs and schedule for reactor licensing and construction vary greatly and a are based on requirements specific to the country. In the USA, there have been discussions concerning the licensing of a MIPR with the U.S. Nuclear Regulatory Commission (USNRC) and a review of the requirements and license review plan for non-power reactors isssued by the USNRC in 1996.

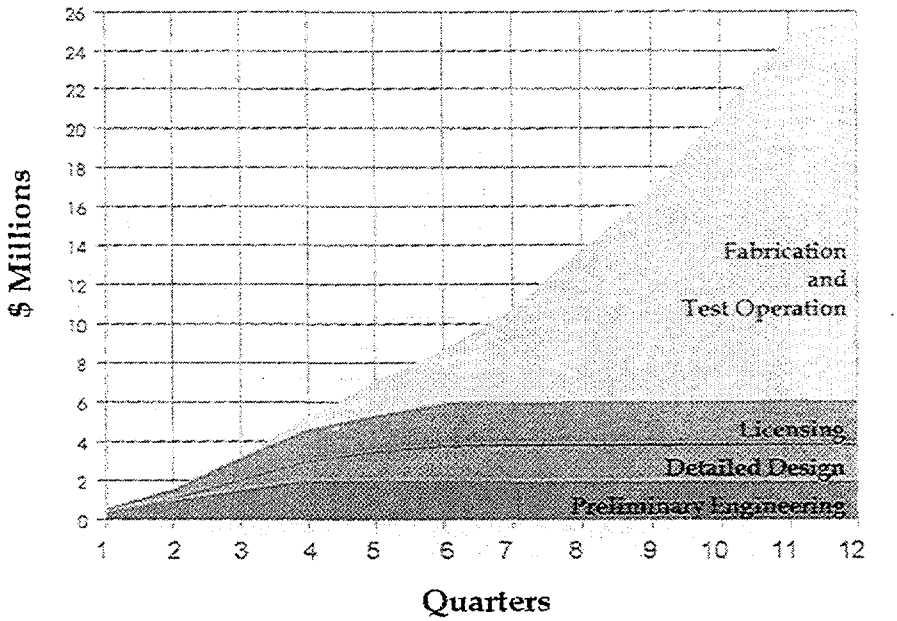

FIG. 7. MIPR cumulative project costs.

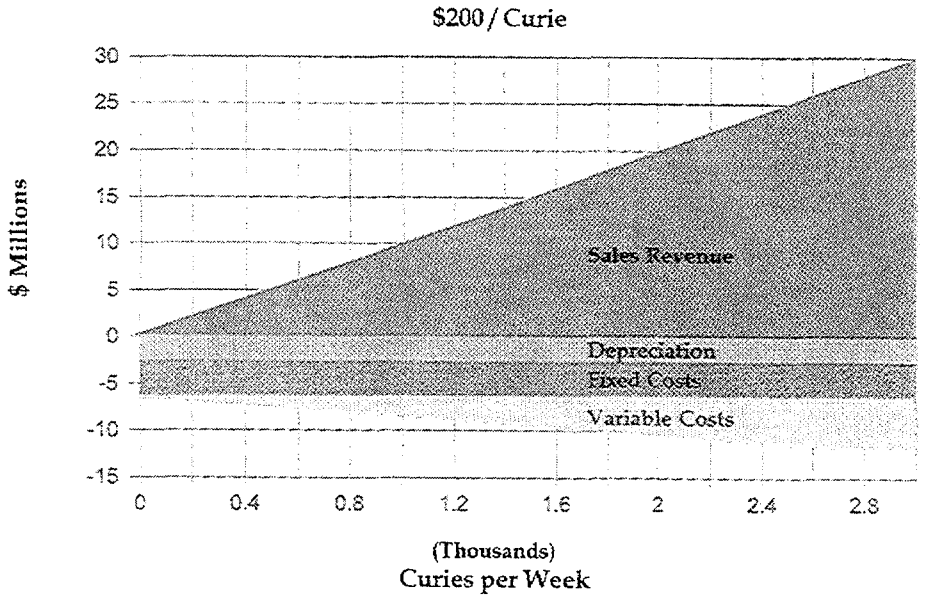

FIG. 8. Cost and sales of ^{99}Mo vs volume for MIPR.

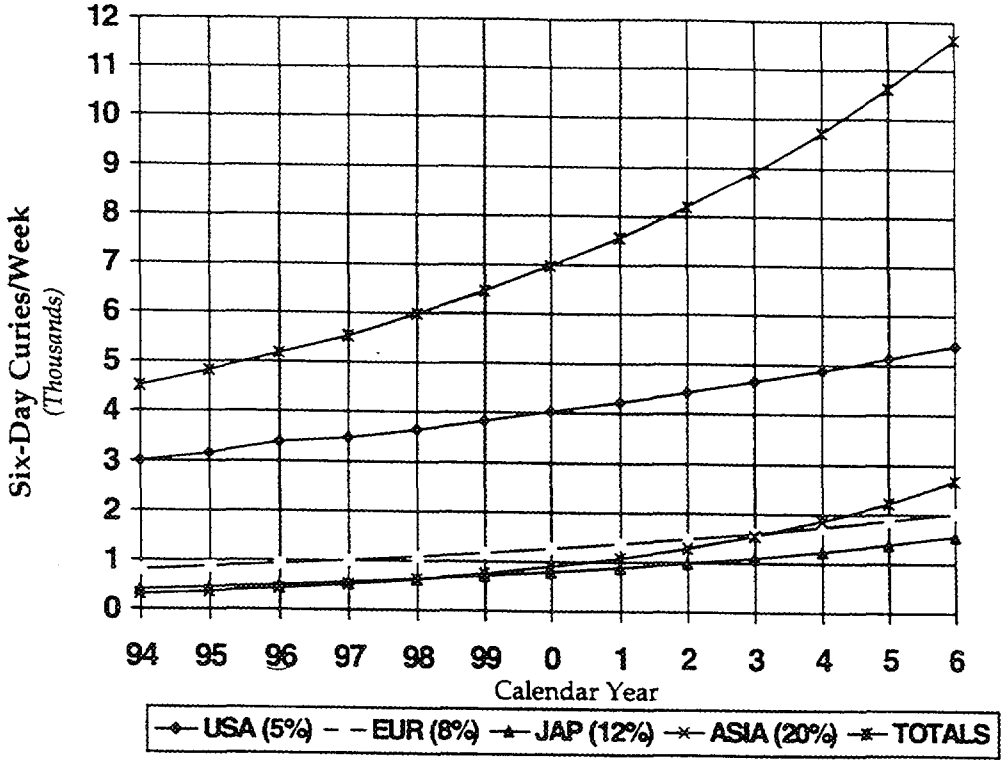

FIG. 9. World demand for Mo-99 vs. years.

Fig. 7 is an estimated expenditure schedule for a MIPR built in the USA and installed in a country with regulations similar to those of the USNRC. The time is approximately three years and a cost of $26 million for the reactor and structures not including hot cell, final purification equipment and any additional administrative space.

If a MIPR system were constructed with investment capital, the costs for the product must include repayment and interest. The other costs are variable costs associated the level of production. The offsetting income from the sale of ^{99}Mo was estimated from a unit sales price of $200 per six-day (calibrated) Curie. Fig. 8 shows graphically these costs and sales versus the volume of sales in Curies per week. The break even point for this example is 800 curies per week. The use of the ^{99m}Tc isotope continues to grow throughout the world and one projection of the quantity worldwide is shown in Fig. 9. The 10 year projection anticipates a need for almost 12000 Curies (six-day calibrated) per week.

1.8. Conclusion

Many reactors are available for target irradiation throughout the world. Often they are multipurpose machines and isotope production is one of many functions. In some cases, the reactors are used less for research and more for commercial work. Reduced research has caused an increase in the cost of the commercial work since the fixed and operating costs do not diminish with reduced usage.

A developing country with an existing reactor can consider using it to irradiate targets. A country planning for a new facility, dedicated to medical isotope production, can consider either an accelerator system or a specialized reactor, such as the MIPR.

REFERENCES

[1] PARRINGTON, J.R., "Nuclides and Isotopes, Fifteenth Edition", 1996, GE Nuclear Energy (Lockheed-Martin).

[2] "Preparation of Tc-99m generators using low power research reactors", Report of a consultants' meeting. Rez, Czechoslovak Socialist Republic, July 6-8, 1981.

[3] "Research Radionuclide Availability in North America", Newsline, J. Nucl. Med., 38, (1997) 7.

[4] "Reactor Physics Constants", ANL 5800 - Second Edition, (1963), 648.

[5] ETHERINGTON, H.L., Nuclear Engineering Handbook, McGraw-Hill, (1958).

[6] GLENN, D., HEGER, S., HLADIK, W., "Comparison of Characteristics of Solution and Conventional Reactors for Mo-99 Production", Nuclear Technology, Vol 118, May 1997.

[7] BALL, R., "The Mo-99 Solution", Nuclear Engineering International, December 1995.

TARGETS FOR THE PRODUCTION OF NEUTRON ACTIVATED MOLYBDENUM-99

E.L.R. HETHERINGTON, R.E. BOYD
Australian Nuclear Science and Technology Organisation,
Lucas Heights, NSW, Australia

Abstract

Neutron activation of natural molybdenum is, ostensibly, the least complex route to ^{99m}Tc. However in most commercial generators the severe limitation in ^{99}Mo specific activity that the route imposes has caused manufacturers to choose the alternative fission process despite its disadvantages of being more expensive and requiring a more complex waste management strategy. The development of a newer generator technology is capable of reviving the demand for neutron activated ^{99}Mo and might encourage the production of ^{99m}Tc by countries possessing less developed nuclear infrastructures. The targets used in the (n,γ) production route consist of analytical grade molybdenum trioxide which has been further refined to remove both rhenium and tungsten trace impurities. The basic methods used by ANSTO to produce a molybdenum target capable of yielding ^{99m}Tc of high radionuclidic purity are described.

1. INTRODUCTION

The almost universal means by which ^{99m}Tc is made available for clinical use is from the elution of generators containing high specific activity fission-^{99}Mo. The manufacture of these generators is controlled by a handful of countries with advanced nuclear infrastructures and the special capabilities of extracting pure ^{99}Mo from irradiated ^{235}U. Despite its almost total commercial dominance, this technology is expensive and is a potential hazard to the environment unless managed appropriately. Direct neutron activation of molybdenum is the least complex route of access to ^{99}Mo. Given the existence of severe limitations on the specific activity attainable, the method is still particularly suited to use in developing countries operating a research reactor but with otherwise limited resources. Solvent extraction technology [1] is the most common method for separating ^{99m}Tc from low specific activity ^{99}Mo. Produced by this technique, the ^{99m}Tc is supplied ready for 'instant' use from a central production laboratory typically at the same site as the reactor. More recently, alternative technologies have been developed in which neutron activated ^{99}Mo is incorporated in solid gel forms of zirconium or titanium molybdate [1,2,3,4] and using these technologies ^{99m}Tc is produced within a nuclear medicine clinic with an ease which is directly comparable to that of the fission ^{99}Mo generator.

The most appropriate target material for low specific activity ^{99}Mo production is molybdenum trioxide (MoO_3); neutron activation occurs via the reaction ^{98}Mo(n,γ)^{99}Mo.

The most common practice is to use targets of natural abundance. The penalty associated with the irradiation of necessarily large target masses is still economically preferred to the use of enriched ^{98}Mo targets, which in any case are only capable of increasing the maximum achievable specific activity by a factor of 4. Analytical Reagent (AR) grade MoO_3 is the best choice for a target material.

2. TARGET CHARACTERISTICS

Natural molybdenum consists of seven stable isotopes; neutron activation gives rise to only three molybdenum radioisotopes - as shown in Table I.

TABLE I. RADIOACTIVE PRODUCTS FROM THE REACTOR IRRADIATION OF MOLYBDENUM

Mo Isotope	% Abundance in Natural Mo	Activation Product	Half-Life
^{92}Mo	14.84	^{93}Mo	6.9 h
^{98}Mo	24.13	^{99}Mo-^{99m}Tc	66.02 h-6.02 h
^{100}Mo	9.63	^{101}Mo	14.6 m

Because of the low yields and short half lives, ^{93}Mo and ^{101}Mo do not contribute significant impurities to extracted ^{99m}Tc. On the other hand AR grade molybdenum trioxide does contain impurities [1] which ought to be removed prior to irradiation in order to minimise the formation of radionuclidic impurities in the separated ^{99m}Tc.

For example ^{186}Re ($t_{1/2}$=90.8 h) and ^{188}Re ($t_{1/2}$=16.8 h) are formed by the ^{185}Re(n,γ)^{186}Re and ^{187}Re (n,γ)^{188}Re nuclear reactions due to the presence of a rhenium impurity in the target material. Both these radionuclidic impurities are substantially removed during the first ^{99m}Tc extraction and as a consequence the first ^{99m}Tc must always be discarded.

A process that has been used at ANSTO to reduce the rhenium level in molybdenum trioxide is given in the ANNEX hereto, however additional processing is justified to eliminate traces of tungsten.

The irradiation of tungsten* produces ^{188}W which decays to its daughter product ^{188}Re. In practice this pair ^{186}W (n,γ) ^{187}W (n,γ) ^{188}W→^{188}Re forms a generator system within the irradiated molybdenum which, because of the chemical similarity between the elements, causes ^{188}Re to be repeatedly extracted along with ^{99m}Tc.

Following the purification process** shown in ANNEX, the tungsten level is approximately 60 ppm. A further processing step [5] can reduce the tungsten level to less than 10 ppm.

** Because it is the product of consecutive neutron activations, the rate of ^{188}W formation varies with the square of the neutron flux; consequently ^{188}Re formation is substantially enhanced in high flux irradiations whenever a significant level of tungsten impurity exists in the molybdenum trioxide target.*

*** The removal of tungsten from MoO_3 relies on the preferential adsorption of tungsten by hydrated stannic oxide [6]. A small scale application of the process consists of stirring for 24 hours one litre of 0.7M $(NH_4)_2MoO_4$ pH 8-9, with 8g of $SnO_2.nH_2O$. The MoO_3 is then precipitated by the addition of concentrated HNO_3 and then calcined at 400 °C for 6 hours.*

TABLE II. PRODUCTION OF ^{99}Mo BY NEUTRON IRRADIATION OF MOLYBDENUM TRIOXIDE IN THE ANSTO RESEARCH REACTOR HIFAR

Reactor Type	10 MW Thermal Research Reactor
Fuel	Enriched Uranium
Moderator	Heavy Water
Irradiation Position	Hollow Fuel Element
Thermal Neutron Flux	$0.5 - 1.0 \times 10^{14}$ n cm^{-2} s^{-1}
Thermal Neutron Activation Cross Section	0.14 barn
Epithermal Flux Index	~0.12
Effective (Westcott [8]) Cross Section	1.2 barn
Effective Cross Section Corrected for Epithermal Flux Depression	0.48 barn (0.12 barn for natural target calculations)
MoO_3 Target Mass per Can	240 g
Can Type	Welded Titanium
^{99}Mo Specific Activity at Flux 1.0×10^{14} $n.cm^{-2}$ s^{-1}	1.5 Ci $.g^{-1}$ Molybdenum (6 day irradiation)

3. NUCLEAR CONSIDERATIONS

The thermal neutron activation cross section for $^{98}Mo(n,\gamma)^{99}Mo$ is 0.14 barns with a resonance integral of 7 barns [7]. Thermal neutron fluxes greater than 1×10^{13} $n.cm^{-2}s^{-1}$ are necessary to produce specific activities of practical importance. The yields of ^{99}Mo can be significantly enhanced by epithermal neutron activation, hence the selection of the irradiation position is critical particularly in lower flux reactors. For all reactors the evaluation of the irradiation positions is essential to achieve optimum yields. Epithermal neutron enhancement of ^{99}Mo is illustrated by the results outlined in Table II.

REFERENCES

[1] INTERNATIONAL ATOMIC ENERGY AGENCY, "Alternate Technologies for ^{99m}Tc Generators", IAEA-TECDOC-852 Vienna 1995.

[2] EVANS, J.V,. MOORE, P.W., SHYING, M.E., SODEAU, J.M., Zirconiummolybdate gel nas a generator for technetium 99m-I. The concept and its evaluation, Appl. Radiat. Isot. **38** (1987) 19.

[3] EVANS, J.V,. MOORE, P.W., SHYING, M.E., SODEAU, J.M., Zirconium molybdate gel as a generator for technetium 99m-II. High activity generators, Appl. Radiat. Isot. **38** (1987) 25.

[4] NARASHIMAN, D.V.S., VANAJA, P., IYER, S.P., MANI, R.S., Development of a new ^{99m}Tc generator using neutron irradiated titanium molybdate as column matrix, Radiochim. Acta. **42** (1987) 49.
[5] DADACHOVA, E., Purification of molybdenum before use in technetium-99m production, Private Communication ANSTO (1997).
[6] SEMENOV, M.I., BLOKHIN, A.A.,.TAUSKANOV, V.P., Use of hydrated oxides of multivalent metals for effective removal of tungsten from molybdenum compounds, Zh. Prikl. Khim. USSR **57** (1984) 1501.
[7] WALKER, W.F., PARRINGTON, J.R., FEINER, F., Chart of the Nuclides, 14th Ed. Knolls Atomic Power Laboratory (1988).
[8] WESTCOTT, C.H., Effective cross section values for well moderated reactor spectra, AECL407 (1957) and AECL1101 (1960).

ANNEX

PURIFICATION OF MOLYBDENUM TRIOXIDE FOR IRRADIATION

A bulk batch of 100 kg is divided into 10 kg sublots

1. The 10 kg sublot of molybdenum trioxide and 40 L distilled water are added to a 50 L container.

2. Approximately 6 L concentrated ammonia solution are added over 30 minutes with vigorous stirring.

3. The resulting solution is filtered using a coarse filter paper.

4. The solution is passed through a 2 cm diameter x 3 m long column of activated charcoal. The flow rate is ~ 1.2 L. h^{-1}.

5. Sufficient concentrated nitric acid (not more than 2-3 L) is added slowly to the solution until no further precipitation occurs.

6. The resulting precipitate of hydrated molybdenum trioxide is filtered out and washed with warm distilled water.

7. The precipitate is dried at 200°C for 24 h, cooled and crushed to a fine powder.

8. The powder is heated in an oven to 380°C for 24 h. Air is blown through the oven during this stage.

9. To confirm thermal stability, 78 g of oxide is heated to 600°C in a gauged pressure vessel. The pressure generated by heating should be not greater than for the system alone.

10. After cooling the powder is stored in plastic containers prior to irradiation.

11. A sample of the purified MoO_3 is irradiated and examined for radionuclidic impurities.

12. Expiry time for the purified target is 5 y.

CONVERTING TARGETS AND PROCESSES FOR FISSION-PRODUCT MOLYBDENUM-99 FROM HIGH- TO LOW-ENRICHED URANIUM

G.F. VANDEGRIFT, J.L. SNELGROVE, S. AASE, M.M. BRETSCHER,
B.A. BUCHHOLZ, D.J. CHAIKO, D.B. CHAMBERLAIN, L. CHEN,
C. CONNER, D. DONG, G.L. HOFMAN, J.C. HUTTER, G.C. KNIGHTON,
J.D. KWOK, R.A. LEONARD, J.E. MATOS, J. SEDLET, B. SRINIVASAN,
D.E. WALKER, T. WIENCEK, E.L. WOOD, D.G. WYGMANS, A. TRAVELLI
Argonne National Laboratory,
Argonne, Illinois,
United States of America

S. LANDSBERGER, D. WU
University of Illinois,
Urbana/Champaign, Illinois,
United States of America

A. SURIPTO, A. MUTALIB, H. NASUTION, H.G. ADANG, L. HOTMAN,
S. AMINI, S. DEDI, R. MARTALENA, A. GOGO, B. PURWADI, D.L. AMIN,
A. ZAHIRUDDIN, SUKMANA, KADARISMAN, SRIYONO, D. HAFID, M. SAYAD
Badan Tenaga Atom National (PUSPIPTEK),
Jakarta, Indonesia

Abstract

Most of the world's supply of ^{99}Mo is produced by the fissioning of ^{235}U in high-enriched uranium targets (HEU, generally 93% ^{235}U). To reduce nuclear-proliferation concerns, the U.S. Reduced Enrichment for Research and Test Reactor Program is working to convert the current HEU targets to low-enriched uranium (LEU, <20% ^{235}U). Switching to LEU targets also requires modifying the separation processes. Current HEU processes can be classified into two main groups based on whether the irradiated target is dissolved in acid or base. Our program has been working on both fronts, with development of targets for acid-side processes being the furthest along. However, using an LEU metal foil target may allow the facile replacement of HEU for both acid and basic dissolution processes. Demonstration of the irradiation and ^{99}Mo separation processes for the LEU metal-foil targets is being done in cooperation with researchers at the Indonesian PUSPIPTEK facility. We are also developing LEU UO_2/Al dispersion plates as substitutes for HEU UAl_x/Al dispersion plates for base-side processes. Results show that conversion to LEU is technically feasible; working with producers is essential to lowering any economic penalty associated with conversion.

1. INTRODUCTION

The Reduced Enrichment for Research and Test Reactor (RERTR) Program was established in 1978 at the Argonne National Laboratory (ANL) by the Department of Energy (DOE), which continues to fund the program and to manage it in coordination with the Department of State (DOS), the Arms Control and Disarmament Agency (ACDA), and the Nuclear Regulatory Commission (NRC). The primary objective of the program is to develop the technology needed to use low-enriched uranium (LEU) instead of high-enriched uranium (HEU) in research and test reactors, and to do so without significant penalties in experimental

performance, economics, or safety aspects of the reactors. Research and test reactors utilize nearly all the HEU that is used in civil nuclear programs, and eliminating their dependence on this material will significantly reduce nuclear proliferation concerns. The RERTR program continues to receive strong support from many international organizations that contribute to this effort.

Most of the HEU used in research reactors is contained in their fuel elements; therefore, a large fraction of the RERTR program activities has been concentrated on developing suitable LEU alternatives for research reactor fuels. However, a non-negligible, wide-spread, and expanding utilization of HEU in research reactors is due to its use in targets for the production of ^{99}Mo through fission. Technetium-99m, the daughter of ^{99}Mo, is the most commonly used medical radioisotope in the world. It is relied upon for over nine million medical procedures each year in the U.S. alone, comprising 70% of all nuclear-medicine procedures. Most ^{99}Mo is produced in research and test reactors by the irradiation of targets containing HEU. Because the worldwide effort to fuel research and test reactors with LEU instead of with HEU has been so successful, HEU is now used only for ^{99}Mo production in some countries. In addition, while there are only a few major producers of ^{99}Mo, many nations with developing nuclear programs are seeking to become producers of ^{99}Mo, both for domestic and foreign consumption. Therefore, an important component of the U.S. RERTR program's goal of reducing world commerce in HEU is the development of means to produce ^{99}Mo using LEU. Initial development work was carried out from 1986 to 1989, when the effort was halted by lack of funding. The DOE authorized resumption of this work in 1993. The two principal aspects of the work are (1) target development and (2) chemical process testing and modification.

As we did for fuel development and testing, the RERTR Program is developing international partnerships for the ^{99}Mo development work. These partnerships are especially important because, at the present time the U.S. does not have facilities suitable for irradiating targets. An agreement was signed with the Indonesian National Atomic Energy Agency (BATAN) in November 1994, and our joint work is well underway. A second agreement was signed with the Korea Atomic Energy Research Institute in December 1996.

Currently, targets for the production of ^{99}Mo are generally either (1) miniature Al-clad fuel plates [1-9] or pins [10,11] containing U-Al alloy or UAl_X dispersion fuel similar to that used, at least in the past, to fuel the reactor or (2) a thin film of UO_2 coated on the inside of a stainless steel tube [12,13]. The ^{99}Mo is extracted first by dissolving either the entire Al-clad fuel plate or pin or by dissolving the UO_2 and then performing a series of extraction and purification steps. Both acid and basic dissolutions are used, and each producer has its own process. The highly competitive nature of the business and the stringent regulations governing the production of drugs make each producer reluctant to change its process. Therefore, the RERTR program's strategy is to minimally modify the most widely used and potentially most useful existing processes.

To yield equivalent amounts of ^{99}Mo, the LEU targets must contain five to six times as much uranium as the HEU targets they replace. Substituting LEU for HEU in targets will require, in most cases, changes in both target design and chemical processing. Three major challenges have been identified: (1) to modify targets and processing as little as possible, (2) to assure continued high yield and purity of the ^{99}Mo product, and (3) to limit economic disadvantage. Keeping the target geometry the same, thereby minimizing the effects of LEU substitution

TABLE I. COMPARISON OF TYPICAL HEU AND LEU TARGETS FOR THE PRODUCTION OF FISSION-PRODUCT ^{99}Mo

	HEU	LEU[1]
^{235}U Enrichment, %	93	19.75
^{235}U, g	15	18.5
Total U, g	16.1	93.7
^{99}Mo yield[2], Ci	532	545
Total Mo, mg	9.8	10.0
^{239}Pu[3], μCi	30	720
(mg)	(0.44)	(12.)
$^{234, 235, 238}$U, μCi	1280[4]	840[5]
Total a, μCi	1310	1560

[1]Assumes the LEU target irradiation was done in an LEU-fueled reactor.
[2]At the time target leaves the reactor core.
[3]Assuming all ^{239}Np has decayed to ^{239}Pu.
[4]Based on a ^{234}U isotopic content of 1.0 wt%.
[5]Based on a ^{234}U isotopic content of 0.12 wt%

on target irradiation, necessitates modifying the form of uranium used. Changing the amount and form of the uranium in the target necessitates modifying at least one or, possibly, two target processing steps--dissolution and initial molybdenum recovery.

One of the issues raised in connection with using LEU to produce ^{99}Mo is the greater amount of ^{239}Pu generated. The ^{239}Pu is generated through neutron capture by the ^{238}U. About 30 times more ^{239}Pu is generated in an LEU target vs. an HEU target for an equivalent amount of ^{99}Mo. However, because significantly more ^{234}U is present in HEU than in LEU as a consequence of the enrichment process, total alpha contamination of an irradiated LEU target is less than 20% higher than that of an equivalent HEU target. Table I shows calculated ^{99}Mo and ^{239}Pu yields and alpha contamination from uranium isotopes in comparable HEU and LEU irradiated targets. Our progress in target and process development is summarized in this paper.

2. CURRENT STATUS OF FISSION-PRODUCT ^{99}Mo PRODUCTION

Except for fission-product ^{99}Mo produced by the Australian Nuclear Science and Technology Organization (ANSTO), which uses uranium enriched to power-reactor fuel levels, all major producers use HEU targets. Table II compares targets and processes used worldwide. The RERTR response to each HEU target and process is also summarized in the Table III.

TABLE II. COMPARISON OF CURRENT PROCESSES FOR ^{99}Mo PRODUCTION (ACID VS. BASE DISSOLUTION)

	Process	
	Acid Dissolution	Base Dissolution
Current Target	Target (1)--UO_2 (HEU) on inside of stainless-steel (SS) cylinder (Cintichem) by Indonesian National Atomic Energy Agency (BATAN), and Sandia National Laboratories (SNL), USA Target (2)--Extruded Al-clad U/Al-alloy pins (HEU), AECL/Nordion, Canada Target (3)--UO_2 pellets (2% ^{235}U), ANSTO, Australia	Aluminum-clad UAl_x/Al-dispersion-fuel plates (HEU)--Institut National des Radioéléments (IRE), Belgium; Comisión Nacional de Energía Atómica (CNEA), Argentina; Atomic Energy Corporation of South Africa Limited (AEC), South Africa; Mallinckrodt, Netherlands
Dissolving Reagent	Nitric acid solution (Cintichem process combines with sulfuric acid)	Sodium hydroxide solution, often with sodium nitrate to avoid H_2 formation
Initial Molybdenum Recovery Step	Target (1)--Precipitation of Mo by a-benzoin oxime followed by dissolution in basic solution for further purification Targets (2) and (3) sorption of Mo by alumina column	Acidification to recover radioiodine and sorption of Mo by (1) alumina or (2) anionic exchange
Advantages	Target (1) • Target cylinder acts also as dissolver vessel--only irradiated UO_2 is dissolved, producing a low volume of waste solution. • Initial Mo recovery is fast with excellent yield and decontamination while concentrating product. Target (2) • Targets are prepared in similar manner to fuel pins. • Targets are miniature fuel pins; therefore, behavior in the reactor is well known. Target (3) • The low enrichment is not a proliferation problem. • Preparation of UO_2 pellet is a well-known technology.	General • Dissolving in base will release the noble fission gases, while retaining radioiodine in the dissolver solution. Fission gases can be recovered separately from iodine. A second step, lowering the pH of the solution, will release iodine isotopes into the gas phase, allowing their separate recovery. • Dissolution of target by base acts as a Mo decontamination step. Basic solution causes precipitation of uranium, other actinides, and many fission products as insoluble hydroxides, which can be filtered from the solution containing the soluble MoO_4^{2-} species. • Targets are essentially miniature fuel plates; therefore, they are easily fabricated, and their behavior in the reactor is well known.

TABLE II. (Cont.)

	Process	
	Acid Dissolution	Base Dissolution
Disadvantages	Targets (1), (2), and (3) • Noble fission gases and iodine gas are released together during uranium dissolution. Target (2) • Large quantity of aluminum must also be dissolved, leading to a large volume of waste solution. • Because reactor fuel will be LEU in the future, targets will need to be made in a dedicated line--separate from that for fuel. Target (3) • Large amount of uranium must be dissolved for ^{99}Mo yield--due to low ^{235}U enrichment.	General (continued) • Entire target is dissolved. A large quantity of aluminum must be dissolved with the uranium, resulting in a large waste volume.
Major Technical Challenges to LEU Substitution	General • To make as little modification to target geometry and processing as possible while increasing the uranium content ~5 times • To produce ^{99}Mo with same or higher specific activity and purity • To obtain same or higher yields of ^{99}Mo and, in some cases, other fission products • To maintain or decrease waste-volume generation • To maintain or increase safety of disposed radioactive waste • To maintain or decrease treatment required for safe waste disposal • To limit economic penalty • To limit concerns from the greater amount of ^{239}Pu in LEU by showing its effective decontamination from ^{99}Mo product • To obtain Reactor Operator acceptance of LEU target design • To obtain Process Safety Officer acceptance of modified process and equipment • To obtain U.S. Federal Drug Administration (FDA) or equivalent national authority approval of the ^{99}Mo product from LEU	General • To make as little modification to target geometry and processing as possible while increasing the uranium content ~5 times • To produce ^{99}Mo with same or higher purity and specific activity • To obtain same or higher yields of ^{99}Mo and, in some cases, other fission products • To maintain or decrease waste-volume generation • To maintain or increase safety of disposed radioactive waste • To maintain or decrease treatment required for safe waste disposal • To limit economic penalty • To limit concerns from greater amount of ^{239}Pu in LEU by showing its effective decontamination from ^{99}Mo product • To obtain Reactor Operator acceptance of LEU target design • To obtain Process Safety Officer acceptance of modified process and equipment • To obtain U.S. Federal Drug Administration (FDA) or equivalent national authority approval of the ^{99}Mo product from LEU

TABLE II. (Cont.)

	Process	
	Acid Dissolution	Base Dissolution
Major Technical Challenges to LEU Substitution (Continued)	Specific for Target (1) • Electrodeposition of UO_2 limited by electrochemistry and equipment. • Too thick layers of UO_2 may cause sintering and, therefore, difficult or incomplete dissolution of UO_2. • If a fully-loaded HEU (~20-g ^{235}U) Cintichem target is used, it is unlikely that an equivalent LEU target can be made using electrodeposited UO_2. Specific for Target (2) • Current design cannot accommodate ~5 times more U as U/Al alloy. • Initial testing with U_3Si_2 targets at Chalk River has shown poor dissolution after irradiation. • It is likely that higher amount of uranium would decrease effectiveness of alumina-column separation. • Chalk River is already developing a new HEU target (likely UO_2) and processing due to current waste-volume problems. Target (3) is already LEU.	Specific • The density of UAl_x is not high enough to allow keeping target geometry the same while accommodating ~5 times the amount of uranium per target. • Alternative, high-density forms of uranium are needed to keep target geometry the same. • Use of alternative forms of uranium may also call for changes in the dispersion medium and the cladding material (both currently aluminum). • The thickness of the cladding may also need to be decreased. • If radical changes to the HEU target are necessary to achieve similar ^{99}Mo yields, opposition could be strong. • Changes to the fuel, the dispersion medium, and the cladding will all affect processing.
Means to Convert to an LEU Target	Target (1) • Use of LEU metal is a strong alternative due to its high density and thermal conductivity, easy dissolution by nitric acid under conditions similar to that for UO_2, and ease of making into a foil. • Initial development was on electro-deposition of U metal on Ni-coated stainless-steel cylinders to give a target/dissolver duplicating the current UO_2-coated one. Concerns that electrodeposition from molten salt was too "high tech" for some potential users shifted R&D to a mechanically formed target. • The LEU target is based on holding a uranium-metal foil between two concentric cylinders with different thermal expansion coefficients. The foil will be provided good thermal contact with the outer, water-cooled cylinder by the higher expansion of the inner cylinder.	U_3Si_2 • Because U_3Si_2's density is higher than that of UAl_x, LEU targets of the same geometry can be fabricated to produce same ^{99}Mo yield as HEU. • Because U_3Si_2 is harder than UAl_x, cladding must be converted from pure Al to a stronger alloy (Al-6061). Alloying elements complicate target dissolution by precipitating as hydroxides. • The U_3Si_2 cannot be dissolved by NaOH solutions or NaOH solutions containing $NaNO_3$. Therefore, the cladding and aluminum powder in the fuel meat are dissolved in one step, and a second step is required using a more powerful reagent to dissolve the U_3Si_2. • Because 15-25% of the ^{99}Mo is lost to the aluminum matrix due to fission recoil, it must be recovered from both solutions.

TABLE II. (Cont.)

	Process	
	Acid Dissolution	Base Dissolution
Means to Convert to an LEU Target (Continued)	Target (1) (Continued) • The outer cylinder is zirconium. Inner cylinders being tested are Al, Mg, 304 SS, and zirconium. Water cooling of outer and no cooling of inner cylinder is still likely to provide some differential thermal expansion, in a target with both cylinders fabricated from zirconium. • Because the U foil bonded to the walls of the target during irradiation, 10-15 μm fission-product-absorption barriers have been added to the U foil. Potential barriers are Ni, Cu, Zn, and Fe. All dissolve quickly in acid; Ni, Zn, and Fe have no activation-products which could generate problems with ^{99}Mo purity. Copper has one major activation product that requires a decontamination factor (DF) of 3300; tracer experiments confirm that this DF can be met. • Adjusted U has been used in targets to minimize the grain size in the foil. An Fe concentration of 450 ppm and Al of 1000 ppm should keep U in the beta form with a 10-20-μm grain size. • Targets with adjusted U, a 304 SS inner cylinder, and Zn or Cu fission-barriers on both sides of the U foil have been irradiated and disassembled successfully. • Early targets have used 10-15 μm Cu, Zn, or Ni foils wrapped around the U foil as fission barriers. In the future, Ni, Zn, or Cu will be electroplated onto the U foil. • A Zn/U compound formed during irradiation dissolves significantly slower in nitric acid than either of the two metals. Conditions for dissolution must be modified to account for this lower dissolution rate.	U_3Si_2 (Continued) • Alkaline hydrogen peroxide will dissolve U_3Si_2 at acceptable rates. However, mechanical means must be employed to break up the agglomerated U_3Si_2 particles following irradiation for rapid dissolution. • An aggressive dissolution solution using concentrated fluoride will dissolve irradiated U_3Si_2 targets in a single step [8]; fluoride complicates waste treatment and disposal. • Future work should either (1) build on the dissolution process using concentrated fluoride described by Sameh [8], (2) look at other aggressive dissolution reagents, or (3) look at other forms of U. U-Metal Foils • Alkaline peroxide will dissolve U foil at acceptable rates. Means have been developed to minimize peroxide autodestruction. • The need for metal barriers in the foil target has complicated basic dissolution. Only Zn can be dissolved in base. Dissolution of Zn in basic sodium nitrate gives high rates. Sodium hydroxide with peroxide dissolves Zn more slowly, but at rates comparable to U dissolution. • Although the Zn/U compound formed during irradiation does not dissolve significantly in basic nitrate solutions, it does dissolve at a higher rate than U or Zn in alkaline peroxide and should not cause dissolution problems.

TABLE II. (Cont.)

	Process	
	Acid Dissolution	Base Dissolution
Means to Convert to an LEU Target (Continued)	Target (2) • The AECL is moving independently on LEU conversion. Until the RERTR program shows successful conversion to LEU, AECL activity will be extremely limited. • Cooperation with the RERTR Program is on an informal, periodic discussion basis. Target (3) • Not applicable	UO_2 • Dispersion-fuel plates with UO_2 loadings up to 40 wt% can provide ~3X the U loading of the UAl_x target--that is about one-half of the ^{235}U needed for an equivalent LEU target. • The UO_2 can be dissolved in basic peroxide at acceptable rates. As an added advantage over U_3Si_2 and U metal, it does not catalyze the autodestruction of H_2O_2. Therefore, its dissolution requires substantially less H_2O_2 and is easier to control. Advanced Fuels • To allow all research and test reactors to convert to LEU fuel, RERTR is developing fuels that will provide higher U loadings [14]. Alloys of U with Mo or with a combination of Zr and Nb are being tested with densities 32-47% higher than that of U_3Si_2. • Due to their lowering the specific activity of the ^{99}Mo, Mo alloys are not appropriate for ^{99}Mo production. • If LEU-Nb-Zr alloys are found to be successful as fuels, they should be tested for use in ^{99}Mo production.
Status of LEU Process Development	Target (1) • Test irradiations of targets continue to optimize their design for consistent removal of the U foil from the target for processing. • The need for fission barriers in targets is established. Zinc, Cu, and Ni are being tested; so far Zn- and Cu-foil-barrier targets have been successful. • Zinc barriers have been electroplated on U foil successfully. Copper electroplating is underway, and that of Ni is yet to be begun. No work has been done using adjusted U. • Dissolution of uranium foil has been developed for unirradiated U foil. Tests in Indonesia confirm that irradiated LEU foil dissolves as fast or faster than unirradiated U foil.	U_3Si_2 • Dissolution by a two-step process is developed to the point where a full-scale demo is needed. Rates and mechanisms of dissolving (1) aluminum in cladding and the fuel matrix and (2) silicide particles are understood. • It is clear that the reason irradiated silicide is slow to dissolve is the bonding of silicide particles during irradiation. A physical means to break up the fused silicide particles before or during dissolution is needed for successful processing. We have not yet designed means to do this. • Use of alloyed-aluminum cladding necessitates a solids-separations step following cladding dissolution. Hydroxide precipitates of alloying elements are suspended in the spent cladding-dissolver solution. Separation of this low-density precipitate from the high-density U_3Si_2 can be accomplished.

TABLE II. (Cont.)

	Process	
	Acid Dissolution	Base Dissolution
Status of LEU Process Development (Continued)	Target (1) (Continued) • We have no dissolution experience for adjusted U. • Tracer-level experiments have shown that Ni, Cu, or Fe fission barriers should not affect dissolution or processing. If a Zn barrier is chosen, conditions must be developed to dissolve Zn/U layer and to show Zn will not affect processing. • Use of a dissolver solution of HNO_3 alone (rather than a mix of HNO_3 and H_2SO_4) has been developed to cut waste treatment and disposal costs. • Tracer-level demonstrations in the U.S. showed that LEU substitution will not adversely affect recovery or purity of ^{99}Mo product. • Indonesian tracer-level demos using (1) ~1000X more activity and (2) the actual solution volumes, reagents, and equipment for a full-size target verified earlier U.S. results and showed the effectiveness of the improved counting and data-analysis methods that were developed. • Design, fabrication, and testing of an experimental dissolver for the full-scale demonstration has been completed. A multi-use production dissolver is yet to be designed. • Agreement was reached with SNL that irradiating and processing of LEU-oxide Cintichem targets will be in the test ^{99}Mo-product-acceptance matrix. Targets are being fabricated at Los Alamos National Laboratory. Target (2) • Status not known.	U_3Si_2 (Continued) • Conditions were found to keep silica in solution during acidification of the dissolver solution prior to I and Mo recovery but must be verified under actual process conditions. • Conditions are known for destroying peroxide and allowing uranium to precipitate following target dissolution. (Precipitation of uranium is necessary prior to acidification and use of an alumina column to recover Mo.) The procedure must still be optimized. • Conditions for alumina recovery of Mo have been determined but must be verified under process conditions. • Full-scale demo yet to be done. U-Metal Foil • Dissolution of U foil with a Zn barrier *may* require a two-step process. • Rate and mechanism of U-foil dissolution by alkaline peroxide are understood and modeled. Affect of adjusted uranium not yet measured. • Zinc that has not reacted with U dissolves quickly in basic nitrate solutions. Dissolution rate using alkaline peroxide may also be adequate. • Dissolver design is only conceptual. • Zinc is the only material currently acceptable as a barrier for base-side processes. The Zn/U compound formed by heat treating is quickly dissolved by alkaline peroxide. • Conditions are known for destroying peroxide and allowing uranium to precipitate following target dissolution. Procedure still to be optimized. • Following dissolution and peroxide destruction, steps for the recovery and purification of molybdenum that were developed for HEU should be appropriate for LEU metal. Must still be verified. UO_2 • Dissolution of UO_2 by alkaline peroxide has been optimized and modeled.

TABLE II. (Cont.)

	Process	
	Acid Dissolution	Base Dissolution
Status of LEU Process Development (Continued)	Target (3) • Not applicable.	UO_2 (Continued) • Conditions for dissolving UO_2/Al dispersions in a two-step process have been developed and tested using heat-treated and low-burnup compacts. • Dispersion-fuel miniplates of UO_2/Al loaded to 40 vol% U have been prepared. Advanced Fuels • No work has yet been done.
Planned Development Activities	Target (1) • At least one full-scale demonstration will be done in Indonesia during 1997. • Following successful demonstration, we will tackle specific tasks necessary for conversion: (1) design and fabrication of the multi-use dissolver, (2) waste treatment and disposal, and (3) economic comparison of production from HEU and LEU. Target (2) • Continued informal communication with AECL staff. Target (3) • No plans.	U_3Si_2 • A decision has been made to suspend R&D activities on this fuel. U-Metal Foils • Destruction of peroxide following dissolution will be optimized for the % recovery and filterability of the U/OH precipitate. • Dissolver system to be developed. • Effects of LEU on ^{99}Mo recovery and purification will be studied using low-burnup targets. • A technical partnership will be established for full-scale demonstration. UO_2 • Samples of miniplates will be irradiated to low burnup and used in tracer studies to test dissolution and ^{99}Mo recovery and purification. • Tasks will parallel those of U foil. Advanced Fuels • As alloys are found acceptable for fuels, they will be tested as ^{99}Mo-production targets.

3. TECHNICAL CHALLENGES TO LEU CONVERSION

Although technical challenges are far from the only impediments to conversion from HEU to LEU, they are the most clearly addressed. They also most clearly define economic factors. The RERTR program's research and development activities need to address all aspects of production but to focus limited resources on technical areas that will give the best return on investment. Molybdenum production can be broken up into the following areas:

- Target fabrication
- Irradiation
- Postirradiation disassembly
- Target dissolution
- Separation and purification of ^{99}Mo
- Waste treatment and disposal

In the case of target development, this requires (1) not modifying target geometry, (2) using materials and fuels that are acceptable to reactor operators, and (3) developing targets that require simple, "low-tech" fabrication methods. In the case of processing it means focusing on target dissolution and the first molybdenum recovery/purification step. The primary differences between LEU and HEU targets shown in Table I (greater amounts of uranium and ^{239}Np/Pu in the LEU target) should only affect dissolution and primary molybdenum recovery. If dissolution of the LEU target is properly designed, the molybdenum fraction should be chemically identical following these two steps.

Waste treatment and disposal have often been neglected in the past but, due to increasing regulations and costs associated with radioactive waste disposal, are becoming an extremely important concern to producers. Modifications to processing required by conversion to LEU could actually be to economic advantage if waste treatment is given proper consideration.

4. LEU TARGET DEVELOPMENT

Target R&D activities are almost completely centered on the uranium-foil target. This target is being developed for both acid- and base-side processing. Fabrication of dispersion-fuel plates for U_3Si_2 and UO_2 has no show-stopping technical issues that need to be addressed. Both are acceptable reactor fuels and are fabricated commercially. Achieving as high as possible uranium loadings is an issue for molybdenum production targets and for reactor fuels. The following sections discuss progress in developing the uranium-foil target and electrodeposition of fission barriers for this target.

4.1. Uranium-foil target

Until 1989, Cintichem, in Tuxedo, NY, produced about one-half of the world's ^{99}Mo supply using targets consisting of high-enriched UO_2 coated on the inside of stainless steel tubes. The same targets are used, under license, in Indonesia today. The standard "Cintichem" target contains up to 25 g of UO_2, or up to 20 g of ^{235}U. Because of concerns that the UO_2 coating thickness could not be increased nearly enough to produce an LEU target with an equivalent ^{235}U content, we had begun to develop electrodeposited metallic uranium targets [15]. However, since we were seeking a target that could be fabricated using "low-tech" methods, we have developed a concept using uranium-metal foils [16, 17].

We have concentrated on the target design illustrated in Fig. 1, where a thin (~130-μm thick) uranium metal foil is sandwiched between slightly tapered inner and outer tubes. The taper is currently 5/1000. In our preferred design, the inner tube is made of a material with a larger thermal expansion coefficient than that of the outer tube material. This differential thermal expansion should assist in maintaining good thermal contact between the foil and the tubes. We have chosen zirconium for the outer tube and, as discussed below, have tested aluminum, magnesium, and stainless steel for the inner-tube material in the differential-thermal-expansion design. Zirconium is also being tested in a design without differential thermal expansion based on differing materials. Aluminum, magnesium, or zirconium is preferred owing to their low neutron absorption cross sections.

Assembly of the target is accomplished by rolling the uranium foil around a mandrel, placing the foil over the inner tube, and inserting the inner tube and foil into the outer tube. A press is used to seat the foil firmly between the tapered inner and outer tubes. Then, the end fittings are welded on, and the assembly is filled with helium gas and sealed. The taper and

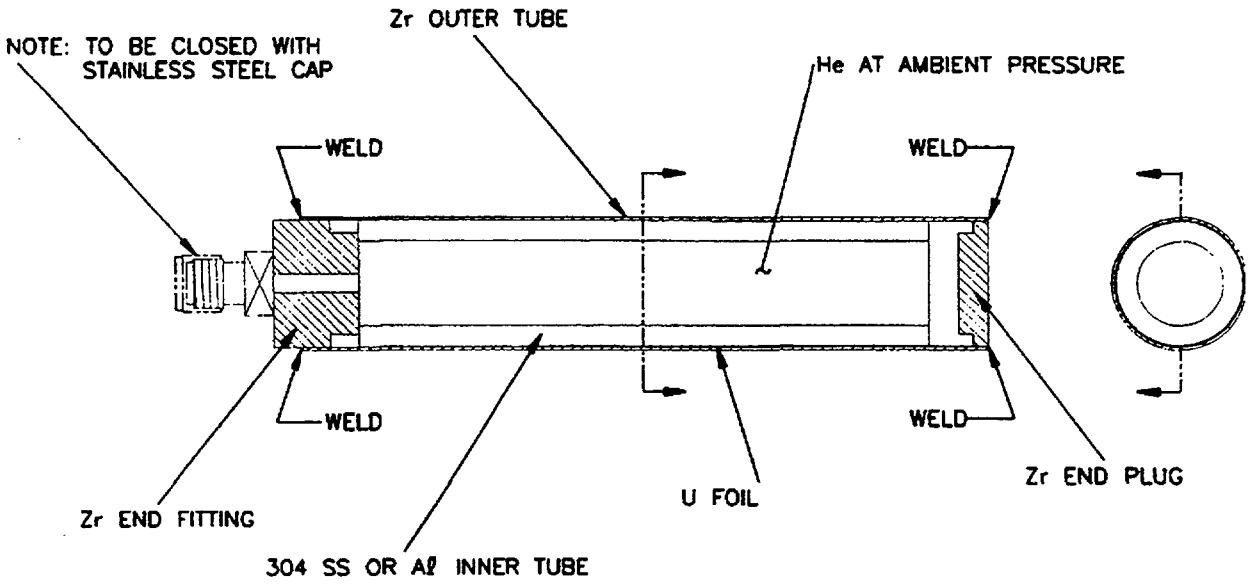

FIG. 1. Uranium metal-foil target.

the greater shrinkage of the inner tube upon cooling after irradiation facilitate disassembly, which is accomplished by cutting off the two ends with a mechanized tubing cutter and using a press to push the inner tube, and the uranium foil, out of the outer tube.

A basic design criterion is to be able to separate the irradiated foil from the tubes, so that only the foil need be dissolved to recover the molybdenum, thereby minimizing waste volume. In our first test, targets with thin oxide layers were produced on the inner and outer tubes to serve as diffusion barriers to inhibit diffusion bonding of the uranium to the tubes. As will be discussed later, we have added fission-fragment-absorbing barriers between the uranium foil and the target tubes. Several targets of this type have been irradiated in the Indonesian RSG-GAS reactor operating at 22.5 MW. Postirradiation examinations have been performed in the adjacent BATAN hot cell facility, under a cooperative research agreement between BATAN and Argonne National Laboratory.

One such target, with a zirconium outer tube and an aluminum inner tube, was irradiated and examined during the summer of 1995. In spite of a thin aluminum-oxide barrier between the uranium foil and the inner tube, which had proven to be sufficient to prevent reaction during thermal testing at elevated temperature, the uranium reacted with the aluminum during irradiation and could not be removed from the inner tube. Metallography showed no apparent interaction of the uranium with the zirconium outer tube, on which a thin zirconium oxide barrier had been placed. Therefore, zirconium appeared to be a suitable target-tube material.

Three additional test targets were irradiated between November 1995 and March 1996 to explore different materials for the inner tube of the target. In one, we coated the aluminum with zirconium by flame spraying, thereby retaining all the features of the first design while adding a zirconium layer between the uranium and aluminum to prevent interaction. In a second target the inner tube was made from magnesium, which also has a larger expansion coefficient than zirconium but forms no compounds with uranium. The third target had a zirconium inner tube. Obviously, the thermal expansion difference was not present in this combination; however, we believe that adequate thermal contact was assured by the assembly process with the tapered tubes. This test was added to verify the apparent nonbonding of uranium foil and zirconium.

Postirradiation examinations performed during April and May of 1996 showed that the uranium foil was bonded to the inner tube of each of these targets. The tentative explanation is that the high fission rate in the uranium and correspondingly high recoil atom flux at the uranium-target tube interface lead to an efficient atomic intermixing at the interface. It appears that bonding by this mechanism will occur with any material. A potential solution to this bonding is inclusion of a thin (10-15 μm) metal barrier between the foil and the target walls. A literature review was undertaken to choose metals that would have the mechanical and chemical attributes suitable for barriers. Important chemical properties were (1) ease of dissolution, (2) noninterference with the recovery of molybdenum from the dissolution, and (3) noninterference with the purification of the ^{99}Mo product. Other important factors were (1) the ability to be electroplated onto uranium or made into foils, (2) low thermal-neutron cross sections for radioisotope formation, and (3) low cost. Based on these criteria and mechanical properties, the best choices for a barrier metal are nickel, iron, and copper for the process of uranium foil target dissolution with acidic solution and zinc for dissolution in base.

Based on the experience gained during the first two series of tests, a third set of irradiations was performed during August 1996. To achieve a smaller grain size and, hence, a more-uniform dimensional change in the uranium during irradiation, we added small amounts of iron and aluminum to produce an "adjusted" uranium alloy containing ~450 ppm iron and ~1000 ppm aluminum. The uranium was reduced to foils by a combination of hot and cold rolling. Following rolling, a ß quench (690°C for 5 min followed by air cooling) was completed to eliminate texture in the foils. We irradiated four targets to test two basic concepts:

1. The inner tube material of one target was changed to austenitic stainless steel. This material was chosen because it will not dissolve in the acid used to dissolve the uranium and because its use will retain the thermal expansion difference since 300 series stainless steel has 2 to 2.5 times the expansion coefficient of zirconium. We expected the uranium foil to bond to the stainless steel inner tube and to be pulled loose from the zirconium outer tube during cooling and disassembly (as was the case for the targets with aluminum and magnesium inner tubes), so that the uranium could be dissolved off the inner tube by placing the entire inner tube into the dissolver. However, the inner tube and foil could not be extracted from the outer tube, indicating some amount of bonding of the uranium foil to the zirconium outer tube.

2. Thin recoil-absorbing barrier foils of ~10-μm thickness were placed between the uranium and one or both target tubes. We expected these barrier foils to bond to the uranium by recoil mixing but not to the target tubes, since the fission fragments will not penetrate the barrier. Since the barrier foils must be dissolved with the uranium foil, only certain materials such as nickel, copper, iron, and zinc are acceptable. We tested both nickel and copper. In one target an aluminum tube with unoxidized surfaces was used, and nickel foils were placed on both sides of the uranium foil. The inner tube with foils was easily extracted, but the foils could not be removed, indicating bonding, presumably by diffusion, of the nickel to the aluminum. We think that introduction of an aluminum oxide layer will prevent such bonding. The other two targets used a stainless steel inner tube. In one a nickel barrier foil was introduced only between the uranium and the zirconium outer tube. The inner tube with foils was easily extracted, and, as expected, the uranium bonded to the inner tube. The uranium and nickel could be dissolved as described above. The final target contained copper barrier foils placed on both sides of the uranium foil. The inner tube with foils was easily extracted, and the foil sandwich was easily removed from the inner tube.

The latter two targets demonstrated the viability of the fission-fragment-barrier concept. Another series of tests was performed in Indonesia during April and May 1997 to test additional barrier-material/target-tube-material combinations. In all of these tests, an oxide diffusion barrier was placed on the target tube surfaces. One of the targets contained copper barrier foils and a stainless steel inner tube, a combination that was successful during the previous test. The remaining targets contained other combinations of copper, nickel, and zinc barrier foils and stainless steel, aluminum, and zirconium inner tubes. None of the targets containing copper or nickel barriers and stainless steel or aluminum inner tubes was successful during this irradiation; the foils were stuck to the stainless steel tubes and the targets with aluminum inner tubes could not be disassembled. The outer surfaces of the copper and nickel barrier foils were speckled, whereas the foil surface in the previously successful target was shiny. However, the target containing zinc barrier foils and a stainless steel inner tube did work; the uranium/barrier foil combination was easily removed from the inner tube. Its surface was shiny, as expected. We now theorize that the uranium foils were rougher than in the previous experiment and that the protruding uranium grains penetrated into the copper and nickel barrier foils to such a depth that the barrier thickness was reduced below the ~7-μm fission fragment range in a number of spots. The zinc barrier foil, which was 5 μm thicker than the copper and nickel foils, apparently was thick enough to absorb the recoils. We must await results of metallographic examinations to be performed in Indonesia to confirm this explanation.

As before, the viability of the fission-fragment-barrier concept has been confirmed, but a number of design details must be addressed to produce a reliable target. We will be examining ways to minimize roughness of the uranium foils. We have also begun to optimize the target. We will be studying (1) the use of aluminum or other low-neutron-absorbing materials for the inner tube in order to decrease the reactivity penalty of the target, (2) the minimization of the thicknesses of the target tubes in order to minimize waste and neutron absorption, and (3) the plating of barrier materials on the uranium foils rather than use of foils in order to minimize fabrication costs.

4.2. Electrodeposition of fission barriers

Electroplating fission barriers on the uranium foil should make target preparation simpler and more economical. Commercial sources for the baths and supplies are literature was available for electrodepositing nickel on uranium metal. A survey of the literature on electroplating uranium located a modest number of papers on the electroplating of nickel on uranium for the purpose of preventing or reducing the surface corrosion of uranium [18-23]. Plating of other elements was not found, but the principles involved in plating nickel should be applicable to the other metals in which we are interested. These are, in addition to nickel, zinc, copper, and, possibly, iron. All the publications agree that the uranium surface must be rough (i.e., have small finger-like projections) for the nickel to adhere. The interface is not a metal bond because uranium oxidizes so readily, but the nickel is attached mechanically. This agrees with earlier experience of one of the authors, who electroplated coatings on uranium in the late 1940s.

We have used plating methods reported in the literature, modifying them as needed as we gain experience. The literature indicates that we must provide a roughened, clean surface. The general method for preparing the uranium surface for nickel plating is to (1) degrease the surface, (2) remove the uranium oxide coating, then (3) etch the surface in a metal chloride salt solution (sometimes containing hydrochloric acid) or a hydrochloric acid/sulfuric acid solution. Because the uranium foils we are attempting to electroplate are only 130-μm thick,

surface preparation has been extremely challenging. We must balance surface roughness against dissolution of the foil. We have used an alkaline zincate bath for plating zinc, an alkaline copper phosphate bath for plating copper, and a nickel sulfamate plating bath for plating nickel. The specific procedure we use consists of:

- Degreasing with xylene
- Removing the xylene by rinsing in methanol
- Rinsing with water to remove any methanol
- Dissolving the oxide layer with 8M HNO_3 (pickling)
- Rinsing with water
- Etching in concentrated ferric chloride solution at 40°C [other chlorides that have been used are those of Sn(II), Ni(II), and Li(I)]
- Rinsing with water
- Immersing in 8M HNO_3 until a metallic surface is obtained
- Rinsing with water
- Electroplating

To minimize oxidation of the uranium surface, the foil is placed in the plating bath with the power supply already on. The success of the procedure was followed by measuring the foil thickness with calipers (0.0001 in.), by weighing the foil before and after treatment, and by performing a microscopic examination. Samples were taken after etching, after electroplating, and, sometimes, after the pickling. In both the pickling and etching steps, uranium is dissolved. Attempts were made to minimize these losses while preparing a surface that produces a continuous, well-bonded barrier metal after electroplating. Zinc plates (12-μm thick) have been prepared with a current density of ~0.12 A/cm^2 at ~1 volt for 15 minutes.

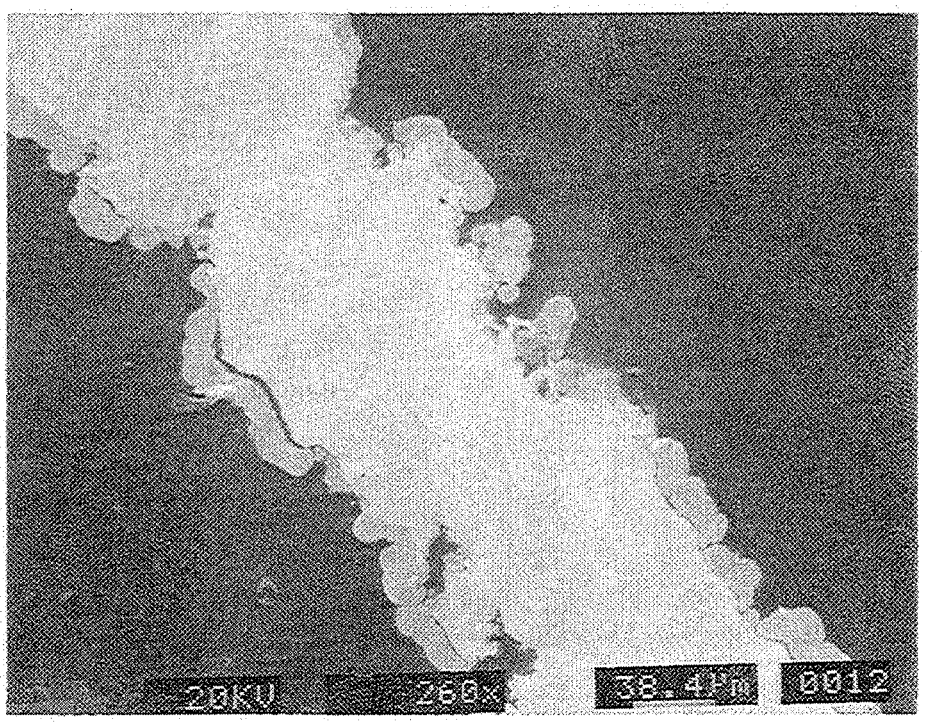

FIG. 2. SEM photograph showing wide variation in Zn plate.

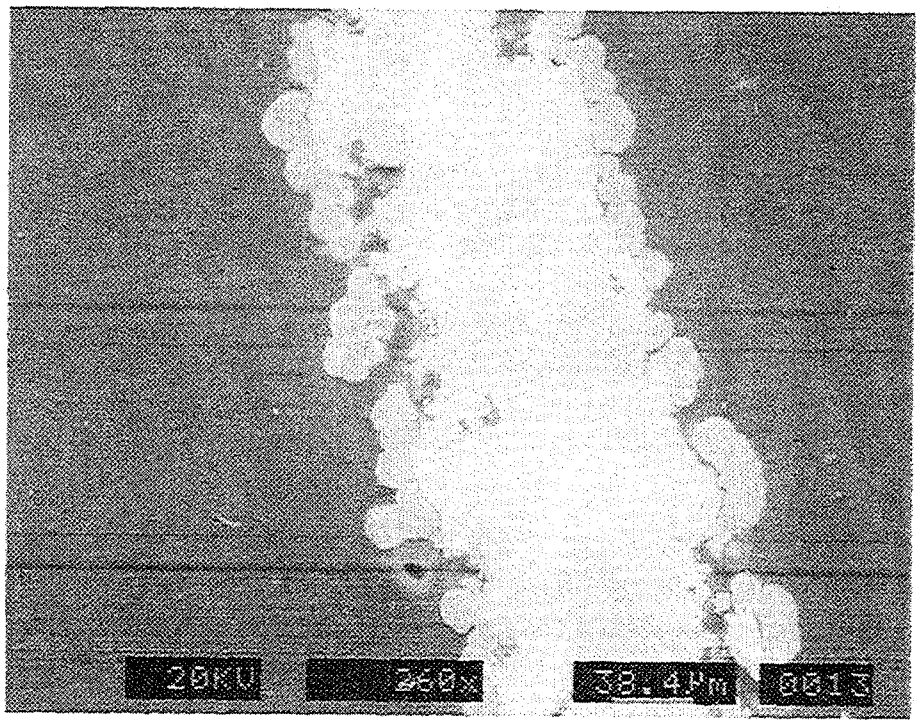

FIG. 3. SEM photograph showing nodular nature of Zn plate.

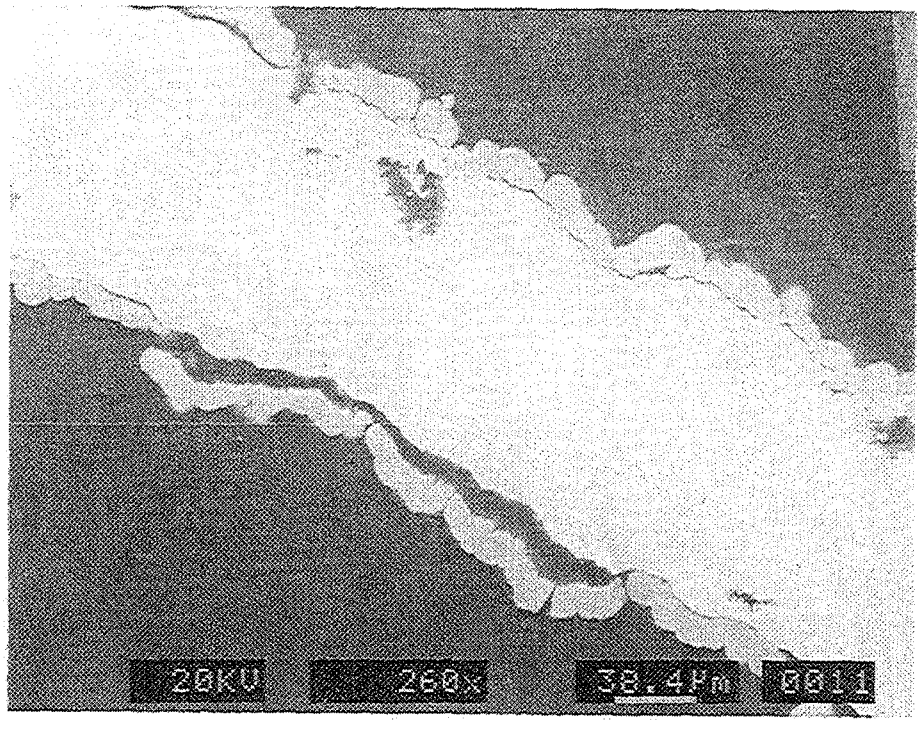

FIG. 4. SEM photograph showing separation of Zn plate from U foil.

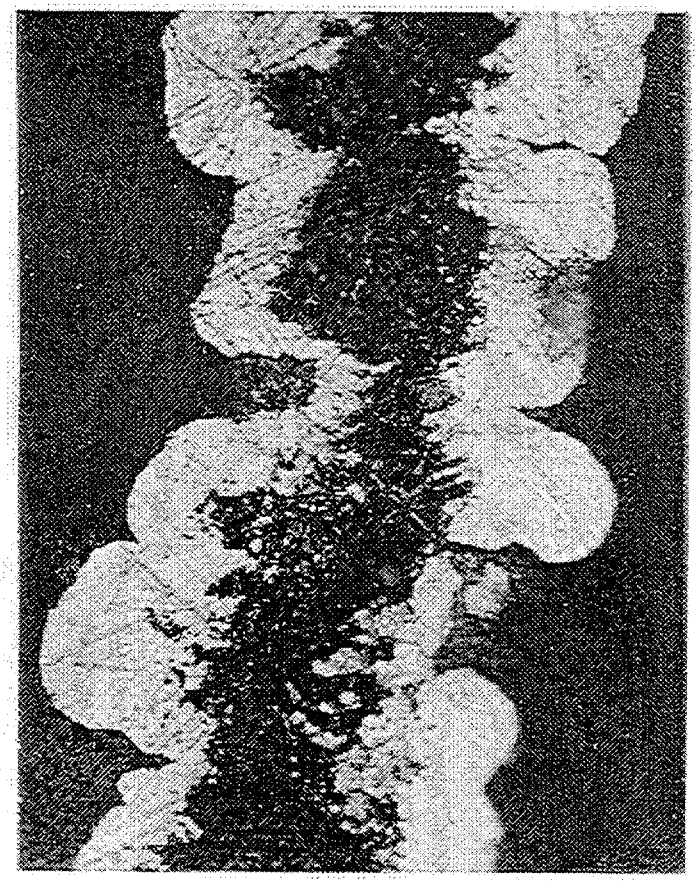

FIG. 5. Early Zn-plated uranium foil showing considerable loss of uranium during etching.

FIG. 6. Optical-microscope photograph of as-delivered uranium foil.

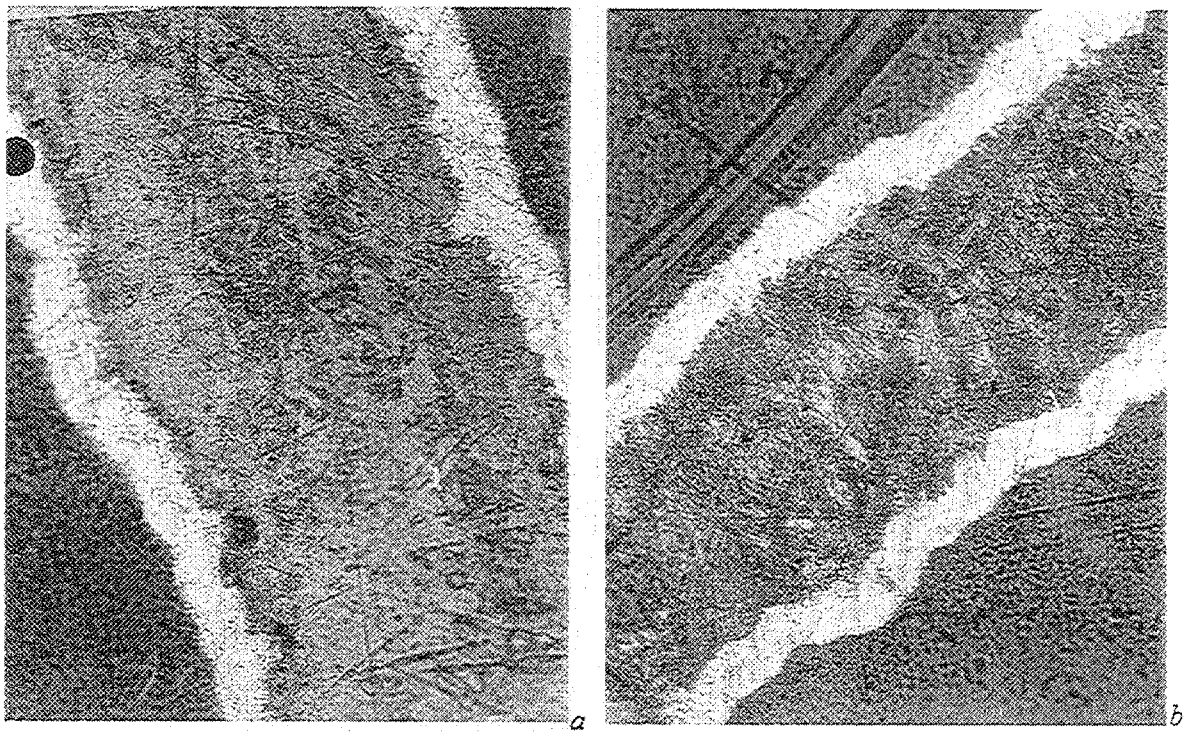

FIG.7. Two examples of acceptable zinc-plated uranium foils.

Scanning electron micrographs of an early attempt at plating uranium with zinc barriers are shown in Figs. 2 through 4. These figures, which show cross sections of the plated foil, reveal a number of interesting features about the zinc plate and the etching and plating process. In these figures, the lightest band across the picture is the uranium foil. The zinc plate is seen as a darker color on either side of the uranium. The black portion is the background--the epoxy matrix holding the foil. Figure 2 shows that the surface of the uranium is considerably deteriorated, containing great variations in thickness as well as some pockets that have been generated by etching. This situation was suspected because of the considerable mass loss from the foil in etching without a proportional loss in thickness. Figure 3 shows a section of foil in which the nodular character of the Zn plate is rather pronounced. Plating began at a number of active sites, which are surrounded by sites that are inactive. As seen, this condition produces a very uneven plate, with the thickness of the Zn plate varying from 0 to 18 μm, with the average being ~8 μm.

Figure 4 shows a section where the separation of the Zn plate from the U foil is especially pronounced. This separation had been visually seen as flaking of the plate when the foil was bent. This flaking occurred on the side of the foil where the Zn plate was in compression, and that is also the case in the photograph. Flaking on the side of the foil on the outside of the bend, where the Zn was in tension, was not visually observed and was much less pronounced than on the compression side, although there are some indications of it on the tension side in the figure. Adhesion of the plate is a factor, but some separation of the plate from the foil will be acceptable provided the plate does not develop gaps or fall off the foil during bending. Figure 5 is an optical micrograph of another early plate. The plating was slightly more uniform (average of 12 μm), but surface etching dissolved far too much of the uranium. Figure 6 shows an optical micrograph of a cross section of the as-received uranium foil, 130 μm thick.

Surface preparation is a compromise between optimal conditions for making a uniform and well-bonded plate and etching away a high fraction of the LEU surface. The best conditions found to date remove about 25 μm of the 130-μm uranium foil. We will deal with the loss in uranium by preparing 150-μm foils. Figures 7a and 7b show zinc-plated uranium foils that meet the criteria of 225 μm uranium loss and uniform, well-bonded zinc electrodeposits. We have yet to produce copper-plated uranium foils that look this good. We are planning to electroplate Zn, Cu, and, time permitting, Ni barriers on LEU foils, which will be irradiated in the Indonesian reactor in September 1997.

5. LEU PROCESS DEVELOPMENT

Throughout the period of our involvement to convert ^{99}Mo production from HEU to LEU, R&D activities have been divided between base- and acid-side processing. Meeting our objective of converting all production of fission-product ^{99}Mo from HEU to LEU necessitates such an approach. This section will be first broken up into base and acid dissolution processes. The next division for each subsection will be made by the two important processing steps for conversion--(1) irradiated target dissolution and (2) the initial molybdenum recovery/purification step. In the case of base-side processing, one further division will be made to discuss the three potential LEU targets--(1) U_3Si_2/Al dispersion fuel, (2) uranium foil, and (3) UO_2/Al dispersion fuel.

5.1. Acid-side processing

Most of the world's supply of ^{99}Mo is produced in the NRU reactor at the AECL's Chalk River Laboratories in Chalk River, Ontario, Canada. It is recovered from irradiated aluminum-clad extruded pins of U/Al alloy by first performing a partial mechanical-decladding and then dissolving the target in nitric acid. The ^{99}Mo is separated from the uranium and other fission products by using an alumina column. Although AECL's conversion from HEU to LEU is vital to meeting the goals of the RERTR program, we have not yet developed a formal program with the AECL or Nordion to assist them in conversion. Our hope is that as we demonstrate the technical and economic feasibility of conversion, such a cooperation will develop. Our efforts directed to acid-side processing have, therefore, been entirely focused on the Cintichem process, which is currently being used by the Sandia National Laboratories and the Indonesian Radioisotope Production Centre located at the PUSPIPTEK Laboratory in Serpong, Indonesia. When the RERTR program first became involved with converting ^{99}Mo production from HEU to LEU, Union Carbide was producing ^{99}Mo at their U.S. reactor in Tuxedo, NY. Cintichem, which took over these operations, produced about half the world's supply of ^{99}Mo before it shut down operations in 1989.

A formal agreement has been in place between ANL and BATAN for about three years to convert the Cintichem process, which BATAN licensed in the late 1980s. Argonne and SNL have cooperated informally for about a year on LEU conversion, and a formal agreement will be signed in the third quarter of 1997. Under this agreement, irradiation and processing of LEU-oxide targets will be added to their test matrix for product acceptance. The LEU-oxide targets are being fabricated at the Los Alamos National Laboratory (LANL), the current fabricator of HEU targets for SNL. Because the United States DOE now owns the licensing rights to the Cintichem process, the RERTR program expects that the LEU-modified Cintichem process can be made available to established and new ^{99}Mo producers under reasonable terms and conditions.

5.1.1. Target dissolution

The Cintichem HEU target is a closed cylinder with an electrodeposited layer of UO_2 on its inner wall. Following irradiation, the target is opened, a cocktail of nitric and sulfuric acid is added, and the target is heated to dissolve uranium and the fission products. Following a degassing step, which removes most of the iodine and noble fission gases, the solution is removed from the target cylinder for further processing. For the LEU-foil target, a slightly different procedure will be followed. After the irradiated uranium foil is removed from its target, it will be placed in a multi-use dissolver and heated. Following dissolution, the resulting solution will be removed from the dissolver and processed by a similar procedure as used for the HEU target.

One of our conversion goals is to make the composition of the spent dissolver solution from the LEU target act as much as possible like that from the current HEU target. Because a comparable LEU target will contain 5-6 times more uranium than an HEU target, the spent LEU dissolver solution must have a higher volume, a higher uranium concentration, or both. Also, because the dissolution of uranium metal is a six-electron oxidation compared to only a two-electron oxidation for UO_2, more of the oxidant (e.g., nitric acid) needs to be present initially. The reactions for oxidation of UO_2 and U metal are shown below:

$$UO_2 + \frac{8}{3}H^+ + \frac{2}{3}NO_3^- \rightarrow UO_2^{2+} + \frac{4}{3}H_2O + \frac{2}{3}NO\uparrow \quad (1)$$

$$U + 4H^+ + 2NO_3^- \rightarrow UO_2^{2+} + 2H_2O + 2NO\uparrow \quad (2)$$

Hydrogen ion can be supplied by sulfuric and/or nitric acid. As seen in Eqs. 1 and 2, the major reduction product of nitric acid is NO. Because (1) up to six times more uranium will be dissolved and (2) uranium metal dissolution will generate three times the amount of NO than for UO_2 dissolution, gas pressures produced and solution volumes used during dissolution were important design criteria for the LEU dissolver.

Uranium-foil dissolution was initially studied as chemical R&D in 1994 [24]. The chemical studies moved into engineering studies in the following years [25, 26]. In 1994, we verified that uranium metal would dissolve in nitric/sulfuric acid mixtures at rates comparable to UO_2. We also measured the heat of dissolution in this system to be 1.10×10^3 kJ/mol-U. In 1995, we measured activation energies for uranium-foil dissolution by the mixed nitric/sulfuric acid system and found it to be 44 kJ/mol-U. Rate-vs.-temperature data are shown in Fig. 8. We also verified (1) that the stoichiometry of Eq. 1 is valid, (2) that no H_2 evolves during dissolution, and (3) that the rate is dependent on hydrogen-ion concentration but nearly independent of whether the hydrogen ion is supplied by sulfuric or nitric acid.

To calculate the rate of dissolution for uranium foil as a function of temperature and the concentrations of HNO_3 and H_2SO_4, all data on dissolution rates were extrapolated to 92°C based on the activation energy of the reaction. Then, the rate of uranium dissolution at 92°C (R_{U92}) was obtained by a least-squares fit of the data using Eq. 3:

$$R_{U92} = a_{n1} \cdot x + a_{s1} \cdot y + a_{n2} \cdot x^2 + a_{s2} \cdot y^2 + a_{22} \cdot x^2 y^2 + a_{s3} \cdot y^3 + a_{33} \cdot x^3 y^3 \quad (3)$$

where the a values are coefficients that were adjusted by using a least-squares fit, x is the molar concentration of HNO_3, and y is the molar concentration of H_2SO_4. For this least-squares fit, the coefficients were constrained to be zero or positive so that R_{U92} is always

positive. This gave a_{22} of 0.0253, a_{33} of 0.01554, a_{n1} of 0.0262, a_{n2} of 0.0389, a_{s1} of 0.0984, a_{s2} of 0.0679, and a_{s3} of 0.01473. The correlation in Eq. 3 yielded the contour plot given in Fig. 9, which shows how the uranium dissolution rates vary in the expected range of operation. A typical reaction path is indicated by the dashed arrow going from point A to point B in Fig. 9. The initial solution would be 3M HNO_3 and 2M H_2SO_4; after reacting to generate a 1M UO_2^{2+} solution, the spent dissolver solution would contain 1M HNO_3 and 1M H_2SO_4. During dissolution, the initial rate that uranium dissolves will be much higher than the final rate. This contour plot also shows that a much simpler correlation can be made to fit the data. The rate at 2M H_2SO_4 is approximately equal to that at 4M HNO_3; the rate at 1M H_2SO_4 is approximately equal to that at 2M HNO_3; etc. The dissolution rate can be simply correlated to the total hydrogen ion concentration in the dissolver solution. This relationship does break down, however, if not enough nitrate ion is present to oxidize the uranium. This revelation led us to consider using a dissolver solution containing nitric acid alone to eliminate problems that sulfate ion causes in waste treatment and disposal.[1]

The next step was to design a closed dissolver that could be used in the PUSPIPTEK hot cells to dissolve the irradiated foil. The design we chose had the same dimensions as the Cintichem target, thus allowing it to be used in the device now used to heat and rotate the HEU target/dissolver. A series of experiments was run at ANL and PUSPIPTEK where various sized pieces of 130-μm depleted uranium (DU) foil were dissolved in 80 mL of 3M HNO_3 and 2M H_2SO_4 with a steady-state temperature of 102 ± 2 °C (Fig. 10). The initial spike in the pressure is caused by the high heat of dissolution (1.10×10^3 kJ/mol-U). The heat released during uranium dissolution causes rapid heatup of the solution and even faster dissolution of the uranium foil. Testing showed that dissolution with HNO_3 alone provided almost identical dissolution times, pressure spikes, and final pressures for the same total hydrogen-ion concentrations as the mixed-acid systems. Figure 11 is a correlation of mass of uranium dissolved vs. final pressure in the dissolver. Some of the points are for UO_2 dissolution; in these cases, the uranium mass was divided by three to account for 1/3 less NO being formed per mole. The model fits the data quite well at 103°C. However, at 25°C, the model pressure is above the observed pressures. This deviation is attributed to the solubility of NO in the dissolver solution. This solubility increases as temperature decreases.

The need for barrier materials further complicates dissolution. However, the perturbation is minor. The overall dissolution reactions for metal barriers of Cu, Ni, Zn, and Fe using nitric acid alone are shown in Eqs. 4 and 5:

$$\text{Cu/Ni/Zn} + \frac{8}{3}\,\text{HNO}_3 \rightarrow \text{Cu/Ni/Zn(NO}_3)_2 + \frac{4}{3}\,\text{H}_2\text{O} + \frac{2}{3}\,\text{NO}\uparrow \qquad (4)$$

$$\text{Fe} + 4\,\text{HNO}_3 \rightarrow \text{Fe(NO}_3)_3 + 2\,\text{H}_2\text{O} + \text{NO}\uparrow \qquad (5)$$

Dissolution rates for Cu, Ni, and Fe were measured over a variety of conditions in a covered, but unsealed, centrifuge tube in a constant-temperature bath. The results indicate that all three metals dissolve faster than uranium: Ni is five times faster, Cu is 190 times faster, and Fe is 560 times faster. Zinc,[2] which was studied later as a potential barrier for the base-side processes, dissolves very quickly in nitric acid. Equations 4 and 5 and the ideal gas law were used in calculating the dissolution pressure for a two-sided barrier on a typical 18-g U-foil target[3] with barrier dimensions of 76 x 102 x 0.010 mm, a dissolver temperature of 103°C,

[1] Studies of the primary ^{99}Mo recovery step (discussed in section 5.1.2.) also showed no penalty for eliminating H_2SO_4.

[2] Complications of using Zn barriers due to its low melting point and reaction with uranium near its melting point will be discussed in section 5.2.1.3.

[3] An 18-g LEU target contains approximately as much ^{235}U as a typical HEU target being used by BATAN.

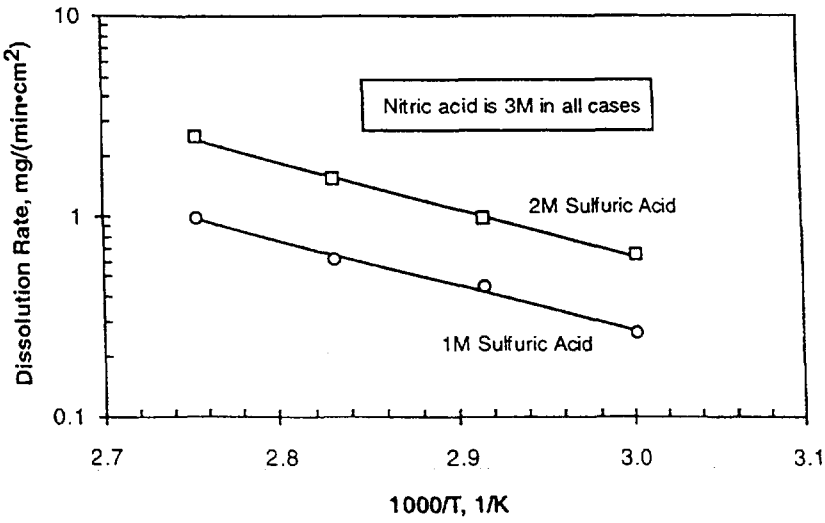

FIG. 8. Effect of temperature on the dissolution rate of uranium foil at two solution compositions.

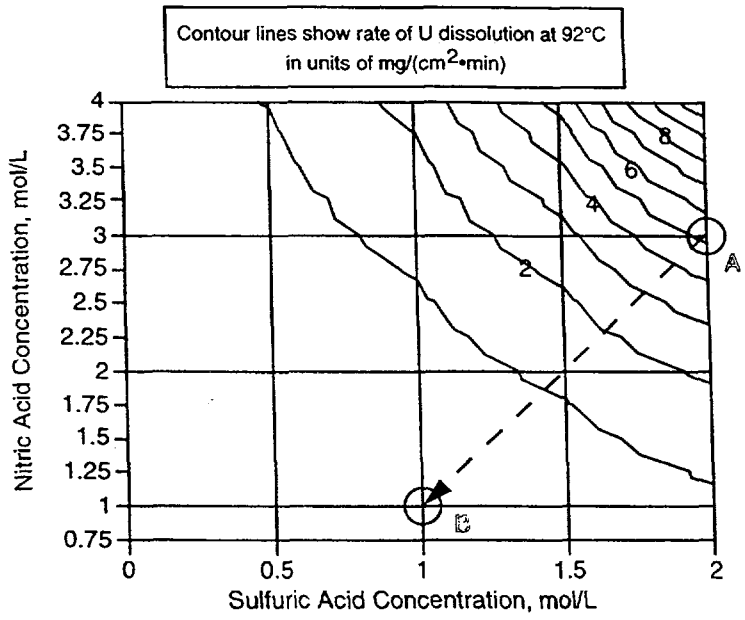

FIG. 9. Modeled effect of the concentration of nitric acid and sulfuric acid on the dissolution rate of uranium foil.

and a gas volume of 282 mL. The results indicate an increase in the final dissolver pressure of about 30 psig for the barriers foils, over that for U alone. Thus, the dissolver pressure will be increased about 10% by the presence of a two-sided barrier. This pressure increase is within the design limits of the stainless-steel dissolver, so that any of these four barrier materials (Zn, Cu, Ni, Fe) can be used without affecting the operation of the U-foil dissolver. In two tests, Ni foil was used in the closed (sealed) stainless-steel dissolver. The results of these tests were very similar. The pressure-time plots (not shown here) indicated that the Ni dissolved easily, as expected. The final gas pressure for this piece of Ni foil was expected to be 159 psia. Instead, a much lower pressure, about 40 psia, was actually realized. The difference in these two pressures may be due to NO gas solubility in the dissolver solution.

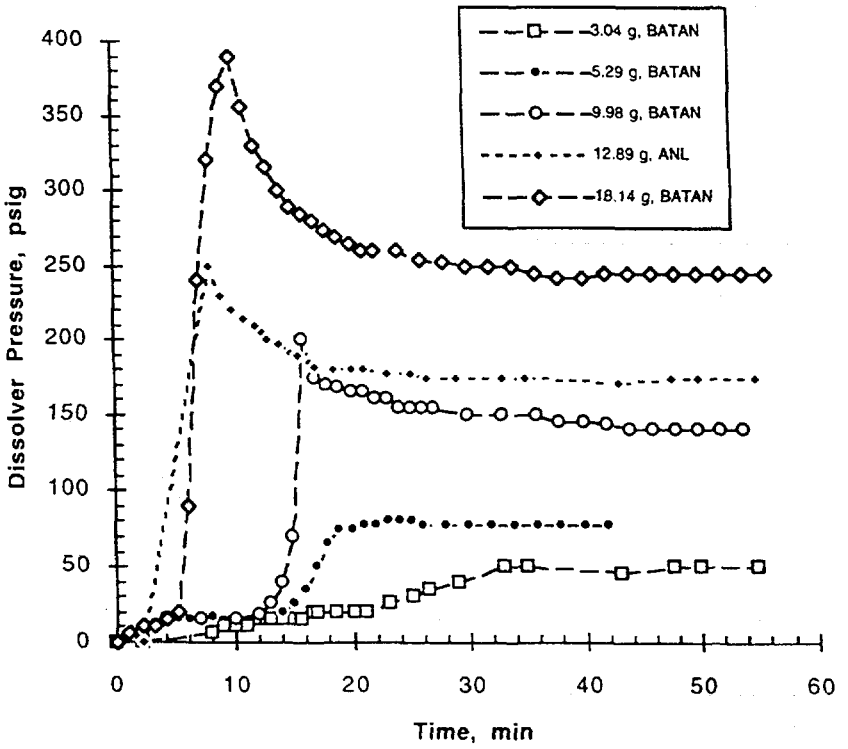

FIG. 10. Variation of pressure with time during dissolution of uranium foil in the stainless-steel dissolver.

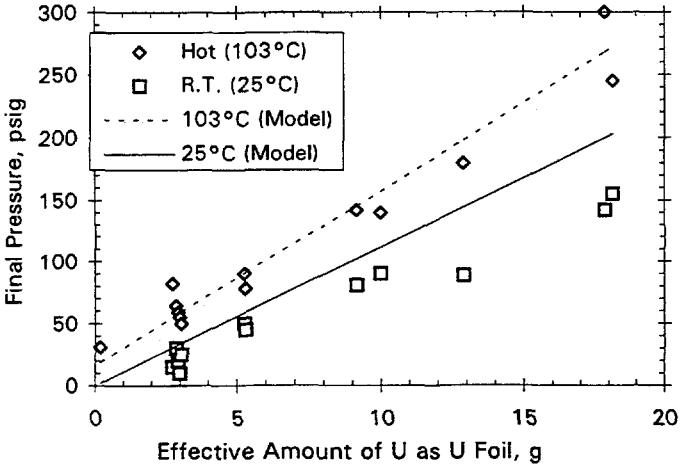

FIG. 11. Effect of uranium mass on final dissolver pressure at room temperature (R.T.) and 103°C.

Researchers at BATAN attempted to dissolve the irradiated Zn-barrier LEU foil that was successfully removed from the target. They used conditions that should have completely dissolved the foil in 30 min. Following this procedure, the gas pressure generated during dissolution and the radioactivity levels in the spent dissolver solution both were far lower than expected. This may be due to (1) the formation of a U-Zn compound at the Zn-foil/U-foil interface during irradiation and (2) this compound dissolving at a lower rate than either uranium or zinc. To test this theory, we heated a zinc-plated DU foil at 375°C overnight. This formed a U/Zn intermetallic that did dissolve at a rate substantially lower than either metal alone. We are undertaking a set of experiments to quantitate the rate of dissolution for this

compound. Although we have been developing the Zn-barrier foils for basic dissolution, using it for acid-side processing is certainly possible if the dissolution rate can be easily handled by increasing dissolver temperature.

Further details on this topic can be found in references 24-26. The dissolver has been set up and tested in the PUSPIPTEK hot cell and is ready for the process demonstration of a fully irradiated foil scheduled for September 1997.

5.1.2. Target processing

The major concern in defining the spent dissolver solution needed for the LEU-modified Cintichem process is to make it compatible with the primary molybdenum recovery and purification step. If this step is successful, differences between HEU and LEU targets are of no consequence to the rest of the process. The initial step in the Cintichem process is the precipitation of Mo(VI) by α-benzoin oxime (a-BO--see Fig. 12). This step is derived from a standard analytical method for molybdenum [27-29]. The standard procedure requires molybdenum in 1M sulfuric acid. Molybdenum precipitation is quantitative, and the precipitate contains very low levels of impurities. Most of our efforts have been focused on this step and on how the yield and purity of ^{99}Mo are affected by the variations in concentrations of uranium, nitric acid, and sulfuric acid.

Early R&D [30, 31] was based on our knowledge of the Cintichem process found in patents [13, 14]. Later R&D [32-35] was based on a firm knowledge of the process due to our cooperative project with BATAN and SNL. Details of the work presented below can be found in these publications. The following summarizes the most important aspects of this work.

A series of experiments was performed to measure the effect of acid (Table III) on the recovery of molybdenum. The conclusion to these studies is that if the hydrogen-ion concentration of the spent dissolver solution is held between 0.5 and 5M (whether from HNO_3 or H_2SO_4), molybdenum recovery will be essentially quantitative. Another set of experiments (Table IV) showed that uranium concentration has no perceptible effect on molybdenum yield. We also determined a range of concentrations for a-BO and molybdate that yielded quantitative recovery. The upshot of this work is that there is wide latitude in the composition of the spent dissolver solution. We, therefore, chose to (1) use only nitric acid and (2) keep the

TABLE III. MOLYBDENUM RECOVERY VS. SOLUTION COMPOSITION

[HNO3], M	% Mo Recovery	[H2SO4], M	% Mo Recovery
0.1	90	0.1	100
0.5	100	0.5	100
1.0	100	1.0	98
2.0	100	2.0	95
4.0	100	4.0	93
6.0	88	6.0	98
8.0	-	8.0	8.7

volume of the dissolver solution low and its uranium concentration high. Although the spent dissolver solution from LEU targets will contain 5-6 times more uranium, the uranium will be at 2-3 times higher concentrations than for the HEU target. Therefore, the LEU feed to the a-BO precipitation will be about twice that for the HEU target.

Although the a-BO precipitation has been our primary concern, we have looked at the entire process. A rather complete description of the process can be found in a document released by SNL [36]. Following precipitation and washing, the a-BO/Mo precipitate is destroyed with alkaline peroxide, and the molybdenum is dissolved in base (as molybdate). The molybdenum solution is further purified by passing it through a column of silver-coated charcoal; performing a silver-iodide precipitation; passing it through a second column containing silver-coated charcoal, hydrated zirconium oxide, and activated charcoal; and finally passing it through a 0.2 μm filter.

TABLE IV. MOLYBDENUM RECOVERY VS. URANIUM CONCENTRATION

$[UO_2(NO_3)_2]$, M	$[H_2SO_4]$, M	% Mo Recovery	
		Precipitate[a]	Filtrate[b]
0.5	1.0	100 ± 2	99.5 ± 0.1
1.0	1.0	100 ± 2	99.3 ± 0.1
1.5	1.0	100 ± 2	99.1 ± 0.1
2.0	1.0	98 ± 2	98.4 ± 0.1
0.5	2.0	-	99.1 ± 0.1
1.0	2.0	-	99.3 ± 0.1
1.5	2.0	-	99.0 ± 0.1

[a]Based on neutron activation analysis (NAA) of molybdenum in the solid.
[b]Based on NAA of molybdenum in the filtered solution.

The allowed levels for radiochemical impurity in ^{99}Mo product are very low, ranging from 10^{-1} to 10^{-7} μCi/mCi-^{99}Mo. Therefore, each purification step must work effectively. The gamma-emitting isotopes that are analyzed in the ^{99}Mo product are tabulated in Table V. Using the ORIGEN2 computer code, we calculated the activities of these radioisotopes in an 18-g LEU target at 24 h after discharge from the Indonesian reactor (RGS-GAS), following a 120-h irradiation at full power (second column of Table V). Columns 3 through 5 contain decontamination factors measured in our tracer experiments for each processing step, the a-BO precipitation and two polishing steps (purifications 1 and 2). The predicted impurity levels in units of μCi/mCi-^{99}Mo in the irradiated LEU target are listed in the last column. The calculations show that, except for ^{103}Ru, the desired radioisotopic decontamination levels can be met easily. Because ^{103}Ru contamination is not a concern in the current Cintichem product from HEU targets and because substitution of LEU will not affect the fission yield, this ^{103}Ru result may indicate a limitation of our tracer experiments more than a problem with LEU substitution. Experiments have also been performed to follow the behavior of uranium and plutonium in the individual Cintichem processing steps. Decontamination factors for both should be more than adequate for meeting alpha impurity levels in the ^{99}Mo product.

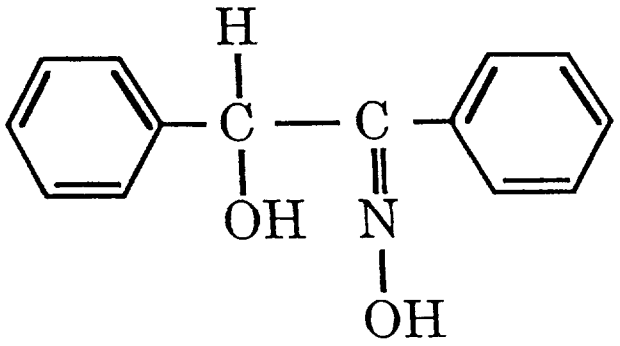

FIG. 12. Chemical form of alpha benzoin oxime.

Development of LEU metal-foil targets has led to the use of thin (10-15 μm) metal barriers between the uranium foil and the target walls. Three metals (Cu, Fe, and Ni) were selected as primary candidates for the barrier material on the basis of their physical, chemical, and nuclear properties.[4] The nuclear properties of interest are the radioisotopes generated in the barrier during target irradiation and their activity levels, which must be removed from molybdenum during processing. By the use of ORIGEN2, we calculated the radioisotopes generated in Fe, Ni, and Cu barriers during LEU target irradiations in the RGS-GAS reactor. The results of these calculations show that only a copper barrier would generate enough radioactivity to be of concern. For its primary activation product, ^{64}Cu, to be less than 0.1 μCi/mCi-^{99}Mo in the molybdenum product, its overall decontamination factor must be >3100.

Neither the barrier materials nor their neutron-activation products are reported to interfere with the precipitation of molybdenum by a-BO [27-29]. Experiments were run to verify the noninterference of these metal ions by using solutions prepared to simulate dissolving the barrier-clad uranium foil in nitric acid. In the same experiments, we measured the amount of each barrier metal that carried with the molybdenum precipitate. Table VI shows the results of these experiments. The molybdenum recovery was high for all experiments, as were the measured decontamination factors. It is likely that the differences in the decontamination factors are more an indication of how well the precipitate was washed in each experiment rather than chemical differences in the barrier-metal ions.

The decontamination factors measured for Fe and Ni are more than high enough to meet impurity requirements for the molybdenum product. However, the removal of ^{64}Cu may require additional decontamination, since the measured value after a-BO precipitation (Table VI) is below the required value of >3100. For this reason, we tested the removal of copper by the two polishing steps; these tests showed that the overall decontamination factor for the two polishing steps should be >10,000. A combination of all three steps should, therefore, effectively reduce ^{64}Cu contamination to well below regulatory concern.

Testing and development activities are continuing at Argonne National Laboratory and the University of Texas to support modification of the Cintichem process for use with LEU targets and to assist BATAN researchers at the PUSPIPTEK Radioisotope Production Center, who are preparing to demonstrate this process on a fully irradiated LEU target. Our collaboration with BATAN is vital to developing and validating this process. Their results continue to show that substitution of LEU in the Cintichem process will be successful and

[4] Zinc, which was primarily selected for base-side process targets, is not discussed below.

TABLE V. CALCULATED IMPURITY LEVELS OF A FULLY IRRADIATED LEU TARGET AND THE ^{99}Mo PRODUCT[a]

Nuclide	Calculated Target Activity, Ci	Measured Decontamination Factors[b]			Calculated Product Impurity Level, μCi/mCi-^{99}Mo
		Precipitation	Purification 1	Purification 2	
Ba-140	292	>516	>162	>165	<3.6E-05
Ce-141	121	>1116	328	419	<1.3E-06
Ce-143	685	>3354	313	641	<1.7E-06
I-131	186	51	28	41	5.3E-03
I-133	628	91	35	51	6.3E-03
I-135	104	121	38	43	8.8E-04
La-140	224	>2409	>104	>149	<1.0E-05
Mo-99	697	1.04	1.05	1.08	—
Nb-95	4.7	4	>13	>9.5	<1.7E-02
Nb-97	480	11	56	1410	9.2E-04
Nd-147	119	208	>62	>59	<2.6E-04
Np-239	1610	>1770	>247	>333	<1.9E-05
Pm-151	45	103	>16	>21	<2.1E-03
Rh-105	102	>276	>34	>46	<4.0E-04
Ru-103	54	113	1.3	3.7	1.7E-01
Sb-127	13.6	>41	1.3	>10	<4.3E-02
Sr-89	65.7	—	—	—	<2.3E-07[c]
Sr-90	0.39	—	—	—	<1.4E-09[c]
Sr-91	209	>3452	235	>586	<7.4E-07
Sr-92	2.65	>2101	>71	>63	<4.7E-07
Te/I-132	464	>5083	327	657	<7.1E-07
Y-93	258	>1294	511	822	<8.0E-07
Zr-95	70	13	27	>49	<6.8E-03
Zr-97	447	17	23	>41	<4.6E-02

[a]Basis is an 18-g LEU target, 24 h after discharge from the RGS-GAS reactor, following a 120-h irradiation at full power.
[b]Ratio of activity in the molybdenum solution before and after treatment.
[c]Predicted from ^{91}Sr behavior.

TABLE VI. EFFECTS OF BARRIER MATERIALS ON a-BO PRECIPITATION[4]

	Cu	Fe	Ni
Molybdenum Recovery, %	99 ± 3	96 ± 3	96 ± 3
Decontamination Factors	1680	258	660

have advanced our progress toward the full-scale demonstration to be done by BATAN. Our unofficial, but soon to be official, cooperation with SNL will move full development of the LEU Cintichem process even faster. Processing of LEU oxide targets will be demonstrated at SNL in the next year.

In summary, our experimental results predict that replacing the current dissolution cocktail, which contains both nitric and sulfuric acids, with nitric acid alone will not compromise the effectiveness of the Cintichem process. In our tracer experiments with this substitution, molybdenum recovery and purity were not degraded. Removal of sulfuric acid from the dissolver solution will decrease waste treatment and disposal costs and increase the stability of the disposed waste form. On the basis of measured decontamination factors from our tracer experiments, molybdenum produced from processing fully irradiated LEU targets is predicted to meet radiochemical purity limits. Its yield will be equivalent to that currently produced from HEU. Likewise, addition of barrier materials will not affect the process. A full-scale demonstration of process will take place in the near future at PUSPIPTEK.

5.2. Base-side processing

As seen in Table II, ^{99}Mo production by IRE, CNEA, Mallinckrodt, and the AEC is all done by irradiating HEU UAl_x/Al-dispersion plates and dissolving the plates in base. The three LEU targets we are studying as the HEU replacement are U_3Si_2/Al and UO_2/Al dispersion plates and a uranium-metal foil with a zinc barrier. For all three targets, base alone is not sufficient to dissolve the uranium fuel; addition of hydrogen peroxide is necessary to achieve acceptable dissolution rates. In processing the two dispersion-fuel targets, the entire target is dissolved before molybdenum can be recovered. In the LEU-metal target, only the uranium foil (and the fission barrier) must be dissolved. The spent dissolver solution will be essentially identical for the two LEU dispersion targets and much like that of the current HEU target.[5] The dissolver solution from the foil target will not have the very high aluminum content like those from the dispersion-fuel targets. However, the dissolver solution from the foil target will contain a significant concentration of zinc. Once dissolved, processing will likely be the same for all three targets. Experimentation on base-side molybdenum recovery and processing steps was done with U_3Si_2 targets; these studies were performed in 1987 and 1988 [31, 37].

5.2.1. Target dissolution

The discussion of target dissolution is divided into three parts--one for each target type. Because the dissolution reagents are the same (NaOH and H_2O_2), the dissolution studies have much in common. In all cases, the purpose of our efforts was first to show the feasibility of target dissolution, then to optimize the dissolution process, and finally to design a dissolver.

5.2.1.1. U_3Si_2/Al dispersion plates

We first began to look at U_3Si_2-target dissolution and processing in 1987, and it was the program's major emphasis through 1989 [31, 37, 38], when all RERTR-^{99}Mo efforts were stopped due to funding problems. Research and development directed toward U_3Si_2 targets began again in 1993 and continued through 1996 [39-43]. A decision was made late in 1996 to suspend this work and to expend limited resources on development of the uranium-metal and UO_2/Al-dispersion targets. The following summarizes the status of U_3Si_2 dissolution; for details, the reader is directed to the above-cited works.

[5]The consequences of dissolving LEU rather than HEU targets on the volume and compositions of the feed to the primary ^{99}Mo recovery step are discussed in section 5.2.2.

An important side reaction that occurs during the silicide dissolution process is the autodestruction of hydrogen peroxide:[6]

$$2\,H_2O_2 \rightarrow 2\,H_2O + O_2 \qquad (6)$$

A literature search revealed very little data about the autodestruction of hydrogen peroxide in sodium hydroxide solutions. One source simply revealed that the autodestruction reaction is catalyzed in base, but no quantitative data were given [44]. A limited kinetic study of dilute hydrogen peroxide (0.01M) in 0.5-6.0M NaOH at room temperature indicated that hydrogen peroxide was stable in highly basic solutions [45]. Experiments at ANL showed the autodestruction of H_2O_2 was first order with respect to H_2O_2 in alkaline solutions between 70 and 100°C. In general, autodestruction of H_2O_2 is catalyzed by metallic surfaces and, in some cases, metal ions in solution.

Hydrogen peroxide is also consumed in the dissolution of the U_3Si_2. The following equations describe the dissolution of U_3Si_2 in alkaline peroxide based on the assumption that it is an intermetallic compound:

$$H_2O_2 + 2e^- \leftrightarrow 2OH^- \qquad (7)$$

$$Si^0 + 6OH^- \rightarrow SiO_3^{2-} + 4e^- + 3H_2O \qquad (8)$$

$$U^0 + 4OH^- \rightarrow UO_2^{2+} + 6e^- + 2H_2O \qquad (9)$$

$$4\,OH^- + UO_2^{2+} + 4H_2O_2 \leftrightarrow UO_2(O_2H)_4^{2-} + 4\,H_2O \qquad (10)$$

Equation 11 is an overall reaction for Eqs. 7 through 10:

$$U_3Si_2 + 25H_2O_2 + 10OH^- \rightarrow 2SiO_3^{2-} + 3UO_2(O_2H)_4^{2-} + 24H_2O \qquad (11)$$

Due to catalyzed autodestruction, the actual H_2O_2 consumption is 10-100 times greater than that predicted by Eq. 11.

We developed a U_3Si_2 dissolution-rate model that can be used in designing a target dissolution procedure. Dissolution rates of U_3Si_2 particles were determined using the initial rate method. A large set of experiments started with ~5.4M H_2O_2 and varied base concentrations at 40, 50, and 60°C. The uranium dissolution rates were normalized to U_3Si_2 particle mass. These normalized rates were then plotted versus initial base concentration (Fig. 13). The uranium dissolution reaction reaches a maximum at approximately 1.5M NaOH for each temperature with both comminuted and atomized U_3Si_2 particles.[7] The reaction rate doubles for a 10°C increase in temperature. The spherical atomized particles dissolve more slowly than the comminuted particles, mostly due to surface area. The atomized and comminuted U_3Si_2 particles have similar uranium dissolution rates at 50°C when surface area

[6] Both uranium metal and U_3Si_2 catalyze this autodestruction, making it orders of magnitude more important than in the dissolution of UO_2, which does not catalyze this reaction.

[7] Most experiments used jagged comminuted powder, crushed from larger pieces and possessing mostly a single-phase structure [46]. Later experiments used atomized powder, spherical particles produced by quenching of molten U_3Si_2 in an inert atmosphere [47].

is considered. The different activation energies for the two particle types show that more than surface area differences are relevant in the dissolution kinetics of atomized and comminuted U_3Si_2 particles.

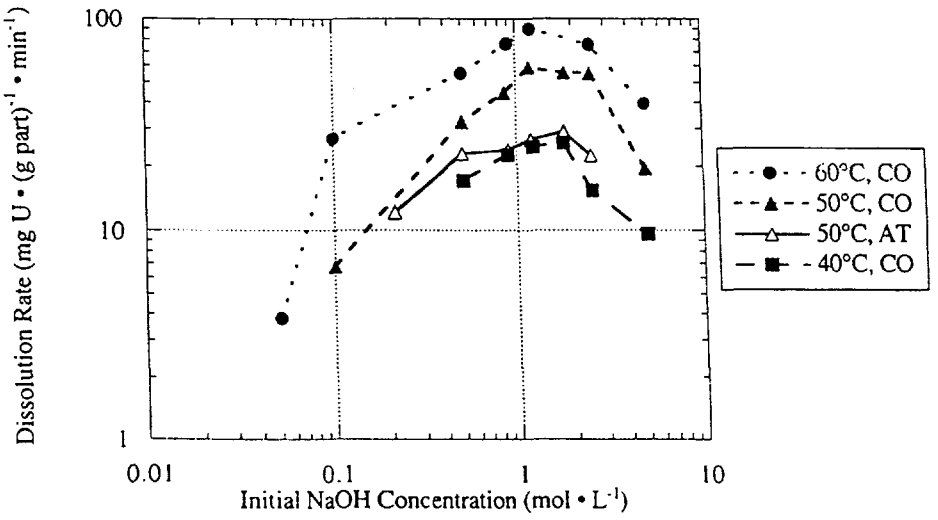

FIG. 13. Variation in uranium dissolution rate normalized to mass of particles (g part) with initial NaOH concentration. The data series in legend give reaction temperature and comminuted (CO) or atomized (AT) particles.

The dissolution activation energies of comminuted and atomized particles were determined by using the Arrhenius equation:

$$k = A\exp(-E_a/RT) \tag{12}$$

where k is the rate constant, E_a is the activation energy, R is the universal gas constant, T is the absolute temperature, and A is a pre-exponential factor.

The reaction mechanism is probably the same for the base range of 0.5-2.5M NaOH, resulting in the same E_a for each particle type. Arrhenius plots are made by plotting the natural logarithm of the uranium dissolution rate constant against the inverse of the temperature (1/T). The slope of the line determines E_a and the y-intercept determines A. Table VII lists the experimentally determined activation energies for comminuted particles dissolved in 0.5-2.5M NaOH and 5.2M H_2O_2. As shown, the average activation energy is 77 ± 15 kJ/mol. The activation energy of the comminuted particles is 40% higher than that of the atomized particles. Differences between their activation energies may be explainable by how they are prepared. The comminuted particles are cooled slowly and contain a single crystalline phase. The atomized particles are condensed quickly from molten U_3Si_2 and contain many different crystalline phases. One or more of these phases has a lower activation energy.

The equilibrium shown in Eqs. 13 and 14 significantly decreases the concentrations of H_2O_2 and OH^- from their as-prepared values:

$$H_2O_2 + OH^- \xleftrightarrow{K=160} HO_2^- + H_2O \tag{13}$$

or

$$160 = \frac{[HO_2^-][H_2O]}{[H_2O_2][OH^-]} = \frac{[HO_2^-]}{[H_2O_2][OH^-]} \tag{14}$$

Figure 14 plots the equilibrium concentrations of O_2H^-, OH^-, and H_2O_2 for a fixed initial peroxide concentration of 5.2M H_2O_2 and variable initial OH^- concentrations. In basic solution the equilibrium H_2O_2 concentration is always less than the initial concentration, and its concentration in high-base solutions is significantly less than in low-base solutions. The maximum peroxide destruction rate occurs at approximately the equilibrium base concentration of 0.1M OH^-, which corresponds to a starting concentration of ~1.2M NaOH.

A model for uranium-silicide dissolution can be developed by assuming that the total uranium on the surface of the U_3Si_2 particles U_s exists in three distinct states, as described by

$$[U_s] = [A] + [B] + [C] \tag{15}$$

where A is the unreacted surface available for reaction, B is the reactive complex from the reaction of A with equilibrium O_2H^-, and C is the unreactive surface produced from the reaction of A with equilibrium OH^-. The complexes B and C are produced by reactions described in Eqs. 16 and 17, where K_1 and K_2 are equilibrium constants:

$$[A] + [O_2H^-]_{eq} \xleftrightarrow{K_1} [B] \tag{16}$$

$$[A] + [OH^-]_{eq} \xleftrightarrow{K_2} [C] \tag{17}$$

The expressions for [B] and [C] can be substituted into Eq. 15 and solved for [B]:

$$[B] = [U_s] \frac{K_1[O_2H^-]_{eq}}{1 + K_1[O_2H^-]_{eq} + K_2[OH^-]_{eq}} \tag{18}$$

TABLE VII. EXPERIMENTAL ACTIVATION ENERGY FOR COMMINUTED U_3Si_2 PARTICLES DISSOLVED IN NaOH AND 5.2M H_2O_2.

[NaOH], mol/L	Activation Energy, kJ/mol
0.5	80
0.9	84
1.2	71
1.8	55
2.5	93
Mean	77±15

Eventually, through a series of fast reactions, complex B becomes the soluble form of uranium that we measure. A uranium dissolution rate model was developed from Eq. 18 and the rate data. Equation 19 gives the uranium dissolution rate R_u as functions of the particle type, and OH^- and O_2H^- concentrations:

$$R_u = A_i \exp\left(-E_{a_i}/RT\right) \bullet \frac{K_1[O_2H^-]_{eq}}{1 + K_1[O_2H^-]_{eq} + K_2[OH^-]_{eq}} \tag{19}$$

The constants K_1 and K_2 were determined by curve fitting of the 50°C data to be 1.2 and 550. The constants for the modified pre-exponential constant A_i and activation energy E_{a_i} (where i denotes AT or CO particles)-A_{AT}, A_{CO}, $E_{a_{AT}}$, and $E_{a_{CO}}$--are 5.10×10^8 mg U·cm^{-2}·min^{-1}, 1.84×10^{12} mg U·cm^{-2}·min^{-1}, 5.5×10^4 kJ·mol^{-1}, and 7.7×10^4 kJ·mol^{-1}, respectively. This temperature-dependent dissolution model for the dissolution of U_3Si_2 particles (Eq. 19) is plotted with experimental data in Fig. 15. The temperature dependence in the exponential fits the data well. The curves fit the data in the desired processing concentration range 0.3-3M O_2H^-. Dissolution rates outside this range are too low for processing an irradiated target.

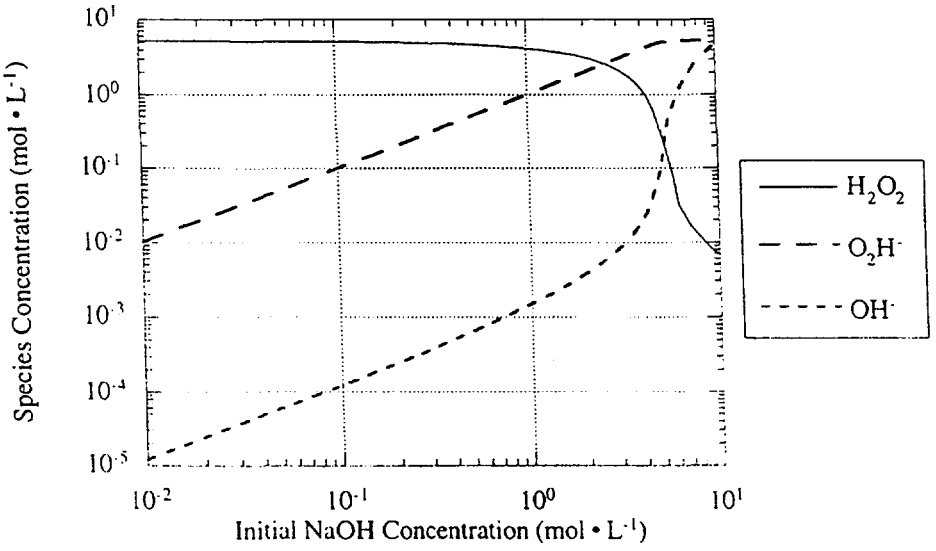

FIG. 14. Calculated variation in equilibrium concentrations of O_2H^-, OH^-, and H_2O_2 for an initial 5.2M H_2O_2 and variable initial OH^- concentration based on Eq. 14.

In conclusion, equilibrium concentrations of peroxyl and hydroxyl ions were used to develop a model for the alkaline peroxide dissolution of U_3Si_2 particles used in dispersion fuel and targets. The uranium dissolution rate reaches a maximum when the equilibrium peroxyl-ion concentration approaches ~1.5M O_2H^-, but the rate changes little over the broader range of 0.5-2.5M O_2H^-. This peroxyl-ion range corresponds to initial concentrations of 0.5-2.5M OH^- with 5.2M H_2O_2 and indicates that the uranium dissolution process is insensitive to small changes in reactant concentrations.

Dissolving unirradiated U_3Si_2 particles is well understood, but we still have a long way to go for dissolving irradiated targets. The current process for basic dissolution involves dissolving the entire target in $NaOH/NO_3$ solution. During the dissolution, uranium and various fission products precipitate as hydrated hydroxide salts. This mixture is diluted and filtered, and molybdenum is recovered from the solution using a column.

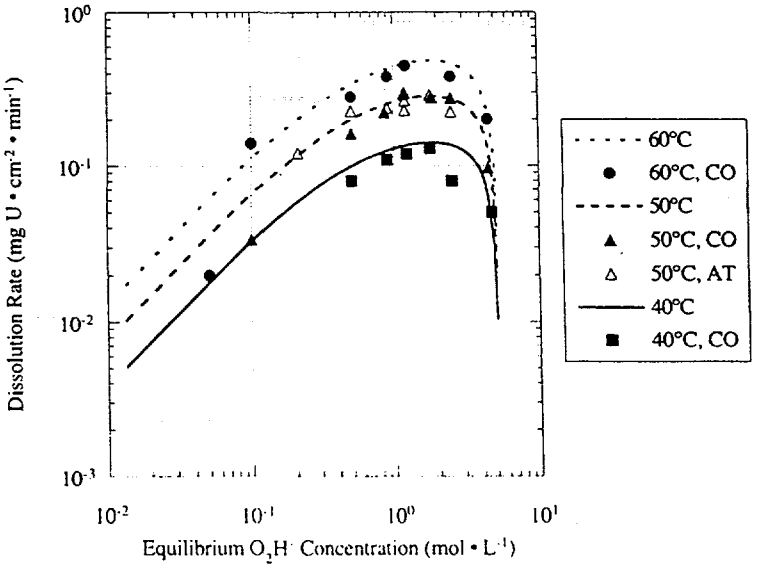

FIG. 15. Variation of uranium dissolution rate with equilibrium peroxyl ion concentration. Data points are denoted by dissolution temperature and particle type (atomized or comminuted), while the empirical model curves generated from Eq. 19 are denoted by temperature only.

In 1987 through 1989 [31,37,38], our results suggested that the targets be digested in a two-step process. In the first step, the aluminum-alloy cladding and the aluminum powder in the fuel meat would be dissolved in 3M NaOH solution. During this step, many of the alloying elements from the cladding (in our case, 6061 Al) would precipitate as hydroxides.The hydroxide slurry would be removed from the U_3Si_2, which could then be dissolved separately with basic hydrogen peroxide. On heating the peroxide solution, peroxide would be destroyed, uranium and many of the fission products would precipitate from the highly basic solution, and the soluble iodine and molybdenum would be separated from them in the filtrate. The two dissolver solutions would be combined for further processing. This scheme is based on three observations:

- Molybdenum-99 loss from the U_3Si_2 fuel due to fission recoil into the aluminum matrix will be in the ~20% range and is likely to represent too high an economic penalty to be ignored.

- The dissolution/digestion rate of U_3Si_2 is too low (<1%/day) in basic solution alone for its practical use in ^{99}Mo-target processing.

- Cladding precipitates must be removed from the dissolver before U_3Si_2 can be dissolved by basic hydrogen peroxide. If they are not, they cause robust autodestruction of hydrogen peroxide before it even contacts the U_3Si_2 particles on the bottom of the dissolver vessel.

In the studies performed in 1988, targets were irradiated in the ANL 180-kW JANUS reactor for 80 min at 1/4 power--a burnup of only 10^{-5}%. This burnup produced 0.9 mCi of ^{99}Mo and enough of the other fission products and ^{239}Np to measure the yield and decontamination of ^{99}Mo through the various steps of the proposed processing scheme. These experiments were performed in glassware at the laboratory-scale level. The next step, to demonstrate this scheme at production levels by using a target with appropriate burnup, was not taken because funding for this project was suspended.

To make a step in that direction, we tested this process using an irradiated miniplate sample that was being stored at ANL following its post-irradiation examination. The miniplate sample that we tested had undergone ~42% burnup in the 30 MW Oak Ridge Reactor (ORR). This miniplate contained uranium enriched to 19.84% ^{235}U before irradiation. Since the miniplate was nearly 9 years old, the short-lived fission products, including ^{99}Mo, had completely decayed. The primary benefit to using a sample with a high burnup is to measure the effects on the dissolution step of changes in the fuel caused by the high degree of fissioning. High burnup of the fuel significantly changes its chemical composition. For example, the chemical composition of the target is modified from that of unirradiated or low-burnup fuels by lowering the uranium content of the fuel, producing ^{28}Si from ^{27}Al, producing ^{31}P from ^{30}Si, and causing the formation of fission products and transuranic elements. Such chemical compositional changes coupled with radiation damage to the fuel caused by energy input (about 200 MeV/fission) form new compounds, especially along the contact between the U_3Si_2 fuel particles and the aluminum matrix. The formation of new compounds in highly irradiated fuels was studied by Gerard Hofman and colleagues at Argonne [48] using both optical and electron microscopy techniques on polished metallographic specimens. The salient aspects of their findings are summarized below:

- A new layer caused by the interaction of uranium silicide with aluminum was formed as a result of high levels of irradiation. The thickness of the layer increased with the duration of irradiation. The layer was about 2-μm thick at 40% burnup.

- The new layer can be represented by the chemical formula $U(Al,Si)_3$, where the Al and Si can form a series of solid solutions represented by the end members UAl_3 and USi_3. At 40% burnup, the chemical composition of the layer is about 65 mol% Al, 25 mol% Si, and 10 mol% U.

- A mixture of nitric acid, hydrofluoric acid, and citric acid etched the unaltered U_3Si_2 but did not attack the $U(Al,Si)_3$ layer.

Unlike the unirradiated target, the irradiated miniplate did not dissolve readily by use of our optimized procedure. The decladding procedure did work as expected. However, after the cladding was removed, the silicide fuel looked like a monolith, not the particles we obtained during the unirradiated testing. This monolith was resistant to dissolution. Heat-treated, unirradiated plates showed the same effect and confirmed that a physical means to break up the fuel meat will be an essential part of target dissolution.

Design of a dissolver system for a two-step process that also provides physical desegregation is a difficult technical problem. This among other problems led us to suspend activity in this area and look toward other targets.

5.2.1.2. Uranium-foil targets

We first dissolved uranium foil in alkaline peroxide in 1988 [37]. Dissolution studies for uranium metal began in earnest in 1995 and are continuing today [42, 49-51]. Studies were moving toward engineering and dissolver design, but chemical aspects were reopened when the use of a zinc fission-recoil barrier became necessary (see section 5.2.1.3).

Dissolution of LEU metal foil with alkaline peroxide solution followed by recovery and purification of ^{99}Mo has been studied at ANL as an option for replacement for the HEU aluminide targets. An LEU-foil dissolution kinetics model was proposed in 1995. During 1996, work was focused on reducing the consumption of hydrogen peroxide during uranium foil dissolution in alkaline peroxide solution and optimizing the uranium dissolution process. In 1997, work has focused on dissolving uranium foil with zinc fission barriers.

Unlike the well-documented acid process, dissolution of uranium metal with alkaline peroxide solutions has received little study. The stoichiometry of uranium metal dissolution by alkaline peroxide is shown in Eq. 20:

$$U + 7H_2O_2 + 2OH^- \rightarrow UO_2(O_2H)_4^{2-} + 6H_2O \qquad (20)$$

In the early 1940s, L. Warf [52] reported that "X (the X stands for uranium) metal dissolved in H_2O_2 + Na_2O_2, NaOH + H_2O_2, and Na_2O_2 + H_2O slowly, and in NaOH + Na_2O_2 very slowly." In their review papers, both Gindler [53] and J. C. Warf [54] mentioned that uranium metal dissolves in a sodium hydroxide solution containing hydrogen peroxide or in a sodium peroxide water mixture, and they both cited L. Warf's report [52]. Larson [55] reported that uranium metal reacts at a moderate rate with a sodium hydroxide/hydrogen peroxide mixture to form a clear solution that is highly colored by the uranyl peroxide complex. However, the kinetics of dissolution of uranium metal foil in alkaline peroxide solutions was basically unknown. The following describes kinetic studies of uranium dissolution in alkaline peroxide solutions. The rate of uranium dissolution was determined by using depleted uranium (DU) foil under various chemical conditions. Much of this study parallels the work and the discussion of the alkaline peroxide dissolution of U_3Si_2. Differences in data treatment reflect differences in perspectives of the principal investigators.

The rate of uranium dissolution versus the equilibrium hydrogen peroxide concentration is shown in Fig. 16 (a log-log plot). Three sets of data were obtained at three fixed base concentrations (0.2, 1.0, and 5.0M) with varying initial hydrogen peroxide concentration (from 1.0 to 4.0M), and the other data set was from experiments in which initial (total) hydrogen peroxide concentration was constant (~3.5M), while the base concentration varied from 0.01 to 5M. Figure 16 clearly indicates that the uranium dissolution data over a broad range of base concentrations can be divided into two groups. The first group, shown by the dashed line on the right-hand side, includes only three data points at base concentrations of 0.01, 0.05, and 0.09M. The second group, the solid line, covers the remaining 20 data points (some data points overlie each other, only 18 can be seen) at base concentrations 0.2M. On

this basis, we concluded that two types of uranium dissolution can be distinguished, a low-base and a high-base process, and that the transition from low-base to high-base process takes place at a base concentration of about 0.2M.

We believe that, in the low-base process (i.e., below 0.2M base), alkali content is the main factor that controls the rate of reaction. An increase in base concentration significantly promotes the rate of uranium dissolution. As shown in Fig. 16, the equilibrium hydrogen peroxide concentration of the three data points in this group varied very little, but the rate of uranium dissolution varied significantly. It is obvious that this dramatic change in the dissolution rate was caused by different base concentrations.

On the other hand, in the high-base process (i.e., above 0.2M base), the rate of uranium dissolution is solely controlled by the equilibrium hydrogen peroxide concentration. Figure 16 indicates that, for base concentrations from 0.2 to 5.0M, the rate of uranium dissolution increased as the equilibrium hydrogen peroxide concentration was increased. All 20 data points fell near or on the same straight line when the uranium dissolution rate was plotted against the equilibrium hydrogen peroxide concentration (in a log-log plot). The slope of the line was 0.25, and the correlation coefficient of the line was 0.89. Therefore, uranium dissolution in the high-base process is a one-fourth order reaction with respect to the equilibrium hydrogen peroxide concentration.

Based on the experimental observations and discussions above, we proposed the empirical kinetics model as shown in Eq. 21:

$$R_u = A\left(e^{\frac{-Ea}{RT}}\right)\left(\frac{K_a\left[OH^-\right]^{n'}}{1+K_a\left[OH^-\right]^{n'}}\right)[H_2O_2]^{n}_{equilibrium} \qquad (21)$$

where R_u is the rate of uranium dissolution ($g \cdot cm^{-2} \cdot s^{-1}$), T is the temperature in Kelvin, E_a (=48.8 kJ/mol) is the activation energy, A (=1.65 x 10^3) is the pre-exponential factor, R is the gas constant, n (=0.25) is a constant, n' (=2) is a constant, K_a (=20.4) is a constant, $[OH^-]$ is the initial (total) hydroxide concentration, and $[H_2O_2]_{equilibrium}$ is the equilibrium concentration of hydrogen peroxide. The mechanism of uranium dissolution is unknown and is out of the scope of this investigation. A factor of $\{K_a[OH^-]^{n'}/(1+K_a[OH^-]^{n'})\}$ was introduced into the model because we believe that OH^- groups are adsorbed on the uranium surface to form an activated compound (Eq. 22) and that uranium dissolution proceeds from a reaction of the activated compound (U^*) with hydrogen peroxide.

$$U^o + n'OH^- \xleftrightarrow{Ka} U^* \qquad (22)$$

Details of how this dissolution model was generated can be found in reference [50]. The predicted rates of uranium dissolution with the model (Eq. 20) were plotted against the experimental data, as shown in Fig. 17. The figure indicates that, in general, the model is good, except that it underestimates the rate of uranium dissolution by approximately 40% at base concentrations of about 0.2M. Notice that a base concentration of 0.2M falls right at the transition point between the low-base and the high-base processes. More parameters are needed to improve the accuracy of this model when applied near the transition regime. However, practical conditions for dissolution are at higher base concentrations.

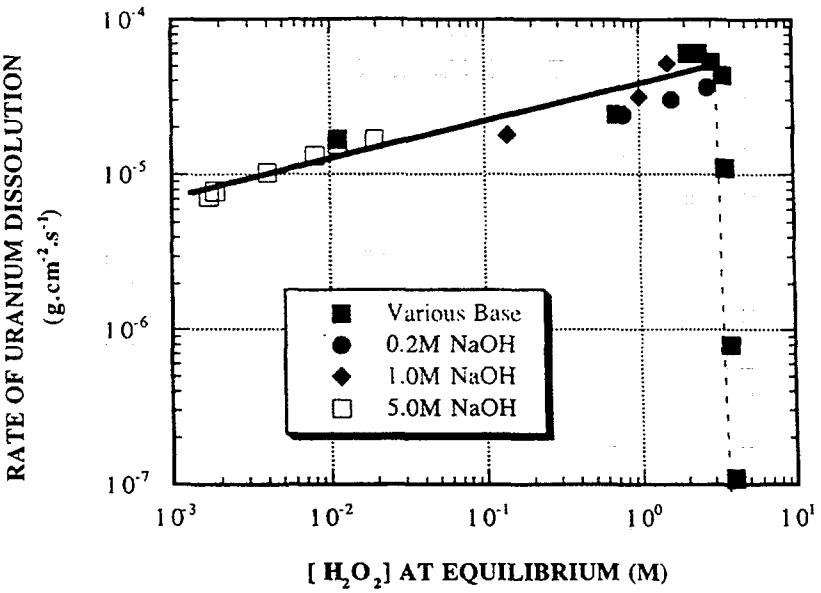

FIG. 16. Effect of equilibrium hydrogen peroxide concentration on rate of uranium dissolution (U Surface Area = 2 cm^2, Temp. = 60°C).

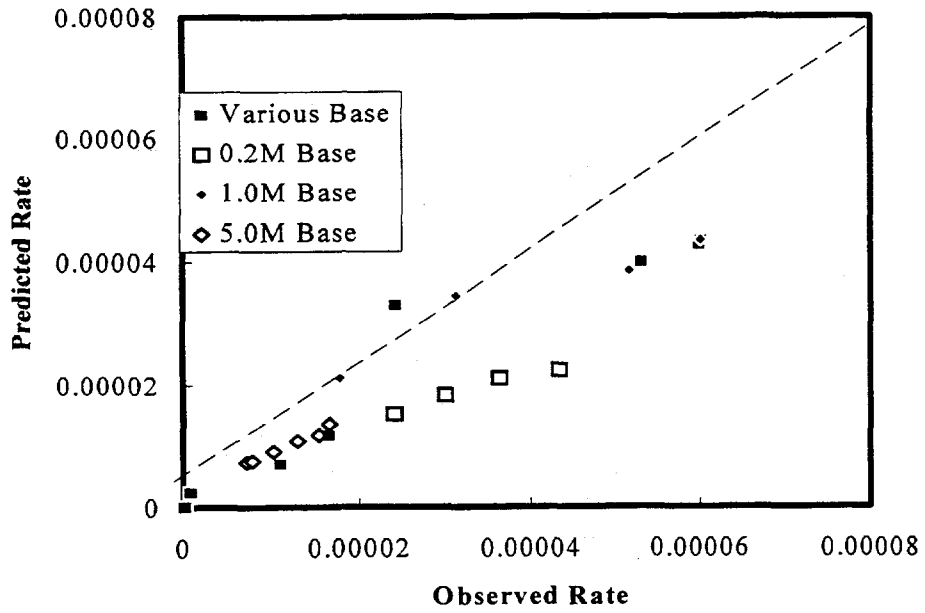

FIG. 17. Predicted vs. observed rate of uranium dissolution.

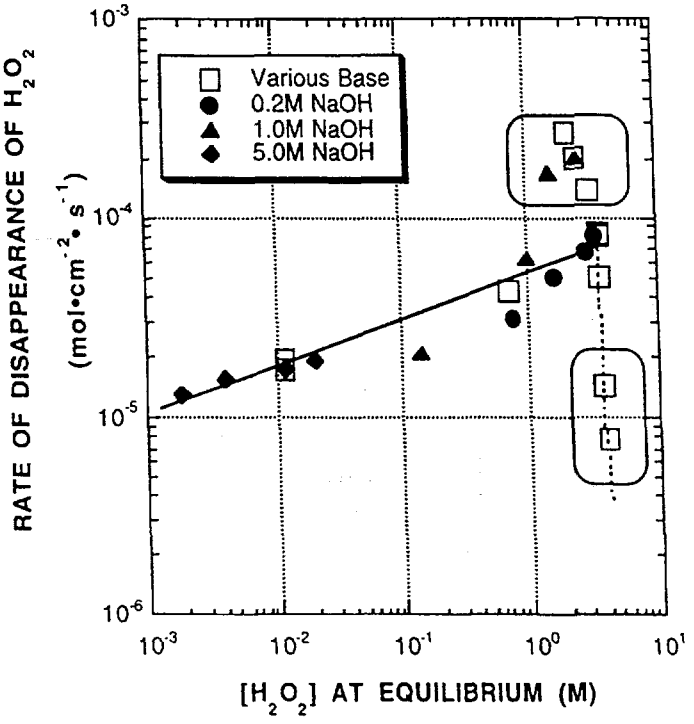

FIG. 18. Effect of equilibrium H_2O_2 concentration on its depletion rate at 60°C.

Dissolution of uranium metal in an alkaline hydrogen peroxide solution involves a complex process in which hydrogen peroxide is consumed by several competing reactions. The uranium surface catalyzes H_2O_2 autodestruction; the rate is orders of magnitude less without the foil present [51]. As a result, a tremendous amount of hydrogen peroxide is depleted during uranium metal dissolution, leading to increased process waste and creating problems in process control. Thus, better understanding the kinetics of hydrogen peroxide decomposition has become a very important factor for reducing the hydrogen peroxide consumption during uranium dissolution.

Figure 18 shows the experimental data for the overall disappearance rates of hydrogen peroxide over a broad range of base concentrations. The depletion of hydrogen peroxide essentially follows the kinetic trend of uranium dissolution and can be divided into two regimes, depending on the hydroxide concentration [51]. In the high-base regime (above 0.2M, indicated by a solid line in Fig. 18), the equilibrium hydrogen peroxide concentration solely controls the rate of hydrogen peroxide disappearance. In other words, the rate of peroxide decomposition is independent of base concentration, and hydroxide ions affect only the acid/base equilibrium between H_2O_2 and O_2H^-. While in the low-base regime (below 0.2M, indicated by the dashed line in Fig. 18), both hydrogen-peroxide and hydroxide concentrations affect the rate of peroxide decomposition. Note that one group of data, shown by the two rectangles, has a common condition of high hydrogen peroxide concentrations and does not follow the trend for the uranium dissolution. This may be explained by the overall rate of hydrogen peroxide decomposition not being solely controlled by the uranium surface under the condition of high peroxide concentration.

Based on the above experimental observations, an empirical kinetics model of the overall disappearance of hydrogen peroxide (R_p) was developed that parallels that for uranium metal dissolution:

$$R_p = A_p \exp\left(-\frac{E_a}{RT}\right)\left(\frac{K_a[OH^-]^{n'}}{1+K_a[OH^-]^{n'}}\right)[H_2O_2]^n_{equilibrium} \quad (23)$$

Values for K_a, n, and n' were determined to be 20.4, 0.25, and 2, respectively, from the uranium dissolution model [50]. The following values were obtained from the experimental data: the pre-exponential factor, A_p, 5.06 x 10^7; and the activation energy, E_a, 76.4 ± 10% kJ/mol.

In this model, the overall disappearance rate of hydrogen peroxide is essentially governed by two terms, OH^- concentration and H_2O_2 concentration. In the high-base regime, the hydroxide ion concentration term becomes near constant. This reveals that the overall consumption of hydrogen peroxide in the high alkaline solution was a 1/4-order function of the equilibrium hydrogen peroxide concentration. While in the low-base regime, the hydroxide concentration term becomes a second-order function of the hydroxide concentration. The hydroxide ion plays a key role in forming an activated complex on the uranium surface to allow the reaction to proceed. It follows that the hydroxide concentration tends to be an important factor in the rate of hydrogen peroxide decomposition, along with the hydrogen peroxide concentrations. This pattern fits the experimental data well, as shown in Fig. 19. However, this model underestimates the rate of hydrogen peroxide decomposition by 6 to 98% over the regime of base concentrations studied.

In an open, batch-type reactor, most of the available hydrogen peroxide is consumed by unwanted autodecomposition. In our previous studies, the hydrogen peroxide consumption ratio (HPCR, moles of hydrogen peroxide consumed per mole of uranium dissolved) was approximately 600. It is critical in this process development to reduce the consumption of hydrogen peroxide to make the process practical.

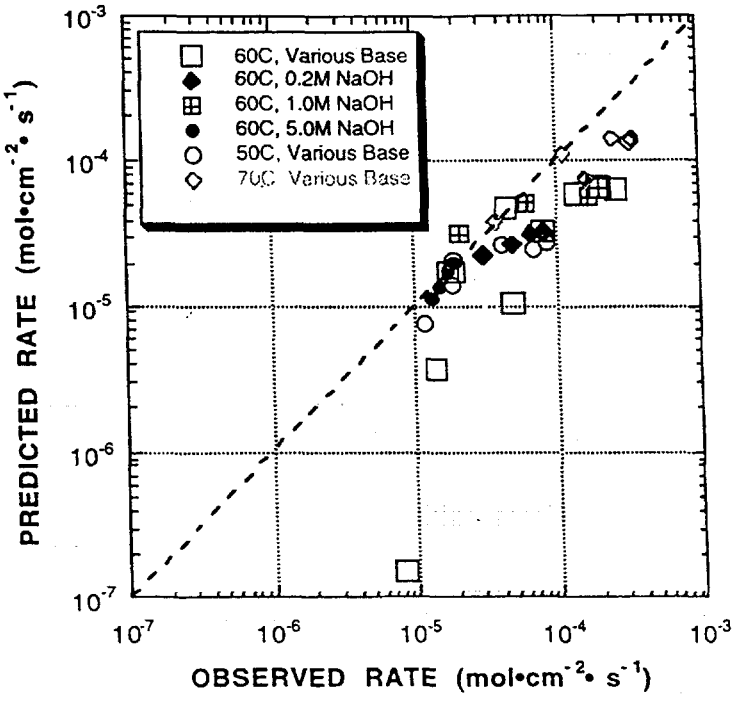

FIG. 19. Predicted rates versus observed rates for depletion of H_2O_2.

An optimized procedure has been developed to reduce the HPCR by using sequential additions of alkaline peroxide [42]. In this sequential procedure, multi-batch processing was employed to replace single-batch processing and thereby avoid decomposition of hydrogen peroxide that remained in the reactor. Results showed that the HPCR could be significantly reduced in a laboratory-scale reactor from ~100 to 5 times the stoichiometric ratio. Because many small-volume additions were actually used in this optimized procedure to frequently replace the dissolving solution or continuously replenish hydrogen peroxide, this opens up the possibility of substituting a plug flow reactor for the multi-batch reactor configuration in the dissolver system.

The HPCR could be further reduced by optimizing the dissolution parameters. We performed a series of experiments to correlate the sodium hydroxide concentration with the uranium dissolution rate and HPCR. The results showed that both the HPCR and the dissolution time were reduced when the base concentrations increased. The effect of dissolution temperature between 50 and 90°C on the uranium dissolution consumption and dissolution time was also determined. As expected, the dissolution time was reduced as temperature increased. However, the HPCR was minimized at 70°C. This probably is due to the competing reactions of uranium dissolution and hydrogen peroxide decomposition, each being affected differently by temperature changes.

Low-enriched uranium metal foils appear to be a viable alternative to the current HEU dispersion-plate targets. Modeling of uranium metal dissolution and hydrogen peroxide decomposition was undertaken to develop an in-depth understanding of the process, and the results should be invaluable in the design of the dissolution process and equipment. Optimization of the dissolution process and minimization of radioactive process waste were achieved by developing a sequential procedure and optimizing the process variables to avoid the rapid decomposition of H_2O_2. At this stage of development, we conclude that (1) HPCR can be significantly reduced by using a multi-stage batch reactor, (2) the optimum composition and temperature are 5.0M H_2O_2/1.5M NaOH and 70°C, respectively, and (3) significant difficulties, such as reactor size and resident time, still need to be resolved. Future work on the dissolution of uranium metal foil will also be concerned with designing the dissolver/off-gas system and integrating ^{99}Mo recovery and purification steps to the dissolution. Complications due to the need of a base-soluble fission barrier are discussed in the following section.

5.2.1.3. Zinc fission barriers

Post-irradiation examination of the ANL LEU-foil test targets showed that bonding of the uranium-metal foil to the target walls was occurring during irradiation. Because of this, it was impossible to remove the foil from the target. Neither Cu, Ni, nor iron dissolve in base. Therefore, a challenging task in process development was identifying a suitable metal for a barrier material that could dissolve in alkaline solution and meet other mechanical and chemical criteria. A literature survey found the following elements that dissolve in alkaline solutions: aluminum, zinc, beryllium, gallium, tin, arsenic, niobium, and tantalum. Aluminum dissolves at about the same rate as uranium metal in 5.0M H_2O_2/1.5M NaOH solution at 70°C. However, there is a strong concern that uranium would react with aluminum during the target irradiation. Germanium and rhenium, although not amphoteric, are reported to dissolve readily in dilute hydrogen peroxide. Of the elements mentioned above, the toxicity of beryllium metal and the low melting point of gallium (30°C) preclude their use. Arsenic is classified as a non-metal and may not have sufficient metallic properties to be made into a

foil. Zinc is an active electropositive element and forms a strong anion with oxygen. It also dissolves readily in sodium-hydroxide/nitrate solution. Work on barrier materials for targets to be processed by dissolution in base has, therefore, focused on zinc.[8]

Three methods of forming the zinc barrier were considered: (1) pressing together zinc and uranium foils, (2) hot dipping the uranium target in molten zinc, and (3) electroplating the zinc onto the uranium foil. One of the most important constraints on the barrier is that it should be of relatively uniform thickness of not much greater than 15 μm to minimize the material to be dissolved after irradiation. Use of pre-formed zinc foil pressed onto the uranium target was eliminated by the high cost and porous nature of the zinc foils thinner than 20 μm. Hot dipping provides a coating of rather poorly controlled thickness, and thicknesses less than 20 μm are unlikely. Electroplating of zinc, on the other hand, seems to provide a relatively simple and inexpensive process with good control over the thickness.[9]

The first task was to develop means to dissolve the zinc barriers. Three types of solutions for dissolving zinc were studied: NaOH, $NaOH/H_2O_2$, and $NaOH/NaNO_3$. A variety of solutions containing NaOH or $NaOH/H_2O_2$ showed dissolution rates less than the desired 2 mg/(cm^2•min). On the other hand, a variety of solutions containing NaOH and $NaNO_3$ gave dissolution rates well above that. A solution of 2.5M NaOH/1M $NaNO_3$ at 70 °C is our standard for rapid dissolution of pure zinc metal. Experiments have confirmed that a zinc coating electroplated onto the uranium-foil surface is also dissolved rapidly by this solution. Analysis by energy dispersive spectroscopy (EDS) of the foils left after dissolution showed that all of the zinc plate was dissolved from the uranium. Liquid scintillation counting of the dissolution solution showed that virtually none of the uranium foil was dissolved with the zinc.

Due to radioactive-decay heat generated within the irradiated LEU, a concern arose regarding whether or not a zinc barrier would melt during transport of the target from the reactor pool to the processing hot cells. The biggest hindrance to the transfer of heat from the target is the relatively small surface area from which heat can be transferred. Sample calculations were made for natural convection in the air immediately after the target leaves the cooling pool and for the possibility that the target will be placed in a cask and shipped over a 24-hour time frame. Although exact temperatures to be experienced by the zinc barriers cannot be predicted, calculations show that temperatures in the range of 300-400°C are likely. Although this is very close to zinc's melting point (420°C), it is expected that the melting point of zinc will not be reached. However, when a zinc-plated uranium foil was heat treated at 375°C overnight in an evacuated glass tube, an intermetallic U/Zn compound was formed.

The intermetallic U/Zn compound is visually distinct from the unheated zinc-plated uranium foil when viewed through a microscope with a magnification of about 440X. Figures 20a and b are micrographs of the Zn-plated DU foil shown in Fig. 5 following this heat treatment. With this intermetallic compound, the interface between the zinc and the uranium is almost indistinguishable, whereas it had been pronounced before. Notice the dendrite formations along the edge of the foil in Fig. 20a. Even if the target is held at low overall temperatures during transport, the fission-product recoil that the zinc barrier is designed to absorb will cause localized heating and most likely cause the formation of this intermetallic compound at the U/Zn interface.

---

[8] As discussed in section 4.2., a zinc fission-barrier is also being considered for acid-side processing targets. This would have the advantage of developing just one target for all processes.

[9] Zinc plating is described in section 4.2.

Solutions suitable for dissolving the intermetallic U/Zn compound were pursued. Attempts to dissolve the zinc from this foil showed that this intermetallic would not dissolve as the zinc plate had from the unheated foils (at 70°C with 50 mL of 2.5M NaOH and 1M $NaNO_3$). A solution of 8M HNO_3 at 70°C dissolved the intermetallic compound but too slowly to be useful.[10] On the other hand, a solution of 1.5M NaOH/5M H_2O_2 appears to dissolve the intermetallic compound faster than it does pure zinc or pure uranium. This solution may be useful for this task, although more experimental work is necessary to clarify the rate of dissolution.

5.2.1.4. UO_2/Al dispersion plates

Work on the alkaline-peroxide dissolution of UO_2/Al dispersion plates is new in 1997. This is the first report of our activities. The density of UO_2 is greater than uranium aluminide, and if the UO_2/Al dispersion is loaded to 40 vol%, an LEU target could contain about three times more uranium than an HEU aluminide target of equivalent geometry. Between five and six times more uranium is needed for an equivalent substitution of LEU for HEU in a ^{99}Mo-production target. Although these LEU targets will contain about one-half the ^{235}U of HEU aluminide targets, (1) expertise is already available for their fabrication, (2) dissolution and processing chemistry will be simpler than that for U_3Si_2, and (3) the time to develop the processing method will be significantly shorter than that for either the U_3Si_2 or uranium-foil targets. Therefore, they may be useful as interium LEU targets while development of the uranium-foil targets is still underway.

Work on recovering ^{99}Mo from a UO_2/Al dispersion target by dissolution in alkaline peroxide solution is underway. Dissolution data were collected by separately adding hydrogen peroxide and a solution of sodium hydroxide to particles of UO_2. All solutions had an initial temperature of 50°C. Typically the reaction between the base and the peroxide caused the temperature to increase rapidly on mixing. From these experiments an empirical rate model was generated of the form:

$$R_u = k \bullet \left[H_2O_2\right]_i^{0.5} \bullet \left[OH^-\right]_i^{0.5} \qquad (24)$$

where R_U is the rate of uranium dissolution in units of mg/(cm^2•min) k is an empirical rate constant, and $[H_2O_2]_i$ and $[OH^-]_i$ are the initial hydrogen peroxide and base concentrations, respectively, in mol/L. A plot of rate vs. $\left[H_2O_2\right]_i^{0.5} \bullet \left[OH^-\right]_i^{0.5}$ is shown in Fig. 21. As seen in Fig. 21, a fairly linear relationship is present. The slope of the best fit line is equal to the rate constant, k = 1.26 mg-L/mol-cm^2-min. Final uranium concentrations as high as 0.35M have been attained in spent dissolver solutions. Uranium precipitates when the peroxide is destroyed. Pressed compacts of aluminum powder and UO_2 have been prepared. The compacts are similar to the "meat" of a UO_2/Al dispersion target. (Figure 22 shows a micrograph of one of these compacts and a drawing showing how the dispersion plate would look.) Dissolution experiments were completed using these compacts. First the aluminum in the compact was dissolved with a solution of 3M sodium hydroxide and 3M sodium nitrate. The aluminum was easily dissolved, and the remaining UO_2 was free-flowing particulate. The UO_2 particles were washed several times with water to remove any residue from the

[10] As discussed in section 5.1.1., BATAN researchers appeared to have had some difficulty in dissolving an irradiated zinc-barrier target in nitric acid.

aluminum dissolution. Finally, the UO_2 was easily dissolved in a solution of 0.5M sodium hydroxide and 5.0M hydrogen peroxide.

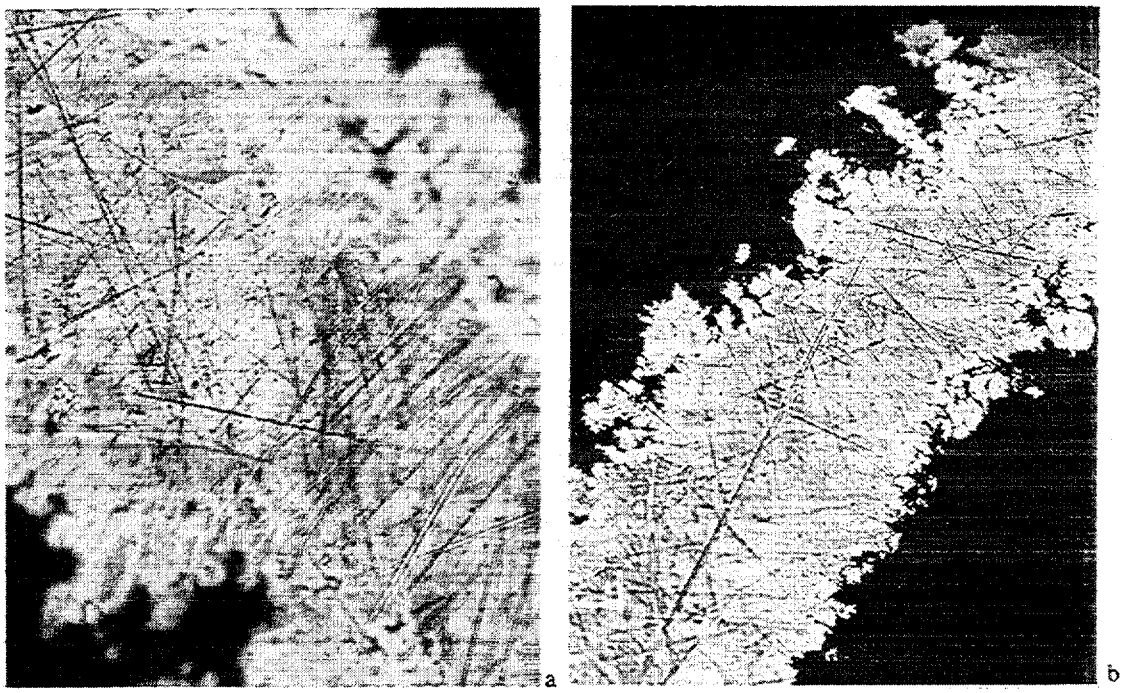

FIG. 20. Two sections of Zn-plated DU foil after heating at 375°C overnight (compare to FIG. 5).

To simulate the reaction between the aluminum matrix and UO_2 during irradiation [56]:

$$Al + UO_2 \rightarrow UAl_x + Al_2O_3 \quad (25)$$

several compacts were heat treated under vacuum at 350°C for 6 and 24 hours. For these compacts, the aluminum could also be easily dissolved, and the remaining UO_2 was also a free-flowing particulate that was easily dissolved in alkaline peroxide. This behavior was vastly different and superior to heat-treated uranium silicide particles, which formed a solid monolith that was difficult to dissolve. Results from low-burnup irradiations of these targets showed that (1) fission-product behavior was as expected based on the UO_2 particle size, and (2) the reaction between UO_2 and the aluminum matrix had no effect on dissolution of the uranium. Although the effects of the longer heating were observed by the swelling and near disintegration of the 24-hour compact, the 6- and 24-hour heat-treated compacts gave the same results following irradiation. In both cases, about 8% of fission products dissolved with the aluminum matrix, while less than 0.2% of the ^{239}Np was found in this solution. (Because ^{239}Np is an activation product and not a fission product, it would remain in the uranium particle after formation. Its low concentration in the aluminum dissolver solution is, therefore, indicative of the small amount of uranium that dissolved.)

Two additional UO_2/Al powder dispersion compacts were prepared. These compacts have been formed into miniplates. Cores punched from the miniplate will be used to study the dissolution of clad miniplates in basic peroxide solutions. In addition, these cores will be

irradiated to a very low burnup using either the ANL Intense Pulsed Neutron Source (IPNS) or the University of Texas reactor. Irradiation of the targets will allow us to conduct tracer-level experiments of the target dissolution and ^{99}Mo recovery and purification steps.

5.2.2. Target processing

Work on base-side processing for the recovery and purification of ^{99}Mo was begun in 1987 and concluded in 1988 [31,37]. All this work was based on use of the LEU silicide targets and the IRE process [2,3]. Conclusions that can be derived from this work are:

- Silica gel formed from acidification of the spent dissolver solution could be a severe problem to molybdenum recovery but can be controlled by keeping silica's concentration below ~0.1M. Even at lower concentrations, soluble silicate decreases the sorption of Mo(VI) onto alumina.

- Uranium precipitation following dissolution by alkaline peroxide must be nearly quantitative so that uranium in solution will not interfere with Mo(VI) sorption on alumina. This means that peroxide destruction must be complete, allowing uranium hydroxides to precipitate.

- In spite of these two potential problems, experiments where U_3Si_2 miniplates were irradiated to low burnup showed that the LEU target would give satisfactory performance using the modified dissolution followed by the standard HEU process.

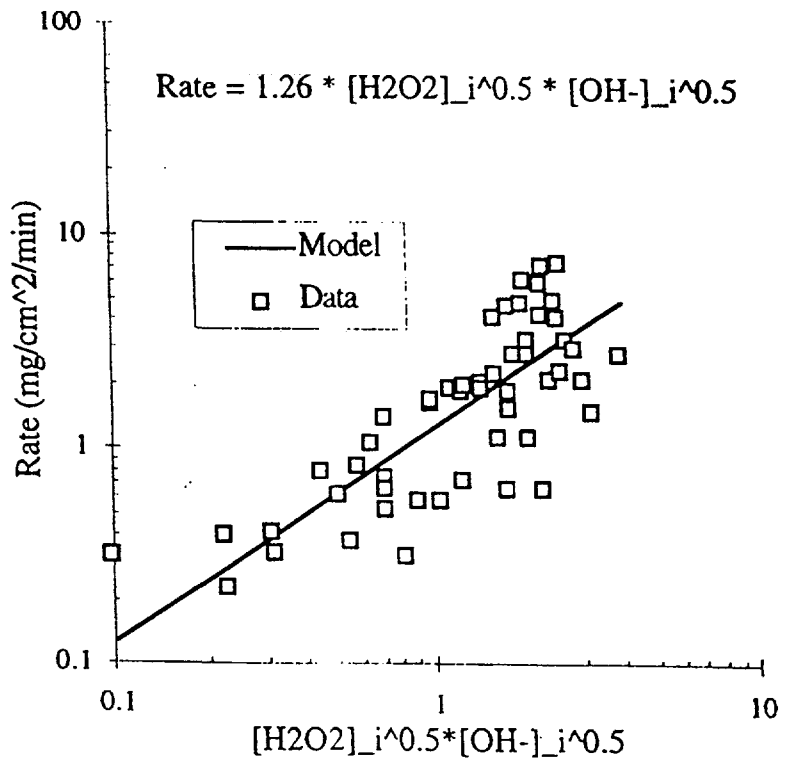

FIG. 21. Rate data and model fit for the dissolution of UO_2 in alkaline peroxide. Initial temperature of reagents was 50°C.

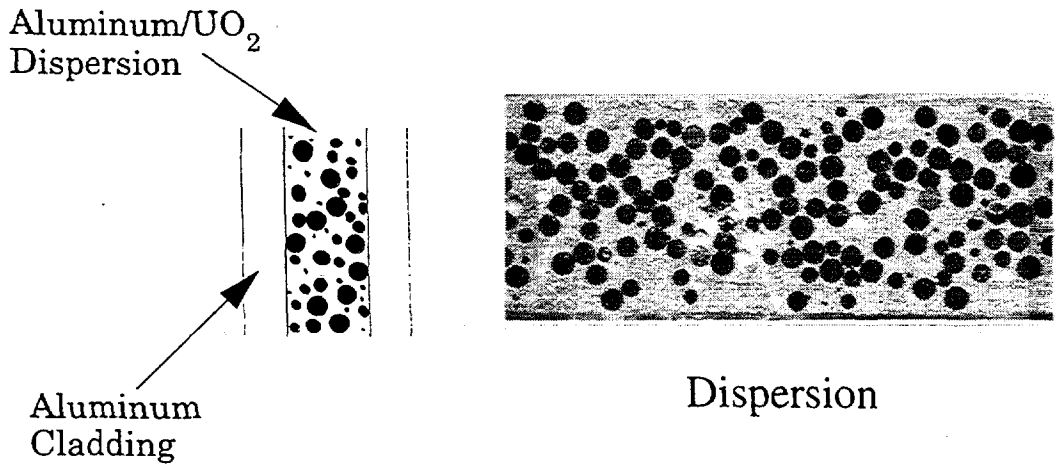

FIG. 22. Illustration of a UO_2/Al-dispersion plate and micrograph of a UO_2/Al-dispersion compact.

- Molybdenum recovery was high, and purification was as expected when the two-step dissolution was followed by acidification and molybdenum sorption on an alumina column.

Because the spent dissolver solutions of LEU foil or oxide targets will not contain significant concentrations of silica, the major concern of U_3Si_2 processing will be eliminated. Because of the need for zinc fission barriers, the feed to the primary recovery step from foil target will contain significant quantities of zinc, which may affect the recovery. However, it will not contain the extremely high concentrations of aluminum found in the plate-type targets.

In the IRE process, three 4.2-g uranium targets are dissolved in 1.6 L of base. This produces a spent dissolver solution near saturation in $NaAlO_2$ (2.1M). The volume of the feed to the primary molybdenum-recovery step would be increased significantly by two of the three LEU targets. With the IRE process,

- Dissolution of a silicide target (with 5 times the uranium) would require about twice the solution volume due to its being a two-step process. The volume to dissolve the aluminum would be the same for the HEU and LEU-silicide targets. The uranium silicide could be dissolved in about 50% of that volume. Rinse solutions would account for the remaining volume. The feed to the primary recovery step might need to be increased further to keep silica in solution.

- Dissolution of two LEU oxide targets (each containing about three times the amount of uranium) would generate about three times the volume of the HEU target. A two-step process is also required for their dissolution. Twice the aluminum would require twice the volume to dissolve it. Dissolution of the UO_2 would require about 50% of that volume, with the remainder due to rinse solutions.

- Dissolution of the LEU-foil target would require the same or less volume than the HEU target to dissolve the Zn-coated LEU foil. Approximately 50% of the HEU-target volume would be to dissolve the uranium, another 20% to dissolve the zinc, and the remainder for rinse solutions.

Once conditions for LEU target dissolution are firm, we will need to reinvestigate the effects of these compositional and volume differences on the primary molybdenum-recovery step.

6. PLANNED R&D ACTIVITIES

We will continue our development activities on both acid- and base-side processes. The LEU-modified Cintichem process needs to be demonstrated on a commercial scale before it can be accepted. Demonstrations are planned at both the Indonesian PUSPIPTEK facility and Sandia National Laboratories. Sandia will actively take part in obtaining FDA approval for LEU Cintichem-type targets, while BATAN will assist in developing economic factors related to the conversion to LEU.

Target fabrication for LEU foils still needs to be optimized in terms of both (1) reproducibly successful disassembly following irradiation and (2) ease of fabrication. The effectiveness of electrodeposited fission barriers must also be demonstrated.

A commercial partner must be acquired for the base-side processing. The partner will assist in (1) refining our design of the dissolution system, (2) focusing our development activities, and (3) demonstrating processing of irradiated full-scale targets.

The RERTR Program wishes to work with all current and future producers of ^{99}Mo to assure that, ultimately, no HEU is needed for ^{99}Mo production.

7. CONCLUSIONS

Conversion of fission-product ^{99}Mo production from HEU to LEU has been proven technically feasible. However, full-scale demonstrations and partnerships with producers world-wide are needed to (1) complete development activities, (2) clarify economic disincentives to conversion, and (3) gain acceptance of the targets, processes, and ^{99}Mo product from LEU. The US Department of Energy and the RERTR Program are committed to eliminating HEU as reactor fuel and as target material for radioisotope production.

REFERENCES

[1] KONRAD, J., "Facilities for the Irradiation of ^{235}U for the Production of ^{99}Mo at the HFR Petten", Irradiation Technology, Proc. of the Int. Topical Mtg., Grenoble, France (1982) 677-683.

[2] SALACZ, J., "Production of Fission Mo-99, I-131 and Xe-133", Revue IRE Tijdschrift, Vol. 9, No. 3 (1985).

[3] FALLAIS, C.J., MOREL de WESTGAVER, A., HEEREN, L., BAUGNET, J.M., GANDOLFO, J.M., BOEYKENS, W., "Production of Radioisotopes with BR2 Facilities", BR2 Reactor Mtg., Mol, Belgium, INIS MF 4426, pp. IX-1 to -11 (1978).

[4] SAMEH, A.A., ACHE, H.J., Production techniques of fission molybdenum-99, Radiochimica Acta **41** (1987) 65-72.

[5] MARQUES, R.O., CRISTINI, P.R., FERNANDEZ, H., MARZIALE, D., "Operation and Installation for Fission ^{99}Mo Production in Argentina", Fission Molybdenum for Medical Use, Proc. of Technical Committee Mtg. Organized by the International Atomic Energy Agency, Karlsruhe, October 13-16, 1987, IAEA-TECDOC-515 (1989) 23-33.

[6] SAMEH, A.A., ACHE, H.J., "Production Techniques of Fission ^{99}Mo", Fission Molybdenum for Medical Use, Proc. of Technical Committee Mtg. Organized by the International Atomic Energy Agency, Karlsruhe, October 13-16, 1987, IAEA-TECDOC-515 (1989) 47-64.

[7] SALACZ, J., "Processing of Irradiated ^{235}U for the Production of ^{99}Mo, ^{131}I, and ^{133}Xe Radioisotopes", Fission Molybdenum for Medical Use, Proc. of Technical Committee Mtg. Organized by the International Atomic Energy Agency, Karlsruhe, October 13-16, 1987, IAEA-TECDOC-515 (1989) 149-154.

[8] SAMEH, A.A., BERTRAM-BERG, A., "HEU and LEU MTR Fuel Elements as Target Materials for the Production of Fission Molybdenum", Proc. of the 1992 International Meeting on Reduced Enrichment for Research and Test Reactors, Roskilde, Denmark, September 27-October 1, 1992, Argonne National Laboratory Report, ANL/RERTR/TM19, CONF-9209266 (1993) 313-333.

[9] COLS, H., CRISTINI, P.R., MARQUES, R.O., "Preliminary Investigations on the Use of Uranium Silicide Targets for Fission Mo-99 Production", Proc. of 1994 International Meeting on Reduced Enrichment for Research and Test Reactors, Williamsburg, Virginia, September 18-23, 1994, Argonne National Laboratory Report, ANL/RERTR/TM-20 (in press).

[10] JONES, R.T., "AEC-2 Experiments in Support of ^{99}Mo Production in NRU", AECL-7335 (1982).

[11] BURRIL, K.A., HARRISON, R.J., "Development of the ^{99}Mo Process at CRNL", Fission Molybdenum for Medical Use, Proc. of Technical Commnittee Mtg. Organized by the International Atomic Energy Agency, Karlsruhe, October 13-16, 1987, IAEA-TECDOC-515 (1989) 35-46.

[12] ARINO, H., KRAMER, H.H., McGOVERN, J.J., THORNTON, A.K., "Production of High Purity Fission Product Molybdenum-99", U.S. Patent 3, 799, 883 (1974).

[13] ARINO, H., COSOLITO, F.J., GEORGE, K.D., THORNTON, A.K., "Preparation of a Primary Target for the Production of Fission Products in a Nuclear Reactor", U.S. Patent 3, 940, 318 (1976).

[14] SNELGROVE, J.L., HOFMAN, G.L., TRYBUS, C.L., WIENCEK, T.C., "Development of Very-High-Density Fuels by the RERTR Program", Proc. of the 19th International Meeting on Reduced Enrichment for Research and Test Reactors, Seoul, Korea, October 7-10, 1996 (1997) 46-54.

[15] MARSHALL, S.L., REDEY, L., VISSERS, D.R., VANDEGRIFT, G.F., MATOS, J.E., "Continuing Investigations on Electrochemical Preparation of LEU Targets for ^{99}Mo Production", Proceedings of the 1988 International Meeting on Reduced Enrichment for Research and Test Reactors, San Diego, California, September 18-24, 1988, Argonne National Laboratory Report, ANL/RERTR/TM-13, CONF-8809221 (1993) 443-450.

[16] WIENCEK, T.C., HOFMAN, G.L., WOOD, E.L., WU, C.T., SNELGROVE, J.L., "LEU ^{99}Mo Target Fabrication and Testing: Overview, Status, and Plans", Proceedings of the 1994 International Meeting on Reduced Enrichment for Research and Test Reactors, Williamsburg, Virginia, September 18-23, 1994, Argonne National Laboratory Report, ANL/RERTR/TM-20 (in press).

[17] HOFMAN, G.L., WIENCEK, T.C., WOOD, E.L., SNELGROVE, J.L., "Irradiation Tests of ^{99}Mo Isotope Production Employing Uranium Metal Foils", presented at the 19th International Meeting on Reduced Enrichment for Research and Test Reactors, October 7-10, 1996, Seoul, Korea (1996).

[18] O'LEARY, W.J., CARLSON, R.J., SLUNDER, C.J., FIORENTINO, R.J., BEACH, J.G., GRAHAM, A.K., NILAND, T.B., McBRIDE, C.C., MAY, R.C., "Meeting at BMI on Electroplating Uranium for Extrusion Cladding", du Pont de Nemours & Company Report, DPW-56-405 (November 8, 1956).

[19] LUNDQUIST, J.R., BRAUN, R.L., STROMATT, R.W., "Nickel Plating Uranium: Review of Laboratory Studies", Plating, Vol. 54, No. 7 (1967) 829-837.
[20] DINI, J.W., CORONADO, P.R., "Electroplating Uranium with Nickel", SCL-DR-67-44 (1967).
[21] DINI, J.W., CORONADO, P.R., "Preparation of Uranium for Electroplating with Nickel", SCL-DC-68-50 (1968).
[22] DINI, J.W., CORONADO, P.R., "Preparation of Uranium for Electroplating with Nickel", Trans. Inst. Metal Finish. Vol. 47(Pt. 1) (1969) 1-6.
[23] DINI, J.W., JOHNSON, H.R., HELMS, J.R., "Nickel Plated Uranium Bond Strength", Plating, Vol. 61, No. 1 (1974) 53-56.
[24] SRINIVASAN, B., HUTTER, J.C., JOHNSON, G.K., VANDEGRIFT, G.F., "Development of Dissolution Process for Metal Foil Target Containing Low Enriched Uranium", Proceedings of the 1994 International Meeting on Reduced Enrichment for Research and Test Reactors, Williamsburg, Virginia, September 18-23, 1994, Argonne National Laboratory Report, ANL/RERTR/TM-20 (in press).
[25] SRINIVASAN, B., LEONARD, R. A., AASE, S., VANDEGRIFT, G. F., MOERIDUN, RAUF, A. A., LUBIS, H., HARDI, A., AMINI, S., and NAMPIRA, Y., "Processing of LEU Targets for ^{99}Mo Production--Dissolution of Metal Foils by Nitric-Acid/Sulfuric-Acid Mixtures", Proceedings of the XVIII International Meeting on Reduced Enrichment for Research and Test Reactors, Paris, France, September 17-21, 1995, paper no. 3-2 (1996).
[26] LEONARD, R.A., CHEN, L., MERTZ, C.J., VANDEGRIFT, G.F., "Progress in Dissolving Modified LEU Cintichem Targets", Proceedings of the 19th International Meeting on Reduced Enrichment for Research and Test Reactors, Seoul, Korea, October 7-10, 1996 (1997) 189-197.
[27] ELWELL, A., Analytical Chemistry of Molybdenum and Tungsten, Pergamon Press, Oxford, (1977) 40-41.
[28] PARKER, A., Analytical Chemistry of Molybdenum, Springer-Verlag, Berlin, New York, (1983) 146-147.
[29] BUSEV, A. I., Analytical Chemistry of Molybdenum (translated by J. Schmorak), Humphrey Science Publishers, Ann Arbor, (1969) 30-31.
[30] VANDEGRIFT, G.F., CHAIKO, D.J., HEINRICH, R.R., KUCERA, E.T., JENSEN, K.J., POA, D.S., VARMA, R., VISSERS, D.R., "Preliminary Investigations for Technology Assessment of ^{99}Mo Production from LEU Targets", 1986 International Meeting on Reduced Enrichment for Research and Test Reactors (RERTR), November 3-6, 1986, Gatlinburg, Tennessee, ANL/RERTR/TM-9,CONF-861185 (1988) 64-79.
[31] VANDEGRIFT, G.F., KWOK, J.D., MARSHALL, S.L., VISSERS, D.R., MATOS, J.E., "Continuing Investigations for Technology Assessment of ^{99}Mo Production from LEU Targets", presented at the 1987 International Meeting on Reduced Enrichment for Research and Test Reactors (RERTR), September 28-October 2, 1987, Buenos Aires, Argentina.
[32] WU, D., BUCHHOLZ, B.A., LANDSBERGER, S., VANDEGRIFT, G.F., "Processing of LEU Targets for Mo Production–Testing and Modification of the Cintichem Process", Proceedings of the XVIII International Meeting on Reduced Enrichment for Research and Test Reactors, Paris, France, September 17-21, 1995, paper no. 3-3 (1996).
[33] WU, D., LANDSBERGER, S., VANDEGRIFT, G.F., Application of neutron activation analysis in a fission molybdenum separation study, J. Radioanal. Nucl. Chem. **216** (1997) 101-105.
[34] ALILUDIN, Z., MUTALIB, A., SUKMANA, A., KADARISMAN, GUNWAN, A.H., VANDEGRIFT, G.F., SRINIVASAN, B., SNELGROVE, J.L., WU, D., "Processing of

LEU Targets for ^{99}Mo Production—Demonstration of a Modified Cintichem Process", Proceedings of the XVIII International Meeting on Reduced Enrichment for Research and Test Reactors, Paris, France, September 17-21, 1995, paper no. 3-4 (1996).

[35] WU, D., LANDSBERGER, S., VANDEGRIFT, G.F., "Progress in Chemical Treatment of LEU Targets By the Modified Cintichem Process", 19th International Meeting on Reduced Enrichment for Research and Test Reactors, Seoul, Korea, October 6-10, 1996 (1996) 172-179.

[36] MASSEY, C.D., MILLER, D.L., CARSON, S.D., WHEELER, T.A., LONGLEY, S.W., COATS, R.L., PARMA, E.J., McDONALD, M., VERNON, M.E., BOURCIER, S.C., MILLS, S.G., TRENNEL, A.J., BOLDT, K.R., "Feasibility Study of Medical Isotope Production at Sandia National Laboratories", SAND95-2703 Rev. O, Sandia National Laboratories (1995).

[37] KWOK, J. D., VANDEGRIFT, G.F., MATOS, J.E., "Processing of Low-Burnup LEU Silicide Targets", Proc. of the 1988 International Meeting on Reduced Enrichment for Research and Test Reactors, San Diego, California, September 18-24, 1988, ANL/RERTR/TM-13, CONF-8809221 (1993) 434-442.

[38] VANDEGRIFT, G.F., KWOK, J.D., CHAMBERLAIN, D.B., HOH, J.C., STREETS, E.W., VOGLER, S., THRESH, H.R., DOMAGALA, R.F., WIENCEK, T.C., MATOS, J.E., "Development of LEU Targets for ^{99}Mo Production and their Chemical Processing--Status 1989", Proc. of the XIIth International Meeting on Reduced Enrichment for Research and Test Reactors, Berlin, September 10-14, 1989 (1991) 421-433.

[39] VANDEGRIFT, G.F., HUTTER, J.C., SRINIVASAN, B., MATOS, J.E., SNELGROVE, J.L., "Development of LEU Targets for ^{99}Mo Production and Their Chemical Processing Status 1993", Proc. of the 16th International Meeting on Reduced Enrichment for Research and Test Reactors, Oarai, Japan, October 4-7, 1993, JAERI-M 94-042 (1994) 394-400.

[40] HUTTER, J.C., SRINIVASAN, B., VICEK, M., VANDEGRIFT, G.F., "Production of Mo-99 Using Low-Enriched Uranium Silicide", Proc. of the 1994 International Meeting on Reduced Enrichment for Research and Test Reactors, Williamsburg, Virginia, September 18-23, 1994, Argonne National Laboratory Report, ANL/CMT/CP-84245 (1994).

[41] BUCHHOLZ, B.A., VANDEGRIFT, G.F., "Processing of LEU Targets for ^{99}Mo Production—Dissolution of U_3Si_2 Targets by Alkaline Hydrogen Peroxide", Proc. to the XVIII International Meeting, Reduced Enrichment for Research and Test Reactors, Paris, France, September 18-21, 1995, paper 3-6 (1996).

[42] CHEN, L., DONG, D., BUCHHOLZ, B.A., WU, D., VANDEGRIFT, G.F., "Progress In Alkaline Peroxide Dissolution of LEU Metal And Silicide Targets", Proc. to the 19th International Meeting on Reduced Enrichment for Research and Test Reactors, Seoul, Korea, October 7-10, 1996 (1996) 180-187.

[43] BUCHHOLZ, B. A., HUTTER, J.C., VANDEGRIFT, G.F., Dissolution kinetics of U_3Si_2 particles in alkaline hydrogen peroxide, Nucl. Tech. **118** (1997) 225.

[44] SCHUMB, W.C., SATTERFIELD, C.N., WENTWORTH, R.L., Hydrogen Peroxide, Reinhold Publishing Corp., New York (1955).

[45] KARRAKER, D.G., "Radiation Effects on the Solubility of Plutonium in Alkaline High Level Waste", WSRC-MS-94-0278X, Westinghouse Savannah River Center (1994).

[46] DOMAGALA, R.F., WIENCEK, T.C., THRESH, H.R., U-Si and USi-Al dispersion fuel alloy development for research and test reactors, Nucl. Tech. **62** (1983) 353.

[47] KIM, C.K., KIM, K.H., JANG, S.J., JO, H.D., KUK, I.H., "Characterization of Atomized U_3Si_2 Powder for Research Reactor", Proceedings of the 1992 International Meeting on Reduced Enrichment for Research and Test Reactors, Roskilde, Denmark, September 27-October 1, 1992, Argonne National Laboratory Report ANL/RERTR/TM-19 (1993) 76-84.

[48] HOFMAN, G.L., NEIMARK, L.A., OLQUIN, F.L., "The Effect of Fabrication Variables on the Irradiation Performance of Uranium Silicide Dispersion Fuel Plates", Proc. of 1986 International Meeting on Reduced Enrichment for Research and Test Reactors (RERTR), November 3-6, 1986, Gatlinburg, Tennessee, ANL/RERTR/TM-9, CONF-861185 (1986) 201.

[49] DONG, D., VANDEGRIFT, G.F., AMINI, S., HERSUBENO, J.B., NASUTION, H., and NAMPIRA, Y., "Processing of LEU Targets for ^{99}Mo Production--Dissolution of U_3Si_2 Targets by Alkaline Hydrogen Peroxide", Proc. of the XVIII International Meeting on Reduced Enrichment for Research and Test Reactors (RERTR), Paris, France, September 18-21, 1995, paper no. 3-5 (1996).

[50] DONG, D., VANDEGRIFT, G.F., Kinetics of dissolution of uranium metal foil by alkaline hydrogen peroxide, Nucl. Sci. and Engin. **124** (1996) 472.

[51] DONG, D., VANDEGRIFT, G.F., Alkaline peroxide processing of LEU targets for ^{99}Mo production-decomposition of hydrogen peroxide, Nucl. Sci. and Engin. **126** (1997) 213.

[52] WARF, L., Technical Report #CC-1194, December 9, 1943.

[53] GINDLER, J.E., The radiochemistry of uranium, U.S. DOE, Technical Information Center (March 1962).

[54] WARF, J.C., "Some Reactions of Uranium Metal", Chemistry of Uranium: Collected Papers, J.J. Katz and E. Rabinowitch, Eds., U.S. Atomic Energy Commission, Technology Information Service Extension (1958) 29-37.

[55] LARSON, R.P., Dissolution of uranium metal and its alloys, Anal. Chem. 31 (1959) 545-549.

[56] HOFMAN, G.L., REST, J., SNELGROVE, J.L., "Irradiation Behavior of Uranium Oxide-Aluminum Dispersion Fuel", Proc. to the 19th International Meeting on Reduced Enrichment for Research and Test Reactors, Seoul, Korea, October 7-10, 1996 (1996) 201-230.

THE ACCELERATOR PRODUCTION OF MOLYBDENUM-99

R.M. LAMBRECHT
Medical and Natural Sciences Research Centre,
University of Tübingen, Germany

T. SEKINE
Department of Materials Science and Department of Radioisotopes,
Japan Atomic Energy Research Institute,
Gunma, Japan

H. VERA RUIZ
Industrial Chemistry and Applications Section,
International Atomic Energy Agency,
Vienna

Abstract

The ALICE code was used to calculate the theoretical excitation functions for proton induced reactions on ^{100}Mo that lead to the production of Nb, Mo and Tc isotopes. The ALICE code predicts a maximum cross section of the order of 100 mb for the ^{100}Mo(p,pn)^{99}Mo nuclear reaction. ALICE predicts that the production of a few Curies of ^{99}Mo is feasible if high intensity (mA) protons are degraded from 50→30 MeV in a target of highly isotopically enriched ^{100}Mo. The ALICE code can not be used to predict the cross sections for the isomeric states for the ^{100}Mo(p,2p)$^{99m+g}$Nb → ^{99}Mo reactions. However, the predicted cross section for protons on ^{100}Mo to yield ^{99}Nb suggests that the (p,2p) reaction channel does not contribute significantly to the thick target yield of ^{99}Mo. Several considerations suggest that accelerator production of ^{99}Mo→^{99m}Tc generators is not a practical economic alternative to fission produced ^{99}Mo. Considerations for the cyclotron production of ^{99m}Tc are discussed.

1. INTRODUCTION

The continuing concerns [1, 2] about the continuing supply of ^{99}Mo for the ^{99}Mo→^{99m}Tc generator motivated us to compare theoretical predictions of the excitation functions for proton induced reactions on ^{100}Mo to the discrepancies between the reports of Beaver and Hupf [3], Almedia and Helus [4], Lagunas-Solar et al. [5], and Levkovskii [6] of the experimental thick target yields for the ^{nat}Mo(p,pn)^{99}Mo nuclear reaction. Beaver and Hupf [3] suggested that a 22 MeV cyclotron is capable of producing a sufficient quantity of ^{99}Mo by the ^{100}Mo(p,pn)^{99}Mo and the ^{nat}Mo → ^{99}Mo nuclear reactions to serve as a reserve ^{99}Mo→^{99m}Tc generator. Almeida and Helus [4] extended the experimental measurements up to 25 MeV, and reported yields in good agreement with Beaver and Hupf [3]. Lambrecht [7] noted the requirement for nuclear data concerning the cyclotron production of ^{99m}Tc and ^{99}Mo at an IAEA Consultants' Meeting on "Data Requirements for Medical Radioisotope Production" that was held in Tokyo in 1988. This stimulated some interest [5,6], but failed to resolve the practical aspects necessary to lead to a conclusion on the feasibility of accelerators as alternative production methods for these medically important radionuclides. However, Lagunas-Solar et al. [5] rationalised that their experimental measurements for reactions leading to ^{99}Mo with 68→ 8 MeV protons on ^{nat}Mo is possible and justifiable under certain circumstances to meet regional needs of developing nations for the ^{99}Mo→^{99m}Tc generator. The predictions of Lagunas-Solar et al. [5,8] were qualified. They extrapolated their data from natural isotopic composition Mo to highly enriched ^{100}Mo targets, and proposed using a 70 MeV H^- (dual beam, 400 μA total) accelerator.

A comparison of the experimental production yields reported in the literature indicates that in all cases Mo of natural isotopic composition was used as the target material. The results were extrapolated to the highest isotopic enrichment ^{100}Mo available (i.e. 97.3%). The natural isotopic composition of ^{100}Mo is 9.6%. Unfortunately, no evaluation details are given in the nuclear data tables of the ^{100}Mo(p,pn)^{99}Mo cross-sections measured by Levkovskii [6].

The nuclear data for proton and deuteron induced reactions on ^{nat}Mo and ^{100}Mo targets leading to ^{99}Mo are sparse. Sonck et al. [6] reviewed the limited production possibilities for deuteron energies up to 50 MeV in another chapter of this TECDOC.

We limited this study to proton induced reactions, namely because it is not common to find an accelerator interested to provide >20 MeV deuterons at high beam currents. To a first approximation one would not anticipate significant differences in the magnitude of cross sections of the (p,pn) and the (d,dn) nuclear reactions on ^{100}Mo.

Therefore, we have investigated the feasibility of accelerator production of ^{99}Mo beginning with the theoretical calculations of nuclear reactions to predict relevant excitation functions using the ALICE code. The hybrid–ALICE code uses the Weisskopf-Ewing evaporation model, the Bohr-Wheeler model for fission, and the geometry dependent hybrid model for precompound decay.

The hybrid model is relevant to the precompound decay, and not to the compound decay. The hybrid means a marriage between two theories on the precompound decay. The geometry dependent hybrid model is a further revision of the hybrid model.

The ALICE code has found applications for estimation of parameters for the production of medical radioisotopes. For example, see: Steyn G. F., et al. [10], Lagunas-Solar et al. [11]; Mustafa [12], Oblozinsky [13,14] and Shigeta et al. [15].

2. CROSS-SECTION CALCULATIONS

The calculations were performed using the framework of the geometry dependent hybrid model [16-20] for the pre-equilibrium emission of neutrons and protons in combination with the Weisskopf-Ewing formalism [21] for the subsequent equilibrium emission of neutrons and protons, deuterons and alpha particles. The calculations are based almost on default options in the code [20]. The initial exciton configuration given by Blann and Vonach [22] were used for the pre-equilibrium calculations. The initial exciton number, the initial excited neutron number and the initial excited proton number were assumed to be 3.0, 0.8 and 1.2, respectively. The exciton includes the particle and the hole in the nucleus. The initial exciton number [3] is the sum of particles and holes. The initial excited proton number (1.2) corresponds to the initial proton particle number, which includes a portion of the projectile proton. The number 3-0.8-1.2 = 1 is the initial hole number. The number 0.8 +1.2 = 2 is the initial particle number. The optical model potential based on the nucleon mean free paths was used to estimate the intranuclear transition rates. Particle binding energies were internally calculated using the Myers and Swiatecki mass formula [23]. Inverse cross sections were also given by the code.

In the calculations of the level densities, the default value of A/8 was taken for the level density parameter and a pairing-energy shift of the effective ground state was calculated from the Myers and Swaitecki (1967) mass formula which was introduced together with a shell effect correction shift.

3. RESULTS AND DISCUSSION

Proton induced reactions on ^{100}Mo could lead to the direct production of ^{99m}Tc via the ^{100}Mo(p,2n)^{99m}Tc nuclear reaction; or the production of ^{99m}Tc by two possible generator routes based on nuclear reactions, namely the ^{100}Mo(p,pn)^{99}Mo $\rightarrow$ ^{99m}Tc and the ^{100}Mo(p,2p)^{99}Nb $\rightarrow$ ^{99}Mo $\rightarrow$ ^{99m}Tc reactions. The ALICE code predictions of excitation functions for the 10 to 70 MeV proton induced reactions on ^{100}Mo that lead to the generator and direct production of Tc radioisotopes are shown in Figures 1-3.

Figure 4 is a comparison of excitation function predicted by the ALICE code to lead to formation of ^{99}Mo by proton irradiation of ^{100}Mo to two sets of experimental cross section measurements. Exp. 1 is the data of Lagunas-Solar et al. (1991), and Exp. 2 is data reported by Scholten, Lambrecht, Cogneau, Qaim and Vera Ruiz [24]. The theoretical excitation function lies between the two sets of experimental data, and is within 30% of the cross section of either curve over most of the energy range studied. A consideration in isotope production is the thick target production yield of the radioisotope of interest. Integration of the excitation function for protons degraded from 50 $\rightarrow$ 30 MeV using >98% isotopic enrichment ^{100}Mo suggests the maximum production rate attainable would be of the order of 27 GBq/μA at saturation. This implies that even with mA beam currents only a few generators could be produced from a cyclotron run. Furthermore, since the ^{99}Mo would not be carrier-free, it would likely be necessary to use the gel generator approach. In addition it would be required to recycle the generators in order to re-use the expensive ^{100}Mo target material. In our opinion the accelerator production of ^{99}Mo is not a viable alternative to fission produced ^{99}Mo. Figure 4 is a comparison of excitation function predicted by the ALICE code to lead to formation of ^{99}Mo by proton irradiation of ^{100}Mo to two sets of experimental cross section measurements. Exp. 1 is the data of Lagunas-Solar et al. (1991), and Exp. 2 is data reported by Scholten, Lambrecht, Cogneau, Qaim and Vera Ruiz [24]. The theoretical excitation function lies between the two sets of experimental data, and is within 30% of the cross section of either curve over most of the energy range studied. A consideration in isotope production is the thick target production yield of the radioisotope of interest. Integration of the excitation function for protons degraded from 50 $\rightarrow$ 30 MeV using >98% isotopic enrichment ^{100}Mo suggests the maximum production rate attainable would be of the order of 27 GBq/μA at saturation. This implies that even with mA beam currents only a few generators could be produced from a cyclotron run. Furthermore, since the ^{99}Mo would not be carrier-free, it would likely be necessary to use the gel generator approach. In addition it would be required to recycle the generators in order to re-use the expensive ^{100}Mo target material. In our opinion the accelerator production of ^{99}Mo is not a viable alternative to fission produced ^{99}Mo.

During this work we noticed an internal discrepancy in the paper of Lagunas-Solar et al. [5] that we were unable to resolve. Numerical data in their Table V are not the same as the data given in Figure 10 in the same paper. See Figure 5. For purposes of the present work we have used only the numerical data.

Cross section measurements for the ^{100}Mo(p,2p)$^{99m+g}$Nb nuclear reaction on isotopically enriched ^{100}Mo are not available mainly due to the fact that ^{99m}Nb has only a 15 sec half life, and the 2.6 min half life of ^{99g}Nb. The isomeric transition yield of ^{99m}Nb has not been reported. ALICE predicts the (p,2p) reaction would have a maximum cross section about a factor of 100 less than the favored (p,pn) nuclear reaction. We note that Lagunas-Solar et al. [5,8] suggested a contribution of the ^{100}Mo(p,2p)$^{99m+g}$Nb $\rightarrow$ ^{99}Mo sequence to the origination of structure in their plot of the excitation function for ^{nat}Mo(p,x)^{99}Mo reactions. We are cautious to accept that the (p,2p) induced reactions are relevant in consideration of the

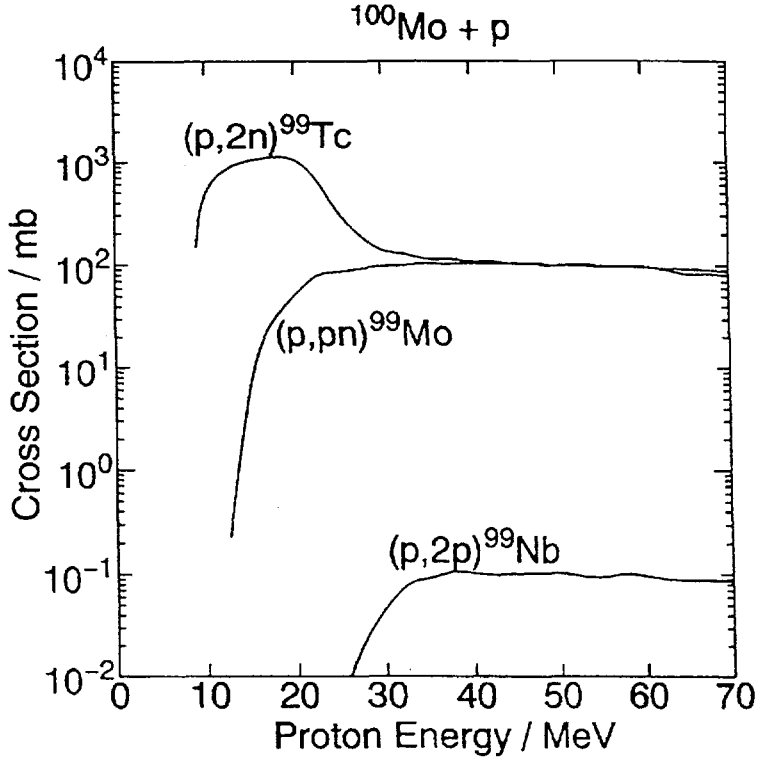

FIG. 1. ALICE code predictions for the proton induced excitation functions for production of ^{99m}Tc.

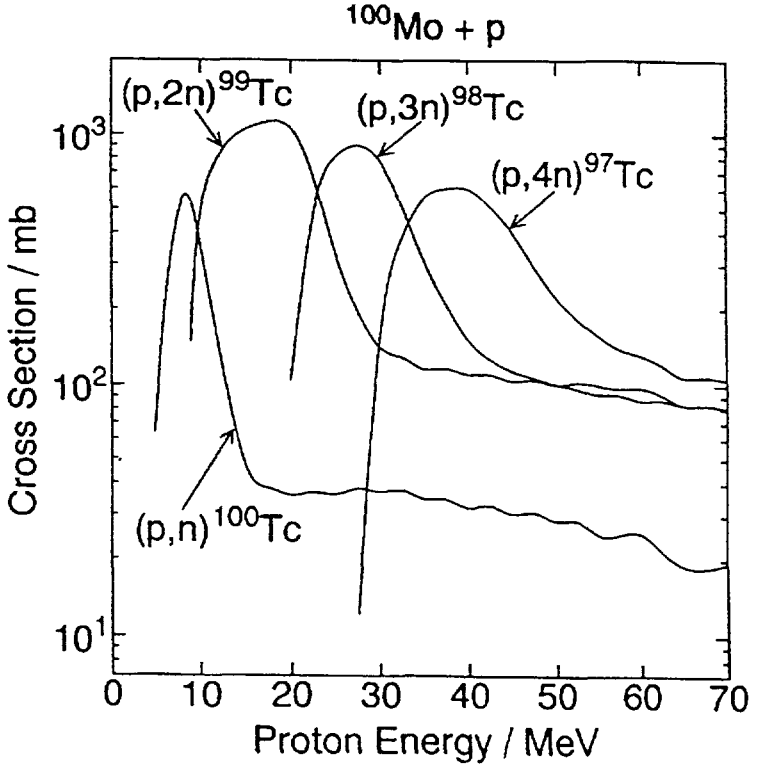

FIG. 2. Excitation functions for ^{97}Tc, ^{98}Tc and ^{99}Tc for proton irradiation of ^{100}Mo.

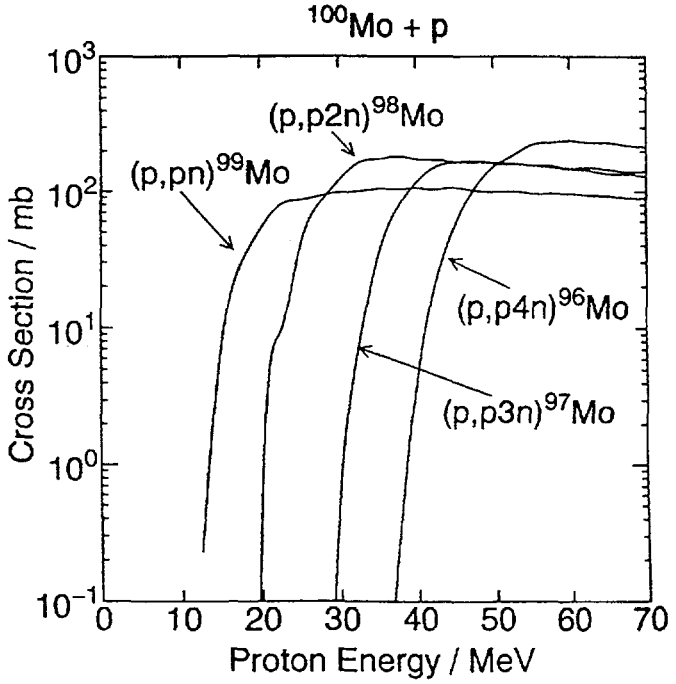

FIG. 3. Excitation functions leading to ^{97}Mo,^{98}Mo and ^{99}Mo for proton irradiation of ^{100}Mo.

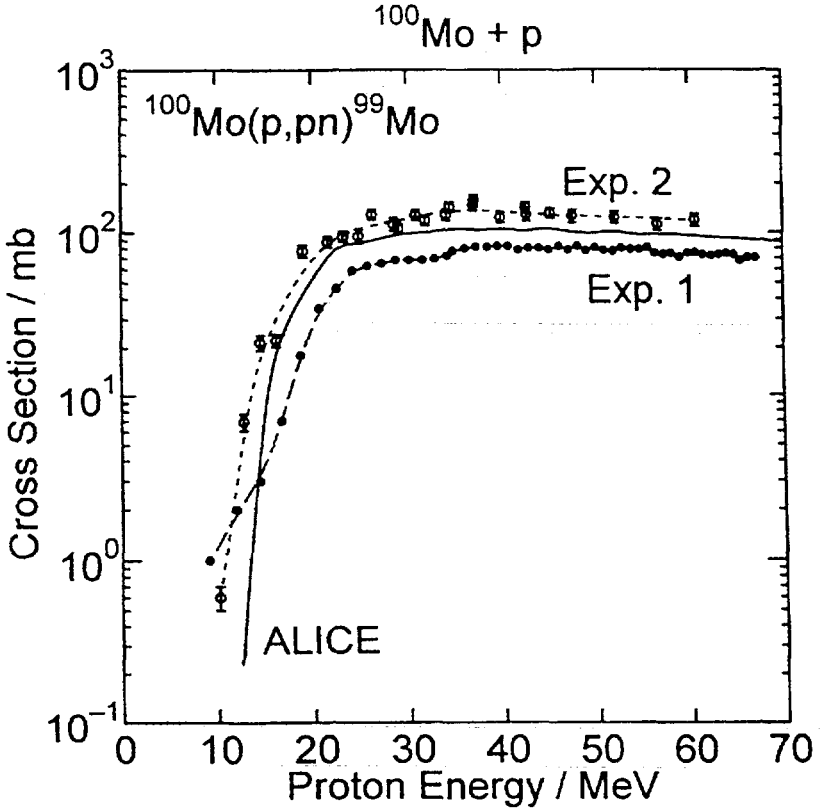

FIG. 4. Comparison of excitation function predicted by the ALICE code to lead to formation of ^{99}Mo by proton irradiation of ^{100}Mo to two sets of experimental cross section measurements Exp. 1 is the data from [5]. Exp. 2 is data reported by [24].

potential accelerator production of the $^{99}Mo \rightarrow {}^{99m}Tc$ generator. In particular, Lagunas-Solar et al. [5], degraded the proton beam from 68 MeV in a stack of ^{nat}Mo foils. Considerable error is anticipated to arise in the calculation of the incident and exit proton beam energy from each of the subsequent targets due to beam energy straggling particularly at low energies. The range-energy errors propogate and may lead to large errors on a result which depends expontentially on energy [12]. Further error could arise in the extrapolation of specific excitation functions to the available ^{100}Mo isotopic enrichment of 98.5% arising from each isotope of Mo when only ^{nat}Mo targets wereused for the experimental measurements. (The natural isotopic composition of ^{100}Mo is only 9.6%) Probably in this procedure different factors were used that are not specifically mentioned in the published reports. In addition, Lagunas-Solar [25] reported that his measurements in 1991 had not taken into account the co-production of a Zr radionuclidic impurity (γ = 141 KeV; not reported) that overlapped in the γ - spectrum of ^{99m}Tc.

Fig. 3 depicts the theoretical excitation functions leading to ^{97}Mo, ^{98}Mo and ^{99}Mo by proton irradiation of ^{100}Mo from the threshold up to 70 MeV. Both ^{97}Mo and ^{98}Mo are stable isotopes. However, repeated long term irradiation and recycling of the enriched ^{100}Mo target material would lead to eventual dilution of the isotopic enrichment of the ^{100}Mo. This would encourage the co-production of other radionuclidic impurities as a result of the proton induced nuclear reactions on ^{97}Mo and ^{98}Mo. Fig. 7 presents the excitation functions leading to ^{94}Nb and ^{95}Nb for proton irradiation of ^{98}Mo. Fig. 8 presents the excitation functions leading to ^{96}Tc, ^{97}Tc and ^{98}Tc for proton irradiation of ^{98}Mo.

Although the ALICE code can not be used to predict the excitation function for the production of ^{99m}Tc, the code does suggest that the maximum yield from the ^{100}Mo (p,2n) ^{99m}Tc reaction will be of the order of 17 MeV. However, the ratio of the ^{99m}Tc /^{99g}Tc cross sections is expected to display variation as function of proton energy. For example, compare the ^{95m}Tc /^{95g}Tc isomeric ratios for the $^{95}Mo(p,n)^{95m}Tc$ nuclear reaction [26]. Experimental measurements summarised (IAEA, 1998) from results of Lagunas-Solar et al., and from a multi-institutional study reported in another chapter of this TECDOC indicated that the optimum energy range for the ^{100}Mo (p,2n) ^{99m}Tc nuclear reaction is between 25–12 MeV with a peak in the excitation function at ~16-18 MeV of >250 mb. The experimentally determined production yield of ^{99m}Tc under these conditions was reported to be in the range of 11 to 13 mCi/μAh under the limited conditions reported using highly isotopically enriched ^{100}Mo targets.

The major concern we see is for the routine use of the $^{100}Mo(p,2n)^{99m}Tc$ is that the co-production of long-lived Tc radionuclides has to be avoided. The long-lived Tc radioisotopes would be a concern, because the long term biological effects of the low dose irradiation of the long-lived radioisotopes are largely unknown. However, the presence of the ^{97}Tc and ^{98}Tc in the ^{99m}Tc would not be expected to distort the quality of medical imaging obtained with generator produced ^{99m}Tc.

The primary problem is the competing nuclear reactions that can occur on impurities of stable Mo isotopes (namely ^{98}Mo) in the ^{100}Mo target. Lagunas-Solar (1997) reported that a commercial source of ultra-high isotopic ^{100}Mo is available. Since the excitation functions have not been measured till now for protons induced reactions on ^{98}Mo (the principal isotopic impurity in isotopically enriched ^{100}Mo). The excitation functions for co-production of Nb isotopes by proton induced reactions on ^{100}Mo are presented in Fig. 6.

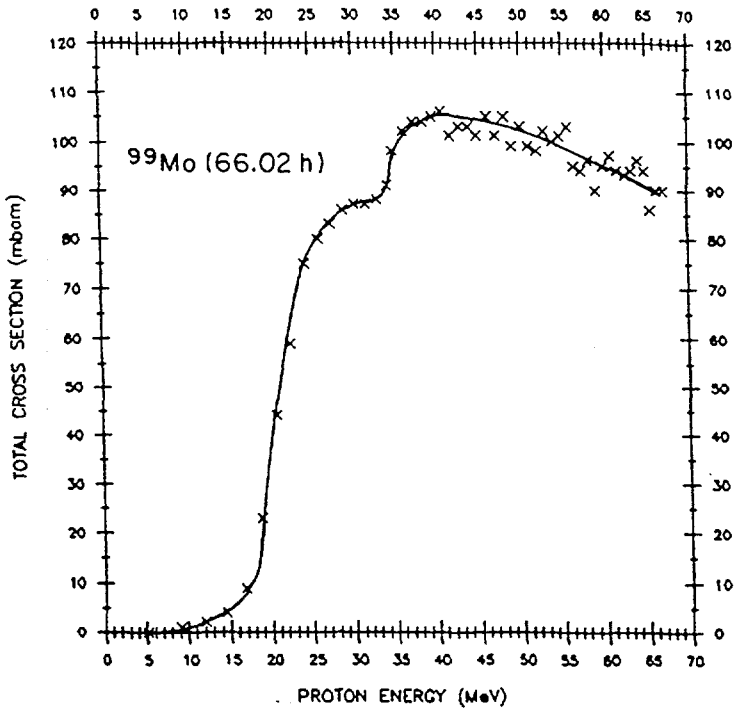

Table 5 (M.C. Lagunas–Solar et al)

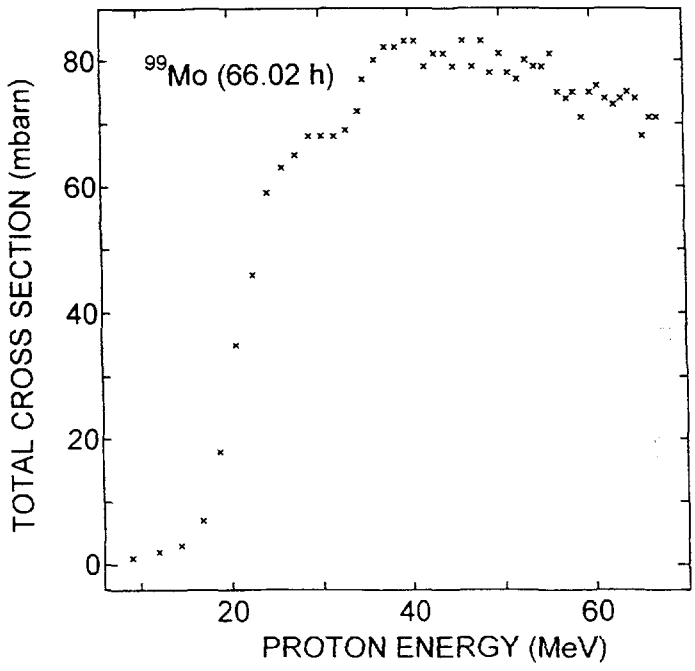

FIG. 5. Comparison of the data reported in Table 5 and Fig. 10 of [5].

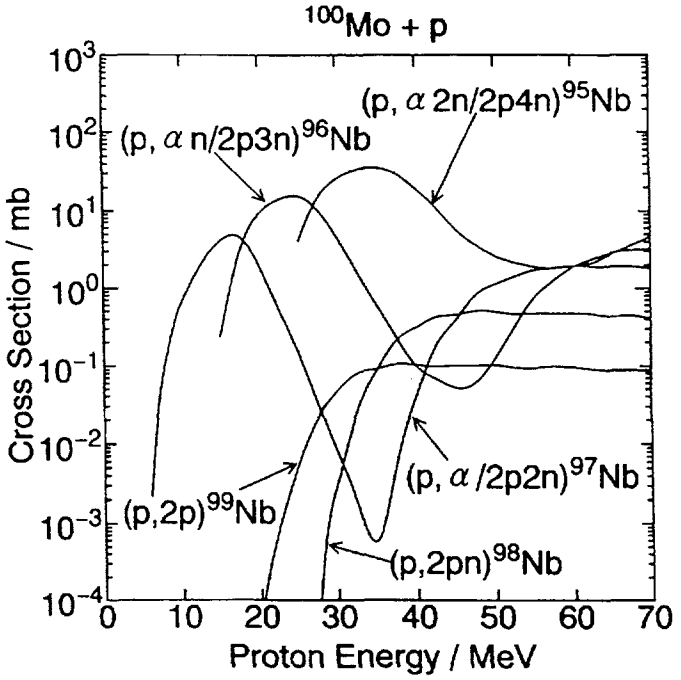

FIG. 6. Excitation functions leading to ^{95}Nb, ^{96}Nb, ^{97}Nb, ^{98}Nb and ^{99}Nb for proton irradiation of ^{100}Mo.

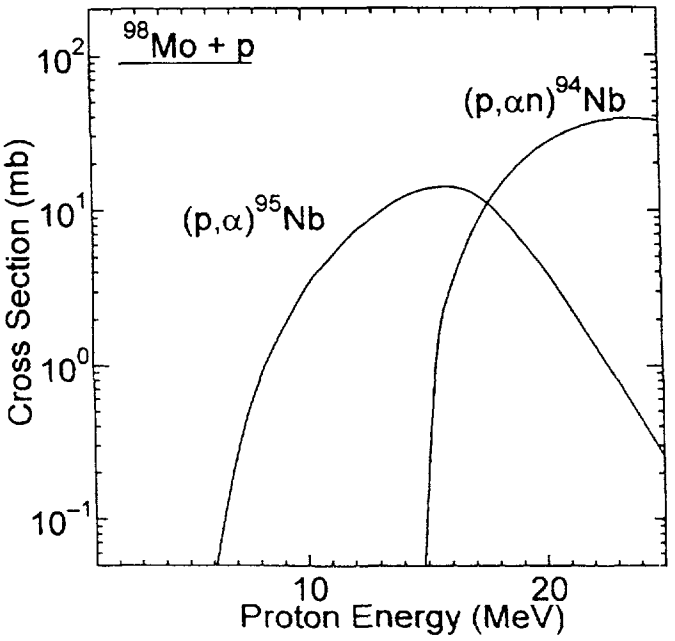

FIG. 7. Excitation functions leading to ^{94}Nb and ^{95}Nb for proton irradiation of ^{98}Mo.

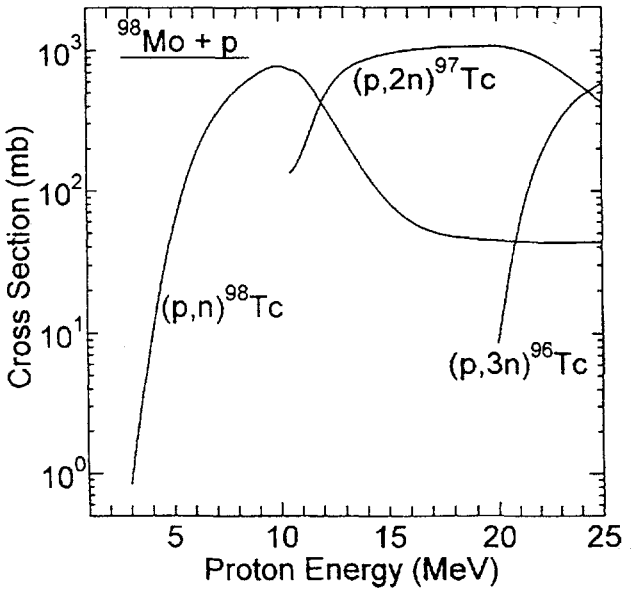

FIG. 8. Excitation functions leading to Tc radioisotopes by proton irradiation of ^{98}Mo.

The ALICE code was useful for defining the upper limit of proton energy to avoid co-production of long lived Tc radionuclidic impurities.

The presence of a low concentration of the stable ^{98}Mo isotope in high isotopic enrichment of ^{100}Mo can lead to the co-production of ^{94}Nb, ^{95}Nb, ^{96}Tc, ^{97}Tc and ^{98}Tc. The Nb radioisotopes decay to stable Mo isotopes, and would not interfere with ^{99m}Tc production. See Figures 7 and 8.

If 100% isotopic enrichment ^{100}Mo were the target material, then the co-production of ^{98}Tc would only be a consideration at proton energies of >20 MeV. The ^{100}Mo(p,n)^{100}Tc reaction is not a factor because of the 15.8 sec half life of ^{100}Tc.

Theoretical estimation of excitation function for the ^{98}Mo(p,γ)^{99m}Tc reaction was not undertaken since capture cross-sections are usually several orders of magnitude too low to be considered for medical radioisotope production.

4. CONCLUSION

The ALICE code predicts the maximum cross section of the ^{100}Mo(p,pn)^{99}Mo to be of the order of 100 mb. The calculated excitation function is in reasonable agreement with sets of experimental cross section measurements reported by two different laboratories. It is concluded that the nuclear reaction even using ^{100}Mo of very high isotopic enrichment and high current accelerators is not particularly attractive as an alternative method for routine production of the ^{99}Mo $\rightarrow$ ^{99m}Tc medical radioisotope generator.

REFERENCES

[1] ROJAS-BURKE J., The future supply of molybdenium-99, J. Nucl. Med. **36** (1995) 15N.

[2] Further steps to ensure moly-99 supply, J. Nucl. Med. **37** (1996) 34N.
[3] BEAVER, J., HUPF, H., Production of ^{99m}Tc on a medical cyclotron: A feasibility study, J. Nucl. Med. **12** (1971) 739.
[4] ALMEIDA, G.L., HELUS, F., On the production of ^{99}Mo and ^{99m}Tc by cyclotron, Radiochem. Radioanal. Letters **28** (1977) 295.
[5] LAGUNAS-SOLAR, M.C., KIEFER, P.M., CARVACHO, O.F., LAGUNAS, C.A., CHA, YA PO, Cyclotron production of NCA ^{99m}Tc and ^{99}Mo, An alternative non-reactor supply source of instant ^{99m}Tc and ^{99}Mo $\rightarrow$ ^{99m}Tc generators, Appl. Radiat. Isotopes **42** (1991) 643-657.
[6] LEKOVSKII N., SCHOPPER H., (Landoldt-Börstein) Middle Mass Nuclides (A = 40–100) Activation Cross Sections by Medium Energy (E = 10–50) Protons and α-Particles (Experiment and Systematics). Inter-Vesti, Moscow (1991) 215 pages.
[[7] LAMBRECHT, R.M. IN K. OKAMOTO, (Ed), Report INDC(NDS)-195/GZ. IAEA, Vienna (1988).
[8] LAGUNAS-SOLAR, M.C., "Production of ^{99m}Tc and ^{99}Mo for nuclear medicine applications via accelerators as an option to reactor methods" presented at the 18th Annual Conference of the Australian Radiation Protection Society, held 6-8 October (1993), University of Sydney, Australia.
[9] SONCK M., TAKACS S., SZELECSENYI F., HERMANNE A., TARKANYI, F., Excitation functions of deuteron induced reactions on ^{nat}Mo up to 21 MeV. An alternative route for the production of ^{99m}Tc and ^{99}Mo", these Proceedings.
[10] STEYN G.F., MILLS S.J., NORTIER F.M., SIMPSON B.R.S., MEYER B.R., Production of ^{52}Fe via proton-induced reactions on manganese and nickel, Applied Radiation Isotopes **41** (1990) 315-325.
[11] LAGUNAS-SOLAR, M.C., HAFF, R.P., Theoretical and Experimental Excitation Functions for proton induced nuclear reactions on Z =10 to Z=82 target nuclides, Radiochim. Acta **60** (1993) 57-67.
[12] MUSTAFA M.G., Nuclear Modeling Applied to Radioisotope Production. Report UCRL-JC-126741, Lawrence Livermore National Laboratory, CA. (1997) 54 .
[13] OBLINSKY P., Development of Reference Charged Particle Cross Section Data Base for Medical Radioisotope Production, Report INDC(NDS)-349, (1996) 33.
[14] OBLINSKY P., Development of Reference Charged Particle Cross Section Data Base for Medical Radioisotope Production. Report INDC(NDS)-349 International Atomic Emergency Agency, Vienna (1996) 45 p.
[15] SHIGETA, N., MATSUOKA H., OSA, A., KOIZUMI, M., IZUMO, M., KOBAYASHI, K., HASHIMOTO, K., SEKINE, T., LAMBRECHT, R.M., Production method of no-carrier-added ^{186}Re, J. Radioanal. Nucl. Chem. **205** (1996) 85-92.
[16] BLANN, M., Hybrid model for pre-equilibrum decay in neuclear reactions, Phys. Rev. Lett. **27** (1971) 337-340.
[17] BLANN, M., Importance of the nuclear density distribution on pre-equilibrum decay, Phys. Rev. Lett. **28** (1972) 757-759.
[18] BLANN M., Overlaid ALICE: a statistical model computer code including fission and pre-equilibrum models.: FORTRAN, cross-sections. Report COO-3494-29, University of Rochester, NY (1975).
[19] BLANN, M., BISPLINGHOFF, J., Code ALICE / Livermore 82".Report UCID-19614, Lawrence Livermore National Laboratory, CA (1982).
[20] BLANN, M., Calculation of Excitation Functions with Code ALICE, in K. Okamoto, (Ed) INDC(NDS)-195/GZ, International Atomic Energy Agency, Vienna (1988).
[21] WEISSKOPF V.F., EWING D.H., On the yield of nuclear reactions with heavy elements, Phys. Rev. **57** (1940) 472-485

[22] BLANN M., VONACH H.K., Global test of modified precompound decay models, Phys. Rev. **C28** (1983) 1475-1492.
[23] MYERS W.D., SWIATECKI W., Anomalies in nuclear masses, J. Ark. Fys. **36** (1967) 343-352.
[24] SCHOLTEN B., LAMBRECHT, R.M., COGNEAU, M., QAIM S.M., VERA RUIZ H., Excitation functions for the Cyclotron Production of ^{99m}Tc and ^{99}Mo. Applied Radiation and Isotopes (to be submitted).
[25] LAGUNAS-SOLAR M., Accelerator production of technetium-99m with proton beams and enriched molybdenium-100 targets, these proceedings.
[26] NAGAME Y., BABA S., SAITO T., Isomeric yield ratio for the ^{95}Mo(p,n)^{95m,g}Tc reaction, Appl. Radiat. Isotopes **45** (1994) 281-285.

ACCELERATOR PRODUCTION OF ^{99m}Tc WITH PROTON BEAMS AND ENRICHED ^{100}MO TARGETS

M.C. LAGUNAS-SOLAR
University of California,
Davis, California,
United States of America

Abstract

The direct production of ^{99m}Tc has been developed based upon the use of the ^{100}Mo(p,2n)^{99m}Tc reaction (Q= -7.9 MeV), using enriched ^{100}Mo targets and accelerated protons of <25 MeV. Cumulative ^{99m}Tc yields measured in this work reached 851 ± 77 MBq/μA/h (23.0 ± 3.0 mCi/μA/h) at end-of-bombardment (EOB) in the 22-12 MeV energy region, with ^{96}Tc (4.35 d) as the only detectable impurity at <0.0003 % at EOB. By using high-intensity beams (i.e. 1 mA) available from modern H^- accelerators, and by extracting multiple H^+ beams to bombard a single or an array of enriched ^{100}Mo targets, this method could provide nearly 851 GBq (23 Ci) of ^{99m}Tc in 1-h bombardments. Because of this large-batch potential, this new method appears to be an effective alternative to the production and distribution of ^{99}Mo → ^{99m}Tc generator systems, although it may be limited to daily, regional/local distribution and use. ^{99m}Tc produced in this fashion has high radionuclidic and radiochemical purity, although its specific activity has not been determined. The accelerator-made ^{99m}Tc has been shown to have similar physical and chemical characteristics than ^{99m}Tc eluted from commercial fission-produced ^{99}Mo → ^{99m}Tc generators. Technical and logistical factors need further study and analysis but the potential and the expected impact of this new method are clear in the context of the operation of large radionuclide distribution centers as well as for small programs in developing regions.

1. INTRODUCTION

The use of ^{99m}Tc (6.02 h) in nuclear medicine is well established worldwide. Its supply and distribution is largely based on the use of reactor technologies to produce its parent ^{99}Mo (66 h), mostly by fissioning ^{235}U with neutrons or, to a lesser extent, by the neutron bombardment of ^{98}Mo targets. After separating and purifying ^{99}Mo from the fissioned or the activated targets, it is used to prepare ^{99}Mo → ^{99m}Tc generators for distribution worldwide. As of this date, no alternative method had been established to replace or as an alternative to these reactor-based techniques.

Since the early 1990's, concerns for the reliability of supply of the weekly batches of ^{99}Mo have arisen because of the age of reactors currently involved, and because of sporadic labor or technical events in some of the reactor facilities involved in its large-scale production. This concern is based on the fact that a large proportion of the current weekly supply of ^{99}Mo rely on a few reactor facilities operating in Canada and in Europe. Production of ^{99}Mo is essential for the timely manufacturing of ^{99}Mo → ^{99m}Tc generators for worldwide distribution. Once on site, this device is used to elute on a daily basis, single or multiple doses of ^{99m}Tc for radiopharmaceutical syntheses. Largely due to the commitment and efficiency of the private sector operating these facilities and the distribution network, a long tradition of reliability and steady worldwide supply have been established and is expected. Over the last few years, however, some disturbances of supply have been encountered as some of the reactor facilities

have suffered from minor but potentially critical interruptions. Furthermore, because an estimated 80-90% of all the diagnostic nuclear medicine procedures performed worldwide are based on the on-site or regional preparation of ready-to-use doses of the various ^{99m}Tc radiopharmaceuticals known today, a steady supply of ^{99}Mo → ^{99m}Tc generators is essential for the economic well being of the industry in general. Therefore, even a few weeks of interrupted supply may cause large economical damage as well as an interruption of clinical services. If the interruption is any longer, many medical services and health-care providers, may be seriously affected causing perhaps irreversible damage to the overall distribution and clinical use communities.

This situation could also affect many of the developing nations with nuclear medicine programs, in particular those located far away from the traditional centers of supply and distribution. Shortage of supply or limited production levels may affect their operating programs and schedules as the priority of commercial supply is usually established based upon demand and, at present, it clearly favors those large use centers located mostly in the developed nations in the northern hemisphere. Clearly, a way to alleviate this situation is to develop many alternative supply centers with capabilities for local or regional supply and based upon more affordable and reachable technologies. Accelerator programs, while still requiring major resources for implementation, and far closer than reactors in the latter category.

Preliminary investigations to develop alternative methods for producing ^{99m}Tc with accelerators were conducted in the mid 1970's. The excitation function for the production of ^{99m}Tc via the ^{100}Mo(p,2n) reaction in the 10 to 25 MeV proton energy region was first reported by Beaver & Hupf in 1971 [1], and was later confirmed by Almeida & Helus in 1977 [2]. However, because of the success of the ^{99}Mo → ^{99m}Tc generator technique developed by Richards in 1966 [3]-no further study was reported until Lagunas-Solar et al. [4-9] developed new data over an extended proton energy range, used enriched ^{100}Mo targets, and further completed an evaluation and demonstrated the feasibility of this new accelerator-based method. The technical feasibility of using modern cyclotrons for the production of ^{99m}Tc was further analyzed by Egan et al. in 1994 [10].

Because of the above scenario, accelerator methods to provide either a direct source of ^{99m}Tc and/or of its parent ^{99}Mo are needed as potential alternatives to the reactor based production of ^{99}Mo. Therefore, also included in this study are measurements of the excitation function leading to the formation of ^{99}Mo via the ^{100}Mo(p,pn)^{99}Mo (Q= - 8.3 MeV) reaction. This latter work is a complement to other investigations regarding the use of proton-induced fission for the production of ^{99}Mo via the ^{238}U(p, fission)^{99}Mo using accelerators [11, 12].

This report summarizes the current data base, includes a detailed accounting of experimental procedures used in this investigation, summarizes the results, and provides a discussion of the rationale behind this new accelerator-based method being developed at the University of California, Davis.

2. EXPERIMENTAL PROCEDURES

2.1. Natural Mo and enriched ^{100}Mo target materials

Natural isotopic abundance Mo, enriched ^{100}Mo (metal) and ^{98}Mo(VI) (oxide) targets were used in all these experiments. In its metal form, Mo [d= 10.22 g/cm^3; m.p. 2610°C; b.p. 5560°C; thermal conductivity @ 100°C 0.325 cal/(s.cm.°C)] is an excellent cyclotron target

and should be able to withstand high current bombardments. The natural and enriched ^{98}Mo(VI) oxide (MoO_3; d= 4.692 g/cm^3; m.p. 795°C; b.p. 1155°C sub.) were used only in experiments conducted with low intensity beams (< 1 μA), as the Mo oxide is not an appropriate target material for high intensity bombardments. Other chemical forms of Mo were not studied as no other compound was found to have equal or better physical and chemical properties than the selected metal and oxide forms.

The isotopic composition of Mo targets that were used or considered in these experiments is given in Table I. It is specially important, in selecting the appropriate enriched ^{100}Mo target, the type and abundance of Mo isotopes present, particularly for ^{96}Mo, ^{97}Mo, and to a lesser extent for ^{98}Mo. These Mo nuclides are also targets and, therefore, are potential sources of several Tc radionuclide impurities.

The isotopic abundance of enriched ^{100}Mo from the The Commonwealth of Independent States (CIS) was selected for use in these experiments. Selection of the enriched ^{100}Mo target material was found to be a significant factor as the relative composition of the impurities from different sources is variable (Table I). The isotopic purity of ^{100}Mo is a critical factor to achieve the highest possible radionuclide purity of the directly-made ^{99m}Tc. The rationale for this choice is discussed below (see section 3.1, Results and Discussion).

Thin natural Mo metallic foils (12.7 μm thick, 99.95% purity, from Alfa, Johnson Matthey Company, MA) were used as single targets for the excitation function measurements. The stacked-foil technique was utilized to cover selected, narrow and broader proton energy ranges for these measurements, although, in order to check for internal consistency, a few single measurements were performed in triplicate at selected proton energies. In addition, thin natural metallic Cu foils (12.7 μm thick, 99.8% purity, from Alfa, Johnson Matthey Company, MA) were used as secondary beam-intensity monitors. Each of the Mo and Cu foils were rectangular in shape (3 x 4 cm) and were weighted and carefully checked for thickness uniformity.

For single natural Mo targets, a Mo foil and a Cu foil were mounted together in a rectangular shaped 35-mm slide frame with the Cu foil facing the proton beam. Such arrangement guaranteed that the Cu foil would be bombarded by protons of known energy and that an essentially identical proton beam would pass through both monitor and target foils. The Cu monitor was used to confirm the total beam charge indicated by the electronic current integrator connected to a Faraday Cup. For the stacked-target experiments, three Cu foils were used: one up front of the Mo stack, one in the middle, and the third at the end of the stacked Mo foils. All three Cu foils were used as beam monitors. The entrance and exit proton energies at each Mo and Cu foils were calculated using a computer code RANGE [17], which is based on the range-energy tables given by Williamson et al. [13].

2.2. Thick enriched ^{100}Mo and ^{98}Mo targets

Enriched ^{100}Mo (97.46 % enrichment level, granular metal powder) and enriched ^{98}Mo oxide (99.45% enrichment) from CIS were used to prepare several thin (< 1 MeV) and thick (> 1 MeV) energy targets. The enriched ^{100}Mo targets were fabricated by pressing the powder into pellets with a diameter of 0.635 cm. Each target was enclosed within thin Cu foils which provided adequate containment in addition to serving as secondary beam monitors. Proton bombardments with up to 100 nA were conducted on a gas-cooled research target provided with the ability to determine yields and purity under various proton-energy conditions. After adequate decay periods (i.e.15-20 d), these targets were reused for further measurements. A

similar enriched ^{100}Mo thick target was also used with up to 1 μA proton beams for yield and radiochemistry experiments (see section 2.6, below). Enriched ^{98}Mo oxide targets were prepared using similar techniques and used to test the existence of the ^{98}Mo(p,γ)^{99m}Tc reaction channel which had been predicted earlier [6].

TABLE I. ISOTOPIC ABUNDANCE OF NATURAL AND ENRICHED Mo TARGETS

Mo Isotope	Natural Mo (%)	Enriched ^{98}Mo (%)	Enriched ^{100}Mo (%) CIS (Russia)[1]	ORNL (USA)
92	14.84	0.02	0.0011	0.55
94	9.25	0.02	0.0008	0.19
95	15.92	0.04	0.0016	0.29
6	16.98	0.06	0.0020	0.35
97	9.55	0.32	0.0026	0.26
98	24.13	99.45	2.54	0.97
100	9.63	0.09	97.46	97.39

2.3. Target irradiation and proton beam monitoring

All the target irradiation were conducted with external proton beams from the 76-inch (1.93 m) isochronous cyclotron at the Crocker Nuclear Laboratory of the University of California, Davis.

All the targets, both single and stacked, natural and enriched, were irradiated under vacuum using a 76-cm diameter scattering chamber (ORTEC 2800 Series, Oak Ridge, TN) insulated electrically from a collimated beam port. An alignment of the beam collimators and the target was well established by means of a laser source prior to each experiment, and the reproducibility of this alignment was verified by video observations during irradiation. The beam size in all irradiation experiments was 0.32 cm in diameter. The proton beam charge was collected in a Faraday Cup fitted with magnetic electron suppression. In addition to the Faraday Cup, beam charge integration was also measured and checked using the ^{63}Cu(p,2n)^{62}Zn reaction induced in the Cu monitor foils [14]. In doing so, two characteristic γ-rays of ^{62}Zn, namely 548.4 keV (14.6%) and 596.7 keV (24.0%) were identified, measured, and used for calibrating beam intensity and for measuring the total charge of protons deposited on the targets.

The incident proton energy was measured using a time-of-flight (TOF) technique known as a γ-flash measurement [15,16]. This method essentially counts the time needed for a proton to travel between two fixed objects, a C stop and a Pb plug, separated 2.0 m apart.

2.4. Radionuclide assays

Each Mo target used in this study was assayed at least twice after irradiation. The first radioassay was conducted and completed within a few hours after the end-of-bombardment

[1] Values reported by ICP measurements.

(EOB). The cumulative activities of directly-made ^{99m}Tc, of indirectly-made ^{99m}Tc (i.e. from the decay of ^{99}Mo), and of directly-made ^{99}Mo were obtained by assaying the 140.5 keV γ-ray.After a 7-day period to allow for the decay of directly-produced ^{99m}Tc, and of other short-lived radionuclides, a second radioassay was performed to measure directly-produced ^{99}Mo, the longer-lived 66 h parent. The activity of directly-made ^{99m}Tc was then determined by analyzing the radioassays in combination, and correcting to EOB. The activity data obtained in this manner was also tested with half-life determinations. A list of radionuclides identified and measured in this work, as well as the decay data used in their respective radioassays, is given in Table II. Several other Tc isotopes were also identified and analyzed by assaying their respective γ-rays. The radioassays of the Cu monitor foils were conducted 1-day after EOB.

The first radioassay measurements were carried out with a high count rate and, therefore, were conducted using a small 0.5-cm^3 high-purity Ge-detector system (Nuclear Data ND-66 MCA). A 60-Hz pulser was counted simultaneously with the Mo foils to correct for dead time and pile-up losses. All remaining radioassays were conducted at a much lower count rate and, therefore, in order to increase statistical accuracy, they were performed using a much larger, higher efficiency 20-cm^3 high-purity coaxial Ge detector. These two Ge detectors were intercalibrated for absolute and relative efficiencies with a mixed-radionuclide point-source standard (National Institute of Standards and Technology, 1988).

2.5. Cross sections, yields, and uncertainties

All measured activities in counts per second (cps) from the assays were converted to cross sections and yields at EOB using the well-known activation formula. Then, the measured yields from natural Mo foils were extrapolated to enriched ^{100}Mo (CIS; 97.46 %) based upon the known isotopic compositions (Table I).The uncertainties in the cross section and yield measurements for the thin natural Mo foils amounted to ±13% and were estimated by combining in quadrature the individual errors listed below:

- beam-current integration (±5%);
- target thickness variation (±4%);
- spectral integration (±4%);
- counting statistics (±3%);
- detector efficiencies (±5%);
- attenuation corrections (±5%);
- γ-ray abundance (±5%); and
- counting geometry (±5%).

The uncertainties in the proton energy determinations were estimated to be ±6%, and included in quadrature the following individual errors:

- incident beam energy (±3%);
- target thickness variation (±4%);
- beam scattering (±1%); and
- range energy values (±3%).

TABLE II. NUCLEAR AND DECAY DATA FOR TECHNETIUM ISOTOPES[1]

Radionuclide	Half life	Principal γ-ray Emissions (keV, % abundance)	Decay Product
^{93}Tc	2.75 h	1363 (66)	^{93}Mo (3.5 x 10^3 a)
^{94}Tc	4.88 h	871 (100) 702.6 (99.8) 849.7 (96.9)	^{94}Mo (Stable)
^{95}Tc	20.0 h	765.8 (93)	^{95}Mo (stable)
^{96}Tc	4.35 d	812.5 (81.5) 849.9 (96.9)	^{96}Mo (stable)
^{99}Tc	2.14 x 10^5 a	β^- decay	^{9}Ru (stable)
^{99m}Tc	6.02 h	140.5 (89)	^{99}Tc (2.14 x 10^5 a)

The uncertainties in the yield measurements for the enriched ^{100}Mo thick targets were estimated to be ±16%. The increased level of uncertainty was due to the accumulated error in the thick-target thickness which was approximately 11 times the thickness of the single thin Mo foil targets. In all the measurements of ^{99m}Tc thick-target yields, the sources of error remained the same and at levels similar to those given above.

2.6. Technetium-99m production tests with enriched ^{100}Mo and ^{98}Mo targets

The enriched ^{100}Mo targets were bombarded with 22.4 MeV protons (1 μA) in a dedicated water-cooled target coupled to an external beam-line for radioisotope production at Crocker Nuclear Laboratory. After irradiation, the target was inspected for integrity, and a series of radiochemistry procedures were performed to dissolve the enriched ^{100}Mo target in 30% H_2O_2 (3 min), followed by a radiochemical separation of ^{99m}Tc radioactivities from Mo using a solvent (methyl ethyl ketone, MEK) extraction technique (< 20 min). After evaporating the organic solvent, isotonic saline was used to dissolve the ^{99m}Tc. This final ^{99m}Tc was radioassayed and the ^{99m}Tc yield and purity were compared with predicted values by extrapolation from excitation function data. The agreement between predicted and measured yield and purity values was excellent (± 12%) providing assurances of the precision of the excitation functions obtained in this work. Similarly, experiments were conducted with protons (20-22 MeV) on enriched ^{98}Mo targets. After the end-of-bombardment, the target was radioassayed and no radiochemistry was performed as the results indicated extremely low production yields for ^{99m}Tc. In this manner, the predicted ^{98}Mo(p,γ) contribution to the ^{99m}Tc yields was tested.

3. RESULTS AND DISCUSSION

3.1. Proton-induced nuclear reactions on Mo targets

Several proton-induced nuclear reactions on Mo targets are possible in the 25-10 MeV energy region covered in this investigation. These reactions are summarized in Table III. For

[1] From "Table of Isotopes" (7th. Ed.). C.M. Lederer and V.S. Shirley (Eds.) John Wiley & Sons (1978).

TABLE III. REACTION CHANNELS FOR ≤25 MEV PROTONS ON ENRICHED MOLYBDENUM-100 TARGETS (CIS, ORNL)

Enriched ^{100}Mo Target (Abundance in %)			Reaction for Production of ^{99m,96,95,94}Tc and ^{99}Mo Isotopes						
	CIS	ORNL	^{99m}Tc	^{96}Tc (6.02 h)	^{95}Tc (4.35 d)	^{94}Tc (20.0 h)	^{99}Mo (4.88 h)	(66.02 h)	
^{92}Mo	0.0011	0.55	n/a[2]	n/a	n/a	n/a	n/a		
^{94}Mo	0.0008	0.19					(p,n) Q=-5.0		
^{95}Mo	0.0016	0.29				(p,n) Q=-2.5	(p,2n) Q=-12.4		
^{96}Mo	0.0020	0.35		(p,n) Q=-3.7	(p,2n) Q=-11.6	(p,3n) Q=-21.6			
^{97}Mo	0.0026	0.26		(p,2n) Q=-10.5	(p,3n) Q=-18.5				
^{98}Mo	2.54	0.97		(p,3n) Q=-19.2					
^{100}Mo	97.46	97.39	(p,2n) Q=-7.9	n/a				(p,pn) Q=-8.3	

each reaction, energetic requirement (Q-value), cross sections, and the isotopic abundance of each Mo target nuclide from which they are produced, determined the overall contribution to the yield of each specific Tc isotope. The physical properties of the Tc isotopes produced from Mo targets were already given in Table II. These properties, when analyzed in combination, provided a clear criteria of their relative significance as potential sources of Tc impurities in directly-made ^{99m}Tc.

Although other Nb, Zr, and Y isotopes are also formed by (p,x) reactions [6], their formation and presence in an irradiated Mo target is not significant as they are effectively separated from Tc radioactivity during target radiochemistry.

Reactions leading to the formation of ^{96}Tc (4.35 d), ^{95}Tc (20.0 h) and ^{94}Tc (4.88 h) are particularly important for the production of high radionuclidic purity ^{99m}Tc from enriched ^{100}Mo targets. These Tc isotopes, as well as the desired ^{99m}Tc, are produced from several Mo impurities present in enriched ^{100}Mo target materials. Therefore, the proper selection of adequately enriched ^{100}Mo is a critical choice, as there are significant differences in the isotopic abundance from the various sources considered in this study (CIS in Russia, and ORNL in the USA). The CIS material was selected, and the decision can be rationalized when inspecting the isotopic composition of ^{100}Mo enriched materials given in Table I, and analyzing it with the proton induced reactions on ^{100}Mo targets producing Tc isotopes, given in Table III.

Clearly, the production of ^{96}Tc, ^{95}Tc, and ^{94}Tc is energetically feasible within the same region of interest for the production of ^{99m}Tc, that is, in the 25-10 MeV energy region studied. Therefore, the production of these Tc impurities must be avoided or minimized by properly selecting the enriched ^{100}Mo target material, and matching its thickness with the selected proton energy region. In order to accomplish this task, several excitation functions were measured and are reported below (see section 3.2). On the other hand, the presence of ^{98}Mo,

[1] Reaction Q values in MeV

[2] Reactions not energetically possible (n/a)

^{97}Mo, ^{96}Mo, ^{95}Mo and ^{94}Mo as target nuclides in the enriched ^{100}Mo targets, was minimized by using a CIS-type rather than the ORNL-type material (Table I), simply because the CIS enriched ^{100}Mo target material had a total of 0.0070% for the combined isotopic composition of these Mo isotopes, as compared to 1.0900% for the ORNL material (a ratio of 1:156).

Among the Tc impurities observed in this investigation, ^{96}Tc (4.35 d) was clearly the main concern. The production of ^{96}Tc from these same Mo isotopic impurities (Table II) and primarily from the more abundant ^{98}Mo via the ^{98}Mo(p,3n) reaction (Q= - 19.2 MeV), can be minimized by limiting the entrance proton energy on the target to ≤ 23 MeV (see section 3.4, below), a proton energy slightly above the energetic threshold for the ^{98}Mo(p,3n) reaction. The results of this strategy and a discussion of the many possible options regarding target material and operating proton energy ranges, is given below.

3.2. Excitation functions for the Mo(p,xn)Tc reactions

Previously reported excitation functions for the proton-induced reactions on natural Mo targets [6] suggested the possibility that two reaction channels, a lower energy ^{98}Mo(p,γ) and a higher energy ^{100}Mo(p,2n), were available for the production of ^{99m}Tc in the 70 to 10 MeV region. However, this interpretation of the empirical data obtained by assaying the typical 140.5-keV γ-ray emission from the 6.02 ^{99m}Tc, was proved as incorrect when it was compared with data obtained in this study with enriched ^{100}Mo targets. The consecutive long-term assays (over 7-10 days after EOB) of the 140.5 keV region taken from the different natural Mo targets used in the previous work, had to be corrected from several potential interference including similar γ-ray emissions from ^{99}Mo (140 keV, 88.7%) and its daughter ^{99m}Tc, to obtain the true count rate for the directly-made ^{99m}Tc. These time-dependent corrections allowed the determination of the true count rate for directly-made ^{99m}Tc by correcting the total count rate for the 140.5 keV region being assayed over time. Although corrections were made to account for the presence of other interfering γ-ray emissions, particularly from the 141-keV (61%) γ ray from ^{90}Nb (14.8 h), it appears that some nuclear decay data is either not correct or does not exist as the corrections produced the doubly peaked excitation function reported earlier [6,7]. In natural Mo targets, ^{90}Nb may be produced indirectly by the ^{92}Mo(14.84%)(p,3n)^{90g,m}Tc (49.2 s; 8.3 s) → ^{90}Mo (5.67 h) → ^{90}Nb (Q=-32.43 MeV) and/or directly by the ^{94}Mo(9.25%)(p,αn)^{90}Nb reaction (Q=-8.97 MeV). Clearly, the presence of ^{90}Nb and/or an unknown contaminant dominated adversely the intended corrections for the "true count rate" due to the directly-made ^{99m}Tc.

In addition, we also used CIS enriched ^{98}Mo targets (Table I) to test the potential of the ^{98}Mo(p,γ) contribution, and limited our observations to below 25 MeV. In this manner, the suspected contribution of the (p,γ) reaction channel was discarded as small cross sections were predicted based on extremely low measured ^{99m}Tc yields (data not shown). Therefore, the interpretation advanced previously [6] on the double "hump" excitation function was proven incorrect and discarded.

The excitation functions measured are summarized in Table IV, and shown in Fig. 1 for ^{99m}Tc; Fig. 2 for ^{96}Tc; Fig. 3 for ^{95}Tc; and Fig. 4 for ^{94}Tc. Because of reaction energetic, target isotopic composition, and proton beam energies, only the ^{99m}Tc cross section data was clearly identified as a single ^{100}Mo(p,2n) reaction channel, and is reported as such. In all other cases, the production of Tc isotopes results from an integration of several reaction channels which are energetically feasible and, thus, allowed in the proton energy range studied and because of the presence of diverse Mo target nuclides being bombarded. The proton energy assigned to

each thin Mo target was calculated as the mean between incident and exit energies. Exit energies were calculated using a computer code RANGE [17] and the corresponding target thickness.

This calculation procedure was employed with all targets, including both single and stacked, natural and enriched, Mo targets and Cu monitor foils, used in this investigation. In addition, the excitation function for the production of ^{99}Mo via the ^{100}Mo(p,pn)^{99}Mo reaction (Q= - 8.3 MeV) is also given in Table IV, and will be discussed in section 3.8, below.

3.2.1. Excitation function for ^{100}Mo(p,2n)^{99m}Tc reaction

The excitation function for the ^{100}Mo(p,2n)^{99m}Tc reaction was measured directly with natural Mo and is shown in Fig. 1. As the only possible contributor in a natural Mo target is the ^{100}Mo nuclide (9.63%), this data provided unequivocal information on this reaction channel. A fit curve of the excitation function for the ^{99m}Tc cross section data shown in Fig. 1, indicated a maximum cross section of 365 ± 47 mb at 16.5 MeV. This maximum cross section is slightly larger than the value of 290 mb reported earlier by Lagunas-Solar et al. [6] and than the 305 mb value reported by Levkovskii [18]. However, the proton energy at which the maximum cross section was measured in this work is in good agreement and within the experimental uncertainty with the 17-MeV maximum reported by Lagunas-Solar [6], and is slightly higher than the 14.8-MeV value reported by Levkovskii [18].

Contrary to what was suggested in previous work [6], no double "hump" excitation function resulted providing an unequivocal solution to the former prediction. The precision of this excitation function is critical for establishing the best operating parameters for ^{99m}Tc yield and purity optimization. This function is also critical in optimizing the incident proton energy and the isotopic purity of the enriched ^{100}Mo target material. To a smaller extent, the exit proton energies, determined by varying the target thickness, is a lesser factor, as the relative contribution to the ^{99m}Tc yield decreases with proton energy. On the other hand, thicker targets shall improve purity as no other Tc impurity is produced significantly, below 19 MeV. This is due to the low abundance of Mo nuclide "impurities" in the CIS ^{100}Mo target material which has 2.54% of ^{98}Mo, but only 0.0026% of ^{97}Mo and 0.0020% of ^{96}Mo, the other potential sources of ^{96}Tc (Table III). Finally, and due to the low abundance of the target Mo nuclides (i.e. ^{97}Mo [0.0026%], ^{96}Mo [0.0020%], ^{95}Mo [0.0016%] and ^{94}Mo [0.0008%]), all other potential Tc impurities such as 20.0 h ^{95}Tc and 4.88 h ^{94}Tc are produced in extremely low yields and were undetectable (below detectable levels) in several ^{99m}Tc production test runs conducted in this study (see section 3.5, below).

TABLE IV. TOTAL CROSS SECTIONS FOR THE PRODUCTION OF ^{99m,96,95,94}Tc AND ^{99}Mo ISOTOPES WITH PROTONS ON NATURAL Mo TARGETS.

Proton Energy (MeV)	^{99m}Tc (mb)	^{96}Tc (mb)	^{95}Tc (mb)	^{94}Tc (mb)	^{99}Mo (mb)
9.54 ± 0.57	51.8 ± 6.7	622 ± 81	123.8 ± 16.1	446 ± 58	
9.87 ± 0.59	83.3 ± 10.8	662 ± 86	212.2 ± 27.6	475 ± 62	
10.2 ± 0.6	124 ± 16	717 ± 93	302.1 ± 39.3	558 ± 73	
10.5 ± 0.6	166 ± 22	789 ± 103	387.3 ± 50.3	546 ± 71	
10.8 ± 0.6	188 ± 24	804 ± 105	553.5 ± 72.0	451 ± 59	
11.1 ± 0.7	216 ± 28	838 ± 109	569.3 ± 74.0	350 ± 46	
11.4 ± 0.7	243 ± 32	879 ± 114	610.7 ± 79.4	331 ± 43	
11.7 ± 0.7	269 ± 35	989 ± 129	588.1 ± 76.5	320 ± 42	
12.0 ± 0.7	279 ± 36	1040 ± 135	565.0 ± 73.5	384 ± 50	

TABLE IV. (Cont.)

Proton Energy (MeV)	^{99m}Tc (mb)	^{96}Tc (mb)	^{95}Tc (mb)	^{94}Tc (mb)	^{99}Mo (mb)
12.2 ± 0.7	288 ± 37	1080 ± 140	612.6 ± 79.6	340 ± 44	
12.5 ± 0.8	297 ± 39	1179 ± 153	657.7 ± 85.5	316 ± 41	
12.8 ± 0.8	303 ± 39	1309 ± 170	692.1 ± 90.0	319 ± 41	
13.0 ± 0.8	304 ± 40	1257 ± 163	661.3 ± 86.0	227 ± 30	
13.3 ± 0.8	327 ± 43	1296 ± 168	768.8 ± 99.9	254 ± 33	4.86 ± 0.63
13.5 ± 0.8	326 ± 42	1229 ± 160	760.1 ± 98.8	300 ± 39	5.83 ± 0.76
13.8 ± 0.8	338 ± 44	1226 ± 159	927 ± 121	340 ± 44	8.97 ± 1.2
14.0 ± 0.8	327 ± 43	1171 ± 152	888 ± 115	361 ± 47	10.8 ± 1.4
14.2 ± 0.9	345 ± 45	1189 ± 155	915 ± 119	380 ± 49	11.3 ± 1.5
14.2 ± 0.9	335 ± 44	1196 ± 155	963 ± 125	389 ± 51	15.3 ± 2.0
14.2 ± 0.9	335 ± 44	1201 ± 156	897 ± 117	387 ± 50	16.0 ± 2.1
14.3 ± 0.9	325 ± 42	1210 ± 157	936 ± 122	404 ± 53	15.9 ± 2.1
14.5 ± 0.9	329 ± 43	1144 ± 149	863 ± 112	431 ± 56	15.5 ± 2.0
14.6 ± 0.9	370 ± 48	1125 ± 146	834 ± 108	597 ± 78	28.8 ± 3.7
14.6 ± 0.9	379 ± 49	1128 ± 147	872 ± 113	609 ± 79	28.8 ± 3.7
14.6 ± 0.9	388 ± 50	1161 ± 151	855 ± 111	557 ± 72	26.2 ± 3.4
14.8 ± 0.9	329 ± 43	1092 ± 142	931 ± 121	563 ± 73	30.5 ± 4.0
16.0 ± 1.0	364 ± 47	1027 ± 134	983 ± 128	698 ± 91	34.9 ± 4.5
16.0 ± 1.0	351 ± 46	1014 ± 132	993 ± 129	681 ± 89	33.9 ± 4.4
16.0 ± 1.0	327 ±43	928 ± 121	1021 ± 133	530 ± 69	33.7 ± 4.4
17.0 ± 1.0	381 ± 50	933 ± 121	956 ± 124	600 ± 78	43.8 ± 5.7
17.0 ± 1.0	362 ± 47	884 ± 115	938 ± 122	707 ± 92	44.6 ± 5.8
17.0 ± 1.0	352 ± 46	897 ± 117	989 ± 129	654 ± 85	48.9 ± 6.4
17.9 ± 1.1	346 ± 45	944 ± 123	941 ± 122	629 ± 82	49.7 ± 6.5
18.1 ± 1.1	343 ± 45	938 ± 122	910 ± 118	627 ± 82	49.9 ± 6.5
18.3 ± 1.1	340 ± 44	956 ± 124	964 ± 125	550 ± 72	54.9 ± 7.1
18.5 ± 1.1	334 ± 43	882 ± 115	906 ± 118	640 ± 83	56.9 ± 7.4
18.7 ± 1.1	330 ± 43	860 ± 112	868 ± 113	685 ± 89	59.1 ± 7.7
19.1 ± 1.1	310 ± 40	965 ± 125	1024 ± 133	634 ± 82	57.8 ± 7.5
19.2 ± 1.2	314 ± 41	861 ± 112	959 ± 125	643 ± 84	60.6 ± 7.9
19.4 ± 1.2	285 ± 37	957 ± 124	927 ± 121	609 ± 79	54.7 ± 7.1
19.6 ± 1.2	273 ± 35	901 ± 117	887 ± 115	544 ± 71	55.3 ± 7.2
19.8 ± 1.2	261 ± 34	920 ± 120	899 ± 117	511 ± 66	55.0 ± 7.2
20.2 ± 1.2	312 ± 41	921 ± 120	944 ± 123	599 ± 78	51.7 ± 6.7
20.2 ± 1.2	319 ± 41	900 ± 117	975 ± 127	725 ± 94	52.1 ± 6.8
20.2 ± 1.2	316 ± 41	910 ± 118	948 ± 123	707 ± 92	53.3 ± 6.9
20.7 ± 1.2	243 ± 32	901 ± 117	901 ± 117	487 ± 63	52.2 ± 6.8
20.9 ± 1.3	239 ± 31	884 ± 115	859 ± 112	498 ± 65	53.3 ± 6.9
21.0 ± 1.3	222 ± 29	870 ± 113	831 ± 108	551 ± 72	52.7 ± 6.9
21.2 ± 1.3	232 ± 30	857 ± 111	873 ± 113	627 ± 82	48.4 ± 6.3
21.4 ± 1.3	203 ± 26	856 ± 111	925 ± 120	489 ± 64	49.1 ± 6.4
21.6 ± 1.3	201 ± 26	877 ± 114	852 ± 111	605 ± 79	48.9 ± 6.4
22.0 ± 1.3	195 ± 25	849 ± 110	893 ± 116	516 ± 67	49.7 ± 6.5
22.1 ± 1.3	183 ± 24	869 ± 113	940 ± 122	480 ± 62	63.7 ± 8.3
22.3 ± 1.3	167 ± 22	901 ± 117	977 ± 127	603 ± 78	62.1 ± 8.1
22.3 ± 1.3	171 ± 22	1049 ± 136	1009 ± 131	650 ± 85	65.3 ± 8.5
22.4 ± 1.3	150 ± 20	1025 ± 133	1088 ± 141	619 ± 80	52.4 ± 6.8
22.4 ± 1.3	137 ± 18	1001 ± 130	1159 ± 151	622 ± 81	60.4 ± 7.9
22.4 ± 1.3	139 ± 18	1015 ± 132	1128 ± 147	643 ± 84	55.3 ± 7.2

TABLE IV. (Cont.)

Proton Energy (MeV)	^{99m}Tc (mb)	^{96}Tc (mb)	^{95}Tc (mb)	^{94}Tc (mb)	^{99}Mo (mb)
22.5 ± 1.4	189 ± 25	998 ± 130	976 ± 127	619 ± 80	60.9 ± 7.9
22.5 ± 1.4	163 ± 21	871 ± 113	907 ± 118	622 ± 81	57.3 ± 7.4
22.7 ± 1.4	168 ± 22	1042 ±135	1092 ± 142	500 ± 65	60.3 ± 7.8
22.7 ± 1.4	151 ± 20	904 ± 118	861 ± 112	530 ± 69	55.3 ± 7.2
22.8 ± 1.4	148 ± 19	1047 ± 136	984 ± 128	605 ± 79	56.3 ± 7.3
22.8 ± 1.4	141 ± 18	968 ± 126	939 ± 122	645 ± 84	57.0 ± 7.4
23.0 ± 1.4	143 ± 19	1057 ± 137	968 ± 126	595 ± 77	59.9 ± 7.8
23.0 ± 1.4	152 ± 20	1001 ± 130	1123 ± 146	506 ± 66	60.8 ± 7.9
23.3 ± 1.4	141 ± 18	1048 ± 136	1017 ± 132	552 ± 72	58.5 ± 7.6
23.5 ± 1.4	131 ± 17	1076 ± 140	1146 ± 149	556 ± 72	61.5 ± 8.0
23.6 ± 1.4	133 ± 17	1205 ± 157	1047 ± 136	570 ± 74	64.4 ± 8.4
23.8 ± 1.4	113 ± 15	1114 ± 145	1242 ± 161	549 ± 71	64.3 ± 8.4
23.9 ± 1.4	118 ± 15	1115 ± 145	1173 ± 152	629 ± 82	65.0 ± 8.5
24.1 ± 1.4	113 ± 15	1133 ± 147	1095 ± 142	596 ± 77	64.7 ± 8.4
24.6 ± 1.5	118 ± 15	1253 ± 163	1252 ± 163	667 ± 87	65.8 ± 8.6
24.6 ± 1.5	124 ± 16	1215 ± 158	1204 ± 157	662 ± 86	67.5 ± 8.8
24.6 ± 1.5	120 ± 16	1235 ± 161	1235 ± 161	654 ± 85	65.4 ± 8.5

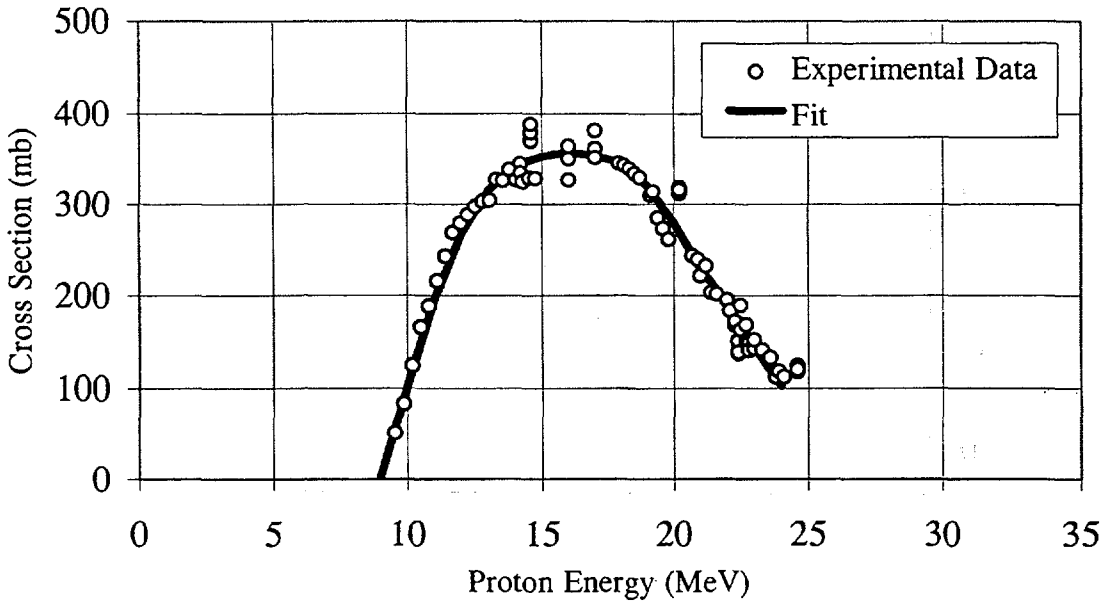

FIG. 1. Excitation function for the ^{100}Mo(p,2n)^{99m}Tc reaction (Q= - 7.9 MeV).

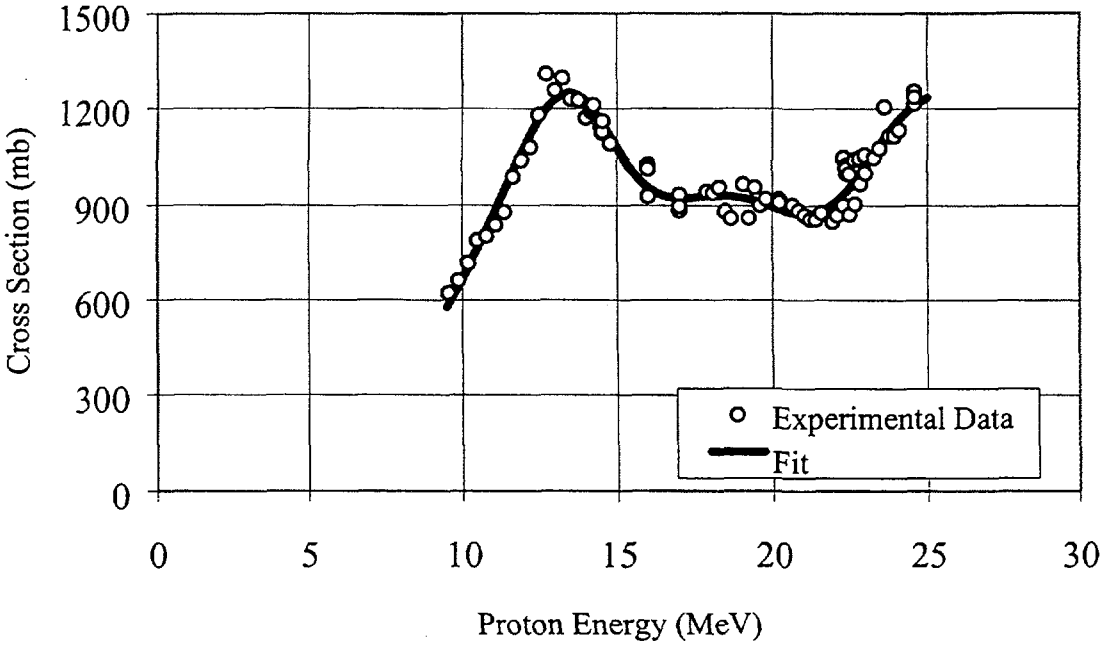

FIG. 2. Excitation function for the $^{nat}Mo(p,xn)^{96}Tc$ reaction.

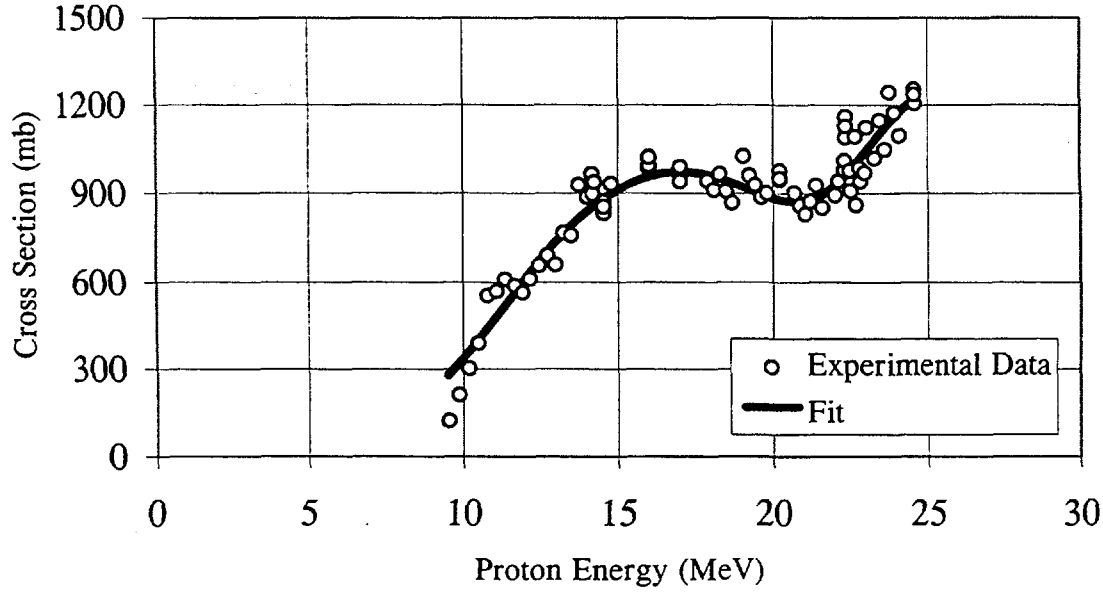

FIG. 3. Excitation function for the $^{nat}Mo(p,xn)^{95}Tc$ reaction.

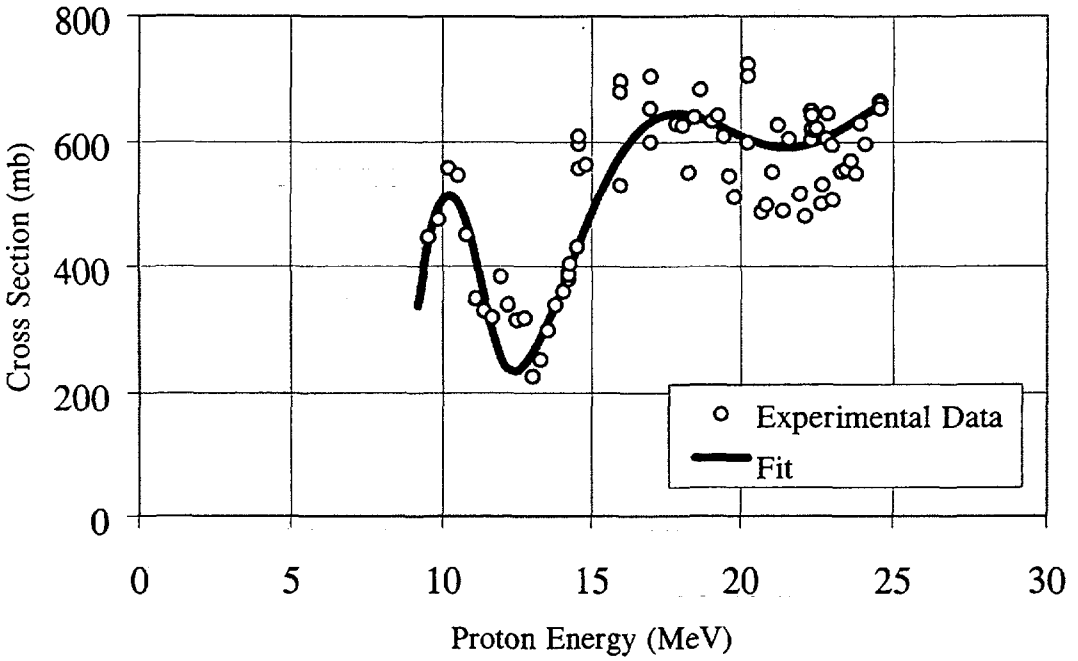

FIG. 4. Excitation function for the ^{nat}Mo(p,xn)^{94}Tc reaction.

3.2.2. Excitation functions for ^{nat}Mo(p,xn)^{96,95,94}Tc reactions

The excitation functions measured for the ^{nat}Mo(p,xn)^{96,95,94}Tc reactions provided with information on the total cross sections for the production of these Tc isotopes as the total activities induced resulted from contributions of several Mo nuclides present in the target (Table II).

In order to get the contribution of individual reaction channels to the production of any of the predicted Tc (^{96}Tc, ^{95}Tc, ^{94}Tc) impurities, the excitation functions given in Table IV were unfolded using the guidance provided by nuclear reaction systematic, reaction energetic, and knowing the isotopic composition of both enriched (CIS) ^{100}Mo and natural Mo target materials. These individual contributions are needed to be able to extrapolate to the isotopic composition of any enriched ^{100}Mo target material considered for this accelerator-based method, and to be able to extrapolate to any of the yields for the ^{96,95,94}Tc impurities.

3.3. Yield estimates with enriched ^{100}Mo (CIS; 97.46%)

The ^{99m}Tc, ^{96}Tc, ^{95}Tc, and ^{94}Tc yields for enriched ^{100}Mo (CIS; 97.46%) targets are given in Table V, and shown in Figures 5-8, respectively. The conversion of cross section data to yield values was direct and straightforward for ^{99m}Tc, as both excitation and the yield functions are identical in shape and boundaries. As expected from the excitation function shown in Fig. 1, the large ^{99m}Tc yield vs. energy function shown in Fig.5, peaked at 16.5 MeV. This yield data also demonstrated that the direct production of ^{99m}Tc in large batches is possible using < 25 MeV protons and enriched ^{100}Mo targets. Integration of the yield data in any selected energy regions allows for the evaluation of yield and purity for all the Tc isotopes of concern, using a variety of proton beam (energy, intensity) and target (thickness, isotopic purity) conditions. Examples of these calculations are given and discussed below.

However, the precision of the yield estimates for ^{96}Tc, ^{95}Tc, and ^{94}Tc, produced by the unfolding method, needed further testing (see section 3.4, below). Further analysis of the yield data to evaluate the potential for the production of Tc impurities (see Figures 6, 7, 8), clearly indicated that the incident proton beam energy should be kept below 23 MeV. There is no limitation regarding purity with respect to exit proton energies. However, as target thickness increases, other concerns regarding target power deposition and its operational reliability, would increase if high intensity proton bombardments are considered.

3.4. Comparison of theoretical and experimental yield and purity values

In order to test the validity of the cross section and yield data summarized above, especially its extrapolation to thick target conditions, several low-intensity production tests were conducted with the enriched ^{100}Mo (CIS; 97.46%) target material. Single targets were bombarded with 20.5 ± 0.1 MeV protons at 100 nA for approximately 10 minutes, using the scattering chamber setup (see section 2.3). The targets were radioassayed immediately and after a decay period, but no radiochemical separations were attempted. The results of these measurements are given in Table VI.

The measured yield and purity for each test compared well-within the levels of the total uncertainty-with extrapolated values obtained from the excitation function data. The proton energy for each ^{100}Mo target was calculated and is reported as the mean value between the

TABLE V. EXTRAPOLATED Tc YIELDS FROM ENRICHED ^{100}Mo (CIS; (97.46%)

Target Energy (MeV)	^{99m}Tc (mCi/μAh/MeV)	^{96}Tc (μCi/μAh/MeV)	^{95}Tc (μCi/μAh/MeV)	^{94}Tc (μCi/μAh/MeV)
9.54 ± 0.57	0.244 ± 0.032	0.00350 ± 0.00046	0.00010 ± 0.00001	0.0228 ± 0.0030
9.87 ± 0.59	0.403 ± 0.052	0.00382 ± 0.00050	0.00030 ± 0.00004	0.0220 ± 0.0029
10.2 ± 0.6	0.615 ± 0.080	0.00420 ± 0.00055	0.00307 ± 0.00040	0.0282 ± 0.0037
10.5 ± 0.6	0.83 ± 0.11	0.00465 ± 0.00060	0.0098 ± 0.0013	0.0282 ± 0.0037
10.8 ± 0.6	0.97 ± 0.13	0.00479 ± 0.00062	0.0143 ± 0.0019	0.0237 ± 0.0031
11.1 ± 0.7	1.15 ± 0.15	0.00506 ± 0.00066	0.0150 ± 0.0020	0.0185 ± 0.0024
11.4 ± 0.7	1.29 ± 0.17	0.00536 ± 0.00070	0.0165 ± 0.0021	0.0223 ± 0.0029
11.7 ± 0.7	1.48 ± 0.19	0.00602 ± 0.00078	0.0219 ± 0.0028	0.0179 ± 0.0023
12.0 ± 0.7	1.54 ± 0.20	0.00640 ± 0.00083	0.0159 ± 0.0021	0.0218 ± 0.0028
12.2 ± 0.7	1.65 ± 0.21	0.00677 ± 0.00088	0.0210 ± 0.0027	0.0125 ± 0.0016
12.5 ± 0.8	1.70 ± 0.22	0.00733 ± 0.00095	0.0185 ± 0.0024	0.0244 ± 0.0032
12.8 ± 0.8	2.13 ± 0.28	0.0080 ± 0.0010	0.0205 ± 0.0027	0.0198 ± 0.0026
13.0 ± 0.8	1.81 ± 0.24	0.0077 ± 0.0010	0.0199 ± 0.0026	0.0252 ± 0.0033
13.3 ± 0.8	2.03 ± 0.26	0.0080 ± 0.0010	0.0236 ± 0.0031	0.0271 ± 0.0035
13.5 ± 0.8	2.02 ± 0.26	0.00761 ± 0.00099	0.0236 ± 0.0031	0.0309 ± 0.0040
13.8 ± 0.8	2.09 ± 0.27	0.00759 ± 0.00099	0.0293 ± 0.0038	0.0348 ± 0.0046
14.0 ± 0.8	2.02 ± 0.26	0.00720 ± 0.00094	0.0285 ± 0.0037	0.0369 ± 0.0048
14.2 ± 0.9	2.16 ± 0.28	0.0079 ± 0.0010	0.0293 ± 0.0038	0.0384 ± 0.0050
14.2 ± 0.9	1.97 ± 0.26	0.0083 ± 0.0011	0.0297 ± 0.0039	0.0406 ± 0.0053
14.2 ± 0.9	2.16 ± 0.28	0.0084 ± 0.0011	0.0312 ± 0.0041	0.0427 ± 0.0056
14.3 ± 0.9	2.09 ± 0.27	0.00739 ± 0.00096	0.0305 ± 0.0040	0.0421 ± 0.0055
14.5 ± 0.9	2.12 ± 0.28	0.00692 ± 0.00090	0.0285 ± 0.0037	0.0462 ± 0.0060
14.6 ± 0.9	2.58 ± 0.34	0.00719 ± 0.00093	0.0281V 0.0037	0.0501 ± 0.0065
14.6 ± 0.9	2.46 ± 0.32	0.00715 ± 0.00093	0.0293 ± 0.0038	0.0598 ± 0.0078
14.6 ± 0.9	2.52 ± 0.33	0.00717 ± 0.00093	0.0287 ± 0.0037	0.0699 ± 0.0091
14.8 ± 0.9	2.12 ± 0.28	0.00698 ± 0.00091	0.0299 ± 0.0039	0.0481 ± 0.0063

TABLE V. (Cont.)

Target Energy (MeV)	^{99m}Tc (mCi/μAh/MeV)	^{96}Tc (μCi/μAh/MeV)	^{95}Tc (μCi/μAh/MeV)	^{94}Tc (μCi/μAh/MeV)
16.0 ± 1.0	2.76 ± 0.36	0.0078 ± 0.0010	0.0363 ± 0.0047	0.0649 ± 0.0084
16.0 ± 1.0	2.66 ± 0.35	0.0077 ± 0.0010	0.0359 ± 0.0047	0.0701 ± 0.0091
16.0 ± 1.0	2.48 ± 0.32	0.00710 ± 0.00092	0.0373 ± 0.0048	0.0545 ± 0.0071
17.0 ± 1.0	2.88 ± 0.37	0.00705 ± 0.00092	0.0365 ± 0.0047	0.0543 ± 0.0071
17.0 ± 1.0	2.73 ± 0.35	0.00705 ± 0.00092	0.0359 ± 0.0047	0.0671 ± 0.0087
17.0 ± 1.0	2.66 ± 0.35	0.00699 ± 0.00091	0.0378 ± 0.0049	0.079 ± 0.010
17.9 ± 1.1	2.67 ± 0.35	0.00668 ± 0.00087	0.0375 ± 0.0049	0.0759 ± 0.0099
18.1 ± 1.1	2.68 ± 0.35	0.00668 ± 0.00087	0.0366 ± 0.0048	0.078 ± 0.010
18.3 ± 1.1	2.67 ± 0.35	0.00684 ± 0.00089	0.0392 ± 0.0051	0.0696 ± 0.0090
18.5 ± 1.1	2.65 ± 0.34	0.00687 ± 0.00089	0.0371 ± 0.0048	0.082 ± 0.011
18.7 ± 1.1	2.64 ± 0.34	0.00686 ± 0.00089	0.0359 ± 0.0047	0.089 ± 0.012
19.1 ± 1.1	2.52 ± 0.33	0.00689 ± 0.00090	0.0430 ± 0.0056	0.084 ± 0.011
19.4 ± 1.2	2.35 ± 0.31	0.00704 ± 0.00092	0.0393 ± 0.0051	0.082 ± 0.0011
19.8 ± 1.2	2.18 ± 0.28	0.00697 ± 0.00091	0.0388 ± 0.0050	0.0705 ± 0.0092
20.2 ± 1.2	2.71 ± 0.35	0.00750 ± 0.00098	0.0414 ± 0.0054	0.104 ± 0.014
20.2 ± 1.2	2.65 ± 0.34	0.0085 ± 0.0011	0.0427 ± 0.0056	0.126 ± 0.016
20.2 ± 1.2	2.68 ± 0.35	0.0095 ± 0.0012	0.0416 ± 0.0054	0.123 ± 0.016
20.7 ± 1.2	2.05 ± 0.27	0.0105 ± 0.0014	0.0377 ± 0.0049	0.0747 ± 0.0097
20.9 ± 1.3	2.03 ± 0.26	0.0120 ± 0.0016	0.0448 ± 0.0058	0.080 ± 0.010
21.0 ± 1.3	1.89 ± 0.25	0.0125 ± 0.0016	0.0434 ± 0.0056	0.089 ± 0.012
21.2 ± 1.3	2.00 ± 0.26	0.0130 ± 0.0017	0.0415 ± 0.0054	0.103V 0.013
21.4 ± 1.3	1.76 ± 0.23	0.0133 ± 0.0017	0.0488 ± 0.0063	0.081 ± 0.011
21.6 ± 1.3	1.75 ± 0.23	0.0138 ± 0.0018	0.0452 ± 0.0059	0.090 ± 0.012
22.0 ± 1.3	1.72 ± 0.22	0.0138 ± 0.0018	0.0450 ± 0.0059	0.078 ± 0.010
22.1 ± 1.3	1.62 ± 0.21	0.0145 ± 0.0019	0.0498 ± 0.0065	0.0732 ± 0.0095
22.3 ± 1.3	1.49 ± 0.19	0.0148 ± 0.0019	0.0521 ± 0.0068	0.093 ± 0.011
22.3 ± 1.3	1.59 ± 0.21	0.0172 ± 0.0022	0.0538 ± 0.0070	0.099 ± 0.013
22.4 ± 1.3	1.38 ± 0.18	0.0179 ± 0.0023	0.0580 ± 0.0075	0.095 ± 0.012
22.4 ± 1.3	1.25 ± 0.16	0.0175 ± 0.0023	0.0618 ± 0.0080	0.095 ± 0.012
22.4 ± 1.3	1.27 ± 0.17	0.0171 ± 0.0022	0.0601 ± 0.0078	0.099 ± 0.013
22.5 ± 1.4	1.68 ± 0.22	0.0177 ± 0.0023	0.0513 ± 0.0067	0.095 ± 0.012
22.5 ± 1.4	1.52 ± 0.20	0.0155 ± 0.0020	0.0477 ± 0.0062	0.0520 ± 0.0068
22.7 ± 1.4	1.42 ± 0.18	0.0186 ± 0.0024	0.0571 ± 0.0074	0.078 ± 0.010
22.7 ± 1.4	1.52 ± 0.20	0.0161 ± 0.0021	0.0451 ± 0.0059	0.083 ± 0.011
22.8 ± 1.4	1.34 ± 0.17	0.0193 ± 0.0025	0.0516 ± 0.0067	0.095 ± 0.012
22.8 ± 1.4	1.33 ± 0.17	0.0164 ± 0.0021	0.0492 ± 0.0064	0.101 ± 0.013
23.0 ± 1.4	1.44 ± 0.19	0.0199 ± 0.0026	0.0510 ± 0.0066	0.094 ± 0.012
23.0 ± 1.4	1.31 ± 0.17	0.0170 ± 0.0022	0.0591 ± 0.0077	0.080 ± 0.010
23.3 ± 1.4	1.34 ± 0.17	0.0205 ± 0.0027	0.0535 ± 0.0070	0.088 ± 0.011
23.5 ± 1.4	1.26 ± 0.16	0.0217 ± 0.0028	0.0598 ± 0.0078	0.089 ± 0.012
23.6 ± 1.4	1.29 ± 0.17	0.0244 ± 0.0032	0.0548 ± 0.0071	0.091 ± 0.012
23.8 ± 1.4	1.09 ± 0.14	0.0232 ± 0.0030	0.0650 ± 0.0085	0.089 ± 0.012
23.9 ± 1.4	1.16 ± 0.15	0.0238 ± 0.0031	0.0645 ± 0.0084	0.102 ± 0.013
24.1 ± 1.4	1.11 ± 0.14	0.0244 ± 0.0032	0.0576 ± 0.0075	0.098 ± 0.013
24.6 ± 1.5	1.17 ± 0.15	0.0242 ± 0.0031	0.0705 ± 0.0092	0.113V 0.015
24.6 ± 1.5	1.15 ± 0.15	0.0242 ± 0.0031	0.0732 ± 0.0095	0.109 ± 0.014
24.6 ± 1.5	1.21 ± 0.16	0.0242 ± 0.0031	0.0703 ± 0.0091	0.107 ± 0.014

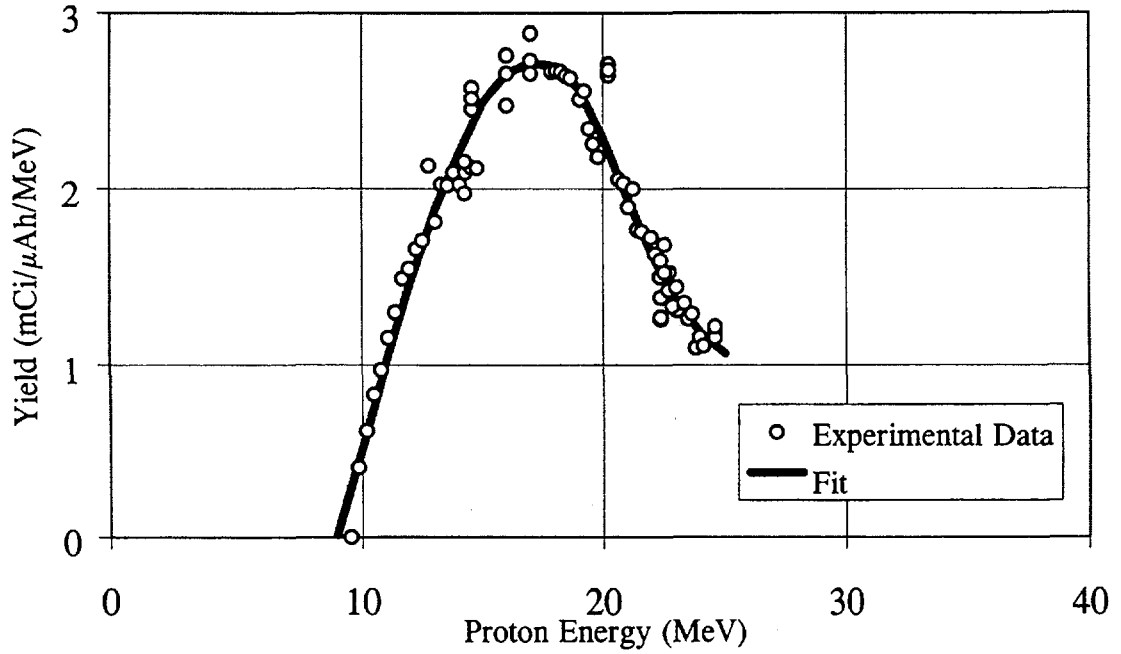

FIG. 5. Extrapolated ^{99m}Tc yields to enriched ^{100}Mo (CIS; 97.46%) targets.

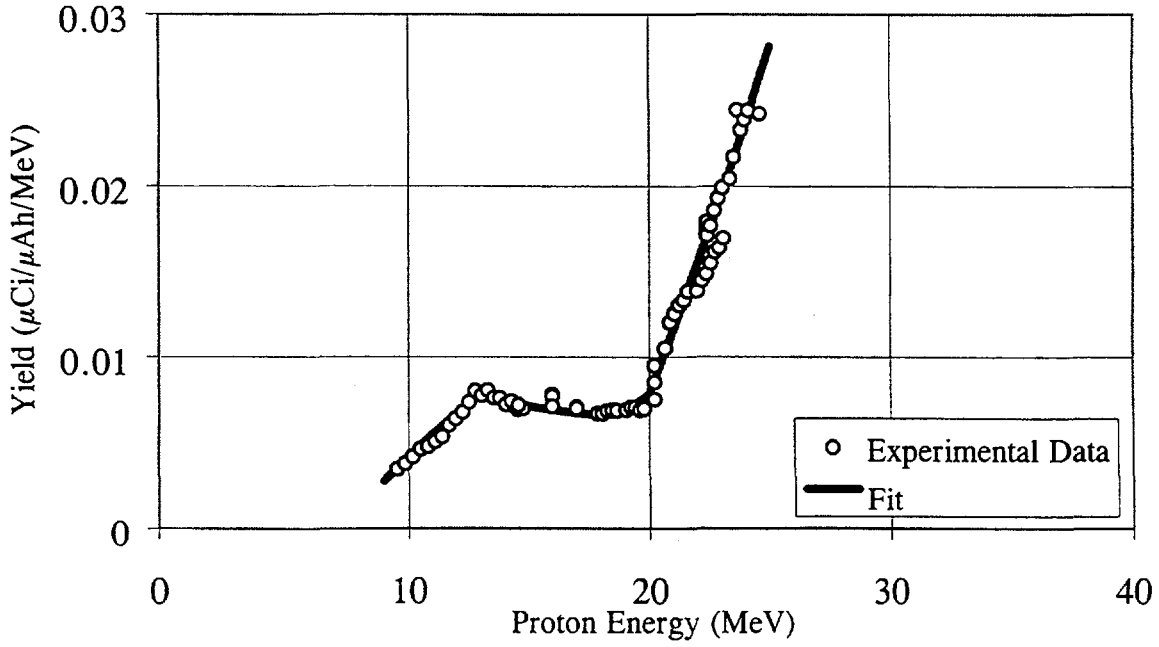

FIG. 6. Extrapolated ^{96}Tc yields to enriched ^{100}Mo (CIS; 97.46%) targets.

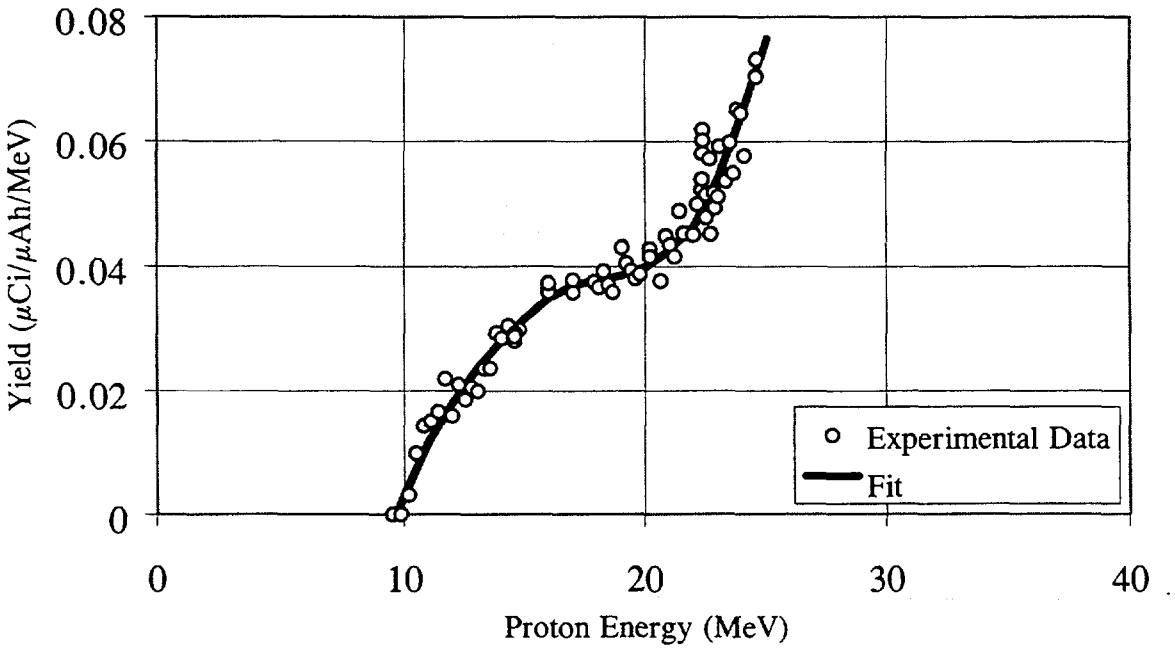

FIG. 7. Extrapolated ^{95}Tc yields to enriched ^{100}Mo (CIS; 97.46%) targets.

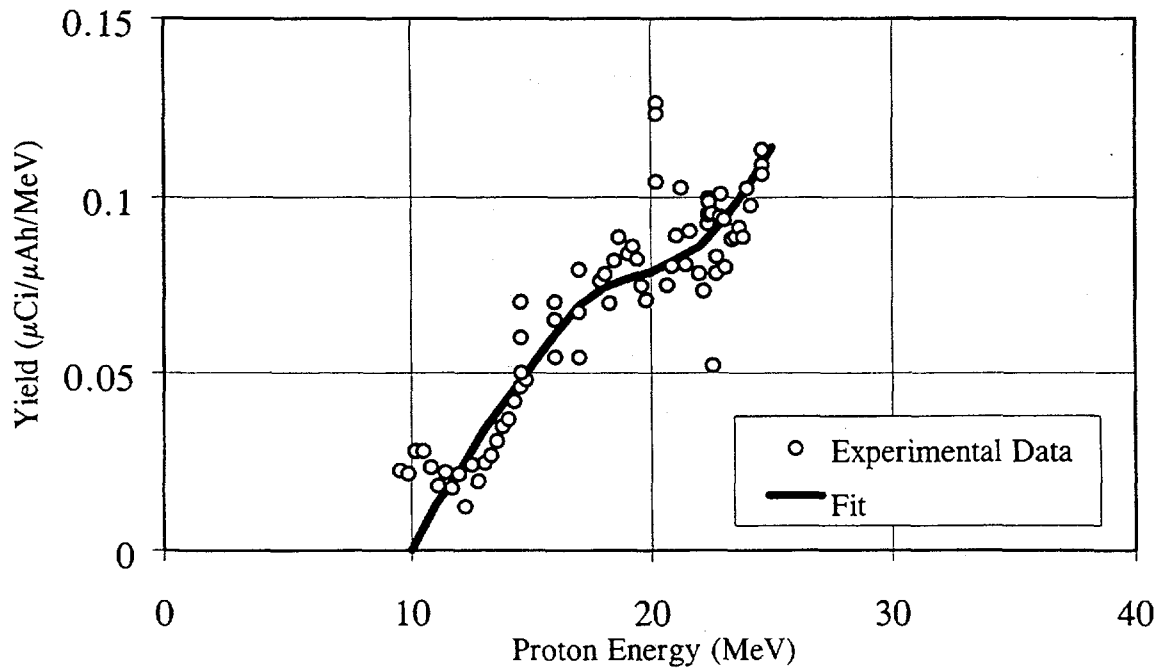

FIG. 8. Extrapolated ^{94}Tc yields to enriched ^{100}Mo (CIS; 97.46%) targets.

TABLE VI. COMPARISON OF MEASURED AND CALCULATED ^{99m}Tc AND ^{96}Tc YIELDS PRODUCED WITH 20.5 MeV PROTONS ON ENRICHED ^{100}Mo TARGETS (CIS; 97.46 %).

Proton Energy[1] (MeV)	Target Thickness (g/cm^2)	Energy Loss in Target (MeV)	^{99m}Tc Yields (EOB) Measured (mCi/μAh)	^{99m}Tc Yields (EOB) Calculated (mCi/μAh)	^{96}Tc Yields (EOB) Measured (μCi/μAh)	^{96}Tc Yields (EOB) Calculated (μCi/μAh)
19.24	0.155	2.17	4.53 ± 0.72	5.20 ± 0.68	0.0158 ± 0.0095	0.0160 ± 0.0021
19.26	0.152	2.12	4.58 ± 0.73	5.01 ± 0.65	0.0254 ± 0.0152	0.0156 ± 0.0020
19.36	0.139	1.93	4.26 ± 0.68	4.49 ± 0.58	0.0245 ± 0.0147	0.0142 ± 0.0018
19.31	0.145	2.02	4.09 ± 0.65	4.74 ± 0.62	0.0220 ± 0.0132	0.0149 ± 0.0019

[1]Mean value (see text).

TABLE VII. COMPARISON OF MEASURED AND CALCULATED ^{99m}Tc AND ^{96}Tc YIELDS PRODUCED WITH A 22.2-13.2 THICK TARGET USING ENRICHED ^{100}Mo (CIS; 97.46 %)[2].

Proton Energy (MeV)	Target Thickness (g/cm^2)	Energy Loss in Target (MeV)	^{99m}Tc Yields (EOB) Measured (mCi/μAh)	^{99m}Tc Yields (EOB) Calculated (mCi/μAh)	^{96}Tc Yields (EOB) Measured (μCi/μAh)	^{96}Tc Yields (EOB) Calculated (μCi/μAh)
22.2 -13.2	0.609	9.0	18.5 ± 7.4	20.6 ± 2.7	0.066 ± 0.040	0.073 ± 0.010
Radionuclide Purity (%)			>99.999	>99.999	0.00036	0.00035

[2] Results from radioassays before and after radiochemistry.

TABLE VIII. THICK-TARGET YIELDS AND PURITIES FOR ^{99m}Tc PRODUCED VIA THE ^{100}Mo(p,2n) REACTION USING CIS ENRICHED ^{100}Mo (97.46%) AND 10-MeV TARGET THICKNESSES.[3]

Target Thickness (Incident/Exit Energy) (MeV)	^{99m}Tc (mCi/μAh)	^{96}Tc (μCi/μAh)	^{95}Tc (μCi/μAh)	^{94}Tc (μCi/μAh)
20 - 10	21.1	0.0676	0.283	0.485
21 - 11	22.5	0.0725	0.317	0.559
22 - 12	23.0	0.0800	0.346	0.625
23 - 13	22.9	0.0904	0.376	0.686
24 - 14	22.1	0.1050	0.409	0.746
25 - 15	20.8	0.1230	0.450	0.808

[3]Calculations done by integration of yields as given in Table 5.

incident and exit proton energies, calculated using the computer code RANGE [17]. In addition, when limiting the incident proton energy on the ^{100}Mo target to less than 20.5 MeV, ^{96}Tc was the only Tc impurity detected in the target. Seven days after EOB, the cumulative ^{96}Tc yields were measured, converted to EOB, and the measured results also agreed with the calculated values obtained by extrapolation (Table VI). The final radionuclide purity for ^{99m}Tc was determined as > 99.99% at EOB, and can be improved further as a thicker target may be utilized to enhance the production of ^{99m}Tc, rather than ^{96}Tc. Limiting the proton incident energy to <20.5 MeV results, however, in a large penalty in ^{99m}Tc yields.

Further experimental testing with a 22.2-13.2-MeV thick ^{100}Mo targets (CIS; 97.46%), and a comparison of measured and calculated yields were also conducted.The results are summarized in Table VII. Once again, yield and purity measurements demonstrated the capabilities of this accelerator-based method to produce high-quality ^{99m}Tc for medical use.

In addition, the results of these tests further demonstrated the internal consistency of the excitation data reported here and the ability to predict yield and purity under a variety of target and proton energy conditions. These test results were then utilized in establishing the optimal proton energy and target thickness parameters for the production of ^{99m}Tc.

3.5. Optimization of the production of ^{99m}Tc from CIS ^{100}Mo (97.46%) targets

In order to maximize ^{99m}Tc yields and radionuclide purity with <23 MeV protons on CIS-type enriched ^{100}Mo (Table I), a series of calculations for 10-MeV thick targets were performed and the results are given in Table VIII. An inspection of these results indicated an optimal proton energy region of 22-12 MeV, under which the maximum cumulative ^{99m}Tc yield of 23.0 ± 3.0 mCi/μAh at EOB, is reached. On the basis of the results given in Table VII and the calculations summarized in Table VIII, we concluded that the optimization of ^{99m}Tc yield and purity should be performed around the 22-MeV proton energy region, with a 10-MeV thick target. Providing a maximum ^{99m}Tc yield and and purity should be performed around the 22-MeV proton energy region, with a 10-MeV thick target. Providing a maximum ^{99m}Tc yield and minimizing the level of ^{96}Tc production were the major factors considered in this conclusion.

3.5.1. Production test for ^{99m}Tc under optimal conditions

Experimental validations of the optimal production conditions defined above, were conducted with 22.4-MeV protons bombarding 22-12 MeV CIS-enriched ^{100}Mo targets. The results are summarized in Table IX, where the calculated ^{99m}Tc production rate and the level of Tc impurities are given as a function of time. The purity of the ^{99m}Tc thus produced is very high, >99.99% at EOB, and larger than 99.9% even 24 hours after EOB. This test confirmed the high purity level for ^{99m}Tc predicted from the excitation function data, and proved once more that the accelerator-based method reported here is suitable for producing ^{99m}Tc for

TABLE IX. TIME DEPENDENT YIELD AND PURITY FOR ^{99m}Tc PRODUCED FROM CIS ENRICHED ^{100}Mo (97.46%) VIA THE ^{100}Mo(p,2n) REACTION IN THE 22-12 MeV PROTON ENERGY REGION

Nuclide	EOB	EOB + 6h	EOB + 12h	EOB + 18h	EOB + 24 h
^{99m}Tc Yield (mCi/μAh)	23.0	11.5	5.78	2.89	1.45
^{99m}Tc Purity (%)	99.995	99.995	99.993	99.989	99.983
^{96}Tc	0.000348	0.000667	0.00128	0.00245	0.00470
^{95}Tc	0.00150	0.00244	0.00395	0.00640	0.0104
^{94}Tc	0.00272	0.00231	0.00197	0.00167	0.00143
Total Impurity (%)	0.00457	0.00542	0.00720	0.01050	0.01650

medical use. Technetium-96 (4.35 d) was the only impurity detected 48-96 h past EOB by using high-resolution γ-ray spectrometry. No further measurements were made due to the low count rates.

3.5.2. High-resolution gamma-ray spectrometry tests

In some test runs, the ^{100}Mo target was dissolved, and a radiochemical separation of Tc isotopes from the target material, and from other radionuclides formed, was conducted (see section 3.7, below). These procedures were followed by radioassays conducted with high-resolution (Ge) gamma-ray spectrometry methods. The results of these tests are shown in several γ-ray spectra of the directly-made ^{99m}Tc (Fig. 9, 100-450 keV γ-ray spectrum) and in Fig.10 (enhanced 650-900 keV γ-spectrum for Tc impurities). In addition, a comparison of radioassays was also made with similar γ-ray spectra taken from samples of ^{99m}Tc eluted from a commercial fission-made ^{99}Mo → ^{99m}Tc generator, which are shown in Figures 11 and 12, respectively. An analysis of these spectra revealed no detectable differences, suggesting that both accelerator-made and reactor-produced ^{99m}Tc products would provide similar quality and imaging resolution.

Additional information regarding the variation of ^{99m}Tc radionuclide purity that would potentially alter the quality of imaging during a 24-h long "usable shelf life" period-assumed for a directly-made source of ^{99m}Tc, is given in Table IX. In this Table, the level of radionuclide purity during different time intervals of the suggested effective shelf life of 24 hours, is given. Although ^{99m}Tc purity is reduced with time, even at the expiration time of ^{99m}Tc (24 h past EOB), its radionuclide purity remains above 99.9%, with <0.1% of Tc impurities (mostly ^{96}Tc) present.

Therefore, based upon the data and results presented here, different operational parameters for an accelerator-based method are available to achieve the desired yield and purity levels suggested from this data. The methodology used in this work, by comparing it with a commercial quality reactor-produced ^{99m}Tc, proved the validity of this conclusion.

3.6. Extrapolated ^{99m}Tc production capabilities

The potential of this new accelerator-based method for the production of ^{99m}Tc, can also be evaluated by using the current and forthcoming capabilities of modern proton accelerators operating with high intensity, mA-beams on targets capable of withstanding several-kW beam power deposition levels. In the 22-12 MeV proton energy region, the

TABLE X. EXTRAPOLATED ^{99m}Tc YIELDS FOR HIGH-INTENSITY, HIGH-POWER PRODUCTION WITH CIS ENRICHED ^{100}Mo (97.46%) TARGETS IN THE 22-12 PROTON ENERGY REGION[1].

Beam Current (mA)	Target Power (kW)	^{99m}Tc Yields per Irradiation Times (Ci/6h)		(Ci/12h)		(Ci/18h)	
		(EOB)	(EOB+24h)	(EOB)	(EOB+24h)	(EOB)	(EOB+24h)
1	10	99.6	6.28	150	9.46	175	11.0
2	20	199	12.6	299	18.9	349	22.0
5	50	498	31.4	748	47.2	874	55.1
10	100	996	62.8	1,496	94.4	1,747	110.2

[1] Corrected for decay during bombardment.

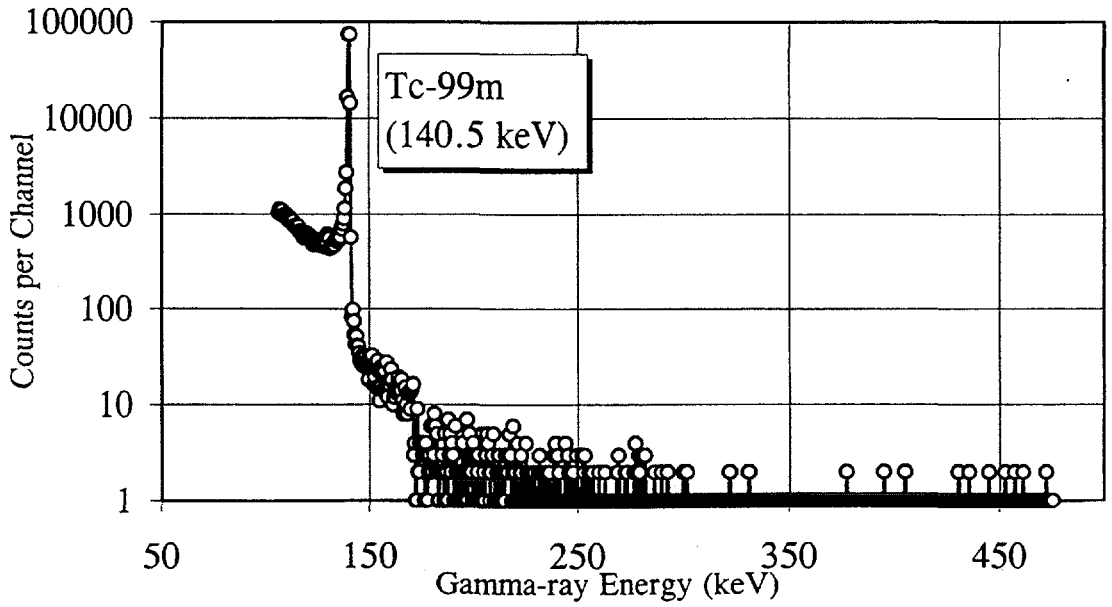

FIG. 9. Gamma-ray spectrum of accelerator-produced ^{99m}Tc from anenriched ^{100}Mo (CIS; 97.46%) thick (22.2-13.2 MeV) target Radioassay at 25 h after EOB.

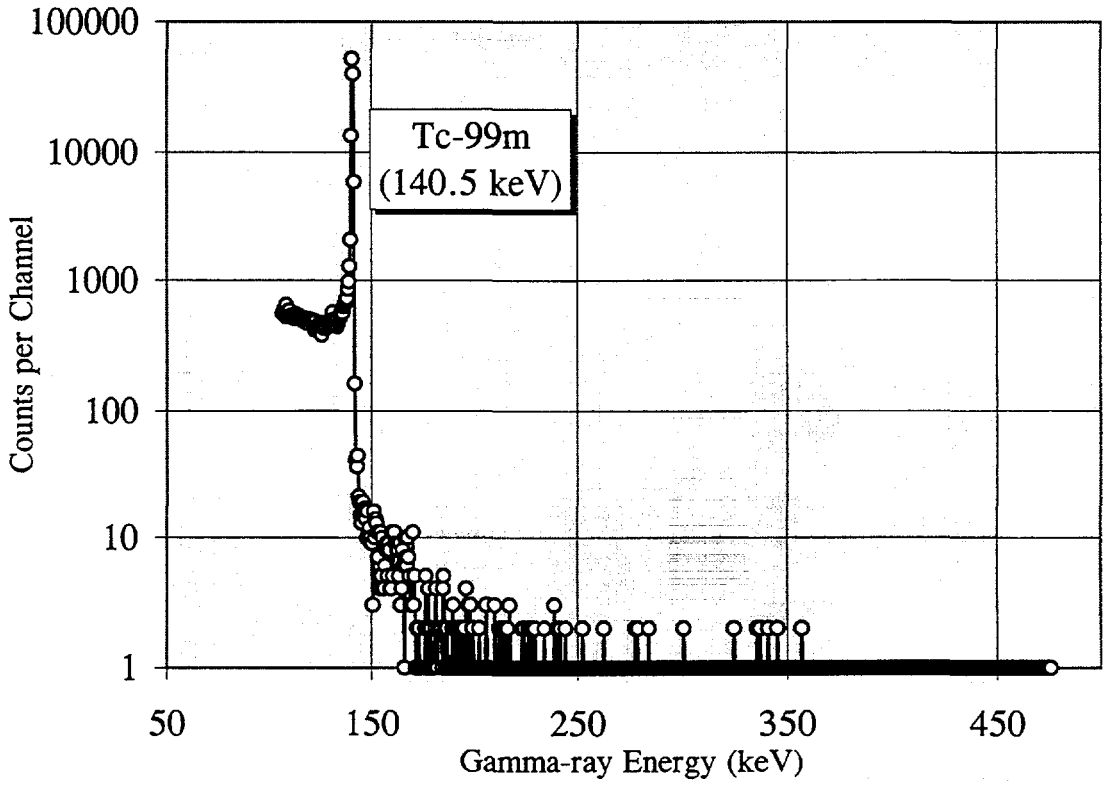

FIG. 10. Gamma-ray spectrum of generator-produced ^{99m}Tc. Radioassay at 24 h after elution.

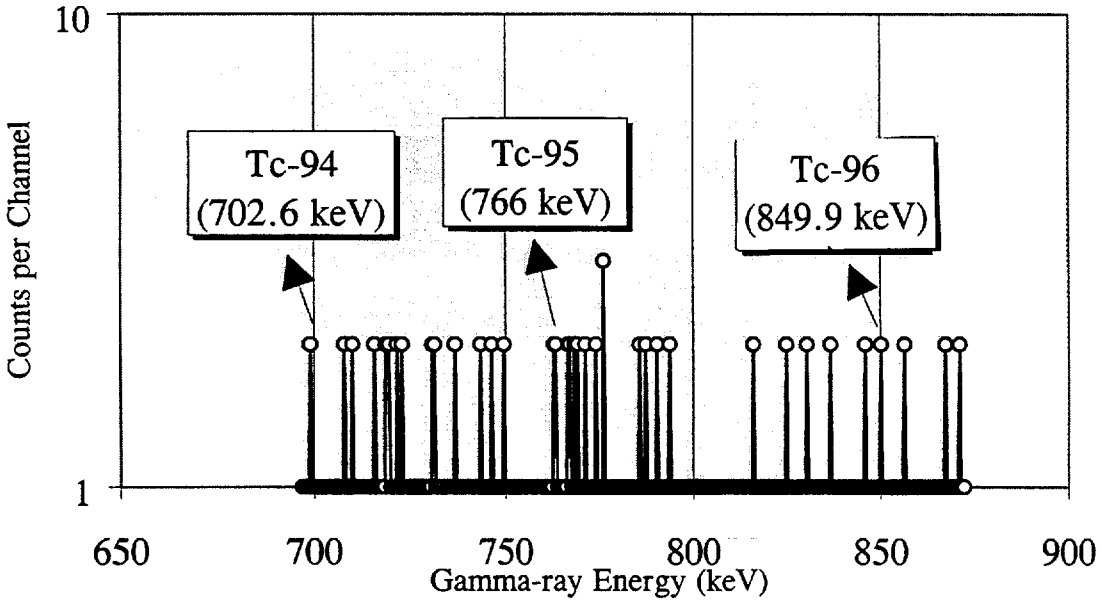

FIG. 11. Gamma-ray spectrum of accelerator-produced Tc impurities from an enriched ^{100}Mo (CIS; 97.46%) thick (22.2-13.2 MeV) target. Radioassay at 25 h after EOB.

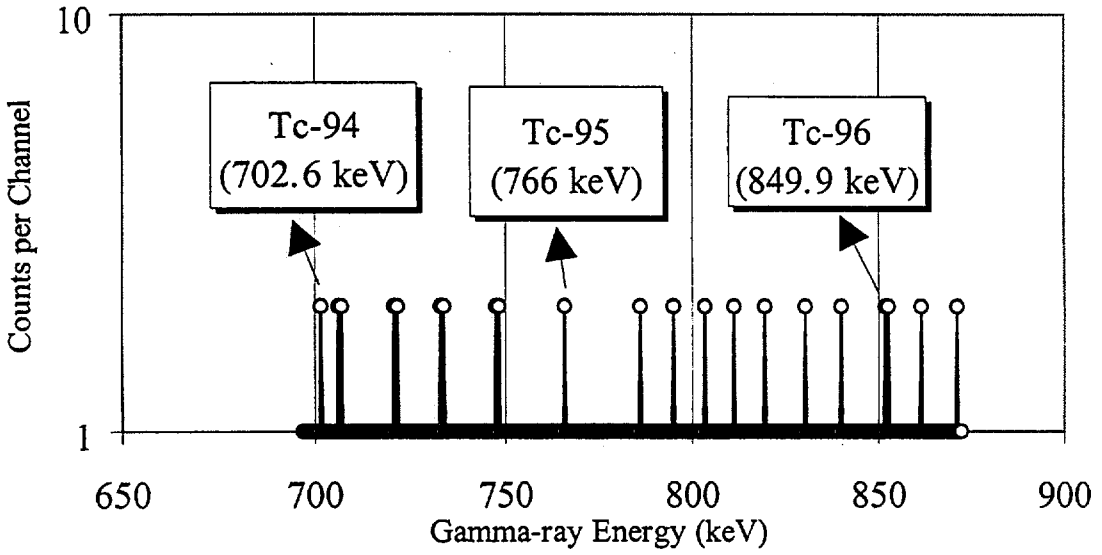

FIG. 12. Gamma-ray spectrum of generator-produced Tc impurities. Radioassay at 24 h after elution.

cumulative ^{99m}Tc yields per target were extrapolated to higher beam intensities and target power using enriched ^{100}Mo (97.46%). Results of these extrapolations, using current accelerator and target capabilities, and those under development, are summarized in Table X.

The use of a large 2-mA cyclotron beam current for radioisotope production was recently reported [19, 20], and higher currents up to 7 mA are being tested and developed [20]. Using high beam current and high power target technologies available today, as many as several hundreds Ci of ^{99m}Tc could be produced each day, indicating that the potential for local and/or regional supply with directly-produced ^{99m}Tc is technically feasible.

3.7. Target radiochemistry: separation and purification of directly-made ^{99m}Tc

The development and testing of rapid and efficient chemical separation methods for Mo-Tc radioactivity's is not a major challenge for the establishment of an accelerator-based method to produce ^{99m}Tc. Since the development of the ^{99}Mo → ^{99m}Tc generator system in the late 1960's by Richards et al, [3], there is ample and well documented information on methods apt for implementation and that can be easily subjected to automation to provide safe, rapid, and efficient Mo-Tc radiochemistry. Therefore, the radiochemistry used in this study was based upon this wealth of information, and was completed in less than 1 hour. This method was not automated, provided an efficient separation of Tc from Mo, an easy recovery of the enriched ^{100}Mo material from an aqueous solution, and was proven to be reliable. The steps and the timing of the method are summarized in Table XI. However, no efforts were made to complete the recovery cycle of the dissolved ^{100}Mo target material and, therefore, this task needs to be investigated. It is suggested, however, that there is ample experience in recovering and reusing enriched materials during commercial cyclotron production activities, and that the properties of Mo as a target, makes this task achievable.

As of this date, the specific activity of directly-made ^{99m}Tc, using the optimal conditions and the radiochemistry generally described above, has not been measured. A high specific activity is desirable as many of the synthesis for various ^{99m}Tc labeled radiopharmaceuticals may be affected. Studies using on-line nuclear spectroscopy methods to measure the relative ratio of excited states of ^{99}Tc (2.4 x 10^5 a) and ^{99m}Tc produced by proton bombardment of CIS enriched ^{100}Mo, are in progress and will be reported elsewhere [21]. Preliminary results and the nuclear properties indicated that a predominant formation of the ^{99m}Tc state is likely, which would suggest that an adequate specific activity can be achieved. Furthermore, the production of ^{99m}Tc from ^{100}Mo targets is conducted in a no-carrier-added condition.

TABLE XI. RADIOCHEMISTRY FOR SEPARATION OF ^{99m}Tc FROM Mo TARGETS

Radiochemistry Step	Time (min)	Elapsed Time (min)
^{100}Mo Target Dissolution with H_2O_2 (30%)	< 5	< 5
^{99m}Tc Separation by Solvent Extraction (MEK)	< 15	< 20
^{99m}Tc Purification by Ion Exchange	< 15	< 35
^{99m}Tc Chemical Formulation in Isotonic Saline	< 10	< 45
^{100}Mo Recovery in Aqueous Solution	< 10	n/a

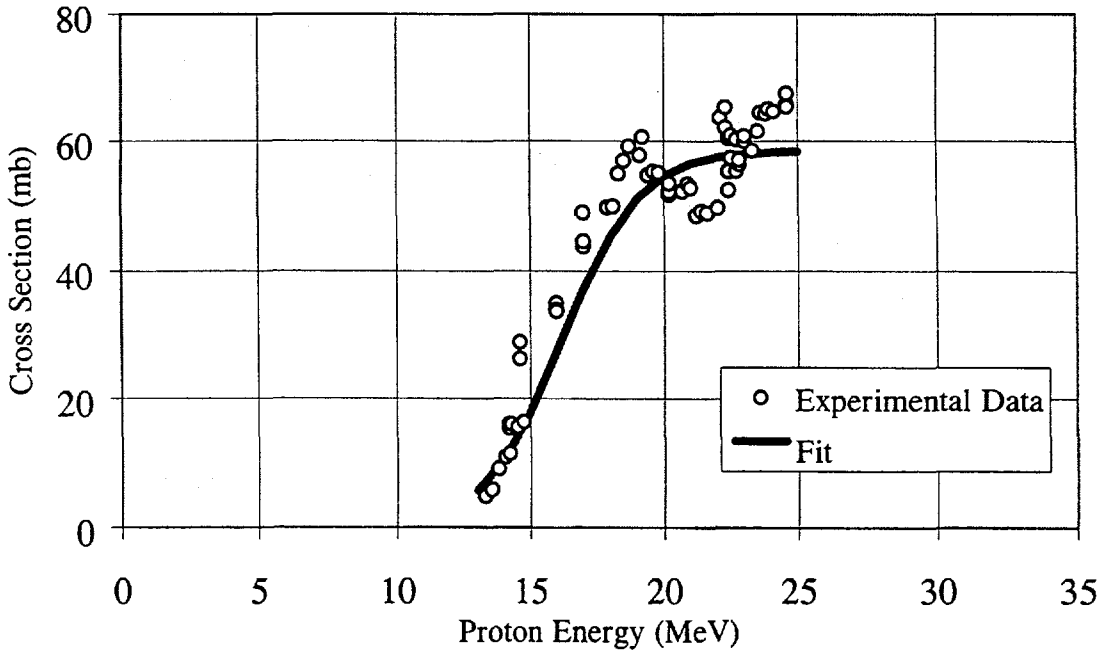

FIG. 13. Excitation function for the $^{100}Mo(p,pn)^{99}Mo$ reaction (Q= - 8.3 MeV).

3.8. Molybdenum-99 production

In addition to completing the experimental work regarding the production of Tc isotopes from Mo targets, the production of ^{99}Mo via the $^{100}Mo(p,pn)^{99}Mo$ (Q=-8.3 MeV) as a potential alternative method, was also investigated. The results of the cross section measurements were listed in Table IV and are shown in Fig. 13. The cumulative yield of ^{99}Mo from CIS enriched ^{100}Mo (97.46%) targets in the 25 to 13 MeV proton energy region, was calculated as 360 μCi/μAh. This result compared well with previously determined yields using natural Mo targets [6]. However, this accelerator-based yield is too low to be competitive with reactor production of ^{99}Mo, which is estimated as 32 Ci/h using neutron-induced fission methods [22]. In addition, ^{99}Mo would be produced in the same matrix as the enriched (and expensive) ^{100}Mo target material, forcing recovery for recycling. Furthermore, the resulting specific activity would be low and not practical for the current generation of high-specific activity fission-produced $^{99}Mo \rightarrow ^{99m}Tc$ generators. Finally, if natural Mo is used to avoid some of the above indicated conditions, the yield would be lowered by a factor of ≈10. An alternative to this approach using proton-induced fission methods, is under study [11,12].

3.9. Future work

Additional large-scale production experiments using enriched ^{100}Mo targets and incident proton energies in the 20-23 MeV region should be undertaken to provide further assurances on an optimal condition for the production of ^{99m}Tc. In these runs, further radioassays to confirm radionuclide purity, specific activity, labeling yields, and imaging characteristics shall be included. Radiochemistry methods must be further evaluated and optimized to confirm that automated, rapid, and efficient processing and recovery of expensive target material are available. Furthermore, the economic and logistical aspects on the potential use of directly-made ^{99m}Tc should be ascertained. Finally, the potential impact of this technique in developing regions must be evaluated. Most if not all these regions are

depending on foreign supply based on the operation of few commercial reactors, and many at present rely on aging reactor facilities facing decommissioning. Accelerator facilities capable of undertaking this operation are more likely to succeed than new or reconditioned reactors in obtaining support and funding, because modern accelerators are capable of supporting a broader spectrum of diagnostic and therapeutic nuclear medicine applications than reactors. Besides, given the current efforts in developing nations to improve medical technologies, accelerator sources are more likely to succeed in securing core support, as they can be applied to many other science & technology development programs.

4. CONCLUSIONS

The production of directly-made ^{99m}Tc via ^{100}Mo(p,2n) reaction on enriched ^{100}Mo targets in a cyclotron with <25 MeV protons has been demonstrated. The detailed excitation function study indicates that with 97.46 % enriched ^{100}Mo, high production rate (a cumulative ^{99m}Tc yield of 23.0 ± 3.0 mCi/μAh at EOB) and high purity (>99.99% at EOB, and >99.9% within 24 h after EOB) are reachable in the yield-optimized proton energy region of 22 to 12 MeV. The directly-made ^{99m}Tc was proved to be of excellent radionuclidic purity as compared with reactor-made commercial ^{99}Mo→^{99m}Tc generator materials.

Instant ^{99m}Tc produced in this fashion would have to be produced in regional/centralized accelerator facilities limiting the supply to local/regional users. In comparison to existing reactor and generator techniques, this method would have several economical advantages as it would minimize nuclear waste production and management costs as well as public and environmental health concerns associated with nuclear reactors.

REFERENCES

[1] BEAVER, J.E., HUPF, H.B., Production of Tc-99m on a medical cyclotron: a feasibility study, J. Nucl. Med. **12(11)** (1971) 739-741.

[2] ALMEIDA, G.L., HELUS, F., On the production of Mo-99 and Tc-99m by cyclotron, Radiochem. Radioanal. Lett. **28(3)** (1977) 205-214.

[3] RICHARDS, P. In: "The Technetium-99m Generator". Andrews, G.A., Kniseley, J.W., and Wagner H.N. Jr., (Eds.). U.S. Atomic Energy Commission (1966).

[4] LAGUNAS-SOLAR, M.C., et al., "Accelerator production of molybdenum-99 as a non-reactor source of Mo-99→ Tc-99m generators". (Abstract). IX Congress of the Latin American Association of Biology and Nuclear Medicine. October 8-11, 1989, Santiago, Chile.

[5] LAGUNAS-SOLAR, M.C., "Cyclotron production of Tc-99m and Mo-99 for nuclear medicine applications: a new alternative to reactor-based methods". (Abstract). 15th. Annual Western Regional Meeting of the Society of Nuclear Medicine, Nov. 1-4, 1990, Long Beach, CA. See: J. Clinical Nuclear Medicine 15(10) (1990) 769.

[6] LAGUNAS-SOLAR, M.C., et al., Cyclotron production of NCA ^{99m}Tc and ^{99}Mo. An alternative non-reactor supply source of instant ^{99m}Tc and ^{99}Mo→ ^{99m}Tc generators, J. Appl. Radiat. Isot. **42(7)** (1991) 643-657.

[7] LAGUNAS-SOLAR, M.C., et al., "Accelerator production of Technetium-99m. targetry and radiochemistry effects on yield and purity (Abstract)". 13th International Conference on the Application of Accelerators in Research & Industry (November 7-10, 1994). Denton, Texas, USA.

[8] LAGUNAS-SOLAR, M.C., Production of Tc-99m and Mo-99 for nuclear medicine applications via accelerators as an option to reactor methods, J. Radiation Protection in Australia, **13(1)** (1995) 16-25.

[9] LAGUNAS-SOLAR, M.C. et al., "An update on the direct production of Tc-99m with proton beams and enriched Mo-100 targets". Annual Meeting of the American Nuclear Society (June 16-20, 1996), Reno, Nevada, USA.
[10] EGAN G., JAMIESON, C., LAGUNAS-SOLAR, M.C., An investigation into the technical feasibility of cyclotron production of Technetium-99m, Journal of Australia & New Zealand Society of Nuclear Medicine (March 1994) 25-31.
[11] LAGUNAS-SOLAR, M.C. et al., "Proton fission for the accelerator production of Mo-99". (Abstract). 205th ACS National Meeting, March 28-April 2, 1993, Denver, Colorado. Book of Abstract # 66.
[12] LAGUNAS-SOLAR, M.C. et al., "Cyclotron production of molybdenum-99 via proton-induced uranium-238 fission". 1996 Annual Meeting of the American Nuclear Society, June 6-12, 1996, Reno, Nevada.
[13] WILLIAMSON, C., et al., Saclay Report No.CEA-R-3042, (1966).
[14] GREENE, M.W., LEBOWITZ, E., Protons reactions with copper for auxiliary cyclotron beam monitoring, Int. J. Appl. Rad. Isot. **23** (1972) 342-344.
[15] JUNGERMAN, J.A. et al., Time-of-flight facility for the absolute measurement of the beam energy of a medium-energy cyclotron, Nucl. Instr. and Meth. **204** (1982) 41.
[16] ROMERO, J.L. et al., A simple time-of-flight method to measure the beam energy of a cyclotron, Nucl. Instr. and Meth. **100** (1972) 551.
[17] CROCKER NUCLEAR LABORATORY COMPUTER CODE (RANGE) (J. Lewis, August 1985).
[18] LEVKOVSKII, V.N., "Activation cross section of nuclides with average masses (A=40-100) by protons and alpha particles with average energies (E=10-50 MeV), Inter Vesi, Moscow, Russia, (1991), p.155.
[19] JONGEN, Y. et al., High intensity H^- cyclotrons for radioisotope production, Ionizing Radiation **15(3)** (1989) 65-74.
[20] JONGEN, Y. et al. Consultants Meeting of IAEA, (April 10-12, 1997), Faure, South Africa.
[21] LAGUNAS-SOLAR, M.C., ZENG, N.X., CASTANEDA, C.M., "Determination of specific activity of accelerator-made ^{99m}Tc by on-line nuclear spectroscopy methods". (Manuscript in Preparation).
[22] MUNZE, R. et al., Large scale production of fission Mo-99 by using fuel elements of a research reactor as starting material, Int. J. Appl. Rad. Isot. **35** (1984) 749-754.

EXCITATION FUNCTIONS OF DEUTERON INDUCED NUCLEAR REACTIONS ON ^{nat}Mo UP TO 21 MeV

An alternative route for the production of ^{99m}Tc and ^{99}Mo

M. SONCK[1]*, S. TAKÁCS[2], F. SZELECSÉNYI[2],
A. HERMANNE[1], F. TÁRKÁNYI[2]

[1] Cyclotron Department, Vrije Universiteit Brussel,
Brussels, Belgium

[2] Institute of Nuclear Research of Hungarian Academy of Sciences,
Debrecen, Hungary

Abstract

Cross sections of deuteron induced nuclear reactions on natural molybdenum have been studied in the frame of a systematic investigation of charged particle induced nuclear reactions on metals for different applications. The excitation functions of ^{92m,95}Nb-, ^{93,94g,94m,95g,95m,96,99m}Tc- and ^{99}Mo were measured up to 21 MeV deuteron energy by using stacked foil technique and activation method. The goal of this work was to study the production possibility of the medical important ^{94m,99m}Tc- and ^{99}Mo-nuclides. Production of ^{99m}Tc and ^{99}Mo is of importance for their use in nuclear medicine, whereas ^{94m}Tc is of interest regarding quantification of kinetics of well-established ^{99m}Tc-radiopharmaceuticals. The production possibilities of ^{99m}Tc and ^{99}Mo above 20 MeV deuteron energies up to 50 MeV were estimated and was found that beside the proton induced reactions the deuteron induced reactions on enriched molybdenum target are very promising.

1. INTRODUCTION

The importance of ^{99m}Tc for nuclear medicine is well known, with almost 90% of the nuclear medicine studies utilising this nuclide. Currently ^{99m}Tc is produced through the mother isotope ^{99}Mo which is a fission product with $T_{1/2}$ = 66 h. Today's world's need of ^{99}Mo is produced in a small number of research reactors which have been in operation for a considerable time and are due for refurbishment or decommissioning. Although at present there is still an overproduction capacity, future problems with the availability of ^{99}Mo can be expected if no new dedicated reactors are licensed rapidly. This leads to a search for alternative production techniques for ^{99m}Tc of which direct cyclotron production and indirect production by cyclotron-driven subcritical assemblies are the most important ones. Searching for other possible production routes the charged particle induced fission on heavy elements (U) and the light charged particle induced nuclear reactions on neighbouring elements of Mo could be important. From the light charged particle induced reactions the proton induced ones are the most promising and the deuteron induced reactions can also be important. The proton induced reactions were investigated in detail, but the deuteron reactions were studied only up to 13 MeV. In this paper we will focus on the possibilities of direct production by deuteron beams of ^{99m}Tc and ^{99}Mo up to 20 MeV deuteron energies and also give some considerations for the production of ^{99m}Tc and ^{99}Mo at higher deuteron energies, up to 50 MeV.

First we collect the preliminary results of our cross section measurements obtained up to 21 MeV deuteron energy on natural Molybdenum. Part of this results were presented at the Conference on Nuclear Data for Science and Technology-97 in Trieste and will be presented at the 2nd International Conference on Isotopes in Sydney.

*Aspirant Fonds voor Wetenschappelijk Onderzoek (FWO), Brussel, Belgium.

In the second part we present the results of our calculations concerning production yields of ^{99m}Tc and ^{99}Mo at higher deuteron energies (up to 50 MeV) in comparison with yields of other charged particle induced reactions. The experimental verification of the estimated yield calculation is in progress.

2. EXPERIMENT

Irradiations were carried out with the external beams of the VUB CGR 560 and the ATOMKI MGC 20E cyclotron. Stacks containing up to 16 foils of 12 μm thick ^{nat}Mo foils (Goodfellow-99.9 % purity) were irradiated for about 1 hour with 200 nA deuteron beams of 10, 16 and 21 MeV primary energies. The beam current was kept constant during each irradiation and was measured in a Faraday-cup. The target holder was equipped with a special "long" collimator and a secondary electron suppressor. The irradiation set-up, the experimental technique, data acquisition and data evaluation were the same or similar as described earlier by us [1,2]. The initial energy of the particles was determined with an accuracy of ± 0.3 MeV by time-of-flight method at the Brussels cyclotron [2] and ± 0.2 MeV by an analysing magnet for irradiations in Debrecen. The effective "on target" energy for each foil was determined using the energy-range formula and tables of Andersen and Ziegler [3]. The activity of the irradiated foils was measured without chemical separation by high resolution gamma-ray spectrometry. The decay of the activity of the samples was followed by measuring each sample several times. All given cross sections are production cross sections and are hence calculated for ^{nat}Mo. The decay data of the investigated isotopes and the Q-values of the contributing processes were taken from Browne and Firestone [4] and are shown in Table I. The average error on the cross section values varies from 10% to 15% and was obtained by quadratic summation of the individual errors.

3. RESULTS AND DISCUSSION

When bombarding ^{nat}Mo with deuteron beams up to 21 MeV, several reaction processes are taking place and contribute to the simultaneous formation of the g-emitting ^{92m,95}Nb, ^{93,94g,94m,95g,95m,96,99m}Tc and ^{99}Mo nuclides. Some of these reactions are measured for the first time above 13 MeV up to 21 MeV. This paper will concentrate more on the production routes for ^{99m}Tc ($T_{1/2}$ = 6.01 h), ^{99}Mo ($T_{1/2}$ = 2.75 d) and ^{94m}Tc ($T_{1/2}$ = 52 min), and investigates the other reactions on ^{nat}Mo which are also important in the practical production point of view. Only a very limited number of other works were found in the literature, all limited to 13 MeV deuteron energy. In the overlapping energy regions our data are mostly in good agreement with the available literature data.

3.1. ^{92m}Nb ($T_{1/2}$ = 10.15 d)

The results obtained for the formation of ^{92m}Nb are shown in Fig. 1. The cross section values were calculated from a spectroscopic analysis performed after a rather long cooling time (>30 days). The 99.0% abundant 934.5 keV g-line was used to characterise this nuclide. Only two literature references by Randa et al. [6] and Anders et al. [5] could be found for this excitation curve, giving slightly lower cross section values. The main contributing reactions are ^{97}Mo(d,a) with Q =+9.95 MeV, ^{98}Mo(d,an) with Q=+1.31 MeV, ^{95}Mo(d,2p) with Q =-2.37 MeV, ^{96}Mo(d,^{3}He) with Q=-3.8 MeV and ^{100}Mo(d,a3n) with Q =-12.9 MeV. At 20 MeV deuteron energy a cross section of 8 mb is reached after a near linear behaviour. No other data on this reaction are available and no extremum is reached in the studied energy band.

TABLE I. NUCLEAR DATA OF THE REACTIONS

Nuclide	Half life	Decay mode	E_γ keV	I_γ %	Contributing reactions	Q values MeV
Molybdenum						
^{101}Mo	14.6 m	β^- (100)	191.9	18.8	^{100}Mo(n,γ)	5.40
			590.9	16.9	^{100}Mo(d,p)	3.17
^{99}Mo	2.75 d	β^- (100)	181.1	12.14	^{100}Mo(d,p2n)	-10.51
			739.5	12.14	^{98}Mo(d,p)	3.70
					^{98}Mo(n,γ)	5.93
					^{100}Mo(n,2n)	-8.29
					^{99}Nb decay	(-5.65)
^{93}Mo	3500 y	EC (100)	30.4	<0.0005	^{94}Mo(d,p2n)	-11.90
					^{92}Mo(d,p)	5.85
					^{92}Mo(n,γ)	8.07
					^{93m}Mo decay	(5.65)
					^{93}Tc decay	(1.86)
^{93m}Mo	6.85 h	IT (99.88)	263.1	56.7	^{94}Mo(d,p2n)	-14.33
		EC (0.12)	684.8	99.7	^{92}Mo(d,p)	3.42
			1477.2	99.9	^{92}Mo(n,γ)	5.65
					^{93}Tc decay	(1.86)
^{91}Mo	15.5 m	β^+ (94.1)	1637	0.329	^{92}Mo(d,p2n)	-14.89
		EC (5.9)			^{92}Mo(n,2n)	-12.67
					^{91m}Mo decay	(-13.33)
					^{91}Tc decay	(-21.88)
^{91m}Mo	65 sec	IT (50.1)	652.98	48.2	^{92}Mo(d,p2n)	-15.55
		EC (49.9)	1507.9	24.4	^{92}Mo(n,2n)	-13.33
					^{91}Tc decay	(-21.88)
Technetium						
^{101}Tc	14.2 m	β^- (100)	306.8	88	^{100}Mo(d,n)	5.22
			545	5.99	^{101}Mo decay	(3.17)
^{100}Tc	15.8 s	β^- (100)	539.5	7.0	^{100}Mo(d,2n)	-3.17
			590.8	5.7		
^{99}Tc	$2.13*10^5$ y	β^- (100)	89.75	$4.9*10^{-6}$	^{98}Mo(d,n)	4.28
					^{100}Mo(d,3n)	-9.94
					^{99}Mo decay	(5.92)
					^{99m}Tc decay	(4.13)
^{99m}Tc	6.006 h	IT (100)	140.5	87.2	^{98}Mo(d,n)	4.13
					^{100}Mo(d,3n)	-10.08
					^{99}Mo decay	(5.92)
^{98}Tc	$4.2*10^6$ y	β^- (100)	652.4	99.7	^{98}Mo(d,2n)	-4.69
			745.4	99.8	^{97} Mo(d,n)	3.95

TABLE I. (Cont.)

Nuclide	Half life	Decay mode	Eγ keV	Iγ %	Contributing reactions	Q values MeV
^{97}Tc	2.6*10^{6} y	EC (100)	no		^{98}Mo(d,3n)	-11.97
					^{97}Mo(d,2n)	-3.33
					^{96}Mo(d,n)	3.49
					^{97m}Tc decay	(3.40)
^{97m}Tc	90.5 d	IT (100)	96.5	0.31	^{98}Mo(d,3n)	-12.07
					^{97}Mo(d,2n)	-3.42
					^{96}Mo(d,n)	3.40
^{96}Tc	4.28 d	EC (100)	778.2	99.76	^{97}Mo(d,3n)	-12.80
			812.5	82	^{96}Mo(d,2n)	-5.98
			850.1	98	^{95}Mo(d,n)	3.18
					^{96m}Tc decay	(3.14)
^{96m}Tc	51.5 m	IT (98)	778.2	1.9	^{97}Mo(d,3n)	-12.83
		EC (2)	1200.2	1.09	^{96}Mo(d,2n)	-6.01
					^{95}Mo(d,n)	3.14
^{95}Tc	20.0 h	EC (100)	765.8	94	^{96}Mo(d,3n)	-13.85
			1073.7	3.75	^{95}Mo(d,2n)	-4.70
					^{94}Mo(d,n)	2.67
					^{95m}Tc decay	(2.63)
^{95m}Tc	61 d	EC (95.8)	204.1	66.2	^{96}Mo(d,3n)	-13.89
		IT (3.9)	582.1	31.4	^{95}Mo(d,2n)	-4.74
		β^+ (0.3)	835.1	27.9	^{94}Mo(d,n)	2.63
^{94}Tc	4.88 h	EC (89)	702.6	99.6	^{95}Mo(d,3n)	-14.63
		β^+ (11)	849.7	95.8	^{94}Mo(d,2n)	-7.26
					^{94m}Tc decay	(-7.34)
^{94m}Tc	52 min	EC (28)	871.1	94.2	^{95}Mo(d,3n)	-14.71
		β^+ (72)	1521.6	4.5	^{94}Mo(d,2n)	-7.34
^{93}Tc	2.75 h	EC (87)	1363.1	66	^{94}Mo(d,3n)	-15.88
		β^+ (13)	1520.3	23.9	^{92}Mo(d,n)	1.86
					^{93m}Tc decay	(1.47)
^{93m}Tc	43.5 m	IT (20)	392.5	60	^{94}Mo(d,3n)	-16.28
		EC (80)	1644.5	15.9	^{92}Mo(d,n)	1.47
^{92}Tc	4.4 m	EC (100)	773.1	100	^{92}Mo(d,2n)	-10.87
			1509.6	100		
^{91}Tc	3.14 m	β^+	810.8	5.1	^{92}Mo(d,3n)	-21.88
		EC	1111.1	3.18	^{91m}Tc decay	(-22.28)
^{91m}Tc	3.3 m	β^+	652.98	70	^{92}Mo(d,3n)	-22.28
		EC	502.99	50.4		

TABLE I. (Cont.)

Nuclide	Half life	Decay mode	Eγ keV	Iγ %	Contributing reactions	Q values MeV
Niobium						
^{99}Nb	15.0 s	β^- (100)	97.7	45	^{100}Mo(d,^{3}He)	-5.65
			137.8	90	^{100}Mo(d,2pn)	-13.37
					^{99m}Nb decay	(-6.02)
^{99m}Nb	2.6 min	β^- (96.2)	97.7	6.7	^{100}Mo(d,^{3}He)	-6.02
		IT (3.8)	253.5	3.7	^{100}Mo(d,2pn)	-13.74
^{98}Nb	2.86 s	β^- (100)	787.3	3.2	^{100}Mo(d,α)	8.05
			1023.9	1.6	^{98}Mo(d,2p)	-6.03
					^{98}Mo(n,p)	-3.80
					^{98m}Nb decay	(7.97)
^{98m}Nb	51.3 m	β^- (99.9)	787.3	71	^{100}Mo(d,α)	7.97
		IT (0.1)	722.7	93	^{98}Mo(d,2p)	-6.11
					^{98}Mo(n,p)	-3.89
^{97}Nb	72.1 m	β^- (100)	658.2	98.34	^{98}Mo(d,n2p)	-17.08
					^{97}Mo(n,p)	-1.15
					^{97m}Nb decay	(-1.9)
^{97m}Nb	1 m	IT (100)	743.32	97.95	^{98}Mo(d,n2p)	-17.83
					^{97}Mo(n,p)	-1.90
^{96}Nb	23.35 h	β^- (100)	1091.3	48.5	^{98}Mo(d,α)	8.20
			1200.2	19.8	^{100}Mo(d,α2n)	-6.01
					^{96}Mo(n,p)	-2.41
^{95}Nb	34.97 d	β^- (100)	765.8	99.79	^{97}Mo(d,α)	9.95
					^{98}Mo(d,αn)	1.31
					^{95}Mo(d,2p)	-2.37
					^{96}Mo(d,2pn)	-11.52
					^{96}Mo(d,^{3}He)	-3.80
					^{95}Mo(n,p)	-0.14
					^{95m}Nb decay	(9.72)
^{95m}Nb	86.6 h	IT (97.5)	235.7	24.9	^{97}Mo(d,α)	9.72
		β^- (2.5)			^{98}Mo(d,αn)	1.07
					^{95}Mo(d,2p)	-2.60
					^{96}Mo(d,2pn)	-11.76
					^{96}Mo(d,^{3}He)	-4.04
					^{95}Mo(n,p)	-0.38
^{94}Nb	2.03*10^4 y	β^- (100)	702.6	99.8	^{96}Mo(d,α)	8.29
			871.1	99.9	^{97}Mo(d,αn)	1.46
					^{94}Mo(n,p)	-1.26
					^{94m}Nb decay	(8.24)

TABLE I. (Cont.)

Nuclide	Half life	Decay mode	Eγ keV	Iγ %	Contributing reactions	Q values MeV
^{94m}Nb	6.26 m	IT (99.5)	871.1	0.5	^{96}Mo(d,α)	8.24
		β^- (0.5)			^{97}Mo(d,αn)	1.42
					^{94}Mo(n,p)	-1.30
^{92}Nb	3.6*10^7 y	EC (100)	561.1	100	^{94}Mo(d,α)	8.75
			934.5	100	^{95}Mo(d,αn)	1.38
					^{92}Mo(d,2p)	-1.80
					^{96}Mo(d,α2n)	-7.77
					^{97}Mo(d,α3n)	-14.59
					^{92}Mo(n,p)	0.43
					^{92m}Nb decay	(8.62)
^{92m}Nb	10.15 d	EC (99)	934.5	99	^{94}Mo(d,α)	8.62
		β^+ (1.0)			^{95}Mo(d,αn)	1.25
					^{92}Mo(d,2p)	-1.93
					^{96}Mo(d,α2n)	-7.91
					^{97}Mo(d,α3n)	-14.73
					^{92}Mo(n,p)	0.29
^{91}Nb	680 y	EC (100)	no γ		^{94}Mo(d,αn)	0.87
					^{92}Mo(d,^{3}He)	-1.96
					^{92}Mo(d,2pn)	-9.68
					^{91}Mo decay	(-12.67)
					^{91m}Nb decay	(0.76)
^{91m}Nb	60.86 d	IT (96.6)	1205.0	4	^{94}Mo(d,αn)	0.76
		EC (3.4)			^{92}Mo(d,^{3}He)	-2.07
					^{92}Mo(d,2pn)	-9.78
					^{91}Mo decay	(-12.67)
^{90}Nb	14.6 h	EC (47)	1129.2	92.7	^{92}Mo(d,α)	6.59
		β^+ (53)	2318.9	82	^{90}Mo decay	(-25)
					^{90m}Nb decay	(6.44)
^{90m}Nb	18.81 s	IT (100)	122.9	64	^{92}Mo(d,α)	6.44
					^{90}Mo decay	(-25)

The only reference found in literature with respect to this excitation curve, published by Randa et al. [6], is in good agreement with our results. Our measurements show a nearly linear behaviour in the observed energy range and the cross section reaches 7 mb at 20 MeV deuteron energy. The contributing reactions in this energy region are ^{94}Mo(d,x) (mainly ^{94}Mo(d,a) with Q=+8.62 MeV), ^{95}Mo(d,x) (mainly ^{95}Mo(d,an) with Q=+1.25 MeV), ^{92}Mo(d,2p) with Q =-1.93 MeV, ^{96}Mo(d,x) (mainly ^{96}Mo(d,a2n) with Q=-7.91 MeV) and ^{97}Mo(d,x) (mainly ^{97}Mo(d,a3n) with Q=-14.73 MeV). As no cross section extremum is reached in the observed energy band additional and independent measurements are needed.

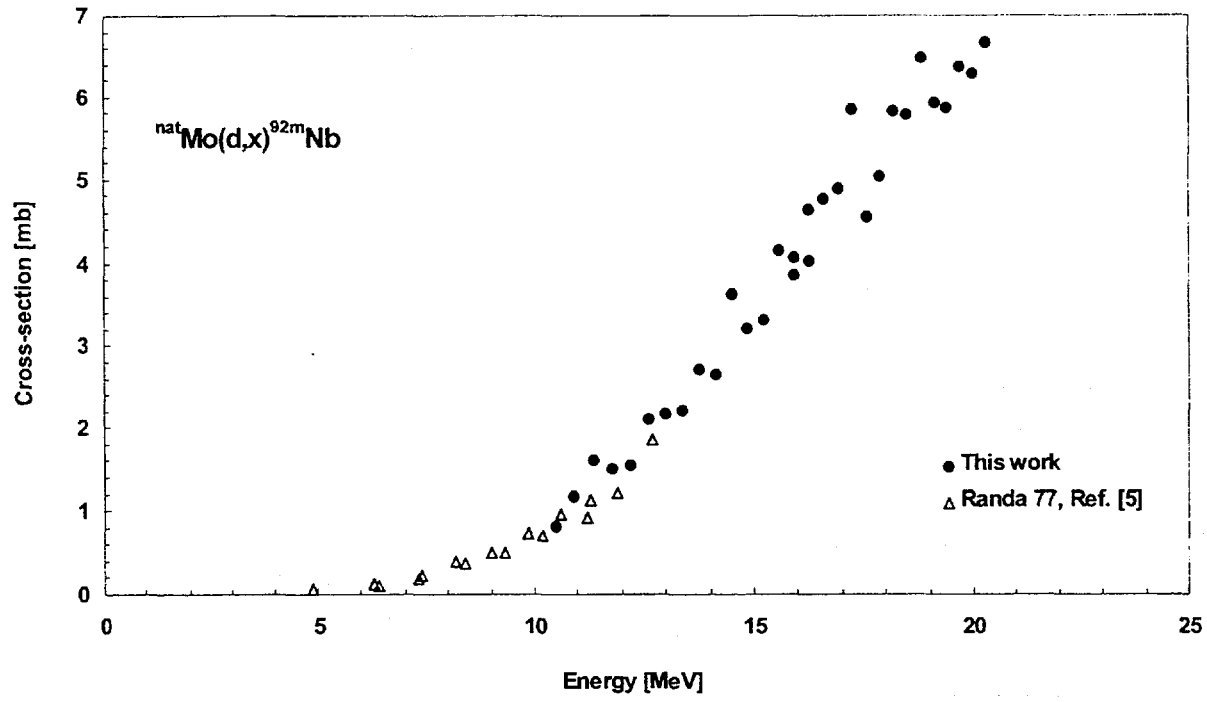

FIG. 1. Cross section for ^{nat}Mo(d,x)^{92m}Nb reaction.

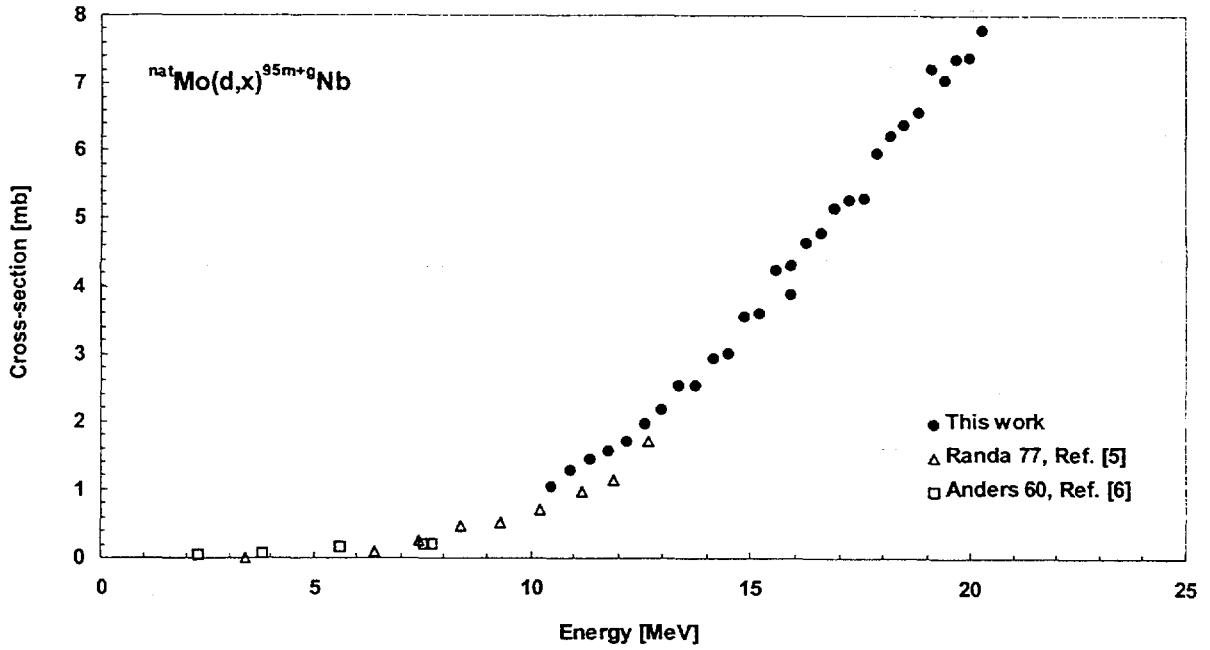

FIG. 2. Cross section for ^{nat}Mo(d,x)$^{95m+g}$Nb.

3.2. $^{95m+g}$Nb ($T_{1/2}$ = 34.97 d)

Both the ^{95g}Tc and ^{95m}Tc (see 3.6 and 3.7) are formed besides ^{95}Nb, and these three nuclides decay finally to ^{95}Mo and as no chemical separation is performed on the irradiated samples, the characteristic g-lines of ^{95}Nb will be contaminated by contribution from ^{95g}Tc and/or ^{95m}Tc. To solve this problem a long cooling time (>30 days) was used to allow decay of ^{95g}Tc ($T_{1/2}$ = 20 h). The 765.8 keV g-line was then used in which the only direct contributions are due to ^{95g}Nb (99.79 %) and ^{95g}Tc (94.0%) and not to ^{95m}Tc. As ^{95m}Tc has several unique characteristic lines (e.g. 582.1 keV, 31.4%) and as all directly formed ^{95g}Tc has decayed, the contribution of ^{95g}Tc (resulting from the isomeric decay of ^{95m}Tc) to the 765.8 keV line can be calculated, yielding the number of counts resulting from the decay of ^{95g}Nb. The results of these calculations are shown in Fig. 2.

Only two literature references by Randa et al. [6] and Anders et al. [7] could be found for this excitation curve, giving slightly lower cross section values. The main contributing reactions are ^{97}Mo(d,a) with Q = + 9.95 MeV, ^{98}Mo(d,an) with Q = + 1.31 MeV, ^{95}Mo(d,2p) with Q = -2.37 MeV, ^{96}Mo(d,^{3}He) with Q = -3.8 MeV and ^{100}Mo(d,a3n) with Q =-12.9 MeV. At 20 MeV deuteron energy a cross section of 8 mb is reached after a near linear behaviour. No other data on this reaction are available and no extremum is reached in the studied energy band.

3.3. $^{93m+g}$Tc ($T_{1/2}$ = 2.75 d)

After total decay of ^{93m}Tc ($T_{1/2}$ = 43.5 min) the results for the production of $^{93m+g}$Tc are shown in Fig. 3 where the undisturbed 1363.1 keV (66%) and the 1477.2 keV (9.6%) g-lines were used to characterise the ^{93}Tc-isotope.The two contributing reactions which can be clearly observed in Fig. 3 are ^{92}Mo(d,n) with Q =+1.86 MeV and ^{94}Mo(d,3n) with Q=-15.88 MeV. Two references were found in literature (Randa et al. [8] and Wolke et al. [9]) giving cross section results for the formation of ^{93g}Tc and ^{93m}Tc by (d,n)-reactions separately. These two production channels were added together appropriately yielding the curve in Fig. 3. Our measurements show a little higher cross section value for the (d,n)-reaction than those from Randa et al. [8] and Wolke et al. [8] in the overlapping energy region.

3.4. ^{94g}Tc ($T_{1/2}$ = 4.883 h)

As ^{94g}Tc has several unique g-lines (e.g. 916.1 keV, 7.6%) and as ^{94m}Tc shows no isomeric transition, the cross section for the production of ^{94g}Tc can be directly calculated from g-spectrometric analysis after a short cooling time (a couple of hours). Results are shown in Figure 4 where two contributing reactions can be observed: ^{94}Mo(d,2n) with Q =-7.26 MeV and ^{95}Mo(d,3n) with Q =-14.63 MeV. Two sets of literature data were found (Randa et al. [8] and Aleksandrov et al. [10]) with results in very good agreement with our data. A cross section value of 100 mb is reached at 20 MeV deuteron energy.

3.5. ^{94m}Tc ($T_{1/2}$ = 52 min)

After a short cooling time (1 to 2 hours) the activity of ^{94m}Tc can be calculated from the 871.1 keV (94.2%) or the 1521.6 keV (4.5%) g-line. The first line is contaminated with ^{94g}Tc (99.9%), while the second one contains contributions of ^{93}Tc (23.9%). The contributions of both ^{93}Tc and ^{94g}Tc can be calculated based on the presence of their unique lines (see 3.3 and 3.4), the abundance of the different lines and the detector efficiency at these g-lines. As a result of these correction calculations a larger scatter on the results can be expected as is seen from Fig. 5.

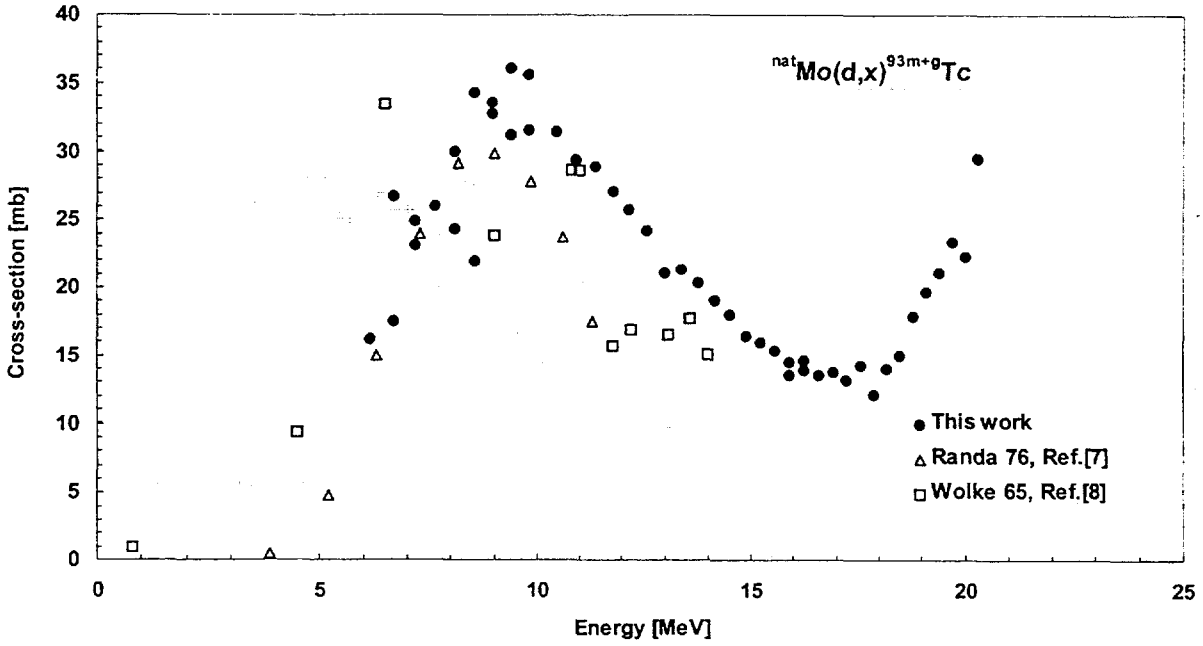

FIG. 3. Cross section for $^{nat}Mo(d,x)^{93m+g}Tc$.

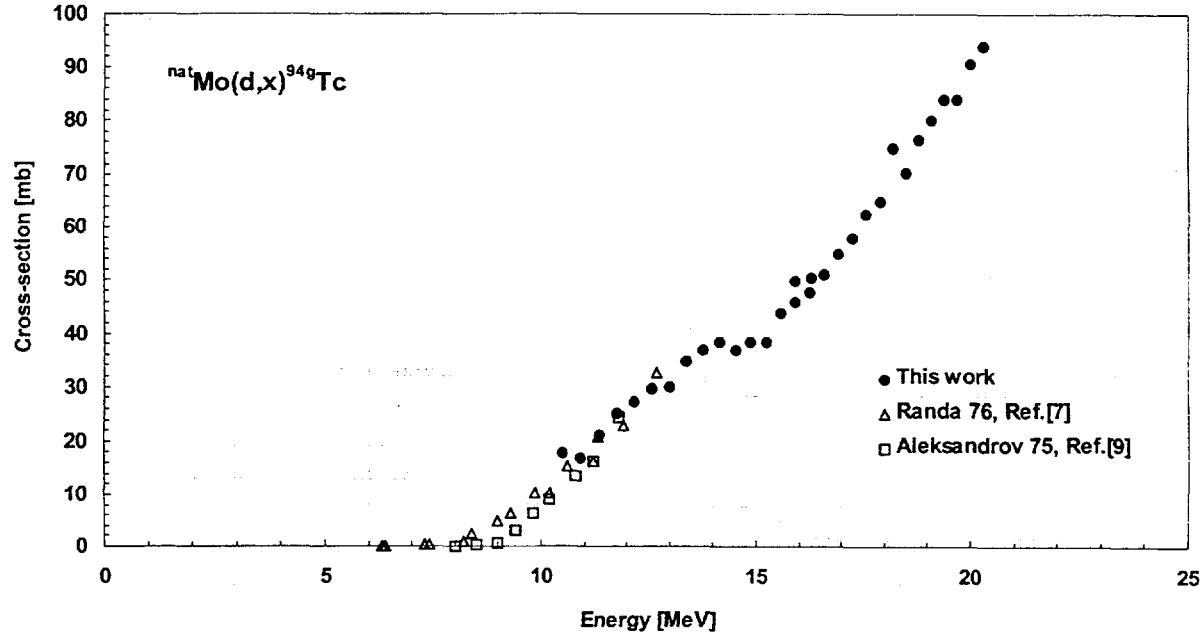

FIG. 4. Cross section for $^{nat}Mo(d,x)^{94g}Tc$.

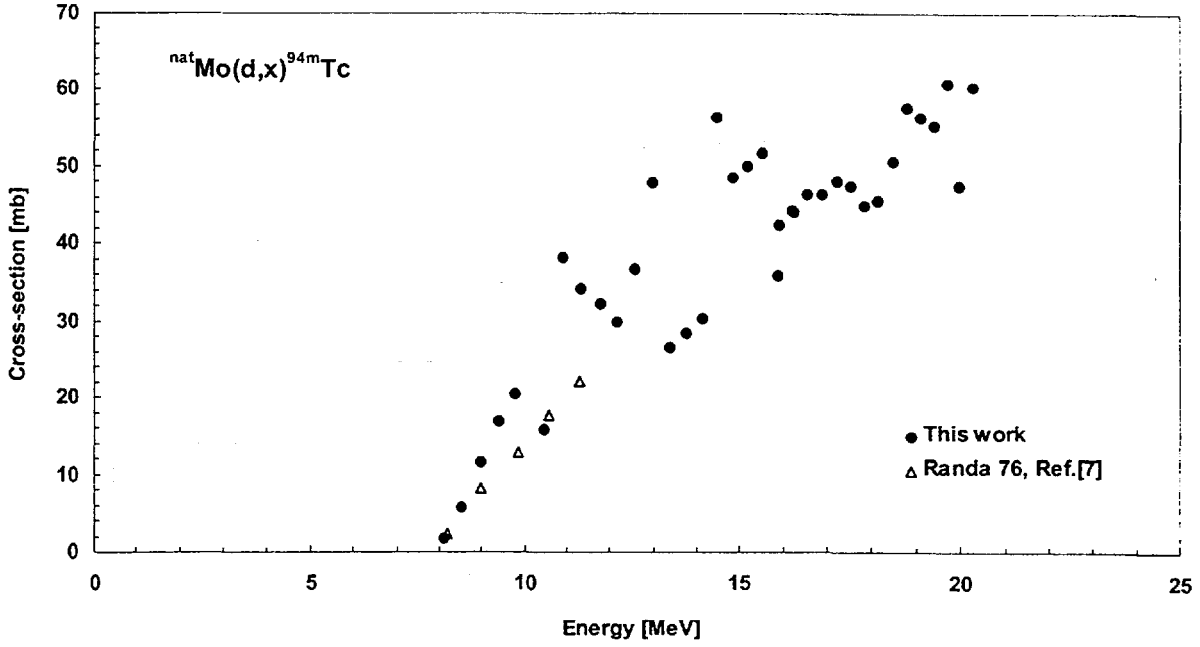

FIG. 5. Cross section for ^{nat}Mo(d,x)^{94m}Tc.

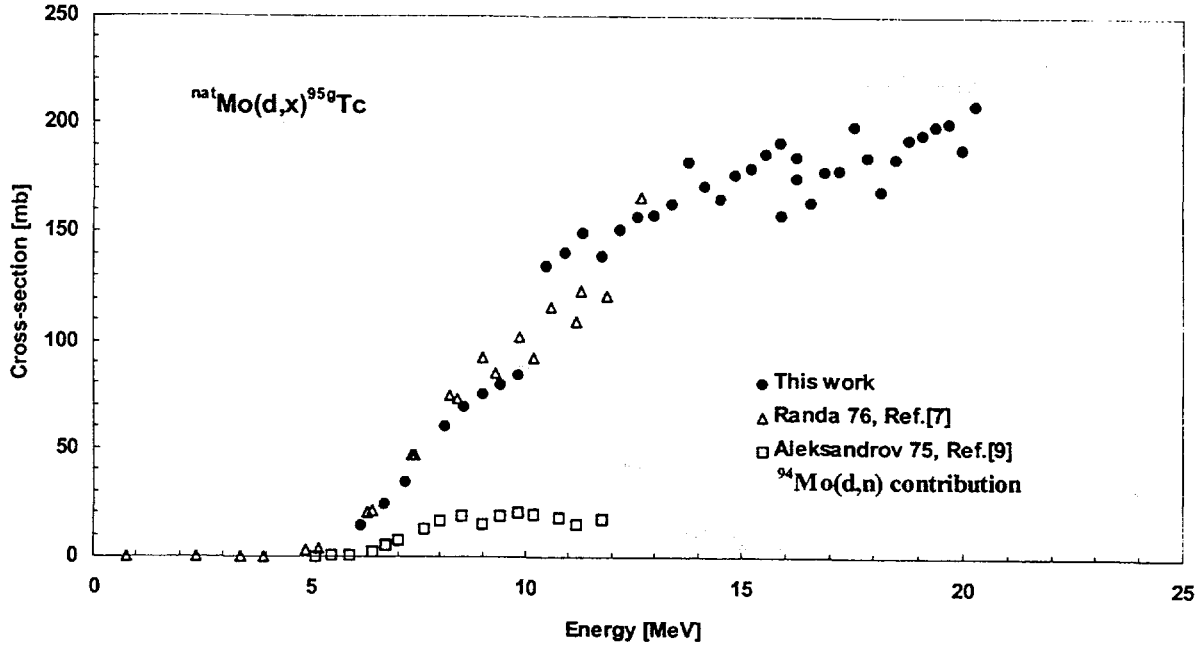

FIG. 6. Cross section for ^{nat}Mo(d,x)^{95g}Tc.

The excitation curve (Fig.5) shows two contributing reactions: ^{94}Mo(d,2n) (Q=-7.34 MeV) and ^{95}Mo(d,3n) (Q=-14.71 MeV), where the (d,2n) reaction on the less abundant ^{94}Mo (9.25 %) reaches a maximal cross section value near 16 MeV, making this the optimal production path using deuteron induced reactions below 21 MeV. From our measured cross section values a physical yield of 3545 MBq/mAh (95 mCi/μAh) is calculated for the energy range 12-17 MeV on enriched ^{94}Mo target. Contamination can be expected through the ^{94}Mo(d,n)^{95g,95m}Tc processes (Figure 6 and 7) and the main contamination arises from ^{95g}Tc ($T_{1/2}$ = 20 h). The data from Aleksandrov et al. [11], obtained on partly enriched ^{94}Mo, show that the contribution of ^{94}Mo(d,n) to the total formation of ^{95g}Tc decreases strongly at 12 MeV incident deuteron energy where production of other Tc-isotopes take over. At the high energy side ^{93}Tc-contamination can occur through the ^{94}Mo(d,3n) process (Q =-15.88 MeV) (Fig. 3), limiting the incident deuteron energy to about 17 MeV. Another contaminating nuclide is ^{94g}Tc (Fig. 4) with a maximal cross section value derived from our measurements on ^{nat}Mo of 100 mb, leading to the conclusion that the production of ^{94m}Tc through deuteron induced reactions is only possible with low isotopic purity. The ^{94}Mo(p,n)^{94m}Tc production channel is hence to be preferred both for the resulting purity, as is shown by Rösch et al. [11], as for the total yield according to both Denzler et al. [12] and Rösch et al. [11]. The ^{92}Mo(a,2n)^{94}Ru→^{94m}Tc will result in even higher purity, however the total yield for this process is considerably lower based on the results of Denzler et al. [12]. Production based on the ^{93}Nb(^{3}He,2n) reaction is not an alternative due to the important isotopic contamination with ^{93g,93m,94g}Tc and due to the rather low yield as shown by Denzler et al. [12].

3.6. ^{95g}Tc ($T_{1/2}$ = 20.0 h)

Figure 6 shows the results of the cross section calculation for the formation of ^{95g}Tc. The results were obtained after a cooling time of 1 to 2 hours and are corrected for the small amount of ^{95g}Tc produced by the isomeric transition ^{95m}Tc→^{95g}Tc.

Contributing reactions are ^{94}Mo(d,n) with Q=+2.67 MeV, ^{95}Mo(d,2n) with Q=-4.7 MeV and ^{96}Mo(d,3n) with Q=-13.85 MeV. Two sets of literature data were found (Randa et al. [8] and Aleksandrov et al. [11]). The results of Randa et al. [8] were, like ours, obtained on ^{nat}Mo and they are in very good agreement with each other, where as the data of Aleksandrov et al. [11] were gathered on partly enriched ^{94}Mo and hence only include the ^{94}Mo(d,n)-reaction with almost no contribution from the ^{95}Mo(d,2n)-process.

3.7. ^{95m}Tc ($T_{1/2}$ = 61 d)

After a long cooling time (>30 days) the results shown in Fig. 7 were obtained for the formation of ^{95m}Tc. Direct calculation of the cross section is possible from the unique g-lines of this isotope (e.g. 582.1 keV, 31.4%).

Again two sets of literature data were found (Randa et al. [8] and Wu Sheng et al. [13]). Data from Wu Sheng et al. [13] are in agreement with our results although our cross section values tend to be slightly higher. The excitation curve given by Randa et al. [8] has a clearly different shape although these results were obtained in comparable experimental conditions. The same contributing reactions as in the ^{95g}Tc case can be observed.

3.8. $^{96m+g}$Tc ($T_{1/2}$ = 4.28 d)

After a long cooling time (>30 days) the activity of ^{96}Tc can be calculated from the 812.5 keV (82%) or the 849.9 keV (98%) g-lines. Results are shown in Figure 8 together with

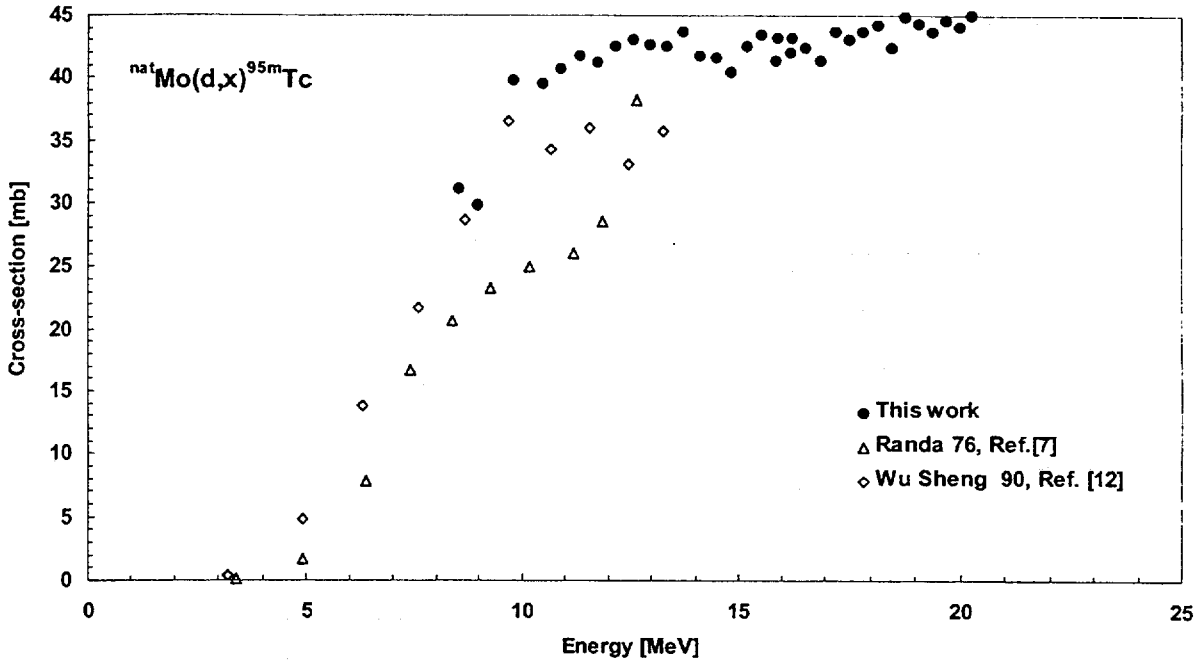

FIG. 7. Cross section for ^{nat}Mo(d,x)^{95m}Tc.

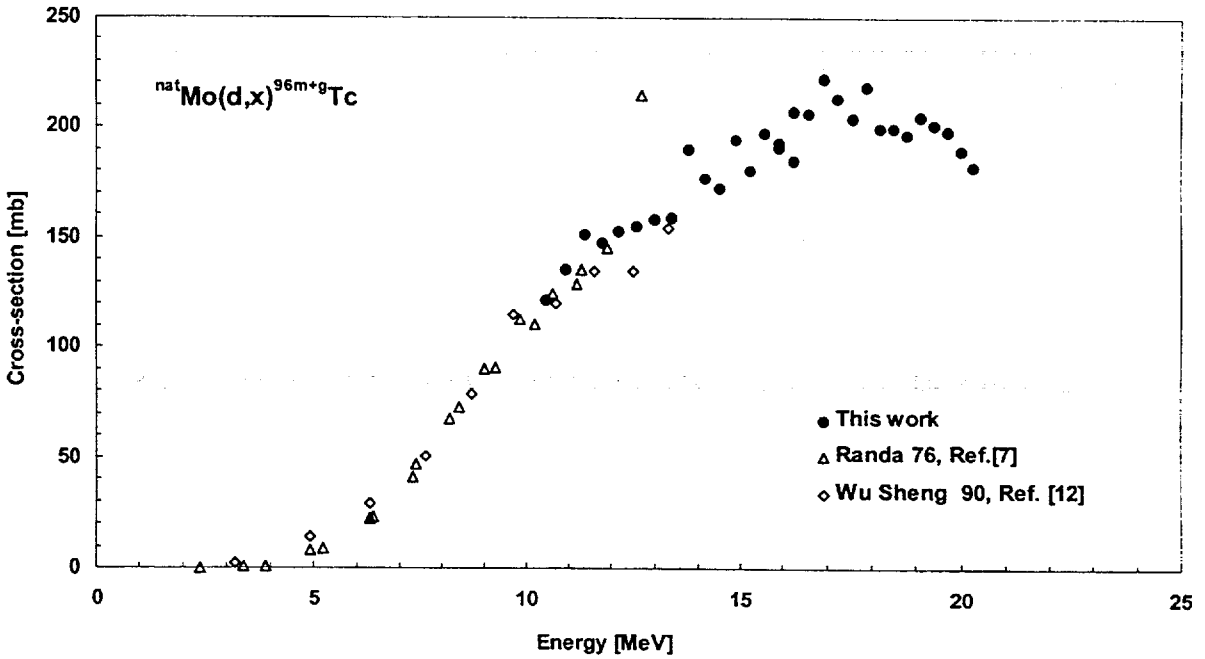

FIG. 8. Cross section for ^{nat}Mo(d,x)$^{96m+g}$Tc.

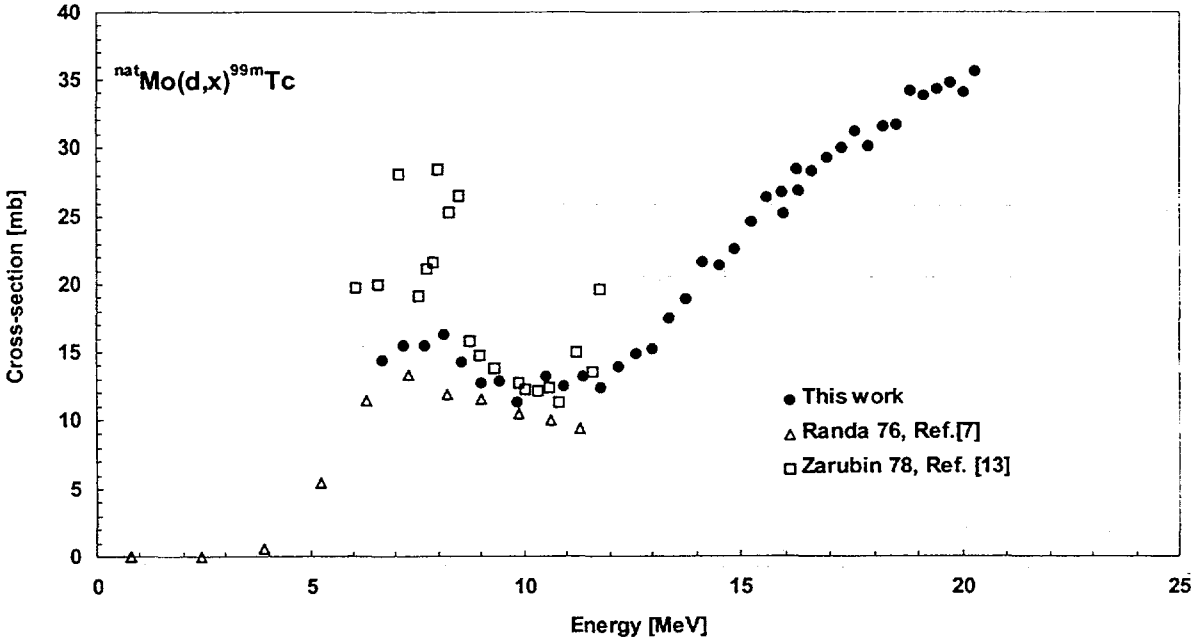

FIG. 9. Cross section for ^{nat}Mo(d,x)^{99m}Tc.

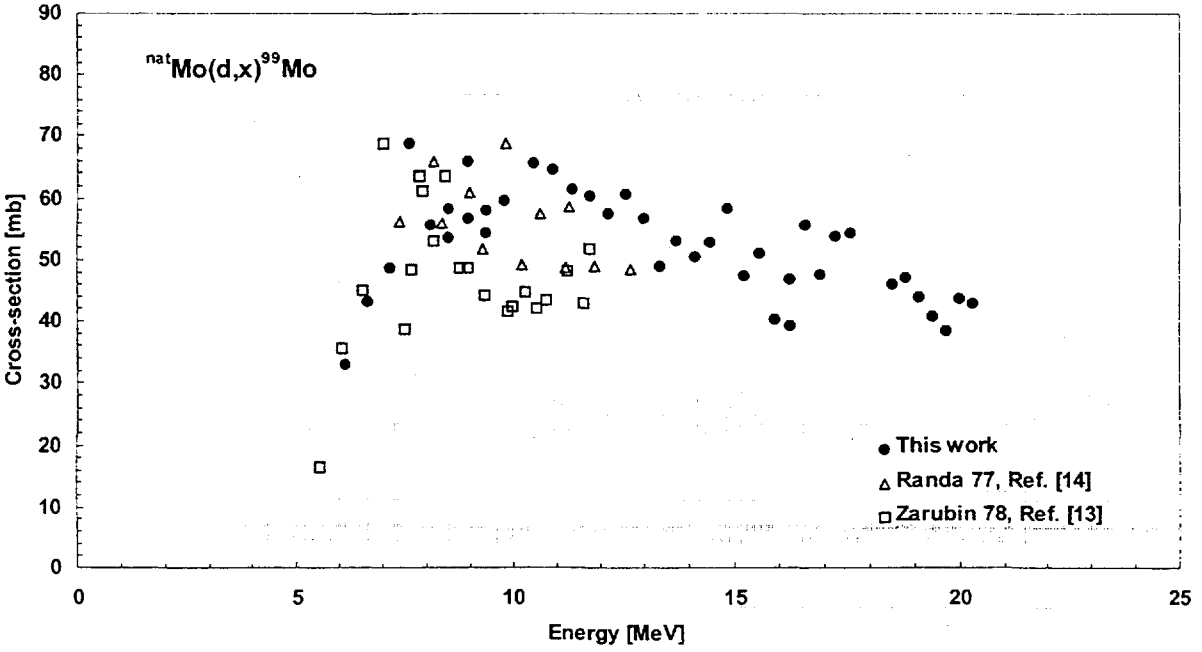

FIG. 10. Cross section for ^{nat}Mo(d,x)^{99}Mo.

the two sets of literature values published by Randa et al. [8] and Wu Sheng et al. [13]. Both literature sets are in reasonable good agreement with our data.Contributing reactions are ^{95}Mo(d,n) with Q=+3.18 MeV, ^{96}Mo(d,2n) with Q= -5.98 MeV and ^{97}Mo(d,3n) with Q=-12.8 MeV together with the isomeric transition of ^{96m}Tc. The ^{96m}Tc-nuclide was not found during this study what is probably due to the low g-abundance in the energy region between 50 keV and 2000 keV and the rather short half life ($T_{1/2}$ = 51.5 min).

3.9. ^{99m}Tc (direct formation) ($T_{1/2}$ = 6.006 h)

After a short cooling time (1 to 2 hours) the activation of ^{99m}Tc can be obtained from the 140.5 keV (87.2 %) g-line. The fraction due to the directly formed ^{99m}Tc is then obtained by subtracting the contribution of the coupled reaction ^{99}Mo→^{99m}Tc. Due to the additional calculations a larger scatter can be expected on the obtained data as is seen from Figure 9. In Figure 9 two contributing reactions to the formation of ^{99m}Tc can be observed : ^{98}Mo(d,n) (Q = 4.13 MeV) and ^{100}Mo(d,3n) (Q =-10.08 MeV), showing a maximal cross section value measured on ^{nat}Mo of 15 mb (at 7 MeV) and 35 mb (at 21 MeV) respectively. The optimal production path for ^{99m}Tc based on deuteron induced reactions is hence the ^{100}Mo(d,3n) process with a maximal cross section s_{max}>360 mb in the studied energy interval. The values reported by Zarubin et al. [14] (Figure 9) are a factor of 2 higher than what is reported by Randa et al. [8] and in this work, which indicates that these results may be obtained without taking the coupling with ^{99}Mo into account or not separating properly the contribution of ^{99}Mo.

Contaminating nuclides in the ^{100}Mo(d,3n)-process are ^{99}Mo (natural decay to ^{99m}Tc), the ^{99g}Tc (which has a very long half life and one low energy very weak gamma line) and the short lived Tc nuclides (^{100,101}Tc, ...). From our measured cross section values a direct production yield of 9.2 mCi/μAh in the 11-21 MeV energy interval is calculated. A larger value is expected for higher incident energies. It can hence be concluded that the direct production of ^{99m}Tc is only economically possible at high energy deuteron beams, but is only practical if daily production facilities are available on site.

3.10. ^{99}Mo ($T_{1/2}$ = 2.7477 d)

When a cooling time of a couple of hours is used, the production of ^{99}Mo can be calculated directly from the 181.1 keV (6.07%) or the 739.5 keV (12.14%) g-lines. Results are shown in Figure 10. Together with the literature references by Randa et al. [15] and Zarubin et al. [14].

Several contributing reactions can be observed : ^{98}Mo(d,p) (Q = + 3.7 MeV), ^{100}Mo(d,x) and decay from ^{99}Nb formed by ^{100}Mo(d,x)-processes (Fig. 10). The maximal cross section for the ^{98}Mo(d,p) reaction is 260 mb [14], while we found >600 mb for the ^{100}Mo(d,x)-reaction, which decreases only slowly with higher deuteron energy due to the contributions of ^{100}Mo(d,t) (Q=-2.0 MeV), ^{100}Mo(d,dn) (Q=-8.3 MeV), ^{100}Mo(d,p2n) (Q=-10.5MeV), ^{100}Mo(d,^{3}He)^{99}Nb→^{99}Mo (Q =-5.65 MeV) and ^{100}Mo(d,2pn)^{99}Nb→^{99}Mo (Q=- 13.37 MeV).

4. PRODUCTION OF ^{99m}Tc and ^{99}Mo AT HIGH DEUTERON ENERGIES

4.1. Calculation of production yields

The systematic behaviour of the excitation functions of deuteron induced reactions and our experimental results up to 21 MeV deuteron energies showed that it is worthwhile to

investigate the production possibility of ^{99}Mo and ^{99m}Tc at higher deuteron energies especially since the energies corresponding to the maximal cross section values of the nuclear reactions leading to the formation of the above two isotopes are above 20 MeV.

As the first estimation of the excitation functions and the impurity levels we performed a calculation study to predict the excitation functions and production yields. The calculation based on the systematics of experimental excitation functions and on the theoretical predictions of the excitation functions of the same type of reactions.

In accordance to the Table II, the main contributing processes at higher deuteron energies for production of ^{99m}Tc are the direct production of the ^{99m}Tc via ^{100}Mo(d,3n) reaction and the decay of the ^{99}Mo by-product during the irradiation. The ^{99}Mo is formed directly via ^{100}Mo(d,p2n) reaction and from the decay of the short lived ^{99}Nb produced via (d,2pn) and (d,^{3}He) reactions on ^{100}Mo.

To obtain the corresponding production yields as a function of the energy we have constructed the excitation functions based on systematics and our experimental values of the related reactions presented above and calculated the thick target yields from this estimated cross sections.

In more detail for construction of excitation functions the following steps and procedure were used:

1. A detailed investigation of the available experimental results on the (d,3n), (d,p2n), (d,^{3}He) and (d,2pn) reactions.
2. Study of the available information of the reported theoretical predictions on the cross sections of the above reactions.
3. Investigations of methods for predictions of cross sections of unknown reactions, based mostly on systematics of parameters of excitation functions.
4. Taking into account that the ^{99}Tc isotope has two longer lived isomeric states, namely the medically important 6 hour ^{99m}Tc isomeric state (1/2$^-$) and the very long lived ($2.13*10^5$ year) ground state (9/2$^+$), the so called isomeric ratio as a function of the energy has to be known to estimate the yield of the "useful part" of the produced ^{99}Tc.

The survey on the high energy deuteron induced reactions shows that only a very few excitation function were measured up to 50 MeV in all mass region and the reliability of the available experimental data sets in many cases are under question. On the other hand only a very few model calculations were found for deuteron induced reactions in all energy ranges, especially for high energies. Regarding the limited number of experimental data and the moderate predictive power of the different models the constructed excitation functions can be considered only as rough estimation.

Production yield of ^{99m}Tc:

The excitation function of the ^{98}Mo(d,n) nuclear reaction used for calculation of the production yield of ^{99m}Tc is shown in Fig. 11a. The values for 100 % enriched target was deduced from the experimental cross sections measured by us on natural target. The yield calculated from the above excitation function is reproduced in Fig. 11b.

TABLE II. DEUTERON INDUCED REACTIONS ON ENRICHED ^{98}Mo AND ^{100}Mo

Radionuclide	Nuclear reaction/Q reaction energy in MeV	
	^{98}Mo	^{100}Mo
	(d,5n)	*(d,7n)*
^{95}Tc		
	-29.35 m	-43.57 m
	-29.31 g	-43.53 g
	(d,4n)	*(d,6n)*
^{96}Tc		
	-21.48 m	-35.69 m
	-21.44 g	-35.66 g
	(d,3n)	*(d,5n)*
^{97}Tc		
	-12.07 m	-26.28 m
	-11.97 g	-26.18 g
	(d,2n)	*(d,4n)*
^{98}Tc		
	-4.69	-18.90
	(d,n)	*(d,3n)*
^{99}Tc		
	4.13 m	-10.08 m
	4.28 g	-9.94 g
	-	*(d,2n)*
^{100}Tc		
		-3.17
	-	*(d,n)*
^{101}Tc		
		5.22
	(d,p); (n,g)	*(d,2pn)^{99}Nb→^{99}Mo*
^{99}Mo		
	3.70, 5.93	-13.74 m
		-13.37 g
		(d,p2n)^{99}Mo; (n,2n)^{99}Mo
		-10.51; -8.29
	-	*(d,p) ;(n,g)*
^{101}Mo		
		3.17; 5.40

The excitation function of the ^{100}Mo(d,3n) reactions was constructed from the systematics of the (d,3n) reactions in this mass region by fitting the curve to the experimental data obtained by us up to 20 MeV. An equal population of the isomeric and the ground state was supposed (isomer/total = 0.5). The curve of the calculated production yield is shown in Figure 11b.

Production yield of ^{99}Mo:

The measured experimental cross sections and the deduced production yield of the $^{98}Mo(d,p)$ reaction are shown in Fig. 11c and Fig. 11d respectively. The results of the investigated low energy region for production of ^{99}Mo on ^{nat}Mo do not allow extrapolation of the pure cross sections of independent reactions going on ^{100}Mo since the threshold energy of the $^{100}Mo(d,p2n)$ and $^{100}Mo(d,2pn)$ reactions are similar and are around 15 MeV.

According to the systematics we found that the magnitude of the (d,2pn) process is significantly lower than that of the (d,p2n) reactions. The production yield of the ^{99}Mo was estimated including the direct production and indirect via decay of ^{99}Nb. The corresponding excitation function is shown in Fig. 11c. The calculated integral yield is reproduced in Fig. 11d.

4.2. Comparison and conclusion

The obtained integral yields show that the low energy nuclear reactions on ^{98}Mo result very low yields for production of both ^{99m}Tc and ^{99}Mo.

To evaluate the production capability of the high energy deuteron reactions on enriched ^{100}Mo targets we reproduced the production yields of the most promising proton induced

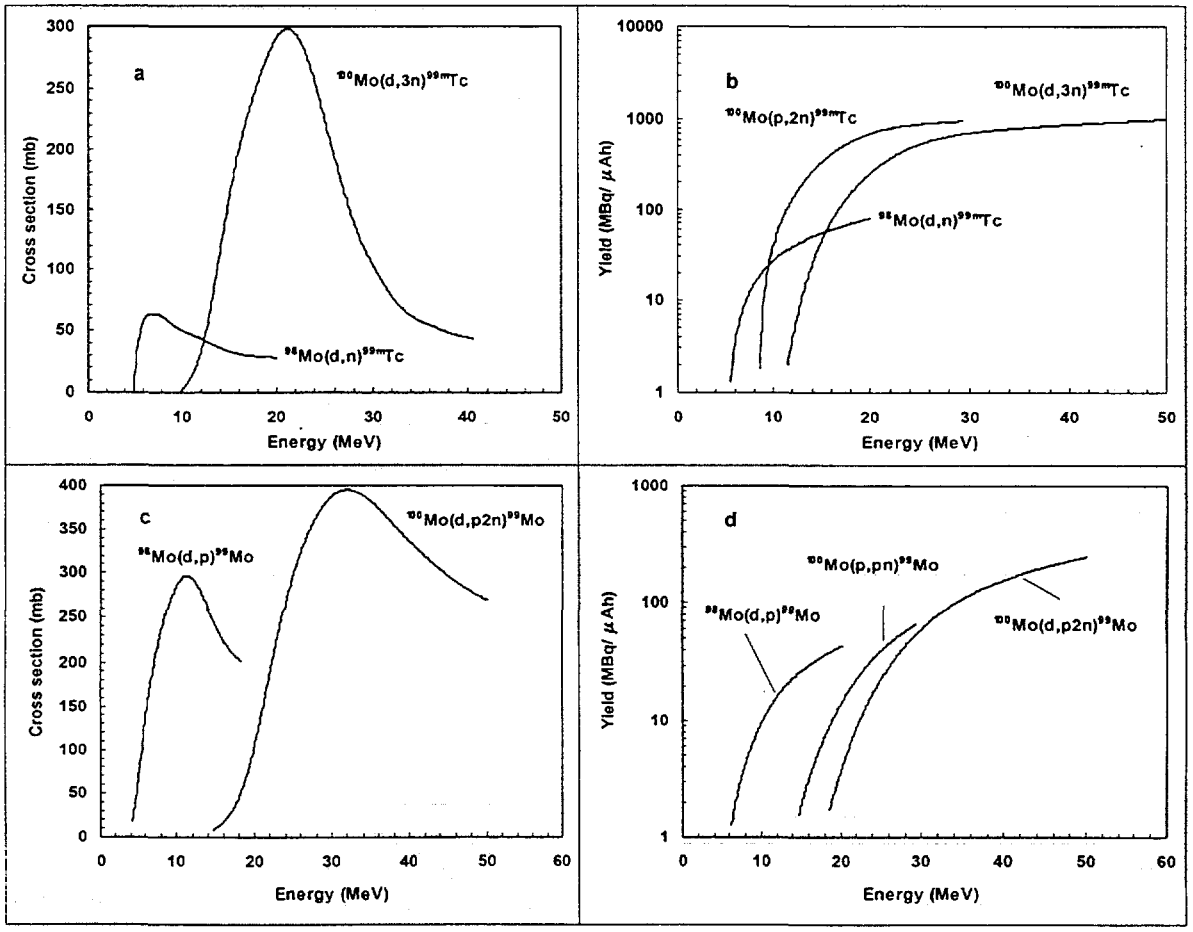

FIG. 11. Summary of production of ^{99m}Tc and ^{99}Mo isotopes.

reactions $^{100}Mo(p,2n)^{99m}Tc$ and $^{100}Mo(p,pn)^{99}Mo$ on Fig. 11 for comparison. The yields for proton were calculated from the experimental excitation functions measured by Levkovski on highly enriched ^{100}Mo [16]. The maximal energy in both cases, for proton and deuteron bombardment, is limited by the production of the unwanted contaminating by-product, the ^{96}Tc isotope (neglecting the ^{97m}Tc having low yield low energy gamma), which has to be avoided (Table I). It is produced by (p,5n) and (d,6n) reactions on ^{100}Mo which limit the energy of the bombarding beam up to 33 MeV in the case of protons and up to 40 MeV for deuterons respectively.

As it is seen in Fig. 11 the estimated physical yield for production of ^{99m}Tc in the $^{100}Mo(d,3n)$ process has a significant about 880 MBq/mAh (24 mCi/mAh) value up to 40 MeV. The physical yield of the $^{100}Mo(d,3n)$ reaction show similar or a little lower value than the yield of the $^{100}Mo(p,2n)$ process (965 MBq/mAh or 26 mCi/mAh up to 30 MeV).

The advantage of the deuteron bombardment is the required smaller amount of enriched target material taking into account the stopping power which is higher for deuteron than in the case of proton bombardment. The need of having deutron accelerators with high beam intensities (~300 μA) is emphasized.

For production of ^{99}Mo the high energy deuterons on ^{100}Mo give higher yield above 30 MeV, than the (p,pn) + (p,2p) process (see Fig. 11d). The energy of the deuteron beam in this case is not limited by the simultaneously produced contaminating isotopes. The $^{100}Mo(d,3n)$ reaction can hence be used in a very wide energy band and will be the preferred reaction path. From the point of the radionuclidic purity no real problem is to be expected as all possible contaminating nuclides are naturally removed by decay. Only at higher deuteron energy the production of ^{97}Tc and ^{96}Tc through (d,5n) and (d,6n) reactions could be a problem, making chemical purification necessary. This reasoning is clearly based on the use of highly enriched ^{100}Mo (>99%), as otherwise numerous contaminating nuclides could be formed in considerable amounts on the other isotopes present. The deuterons have the advantage of the required smaller amount of the target material and the disadvantage of the required high energy. In case of deuterons significant amount of high energy neutrons are produced in the break up process of the deuterons beside the neutron producing reactions. These neutrons can also produce ^{99}Mo in the $^{100}Mo(n,2n)$ process.

The total physical yield at 50 MeV can reach 247 MBq/mAh or 6.7 mCi/mAh. Production of a 2 Ci ^{99}Mo generator is hence possible with 1 hour of irradiation time at a current of 300 μA on target. In order to cover the current weekly world demand of ^{99}Mo by deuteron induced reactions, over 300 dedicated accelerators are needed, making the production of ^{99}Mo by deuteron induced reactions on highly enriched ^{100}Mo not a real alternative to the fission production of ^{99}Mo, despite the physical and chemical feasibility.

Direct production of ^{99m}Tc with higher yield is more promising than production through ^{99}Mo generator but is possible only at high deuteron energies and is only practical if daily production facilities are available on site. In that case the distribution of the produced activity is preferred in the form of ^{99m}Tc rather than to distribute the ^{99}Mo generators since ^{99}Mo generators have to be produced from the highly enriched very expensive ^{100}Mo target material. Distributions of ^{99}Mo generators requires large amount of enriched ^{100}Mo target material and it is essential to organise the collections of the distributed Mo generators. The on site direct distribution of ^{99m}Tc has the advantages that useful amounts of ^{99m}Tc demand only a few ^{100}Mo targets in sequence, separating (milking) the ^{99m}Tc and keeping the expensive ^{100}Mo target(s) always at the production site. During daily production of ^{99m}Tc the simultaneously produced

^{99}Mo can enhance the direct production yield of the ^{99m}Tc by decay and about 1000 MBq/mAh yield of ^{99m}Tc can be reached, depending on the initial activity of the irradiated target.

The status of the currently available very limited experimental yield and cross section data are still rather poor and make it difficult to calculate the proper achievable yields. Therefore new measurements and theoretical calculations are required in the near future to get reliable data for the production of ^{99m}Tc at higher deuteron energies.

REFERENCES

[1] TÁRKÁNYI, F., SZELECSÉNYI, F., KOPECKÝ, P., Excitation functions of proton induced reactions on natural nickel for monitoring beam energy and intensity, J. Appl. Radiat. Isot. **42** (1991) 13.

[2] SONCK, M., Van HOYWEGHEN, J., HERMANNE, A., Determination of the external beam energy of a variable energy multiparticle cyclotron, J. Appl. Radiat. Isot. **47** (1996) 513.

[3] ANDERSEN, H. H., ZIEGLER, J. F., "Hydrogen Stopping Powers and Ranges in All Elements", Pergamon Press, 1977.

[4] BROWNE, E., FIRESTONE, R. B., "Table of Radioactive Isotopes", Wiley, 1986.

[5] ANDERS, O. U., MEINKE, W. W., Absolute (d,a) reaction cross sections of zirconium, molybdenum, titanium and sulfur, Phys. Rew. **120** (1960) 2114.

[6] RANDA, Z., SVOBODA, K., Excitation functions and yields of (d,a) reaction on natural molybdenum up to the deuteron energy of 13 MeV, Int. J. Appl. Rad. Isot. **28** (1977) 555.

[7] ANDERS, O. U., MEINKE, W. W., Absolute (d,a) reaction cross sections of zirconium, molybdenum, titanium and sulfur, Phys. Rew. **120** (1960) 2114.

[8] RANDA, Z., SVOBODA, K., Excitation functions and yields of (d,n) and (d,2n) reactions on natural molybdenum, J. Inorg. Nucl. Chem. **38** (1976) 2289.

[9] WOLKE, R. L., Report TID 21525, Contract AT (30-1)-2771 (1965), data were taken from [7].

[10] ALEKSANDROV, Yu. A., APRELEV, M. V., ZARUBIN, I. I., PADALKO, V. Yu., PODKOPAEV, Yu. N., HRISANFOV, Yu. V., Excitation functions of ground states of ^{95}Tc and ^{94}Tc in (d,n) and (d,2n) reactions, Bull. Russian Ac. Sciences **39** (1975) 103.

[11] RÖSCH, F., QAIM, S. M., Nuclear data relevant to the production of the positron emitting technetium isotope ^{94m}Tc via the ^{94}Mo(p,n)-reaction, Radiochim. Acta **62** (1993) 115.

[12] DENZLER, F. O., RÖSCH, F., QAIM, S. M., Excitation functions of a-particle induced nuclear reactions on highly enriched ^{92}Mo: comparative evaluation of production routes for ^{94m}Tc, Radiochim. Acta **68** (1995) 13 and Radiochim. Acta **75** (1996) 227.

[13] WU SHENG, LONG XIANGUAN, PENG XIUFENG, HO FUQING, LIU MANTIAN, "Excitation Functions for the ^{nat}Mo(d,x)^{95m}TC, ^{nat}Mo(d,x)^{96g}Tc and ^{nat}Mo(d,x)^{97}Tc Reactions", Report, Inst. of Nucl. Sci. and Techn., Sichuan Univ., NST-004, 1990.

[14] ZARUBIN, P.P., PADALKO, V. Yu., HRISANFOV, Yu. V., LEBEDEV, P.P., PODKOPAEV, Yu. N., Excitation function of ^{98}Mo+d reactions, Bull. Russian Ac. Sciences **42** (1978) 145.

[15] RANDA, Z., SVOBODA, K., Excitation functions and yields of the (d,p) reactions on natural molybdenum for deuteron energies less than 13 MeV, J. Inorg. Nucl. Chem. **39** (1977) 2121.

[16] LEVKOVSKIJ, V.N., Cross sections of medium mass nuclide activation (A=40-100 MeV) by medium energy protons and alpha particles (E = 10-50 MeV), Inter Vesi, Moscow, USSR, 1991.

HIGH BEAM INTENSITIES FOR CYCLOTRON-BASED RADIOISOTOPE PRODUCTION

Y. JONGEN
Ion Beam Applications s.a.,
Louvain-la-Neuve, Belgium

Abstract

Cyclotron-based systems devoted to radioisotope production, both for therapy and diagnostics, are commercially available and used since many years. Today, the requirement for high beam intensities is becoming more and more important. As a consequence, and favored by continuous developments in target technology and on ion sources, the maximum beam intensity available from these cyclotrons has increased, with years, from a few hundred μA to a few mA. This paper focus on some of the applications for which high beam intensities are required, as well as on the achievements and developments at IBA in relation to these applications.

1. INTRODUCTION

Cyclotron technology is largely disseminated into the medical and radio-pharmaceutical community. In particular, cyclotron-based systems devoted to radioisotope production, both for therapy and diagnostics, are commercially available and used since many years. Today, the requirement for high beam intensities is becoming more and more important. As a consequence, and favored by continuous developments in target technology and on ion sources, the maximum beam intensity available from these cyclotrons has increased, with years, from a few hundred μA to a few mA. This paper focus on some of the applications for which high beam intensities are required, as well as on the achievements and developments at IBA in relation to these applications.

2. NEGATIVE-ION CYCLOTRONS FOR THE PRODUCTION OF RADIOISOTOPES FOR IMAGING AND DIAGNOSIS IN NUCLEAR MEDICINE

Commercial companies operate several cyclotrons in the same facility and produce different radioisotopes [1] that they market themselves. Many important hospitals and clinics are now also equipped with cyclotrons producing radioisotopes for their own use or for distribution on regional scale. This evolution was possible because of the high degree of automation, reliability and simplicity characterizing the negative-ion cyclotrons used nowadays for radioisotopes production.

2.1. Negative ion technology

The first cyclotrons produced commercially for the production of medical radioisotopes were "classical", positive ion, isochronous cyclotrons, similar to their counterparts built for nuclear physics research. The beam was extracted using an electrostatic deflector. The heat dissipation limits in the deflector septum limited the extracted beam power to a couple of kW, but higher intensities, typically several hundred μA were available on internal targets. The Cyclotron Corporation (TCC), based in Berkeley (Ca), produced between 1968 and 1984 in excess of 30 cyclotrons based on this technology. A major step was made in the early 80's when TCC proposed a 42 MeV cyclotron (CP42) accelerating negative ions, produced by an

internal P.I.G. source, and extracting by stripping. Extracted beam currents exceeding 200 μA up to 40 MeV were available. Thanks to the stripping extraction, variable energy extracted beams could be obtained in a fixed field, fixed frequency cyclotron. The simultaneous extraction of two beams was also, in principle possible. However, the use of an internal ion source meant a poor vacuum in the cyclotron accelerating tank, and significant amounts of beam were lost in the median plane by stripping on the residual gas. The need to deal with these large beam losses resulted in a quite complex design of the dees and of the R.F. systems, and resulted, at least in the beginning, in a lower reliability. This cyclotron was, initially, a commercial success. Six CP42's were ordered and built, even before the prototype was fully tested. Delays in the commissioning of these cyclotrons contributed eventually to the bankruptcy of TCC. After this significant failure, negative ion technology was rejected by radioisotope producers for some time, in favor of more classical positive ion isochronous cyclotrons, like the MC40 model, made by the Scanditronix company in Upsala.

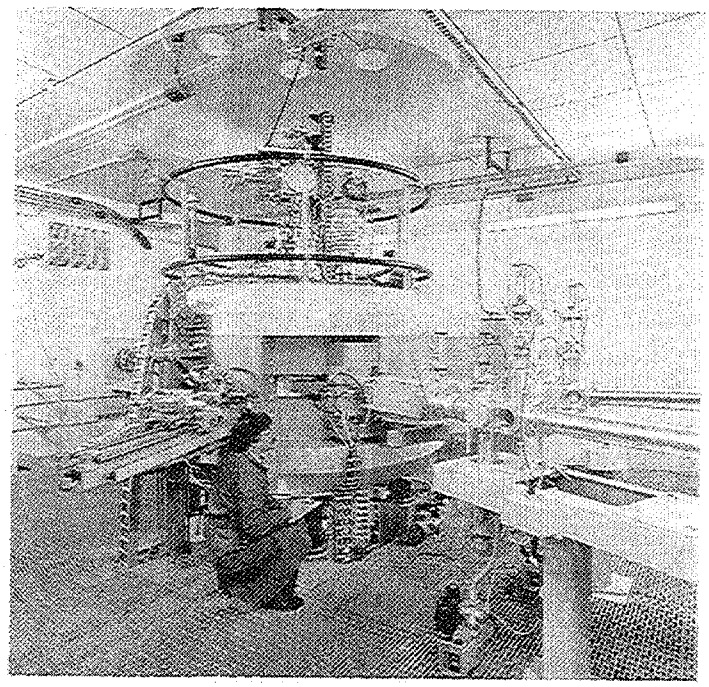

FIG. 1. A CYCLONE 30 cyclotron.

The next major step in radioisotope production cyclotrons was the introduction, in 1987, by IBA, of the CYCLONE 30. It is a 30 MeV, fixed-field, fixed-frequency, H^- cyclotron with extraction by stripping, dual beam and variable energy. The first major improvement of this model was the use of an external, multicusp ion source for the production of the negative ions.

The acceleration of negative H ions in a fixed-field, fixed-frequency cyclotron offers several advantages. Among others, the extraction is straightforward by means of stripping of the H^- ions in a thin carbon foil, leading to an extraction efficiency close to 100%. The negative hydrogen ions are produced by an external multicusp arc discharge ion sources producing an H^- beam. This external source is combined with axial injection. The use of an external source avoids the vacuum problems leading to beam losses and activation of cyclotrons with internal

sources. The adopted solution of an external H^- source with its own pumping system allows the neutral gas to be pumped in the external source system, and moderate size pumps are sufficient to obtain a very low operating pressure in the cyclotron. This reduces beam losses and implies a very low activation of the cyclotron. Maintenance is easier and safer.

2.2. The requirement for higher beam intensities for cyclotron-based production of nuclear medicine radioisotopes

The first CYCLONE 30's used a 2 mA external multicusp ion source, and a 25 kW output R.F. final amplifier. The extracted beam intensity was 500 mA (design value), 350 mA guaranteed, with actual maximum currents varying from machine to machine between 450 mA and 600 mA. These characteristics, in particular the extracted beam intensities, were up to now well adapted to the production constraints, in particular from the point of view of the maximum current the targets may support.

However, recent developments in target technology are at the root of an increasing interest, from the radioisotopes producers, for higher beam intensities. In parallel, there have been important progress in negative ion source technology. In this field, IBA is working in collaboration with A.E.A. Technology, Culham, UK, in negative ion source technology.

As a consequence, high intensity versions of CYCLONE 30 are available today, with maximum extracted beam intensities up to more than 2 mA. These systems include, among others, a new ion source series, able to produce 7 to 25 mA of H^- into a small emittance.

IBA is also proposing an intensity upgrading system allowing a significant increase of the beam intensity (up to 2 mA typically) of any existing Cyclone 30. For the radioisotopes producers, the main advantage of this option is that the isotope production rate of their existing CYCLONE 30 can be increased while keeping unchanged the production facility (no need for an important investment in a new building) and most of the cyclotron operation costs (no need for additional personnel for example). Alternatively, this may be a way of reducing operation costs.

2.3. Radioisotopes for imaging and diagnosis in nuclear medicine: the particular case of ^{99m}Tc

Gallium-67 and thallium-201 are among the most common medical radioisotopes produced with cyclotrons. However, the most frequently used radioisotope for nuclear medicine is produced with nuclear reactors: technetium-99m, distributed as the $^{99}Mo \rightarrow {}^{99m}Tc$ generator. The preferred reaction for the production of ^{99}Mo in nuclear reactors is the neutron induced fission on highly enriched uranium-235 targets. Most of the nuclear reactors used for this production are due, in the next years, for a major refurbishment or for decommissioning [3]. This problem of the future availability of nuclear reactors suitable for ^{99}Mo production has prompted a renewed interest on alternative production methods.

Some alternative production methods are presently under development: one of them is based on the direct accelerator production of ^{99m}Tc or ^{99}Mo, another one is the proton-driven fission neutron source for the production of fission ^{99}Mo [3]. Both methods require the use of high intensity cyclotrons.

As far as the direct accelerator production of ^{99m}Tc or ^{99}Mo is concerned, different possible cyclotron production techniques can be considered [4]. The technical feasibility of these alternative production methods is still being evaluated. Among others, there are questions regarding the specific activity of "instant Tc" and the separation chemistry of ^{99}Mo, as well as licensing and distribution issues. Nevertheless, directly produced Tc could become, in the future, a product complementary to generator produced Tc. In this case, the most promising methods will require high intensity proton beams, in the 2 to 5 mA range.

As far as the production of fission ^{99}Mo is concerned, the proposal is based on a 150 MeV, up to 2 mA cyclotron driving a sub-critical intense neutron source, generating thermal neutron fluxes similar in intensity to those of nuclear reactors used for the production of ^{99}Mo.

Both alternative methods will therefore require several mA of beam. The proposed accelerators will include most of the advanced fundamental characteristics of existing IBA cyclotrons, in particular the negative ion technology. Experience on high efficiency RF power amplifiers developed for the Rhodotron [5], on Cyclone 18+ high beam power conversion efficiency [6], and on the high intensity versions of Cyclone 30 will be valorized.

3. PRODUCTION OF RADIOISOTOPES FOR THERAPY

Medical radioisotopes are generally used for imaging and diagnosis in nuclear medicine. But some of them are used for cancer therapy. Radioisotope production for therapy applications may require extremely high intensity cyclotrons. For example, in 1992 IBA was asked to develop a very high intensity, 18 MeV cyclotron for the production of the radioisotope ^{103}Pd. This radioisotope is marketed, in small sealed sources, for the local treatment of prostate cancer by the American company Theragenics. It can be produced by a (p,n) reaction on Rhodium, a good material for internal target. However, the reaction yield is low and large beam currents are needed to achieve the desired production levels.

The development of this cyclotron, the CYCLONE 18+, was a new step in the evolution of cyclotrons for radioisotope production, in particular from the maximum intensity point of view. Indeed, CYCLONE 18+ operates continuously at 2 mA beam on target. It is therefore demonstrated today, experimentally, that a cyclotron with an internal target can operate routinely at 2 mA beam current. Also currents in excess of 5 mA have been observed during factory tests, and space charge calculations made for cyclotrons that do not require turn separation indicate that the intensity limit is probably around 10 mA average beam current [6]. This applies not only to positive ion cyclotrons using an internal target but also to negative ion cyclotrons where the extraction is made by charge exchange.

4. THE INNOVATIVE CONCEPT OF AUTO-EXTRACTION OR THE REBIRTH OF THE POSITIVE ION TECHNOLOGY

The use of negative ion technology allows an extraction by means of stripping of the H^- ions in a thin carbon foil, leading to an extraction efficiency close to 100%. This technology is therefore, up to now, the technology of choice for applications where high intensity beams must be extracted. However, the requirements on the vacuum quality are high and, to avoid electromagnetic dissociation, low magnetic fields must be used. The consequence is that high energy cyclotrons quickly become very large machines if negative ions are accelerated, which is nevertheless necessary if high intensity extracted beams are required. From this point of view, any technological innovation leading to the use of positive ion technology together with

an extraction system allowing a nearly 100% extraction efficiency would represent an unquestionable improvement.

IBA is presently working on a totally new concept for the extraction of high currents of positive ions [7]. This new concept, called the auto-extraction will provide close to 100% extraction efficiency without the need of extraction elements that could easily be damaged by high currents, like septa for electrostatic or magnetic extractors.

The basic principles are the following. In an isochronous cyclotron, the average field increases with radius to compensate the relativistic mass increase of the accelerated particles. Close to the pole edge, it become impossible to maintain an isochronous radial field profile. The actual field falls below the ideal field, reaches a maximum, and starts to decrease. When the actual field starts departing from the ideal isochronous field, the accelerated particles start to lag with respect to the accelerating voltage on the dee. When the phase lag reaches 90°, the acceleration stops: this point represents the limit of acceleration. At an other (generally larger) radius, the field index, defined as N = R/B dB/dR, reaches the value -1. This point is the limit of radial focusing. Past this point, the magnet is unable to hold the ions, and the ions escape the influence of the magnetic field. We call the radius where N reaches -1 the limit of self-extraction. If the gap is large, like in most existing cyclotrons, the radial fall of the field is quite gradual, and the limit of acceleration is found at a radius significantly smaller than the limit of self-extraction. Transporting the beam from the first limit to the second is the task of the extraction system, including generally an electrostatic deflector.

In a magnet with a smaller gap, the fall of the magnetic field close to the pole boundary is much sharper. As a result, the limit of acceleration falls much closer to the limit of self-extraction, and the extraction is much easier. When the magnet gap at extraction becomes very small (like smaller than 20 times the radius gain per turn at extraction), the limit of self extraction is reached before the limit of acceleration, and the beam escapes spontaneously the magnetic field when the pole edge is reached. This corresponds to the auto-extraction.

Provided that experiences confirm our numerical simulations in progress, this new extraction method for positive ions is likely to replace the use of negative ions in cyclotrons designed for high currents.

5. CONCLUSION

Recently achieved and expected progresses in ion sources and cyclotron technologies allow for the production of multi-milliampere extracted beam intensities. Combined with appropriate target design allowing for high power dissipation, this evolution opens the way for high intensity accelerator-based production of radioisotopes, in particular the direct production of ^{99}Mo and ^{99m}Tc.

REFERENCES

[1] S.M. QAIM, Nuclear data relevant to cyclotron produced short-lived medical radioisotopes, Radiochimica Acta **30** (1982) 147-162.

[2] Y. JONGEN, "The Cyclone 30 a 30 MeV, high intensity H^- cyclotron for radioisotope production", 7th Conference on Applied Accelerators, St. Petersburg, 1992.

[3] Y. JONGEN, "A proton-driven, intense, subcritical, fission neutron source for radioisotope production", Proceedings of the International Conference on Accelerator-Driven Transmutation Technologies and Applications, Las Vegas, July 1994.

[4] G. EGAN, C. JAMIESON, M.C. LAGUNAS-SOLAR, "An investigation into the technical feasibility of cyclotron production of technetium-99m", Newsletter of the Australia New Zealand Society of Nuclear Medicine, March 1994.

[5] Y. JONGEN, M. ABS, J.M. CAPDEVILA, D. DEFRISE, F. GENIN, A. NGUYEN, The rhodotron, a new high-energy, high-power, cw electron accelerator, Nucl. Inst. and Meth. in Phys. Res. **B 89** (1994) 60-64.

[6] Y. JONGEN, "Extremely High Intensity Cyclotrons for Radioisotope Production", Proceedings of the EPAC 94 Conference, London, May 1994.

[7] Y. JONGEN, D. VANDEPLASSCHE, P. COHILIS, "High Intensity Cyclotrons for Radioisotope Production or the Comeback of the Positive Ions", Proceedings of the CYCLOTRONS'95 Conference, Cape Town, October 1995.

ADONIS: THE PROTON-DRIVEN NEUTRON SOURCE FOR RADIOISOTOPE PRODUCTION

Y. JONGEN
Ion Beam Applications s.a.,
Louvain-la-Neuve, Belgium

Abstract

The world production of fission ^{99}Mo is today made in a very small number of research reactors which are getting quite old and are due, in the next years, for a major refurbishment or for decommissioning. The need for reliable sources of ^{99}Mo is becoming more and more urgent. As an attractive, competitive alternative to nuclear reactors used for radioisotope production, but also for research and industrial applications, we propose a cyclotron based spallation neutron source with neutron multiplication by fission. The optimal configuration for ^{99}Mo production has been calculated with neutronic calculation codes. It is shown that such a system, which offers many advantages compared to nuclear reactors, can be used to supply more than 50% of the world demand in ^{99}Mo.

1. INTRODUCTION

The importance of the production of ^{99}Mo is related to the world consumption of ^{99}Mo $\rightarrow$ ^{99m}Tc generators. The availability of Tc generators is crucial: Technetium 99-m is, by a large extent, the most widely used radioisotope in nuclear medicine. The ^{99m}Tc is normally supplied to the hospital as ^{99}Mo $\rightarrow$ ^{99m}Tc generators: the ^{99}Mo has a half life of 66 hours, versus 6 hours for the ^{99m}Tc, making the logistics of distribution much more practical for the ^{99}Mo generator than for the short-lived ^{99m}Tc.

Most of the ^{99}Mo used in nuclear medicine is obtained as a fission product of ^{235}U. The world production of fission ^{99}Mo is today made in a very small number of research reactors which are getting quite old and are due, in the next years, for a major refurbishment or for decommissioning. The need for reliable sources of ^{99}Mo is becoming more and more urgent.

There are, however, alternative methods for producing ^{99}Mo and ^{99m}Tc. As an attractive, competitive alternative to nuclear reactors used for radioisotope production, but also for research and industrial applications, we propose an accelerator based spallation neutron source with neutron multiplication by fission. The optimal configuration for ^{99}Mo production has been calculated with neutronic calculation codes. It is shown that such a system, which offers many advantages compared to nuclear reactors, can be used to supply more than 50% of the world demand in ^{99}Mo. Other alternative methods are presented elsewhere.

2. ADONIS: AN ALTERNATIVE TO NUCLEAR REACTORS

A number of reasons favor the continued use of the ^{235}U fission reaction for the production of ^{99}Mo: the high production yield resulting from the large cross-section of fission of ^{235}U by thermal neutrons, the high density of activity in the irradiated samples (allowing to perform the separation chemistry on reasonably low amounts of material), the possibility to

continue to use the existing and very expensive fission ^{99}Mo chemical separation facilities, and the possibility to avoid or minimize the re-licensing process for all radioactive diagnostic drugs labeled with ^{99m}Tc from ^{99}Mo $\rightarrow$ ^{99m}Tc generators.

The proposed ADONIS-system (Accelerator Driven Optimized Nuclear Irradiation System) [1] is designed for the production of fission ^{99}Mo, among other applications. It is based on [2] and includes the following elements:

(1) a H^- cyclotron, able to accelerate 2 mA of beam at 150 MeV with low acceleration losses and almost 100% extraction efficiency;

(2) a beam transport system, transporting the proton beam without losses to a neutron source;

(3) a neutron source including:
   a) a primary beam target, where the proton beam strikes a molten Pb-Bi target, producing spallation (mostly evaporation) neutrons;
   b) a water moderator surrounding the primary target;
   c) a number of secondary targets made of highly enriched ^{235}U. The neutron multiplication obtained in such a system can be shaped by the amount of secondary targets, but will ultimately remain far from criticality.

If necessary, to allow for different applications with very different source designs, or for backup reasons for example, more than one neutron source can be connected to the same accelerator.

The concept of sub-criticality indicates the completely different nature of this system compared to reactors. Due to the inherent limitation of the maximum amount of uranium put into this system, there can even be no doubt about the non-critical behavior. The use of a cyclotron as a driver also allows the quasi-instantaneous shut-down of the system if necessary. The combination of sub-criticality, externally driven neutron source, and the design of the system itself makes ADONIS inherently safe.

2.1. The 150 MeV, 2 mA H^- cyclotron

The 150 MeV, 2 mA H^- cyclotron takes advantage of the experience of Ion Beam Applications which has built more than 15 lower energy (30 MeV), high current (0.5 mA) H^- cyclotrons for radioisotope production. Such cyclotrons are used today by all major radio-pharmaceutical companies for the production of medical radioisotopes. IBA proposes upgrades allowing to increase the beam current of these cyclotrons, with final extracted currents between 1 and 2 mA. A key component of this upgrade is a higher brightness H^- multicusp ion source developed for IBA by AEA Technology in Culham (GB) [3]. The proposed cyclotron would use such an improved multicusp ion source, able to produce 25 mA of H^-.

Recently experimental results and calculations were presented [4] showing that the space charge limit for current designs of H^- cyclotrons was between 5 and 10 mA of beam current. These results show also that very high beam loading of the cyclotron RF system - up to 80% - is possible. The results of another IBA accelerator, the Rhodotron [5] show that mainline to RF efficiencies in excess of 70% can be achieved at 200 kW RF power and 107 MHz.

The total power efficiency of such a 150 MeV, 2 mA H^- cyclotron could therefore reach 50%, i.e. a total electrical power of only 600 kW for 300 kW of beam power.

The problem of the electromagnetic dissociation of H^- imposes the use of lower magnetic fields at higher energies. For a 150 MeV cyclotron, the maximum sector field would be 1.1 T, and the average field 0.6 T at the center. This would result in a pole radius of 2.75 m, and an external diameter of 8 m for the accelerator.

2.2. The production of the primary (spallation) neutrons

The 150 MeV, 300 kW proton beam is used to produce spallation neutrons in a molten Pb-Bi target.

A first estimation of the number of neutrons per incident proton was obtained through interpolations using available data. The neutron production yield from protons on lead targets has indeed been measured by Bell et al. [6] at energies below 80 MeV, and by Carpenter [7] between 0.5 and 1.5 GeV. There is also a measurement of the total neutron yield at 100 MeV made by Lone et al. [8] showing a value of 0.35 neutron/incident proton at 100 MeV, in excellent agreement with our calculations.

This first estimation was confirmed by more detailed calculations of the neutron production from the spallation reaction and the neutron transport using the computer codes HETC and DORT. The calculations are described in detail elsewhere [9]. The geometry for these calculations consisted of a cylinder of Pb-Bi with a radius of 3 cm and a length of 15 cm. The proton beam and the target tube are coaxial. The proton beam was supposed to have a gaussian distribution with a FWHM of 1.5 cm.

As a result of these calculations, the total primary neutron yield is estimated to be 0.8 neutrons per incident proton at 150 MeV.

2.3. The neutron source

The proposed target assembly is schematically illustrated in Fig.1. A flowing liquid lead-bismuth eutectic alloy is currently proposed as the spallation target material. The flowing target allows the heat to be transported through convection of the target material itself.

The proposed primary target is vertical with the liquid lead-bismuth flowing out of a ring-type nozzle into an open channel. Here the fluid interacts with the proton beam and is in direct contact with the vacuum. The flow exits the bottom of the target region, and is pumped through a heat exchanger, and then returns back to the target. A drain tank is used to hold the solid and liquid alloy during start-up or shut-down: the liquid can therefore be pre-heated and cooled down in a controlled manner. Electro-magnetic pumps were chosen to deliver the forced circulation in the Pb-Bi circuit.

The primary target will be surrounded in all directions by a water moderator, in order to thermalize the primary spallation and secondary fission neutrons. The ^{235}U secondary targets are planar and placed around the spallation source in a separate circuit. They are positioned in three concentric zones as illustrated in Fig. 2. The optimal configuration may vary in function of the application and has been calculated with neutronic calculation codes for the case of the production of ^{99}Mo.

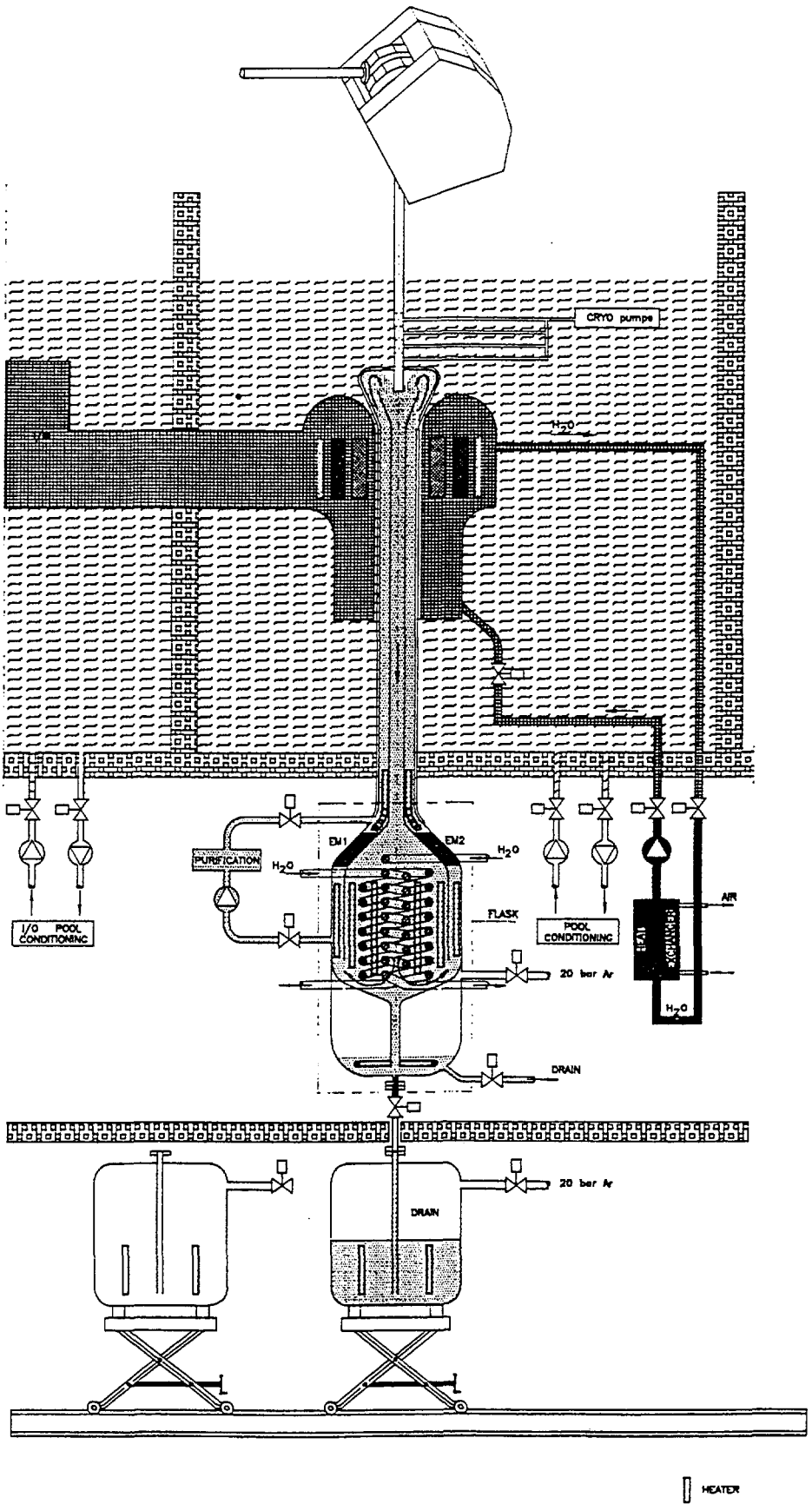

Fig. 1. Schematics of the sub-critical facility

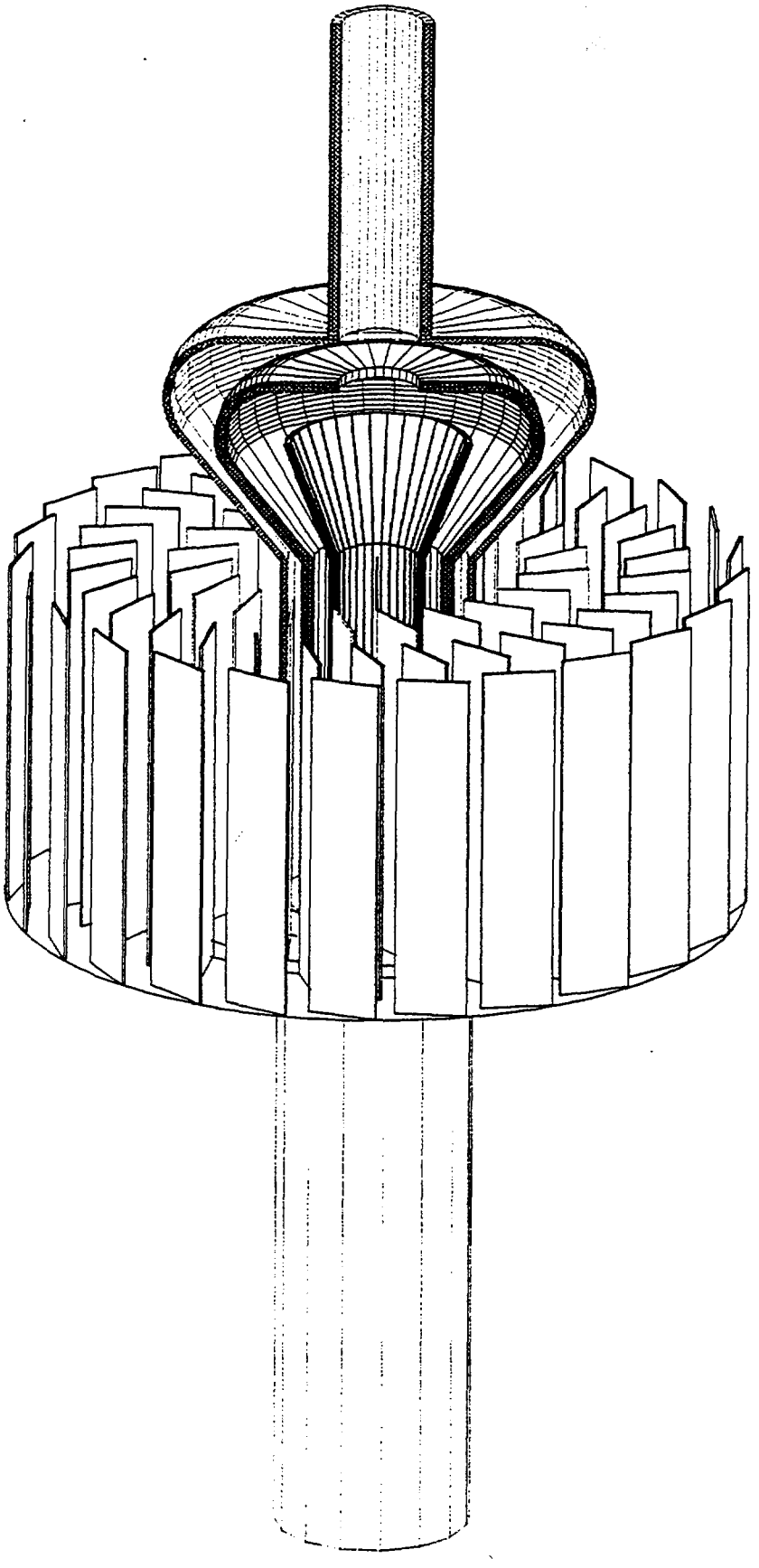

Fig. 2. Positioning of the uranium targets

All the above components are located in a main irradiation pool, for moderation and shielding purposes. Adjacent to the main pool is an annex pool (see Fig.1) allowing the remote handling of new and irradiated targets and used also as an intermediate storage pool. The manipulation and transfer of the uranium targets is realized by using a combined system of teleoperation and guiding tubes.

Among the advantages of the proposed assembly, let us note the absence of an entrance window for the proton beam, the uncoupling of the primary spallation target circuit and the uranium target circuit and surrounding feeding zone, and the simple one-circuit operation for Pb-Bi serving both heat-transport needs and spallation target needs.

3. OPTIMIZATION OF THE SYSTEM FOR RADIOISOTOPE PRODUCTION

In view of this important application, the design of such a sub-critical facility was optimized for ^{99}Mo production. To obtain the maximum fission rate in the ^{235}U targets and therefore the maximum multiplication factor, these targets have to be placed in a position where the thermal flux resulting from the slowing-down of the energetic spallation neutrons is maximum. Another parameter of importance is the amount of uranium targets that can be placed in that position, in order to maximize the total ^{99}Mo production rate, but limiting the shadowing effects between them. In fact, the proposed ADONIS system results into a high operational flexibility. One can load independently different amounts of ^{235}U targets in the three irradiation zones, such that one can maximize either the total ^{99}Mo production or the specific activities. Any production scheme in between is of course possible.

The neutron transport, thermalisation and multiplication in this assembly were simulated using numerical neutron transport codes at SCK-CEN. In particular, the DORT S_N [10] neutron transport code was used, associated to the MOL-BR2-40GR library, to calculate the multiplication factor of the ADONIS system as well as the thermal flux distribution in the water pool surrounding the spallation source, in the presence of the secondary targets or not. These calculations were completed in the fixed source mode with multiplication allowed in the fissile zones. A cylindrical geometry modeling was used to describe the Pb-Bi spallation source, the structural external double wall (Stainless Steel), the water-pool and the three rings of ^{235}U targets. By using different loading schemes, one can obtain an extended set of attainable flux distributions. One of them is shown in Fig. 3 (relative units).

The presence of two-side wings is due to the effect of the thermalization and the reflection of fast neutrons created during the fission process in the ^{235}U plates. Typical thermal neutron fluxes at targets location are around 6.10^{13} n .s^{-1}cm^{-2}.

Table I presents the activity of ^{99}Mo which can be achieved for two different loading schemes of the uranium targets.

TABLE I. EXAMPLE OF LOADING SCHEMES FOR ^{99}MO PRODUCTION (ACTIVITIES END OF IRRADIATION, PER WEEK)

Type of Loading	Total Activity (Ci)	Specific Activity (Ci.g^{-1})
Maximum total production	35000	100
Maximum specific activity	22500	180

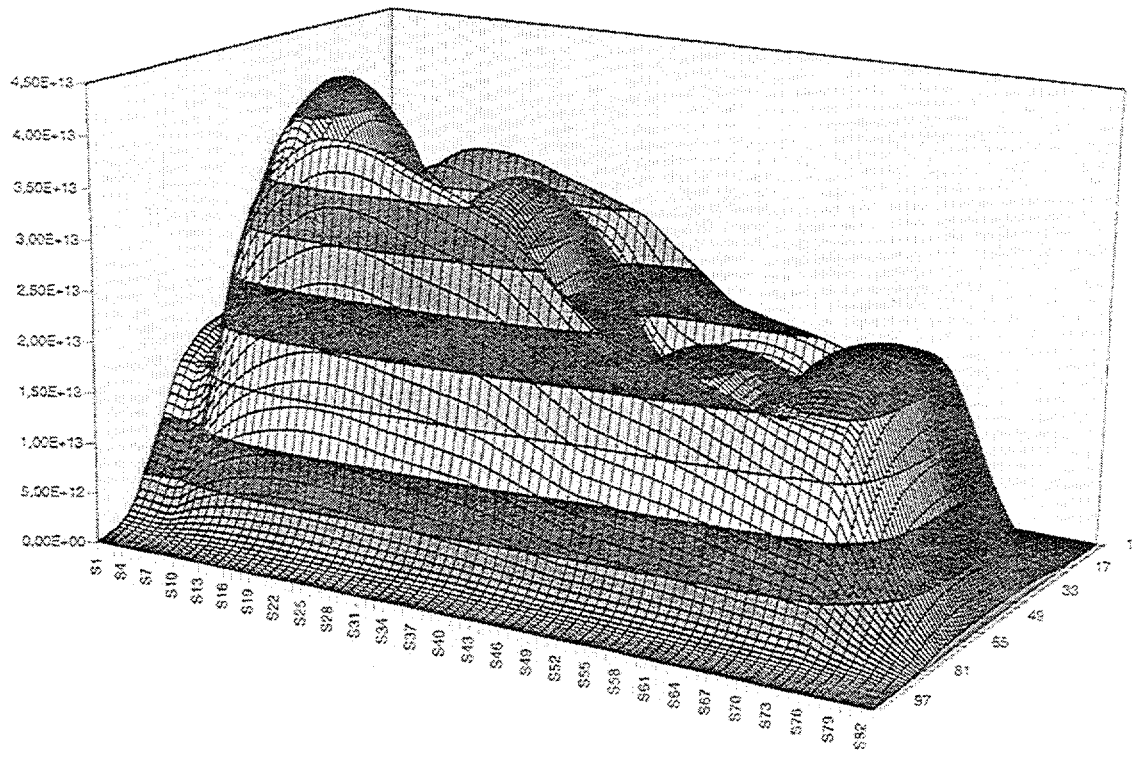

Fig. 3. Neutron flux distribution

The maximum total production corresponds, at the end, to more than 50% of the world's demand, while the obtained mean specific activities are comparable to those presently obtained in most nuclear reactors used for ^{99}Mo production.

4. CONCLUSION

The ADONIS system is proposed as an alternative to nuclear reactors currently used for the production of fission-based radioisotopes, for research and for industrial applications. Compared to nuclear reactors, the proposed system is unquestionably safe. Other advantages are the modularity of the system and its flexibility in operation. As far as the production of ^{99}Mo is concerned, one such system could in principle supply more than 50% of the world demand and would cost significantly less than a commercial, 10 MW isotope production reactor. Operational costs, including personnel, operational fuel and waste, and final dismantling costs, would be significantly lower also. The existing fission-molybdenum processing technologies could be used further on. Finally, the non critical nature of the system would make it more acceptable for the public opinion than a nuclear reactor, and should simplify the licensing process as well.

REFERENCES

[1] COHILIS, P., JONGEN, Y., LANNOYE, G., D'HONDT, P., VAN DEN DURPEL, L., AÏT ABDERRAHIM, H., "Recent Advances in the Design of a Cyclotron-Driven, Intense, Subcritical Neutron Source", Proceedings of EPAC 96, Sitges, June 1996, (to be published).

[2] JONGEN, Y., "A Proton-Driven, Intense, Sub-critical, Fission Neutron Source for Radioisotope Production", International Conference on Accelerator-Driven Transmutation Technologies and Applications, Las Vegas, NV, July 1994.
[3] MC ADAMS, R., KING, R.F., PROUDFOOT, G., HOLMES, A.J.T., "Pure and Cesiated CW Volume Source Performance at the Culham Ion Source Test Stand", Proceedings of Sixth Intl. Symposium on Production and Neutralization of Negative Ions and Beams, Brookhaven, Nov. 1992, AIP conf. proceedings No 287, pp. 353-367.
[4] JONGEN, Y., "Extremely High Intensity Cyclotrons for Radioisotope production" Proceedings of EPAC 94, London, July 1994, (to be published).
[5] JONGEN, Y., ABS, M., DEFRISE, D., GENIN, F., CAPDEVILLA, J.M., GAL, O., NGUYEN, A., First beam tests results from the 10 MeV, 100 kW Rhodotron, (ibid., to be published).
[6] BELL, R.E., SHARSGARD, H.M., Cross-sections of (p,xn) reactions on the isotopes of lead and bismuth, Can. Journal of Physics **34** (1956) 745-766.
[7] CARPENTER, J.M., Pulsed spallation sources for slow neutron scattering, NIM **145** (1977) 91-113.
[8] LONE, M.A. et al., Total neutron yields from 100 MeV Protons on Pb and 7Li targets, NIM **214** (1983) 333-339.
[9] D'HONDT,P., VAN DEN DURPEL, L., AÏT ABDERRAHIM, H., JONGEN, Y., COHILIS, P., "An Alternative to Nuclear Research Reactors: the ADONIS-Concept", to be presented at the International Conference on Neutrons and their Applications, Creté, June 1996.
[10] RHOADES, W.A., MAYNATT, F.R., "TORT-DORT, Two and Three-Dimensional Discrete Ordinates Transport Code, version 2.7.3", RSIC CCC-543, May 1993.

THE GEL GENERATOR OPTION

R.E. BOYD
Australian Nuclear Science & Technology Organisation,
Lucas Heights, NSW, Australia

Abstract

The development of a national policy for guaranteeing an ample supply of ^{99m}Tc to nuclear medicine, involves issues which go beyond the means by which radioactivation is achieved. Indeed, in such an exercise the pragmatic dictates of business and the sensitivities of politics must also be taken into account. Furthermore where a preference towards the nuclear reactor or the potential of cyclotrons is being questioned, the debate is incomplete if the only options that are considered are the fission-based ^{99}Mo generator versus the direct cyclotron production of ^{99m}Tc. There is a third option (also neutron γ-based), an alternative to the fission ^{99}Mo generator, which ought not be overlooked. The application of low specific activity (n,γ) ^{99}Mo to a new type of generator, the Gel Generator, has been the focus of much research, particularly in Australia and more recently in China. After the initial concept had been established in the laboratory, the Australian researchers then undertook a comprehensive program of tests on the Gel Generator to assess its potential, either in the clinical laboratory or the centralised radiopharmacy, for supplying ^{99m}Tc suitable for nuclear medicine. The outcome of this program was a clear indication that the Gel Generator innovation had the capability to provide both technical and economic advantages to the nuclear medicine industry. These advantages are described. Since that time the Gel Generator has been selected for routine use in China where it now satisfies more than 30% of the ^{99m}Tc demand.

1. INTRODUCTION

The majority of the world's supply of ^{99m}Tc is derived from generators containing fission-based ^{99}Mo. While such systems consistently produce ^{99m}Tc with excellent physico-chemical and biomedical qualities, the process of manufacturing fission-based ^{99}Mo involves so many complications that few commercial organisations are willing to be involved, despite the size of the world market. The need for elaborate heavily shielded processing facilities, the need to protect the environment from volatile fission products and the generation of medium level, liquid and solid radioactive wastes are all attendant difficulties which incur substantial economic penalties. These penalties are endured because the nuclear medicine industry has traditionally accepted the view that the fission-based ^{99}Mo generator is the unique solution to the continuously growing demand for an efficient, clinically acceptable and user-friendly source of its mainstay radionuclide. This view is still current, as reflected by the US Government's decision [1] to establish an indigenous capability for manufacturing fission-based ^{99}Mo; but it is also being challenged.

There are modern alternatives to the fission-based ^{99}Mo generator which deserve to be given serious consideration by the nuclear medicine industry. Novel alternatives utilising the particle accelerator, either to produce ^{99m}Tc directly by the proton bombardment of molybdenum [2] or by inducing uranium-238 to fission under the influence of proton bombardment [3], are being proposed. Another alternative follows on from research conducted in Australia in which reactor irradiated molybdenum (ie low specific activity) was incorporated into a zirconium molybdate gel [4]. It was shown that ^{99m}Tc can be separated from such a gel in an exactly the same manner (saline elution) and with identical qualities to that obtained from the fission-based ^{99}Mo generator [5].

Although some general comments are offered on the relative values of the cyclotron and the nuclear reactor as a tool for producing radionuclides, the main thrust of this work is to increase the general awareness of the reactor-based alternative to the present fission-based ^{99}Mo generator. It is intended to demonstrate that this alternative can offer the nuclear medicine industry all the operational advantages of today's generators without the more obvious disadvantages incurred through the processing of irradiated uranium.

2. THE NUCLEAR REACTOR VERSUS THE ACCELERATOR

The production of a radioactive product is more easily achieved via neutron irradiation of a target in a nuclear reactor than by a cyclotron bombardment with charged particles for the following reasons:-

- Reactor targets are easier to design and construct
- Reactor targets require less cooling during activation
- Reactor targets are easier to load and unload

In general, neutron activation cross-sections are orders of magnitude greater than those for charged particles; this leads to higher yields. There are fewer channels of activation with neutrons and as a result it is easier to predict the outcome(s) from neutron activation; this implies lower impurity levels. Nuclear reactors are invariably used to perform simultaneous activation of many targets and as a consequence the nuclear reactor is better suited to large scale commercial production programs.

In the context of ^{99}Mo $\rightarrow$ ^{99m}Tc production, the nuclear reactor offers two independent, high yielding routes of activation both of which have been commercially exploited on a world-scale. On the other hand we see the method proposed for the direct cyclotron production of ^{99m}Tc as having only limited application in a few specialised circumstances. The production of high specific activity ^{99}Mo by the proton induced fission of ^{238}U is still too new a concept to be evaluated with any certainty.

3. THE GEL GENERATOR CONCEPT

The Gel Generator utilises low specific activity (n,γ)^{99}Mo which is processed post-irradiation into an insoluble zirconium molybdate hydrous gel structure. The dried gel contains about 25% by weight of molybdenum and has properties consistent with a cation exchanger*. The process for synthesising the gel is shown in Fig. 1.

The passage of an aqueous eluant (typically either pure water or physiological saline) through a column of the gel releases the ^{99m}Tc; the chromatographic separation can be performed with the same degree of ease as that applying with the fission ^{99}Mo generator.

The gel generator may experience radiolytically induced losses in efficiency similar to those exhibited by the fission ^{99}Mo generator however this effect can be minimised by replacing 5% of the zirconium in the initial gel reactants with cerium [Ce(IV)].

*Synthesising the gel prior to neutron activation produces a relatively useless product because of damage sustained by the gel from the effects of nuclear heating which cause it to lose its ion-exchange properties.

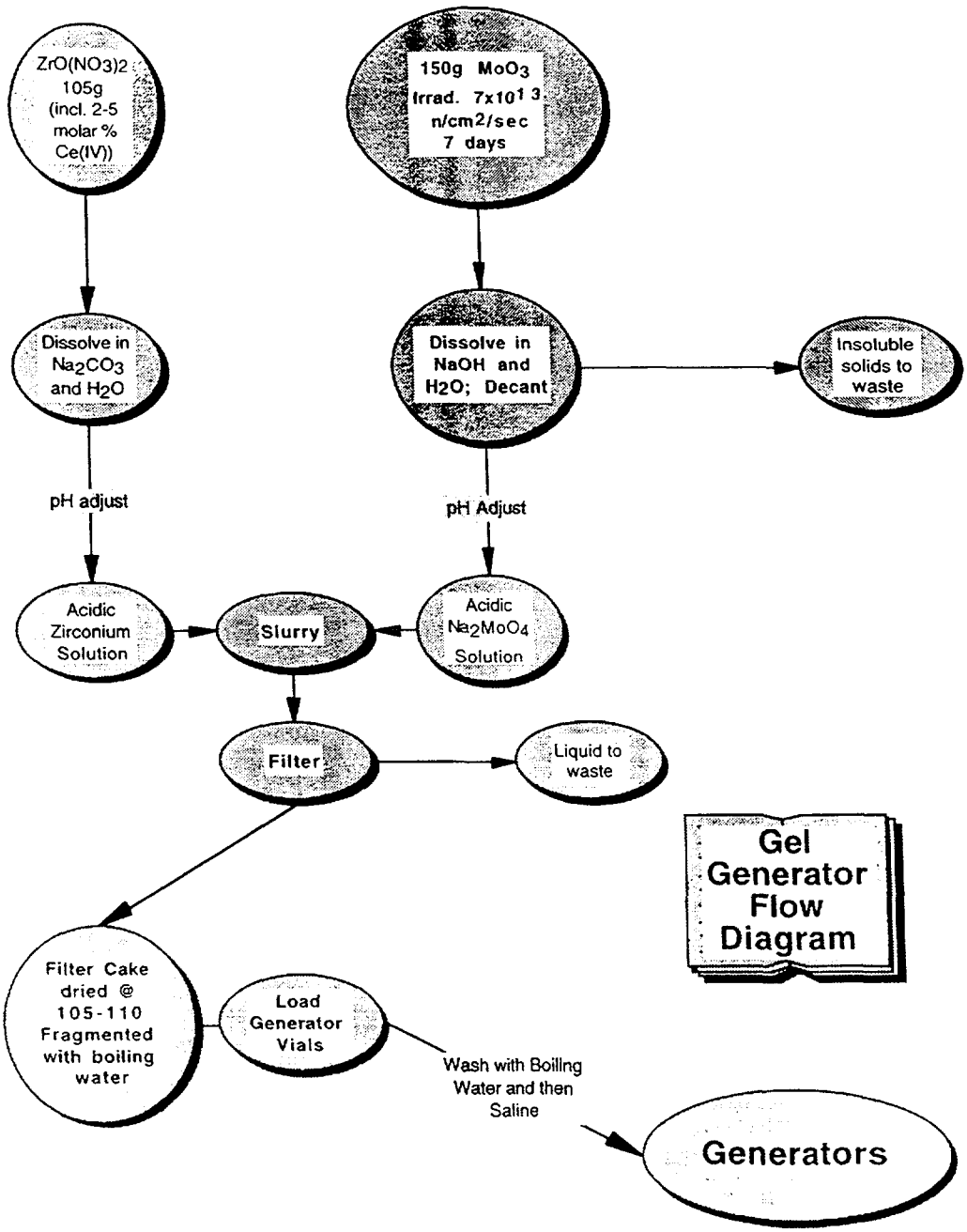

FIG.1. Flow diagram for the preparation of zirconium molybdate (^{99}Mo) gel.

The gel is insoluble and chemically stable within the pH range 2-9. It successfully withstands thermal (wet steam) autoclaving; consequently the gel generator may be presented as a terminally sterilised product.

4. PERFORMANCE TESTING THE GEL GENERATOR

Following the initial research period in which the gel was chemically characterised and its optimum preparation conditions established, a pilot plant was constructed to produce prototype generators in two ranges of activity-firstly a range covering the radioactivities routinely used within nuclear medicine departments (ie the transportable ^{99m}Tc generators) and

then another range of much higher radioactivities typical of those used in centralised radiopharmacies (the "jumbo" generators). A comprehensive program of performance testing was applied to the prototype generators with the following results:

4.1. Elution efficiency

The efficiency with which ^{99m}Tc could be separated from the generators is summarised in Tables I and II.

TABLE I. ELUTION EFFICIENCY OF TRANSPORTABLE GEL GENERATORS

No. of Generators	Range of Activities GBq	Total No. of Elutions	Mean Efficiency %
43	15 to 64	411	82.4 ± 1.2

TABLE II. ELUTION EFFICIENCY OF "JUMBO" GEL GENERATORS

No. of Generators	Range of Activities GBq	Total No. of Elutions	Mean Efficiency %
5	669 to 2023	45	89.3 ± 7.4

TABLE III. ^{99}Mo BREAKTHROUGH

No. Eluates Tested	^{99}Mo Breakthrough		Mean Expiry Time
	Range of Values %	Mean Value %	(h)
408	0.000 to 0.014	0.003	44

4.2. Molybdenum-99 breakthrough

The ^{99}Mo content of the eluates was measured gamma-spectroscopically and the results are summarised in Table III*.

*Because the ^{99}Mo level in an eluate increases with the age of the sample, an alternative statement of radionuclidic purity is employed. The **Expiry Time** is that period of time post-elution necessary before the ^{99}Mo reaches the maximum level allowed by the pharmacopoeia monograph- typically 0.1%)

4.3. Other radionuclidic impurities

After the short-lived radioactivities had decayed (a few days), several of the eluates were re-examined for the presence (identity and concentration) of other radionuclidic impurities. The results of these measurements are shown in Table IV.

TABLE IV. LONG-LIVED RADIO-CONTAMINANTS

No. Eluates Tested	Frequency of Making a Positive Finding	Radionuclide(s) Identified	Concentration %
133	17/133	^{134}Cs	<0.005

TABLE V. CHEMICAL PURITY OF THE ELUATES

No. Eluates Examined	131 Samples
pH	4.5 to 6.0
Zr^{4+} ppm	<5
NO_3^- ppm	<20
Ce^{3+} and Ce^{4+} ppm	<5 to <10

TABLE VI. RADIOCHEMICAL PURITY

Early Eluates		Mid-cycle Eluates		Late Eluates	
No. Samples	% ^{99m}Tc as $^{99m}TcO_4^-$	No. Samples	% ^{99m}Tc as $^{99m}TcO_4^-$	No. Samples	% ^{99m}Tc as $^{99m}TcO_4^-$
42	99.2 to 99.9	43	99.1 to 99.9	43	99.1 to 99.9

4.4. Chemical purity

Eluate samples, taken at the beginning, the mid-point and at the end of a series of elutions were assayed for trace chemical impurities likely to compromise pharmaceutical quality. The results of these tests are summarised in Table V.

4.5. Radiochemical Purity

Radiochemical impurities often arise due to the effects of radiation on the solvent(radiolysis), changes in temperature or pH, or the presence of reducing/oxidising agents. The pertechnetate ion is a strong oxidising agent capable of reacting with traces of reducing substances to produce lower valency species. Using thin layer chromatographic techniques the radiochemical species present in the eluates were investigated (Table VI).

4.6. Elution Profile

The elution profile of column based generators is influenced strongly by physical size and shape [6]. In the case of the gel generator a third factor applies: the bed can be pre-conditioned by extensive washing with saline to remove pertechnetate-retarding anion exchange sites. Following this treatment the elution profile is substantially sharpened and the elution efficiency improved.

At moderate levels of ^{99}Mo specific activity (circa 75GBq ^{99}Mo per g Mo) the elution process is essentially complete within the passage of 10 mL. Some complications arise with very low specific activities because the ^{99m}Tc concentration of the eluates is too low for practical application. However an important property of the gel generator is its ability to be eluted effectively with pure water, in place of saline. This difference can then be exploited to provide the means for overcoming the low ^{99m}Tc concentrations that are characteristic of the large bed "Jumbo Generator".

The following technique for concentrating ^{99m}Tc was developed:-

- A 1g Al_2O_3 column is located downstream of the main generator bed,
- The generator is eluted with just 50mL of pure water,
- Issuing from the base of the generator, the aqueous ^{99m}Tc is pumped through the Al_2O_3 column which strips out the ^{99m}Tc activity. The water is recycled to the top of the generator column and the elution process is repeated 3-4 times.
- A highly concentrated ^{99m}Tc solution can then be recovered ,simply by flushing the small Al_2O_3 column with 5 mL saline.
- The process is amenable to automation and laboratory results indicate that the ^{99m}Tc can be recovered with >90% efficiency and be concentrated by a factor of 20.

4.7. Pre-clinical biological testing

Experiments were performed* in which the relative bio-distributions were compared for several radiopharmaceutical 'cold-kits' reconstituted with either gel ^{99}Mo-derived or fission ^{99}Mo-derived pertechnetate solutions.

The respective bio-distributions, in age-matched groups of 12 rats, were shown not to be significantly different (Unpaired Student t-Test) [5].

*According to the Australian Code of Practice for the Care and Use of Animals for Scientific Purposes

The quality of the ^{99m}Tc produced by the gel generator is sufficiently high to presume that this generator should anticipate receiving a wider clinical acceptance than it currently enjoys. When presented either for use in the nuclear medicine clinic or in the setting of a centralised radiopharmacy, the gel generator deserves to be considered as a potential adjunct to, or replacement for the fission ^{99}Mo generator.

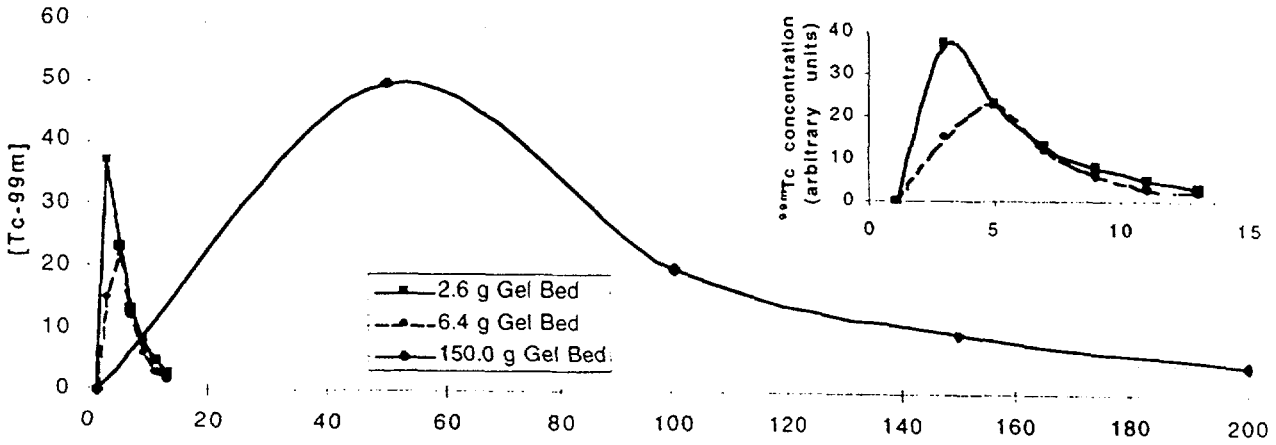

FIG. 2. The effect of bed size on the elution profile.

4.8. Clinical experience

The Gel Generator has not yet progressed to clinical trials in Australia, however it is in routine use in China where it was reported [7] that clinical results are indistinguishable from those obtained from its fission ^{99}Mo counterpart in comparable clinical studies.

4.9. Summary of test results

^{99m}Tc derived from gel generators has been assessed by a battery of tests and has been compared against the international standards of acceptability that would apply to presently available generators. Without exception, the performance characteristics of the gel generator were found to be at least as good as those exhibited by the fission ^{99}Mo generator.

5. OTHER CONSIDERATIONS

Given the close similarity in the technical performances of the two generator types, it is profitable to examine other considerations to find the incentives for change.

5.1. Economic considerations

The cost of producing (n,γ)^{99}Mo is less than that for fission ^{99}Mo. One analysis [5] shows that this differential can be quite substantial; eg $US 0.83 per Ci as compared to $US 57 per Ci. However when the fixed costs associated with generator manufacture are included in the comparison much of this relative advantage is eroded away. Effective costs are also complicated by such considerations as the post delivery calibration time for the ^{99}Mo activity and the type of elution regime. However it would be reasonable to presume that the gel generator technology offers some savings.

5.2. Waste and environmental issues

The processing of uranium targets for the production of fission ^{99}Mo generators gives rise to quantities of medium-level liquid and solid wastes containing uranium, plutonium and several long-lived fission products which require substantial treatment before final disposal can be contemplated.

The gaseous releases from the processing hot-cells are very much reduced by the use of delaying absorbent filters in the dissolver off-gas lines and in the cell ventilation ductwork.

The processing of irradiated molybdenum trioxide to zirconium molybdate gel does not require as sophisticated a waste management strategy.

6. DISCUSSION

The Gel Generator has been shown to be technically equivalent to the fission ^{99}Mo generator.

- From the perspective of the end-user, the Gel Generator retains the simple-to-operate attribute that is an important characteristic of the fission ^{99}Mo generator.
- ^{99m}Tc can be obtained from the Gel Generator with an efficiency close to that of the fission ^{99}Mo generator.
- The overall quality of ^{99m}Tc from the Gel Generator is, to all intents and purposes, indistinguishable from the alternatives.
- There appears to be no special restriction on the field of application for ^{99m}Tc obtained from the Gel Generator.
- Manufacturing zirconium molybdate gel from neutron activated molybdenum trioxide does not require the elaborate processing facilities that are a pre-requisite of all processes treating fissioned uranium.
- The Gel Generator minimizes waste.
- ^{99m}Tc from the Gel Generator is cheaper than that obtained from the fission ^{99}Mo generator
- Gel generator can be presented to the marketplace in the same packaging format, if so required.
- Since more than 80% of nuclear medicine's imaging procedures require the administration of a ^{99m}Tc radiopharmaceutical* the Gel Generator is capable of bringing the benefits of nuclear medicine to a wider population of patients.

China is the first country to attempt to satisfy a significant portion of the national demand for ^{99m}Tc by utilising the gel generator technology. Other Asian countries have also explored the possibility of change.

In the commercial pharmaceutical world, the need to protect society by requiring all new drugs to be formally registered has had the unavoidable side-effect of slowing down the rate of innovation. However the demonstrated potential benefits of the gel generator technology could be sufficient incentive to persuade the radiopharmaceutical industry to consider a change.

**to some 100,000 patients per day world-wide*

REFERENCES

[1] COATS, R.L., "The ^{99}Mo Production Program at Sandia National Laboratories", Proc. Conf. American Nuclear Society, (Philadelphia, June 1995).

[2] LAGUNAS-SOLAR, M. et al, Cyclotron production of NCA ^{99m}Tc and ^{99}Mo. An alternative non-reactor supply source of instant ^{99m}Tc and ^{99}Mo, Appl. Radiat. Isot. **42** (1991) 643-657.

[3] JONGEN, Y., "A Proton-Driven, Intense, Sub-critical, Fission Neutron Source for Radioisotope Production", Accelerator-Driven Transmutation Technologies and Applications (Proc. Intl. Conf, Las Vegas, July 1994).

[4] EVANS, J.V., MOORE, P.W., SHYING, M.S., SODEAU, J.M. "Zirconium Molybdate Gel as a Generator for Technetium-99m", Proc. 3rd World Congress of Nuclear Medicine and Biology, (Paris, Aug. 1982).

[5] BOYD, R.E., The gel generator: a viable alternative source of technetium-99m for nuclear medicine, Appl. Radiat. Isot. **48** (1997) 1027-1033.

[6] BOYD, R.E., "Recent Developments in Generators of ^{99m}Tc", Radiopharmaceuticals and Labelled Compounds, (Proc. Symp. Copenhagen, March 1973).

[7] TAN TIAN-ZHI, MO TING SHU, West China University of Medical Sciences, Chengdu, Sichuan, China, personal communication, (1996).

LIST OF PARTICIPANTS

Ball, R.M.	Ball Systems Company Lynchburg, Virginia, United States of America
Barich, T.S.	MDS Nordion, 47 March Road, P.O. Box 13500, Ontario, Canada
Boyd, R.	Radiopharmaceuticals Division, Australian Nuclear Science & Technology Organisation, New Illawara Road, Lucas Heights 2234, NSW, Australia
Deblaton, M.	Institut National des Radioelements (IRE), B-6220 Fleurus, Belgium
Gudge, R.	Isotope Supplier Development, Amersham International plc, Amersham, BUCKS HPP7 9ll, United Kingdom
Jongen, Y.	Ion Beam Applications s.a., Chemin du Cyclotron, rue J.E. Lenoir 6, B-1348 Louvain-La-Neuve, Belgium
Lagunas-Solar, M.	Crocker Nuclear Laboratory Radioisotope Programme, University of California, Davis, California 95616 United States of America
Lambrecht, R.	Medical and Natural Science Research Centre, University of Tübingen, ob dem Himmelreich 7, D-72074 Tübingen, Germany
Oblozinsky, P.	International Atomic Energy Agency, Nuclear Data Section, Wagramer Strasse 5, P.O. Box 100, A-1400 Vienna, Austria
Scholten, B.	Institut für Nuklearchemie, Forschungszentrum Jülich GmbH, Postfach 1913, D-52425 Jülich, Germany
Tarkanyi, F.T.	Institute of Nuclear Research of the Hungarian Academy of Sciences, H-4001 Debrecen, P.O. Box 51, Hungary
Van Zyl De Villiers, W.	Atomic Energy Corporation of South Africa Ltd, Building 1600 P.O. Box 582, Pretoria 0001, South Africa

Vandegrift, G.F.	Argonne National Laboratory, Argonne, Illinois, United States of America
Vera Ruiz, H. *(Scientific Secretary)*	International Atomic Energy Agency, Wagramerstrasse 5, P.O. Box 100, A-1400 Vienna, Austria